

Switzerland

Swiss Geodetic Commission



Suisse

Commission Géodésique Suisse

**Swiss National Report on the
GEODETIC ACTIVITIES
in the years 2019 to 2023**

Presented to the XXVIII General Assembly
of the International Union of Geodesy and Geophysics
in Berlin, Germany, July 2023



**Rapport National Suisse sur les
ACTIVITÉS GÉODÉSIQUES
exécutées de 2019 à 2023**

Présenté à la vingt-huitième Assemblée générale
de l'Union Géodésique et Géophysique Internationale
tenue à Berlin, Allemagne, Juillet 2023

Zurich 2023

Swiss Geodetic Commission/Commission Géodésique Suisse

ETH Zurich

Robert-Gnehm-Weg 15

8093 Zurich

Switzerland

<http://www.sgc.ethz.ch/publications>

Edited by:

J. Mueller-Gantenbein

E. Brockmann

U. Marti

M. Rothacher

B. Merminod

Secretary of the SGC

(Commission 1)

(Commission 2)

(Commission 3)

(Commission 4)

In addition to the bibliographies at the end of each section we recommend the following
www-sites:

Astronomical Institute of the University of Bern (AIUB): <http://www.aiub.unibe.ch/>

Institute of Geodesy and Photogrammetry,
Eidgenössische Technische Hochschule, ETH Zurich: <http://www.igp.ethz.ch/>

Office federal de topographie (swisstopo)
Federal Office of Topography (swisstopo): <http://www.swisstopo.ch/>

Geodetic Engineering Laboratory,
École polytechnique fédérale de Lausanne EPFL: <http://topo.epfl.ch/>

Haute Ecole d'Ingénierie et de Gestion du Canton de Vaud: <http://www.heig-vd.ch/>

University of Applied Sciences Northwestern Switzerland,
Fachhochschule Nordwestschweiz: <http://www.fhnw.ch/>

ISBN 978-3-908440-55-0

©2023 Swiss Geodetic Commission

PREFACE

The Swiss Geodetic Commission (SGC) is an organisation within the Swiss Academy of Sciences (SCNAT). It is devoted to research into scientific problems of geodesy including the transfer to practical applications in national surveying. Of particular importance is the promotion of international cooperation and national coordination. The SGC has close links to the Swiss Geophysical Commission, in particular in the field of gravimetry where research projects are being pursued jointly on an interdisciplinary basis.

For the compilation of the national report covering the scientific activities of the past 4 years it was decided to follow the structure of previous national reports and divide it into 4 commissions according to the structure of the International Association of Geodesy (IAG):

- 1 Reference Frames
- 2 Gravity Field
- 3 Earth Rotation and Geodynamics
- 4 Positioning & Applications

These main chapters were compiled by an editorial staff consisting of E. Brockmann (Commission 1), U. Marti (Commission 2), M. Rothacher (Commission 3), B. Merminod (Commission 4). Our special thanks go to J. Mueller-Gantenbein, secretary of SGC, for the careful editing and preparation of the layout. Without her efforts this report could not have been realized in due time.

The SGC expresses its appreciative thanks to all colleagues who have contributed to this report and who are promoting Geodetic Sciences in Switzerland. Financial support was provided by the SCNAT. Its valuable help is gratefully acknowledged.

On behalf of the Swiss Geodetic Commission, June 2023

Urs Marti
Vice-President of SGC

Adrian Jäggi
President of SGC

1	REFERENCE FRAMES	5
	SATELLITE LASER RANGING AT ZIMMERWALD.....	7
	<i>T. Schildknecht¹, L. Kleint¹, P. Lauber¹, M. Prohaska¹, A. Jäggi¹</i>	
	CODE CONTRIBUTIONS TO THE IGS.....	10
	<i>R. Dach¹, S. Schaer^{1,2}, D. Arnold¹, M. Kalarus¹, L. Prange¹, P. Stebler¹, D. Sidorov^{1,3}, A. Villiger^{1,4}, A. Jäggi¹</i>	
	EUREF ACTIVITIES AT CODE.....	13
	<i>S. Schaer^{1,2}, D. Arnold¹, R. Dach¹, L. Prange¹, D. Sidorov¹, P. Stebler¹, A. Sušnik^{1,3}, A. Villiger¹, A. Jäggi¹</i>	
	THE SWISS OPTICAL GROUND STATION AND GEODYNAMICS OBSERVATORY ZIMMERWALD.....	15
	<i>L. Kleint¹, T. Schildknecht¹, P. Lauber¹, M. Prohaska¹, A. Jäggi¹</i>	
	UNIFYING THE THREE PILLARS OF GEODESY USING SPACE TIES.....	18
	<i>A. Jäggi¹, E. Calero¹, L. Geisser¹, C. Kobel¹, D. Arnold¹, G. Bury¹, R. Dach¹, T. Grombein¹, M. Kalarus¹, X. Mao¹, S. Schaer¹, A. Villiger¹</i>	
	DIFFERENCING STRATEGIES FOR SLR OBSERVATIONS	20
	<i>I. Herrera Pinzón^{1,2}, M. Rothacher¹</i>	
	RIGOROUS COMBINATION OF GNSS AND VLBI OBSERVATIONS.....	23
	<i>I. Herrera Pinzón¹, M. Rothacher¹</i>	
	SHAPING THE FUTURE OF VLBI GLOBAL OBSERVING SYSTEM OBSERVATIONS AT ETH ZURICH.....	25
	<i>M. Schartner¹, B. Soja¹</i>	
	ANALYSIS OF PERMANENT GNSS NETWORKS AT SWISSTOPO (PNAC)	27
	<i>S. Lutz¹, D. Ineichen¹, S. Schaer¹, E. Brockmann^{1,2}</i>	
	GNSS2022: 5 TH RE-OBSERVATION OF THE NATIONAL GNSS NETWORK LV95.....	33
	<i>J. Carell¹, G. Palma¹, E. Brockmann^{1,2}, S. Condamin¹, M. Mäusli¹, Ch. Theler¹, A. Schlatter¹, T. Seiler¹, M. Smolik¹, D. Willi¹</i>	
	MEASUREMENTS FOR THE NATIONAL HEIGHT SYSTEM	36
	<i>A. Schlatter¹, U. Marti¹, D. Willi¹</i>	
	TABLE OF CONTENTS	39
	BIBLIOGRAPHY COMMISSION 1	39
2	GRAVITY FIELD.....	43
	ABSOLUTE AND RELATIVE GRAVITY MEASUREMENTS.....	45
	<i>U. Marti¹, H. Baumann²</i>	
	DEVIATIONS OF THE VERTICAL MEASUREMENTS IN SWITZERLAND	49
	<i>D. Willi¹, J. Carell¹, U. Marti¹, S. Guillaume², S. Brossi³</i>	
	GEOID DETERMINATION	53
	<i>U. Marti¹</i>	
	GEOID VALIDATION DATASET FROM PROFILE MEASUREMENT CAMPAIGNS FOR THE FCC AT CERN.....	56
	<i>J.A. Koch¹, D. Willi², U. Marti², B. Soja¹, M. Rothacher¹</i>	
	COMBINATION SERVICE FOR TIME-VARIABLE GRAVITY FIELDS (COST-G).....	60
	<i>U. Meyer¹, M. Lasser¹, A. Jäggi¹</i>	
	NOISE MODELLING FOR GRACE FOLLOW-ON OBSERVABLES IN THE CELESTIAL MECHANICS APPROACH	63
	<i>M. Lasser¹, U. Meyer¹, A. Jäggi¹</i>	

AIUB CONTRIBUTION TO THE GLOBAL GRAVITY-BASED GROUNDWATER PRODUCT (G3P).....	66
<i>A. Jäggi¹, N. Darbeheshti¹, M. Lasser¹, U. Meyer¹, A. Güntner²</i>	
SIMULATION STUDY FOR GEODETIC PARAMETER RECOVERY AT EUROPA AND CALLISTO	68
<i>W. Desprats¹, D. Arnold¹, A. Jäggi¹</i>	
TABLE OF CONTENTS	73
BIBLIOGRAPHY COMMISSION 2	73
3 EARTH ROTATION AND GEODYNAMICS.....	77
ALPINE METROLOGY LAB FOR THE MONITORING OF STATION MOVEMENTS IN THE MATTER VALLEY.....	79
<i>G. Moeller¹, T. Medic¹, M. Aichinger-Rosenberger², L. Schmid¹, A. Wieser¹, M. Rothacher¹</i>	
ROTATIONAL SENSORS, ACCELEROMETERS AND GNSS FOR STRONG GROUND MOTION	81
<i>Y. Rossi^{1,2}, K. Tatsis³, M. Awadaljeed¹, K. Arbogast¹, R. Hohensinn¹, J. Clinton², E. Chatzi³, M. Rothacher¹</i>	
OPERATIONAL PREDICTION OF EARTH ORIENTATION PARAMETERS WITH MACHINE LEARNING.....	83
<i>M. Kiani Shahvandi¹, M. Schartner¹, J. Gou¹, B. Soja¹</i>	
TABLE OF CONTENTS	87
BIBLIOGRAPHY COMMISSION 3	87
4 POSITIONING AND APPLICATIONS.....	89
BERNESE GNSS SOFTWARE.....	91
<i>R. Dach¹, P. Fridez¹, D. Arnold¹, E. Calero¹, N. Darbeheshti¹, W. Desprats¹, C. Gattano¹, L. Geisser¹, T. Grombein¹, M. Kalarus¹, C. Kobel¹, M. Lasser¹, X. Mao¹, U. Meyer¹, L. Prange¹, S. Schaer¹, L. Schreiter¹, D. Sidorov¹, P. Stebler¹, A. Villiger¹, A. Jäggi¹</i>	
SELECTED PRODUCTS FROM THE CODE ANALYSIS CENTER.....	94
<i>R. Dach¹, S. Schaer^{1,2}, D. Arnold¹, M. Kalarus¹, L. Prange¹, P. Stebler¹, D. Sidorov^{1,3}, A. Villiger^{1,4}, A. Jäggi¹</i>	
AIUB CONTRIBUTION TO THE COPERNICUS POD SERVICE	99
<i>D. Arnold¹, C. Kobel¹, X. Mao¹, A. Jäggi¹</i>	
ANALYSIS AND QUALITY ASSESSMENT OF LEO GPS DATA FOR GEOPHYSICAL AND IONOSPHERIC APPLICATIONS.....	101
<i>L. Schreiter¹, D. Arnold¹, A. Jäggi¹</i>	
REAL-TIME NAVIGATION SOLUTIONS OF LOW-COST OFF-THE-SHELF GNSS RECEIVERS ON BOARD THE ASTROCAST SATELLITES	103
<i>L. Müller¹, M. Rothacher¹, K. Chen¹, G. Moeller¹, B. Soja¹, L. Lopez²</i>	
A HIGH-PRECISION COMMERCIAL OFF-THE-SHELF GNSS PAYLOAD BOARD FOR NANOSATELLITE ORBIT DETERMINATION AND TIMING	105
<i>G. Moeller¹, F. Sonnenberg¹, A. Wolf¹, B. Soja¹, M. Rothacher¹</i>	
LOW-COST GNSS AND REAL-TIME PPP: ASSESSING THE PRECISION OF THE U-BLOX ZED-F9P FOR KINEMATIC MONITORING APPLICATIONS	107
<i>R. Hohensinn¹, R. Stauffer¹, M.F. Glaner², I.D. Herrera Pinzón¹, E. Vuadens¹, Y. Rossi^{1,3}, J. Clinton³, M. Rothacher¹</i>	
SENSING SMALL-SCALE STRUCTURES IN THE LOWER ATMOSPHERE WITH TOMOGRAPHIC PRINCIPLES.....	109
<i>G. Moeller¹, E. Shehaj¹, W. Zhang^{1,2}</i>	
ABSOLUTE PHASE CENTER CALIBRATION OF LOW-COST GNSS PATCH ANTENNAS.....	112
<i>G. Moeller¹, N. Ryther¹, A. Brown¹, M. Rothacher¹</i>	
ESTIMATION OF TROPOSPHERIC PARAMETERS WITH GNSS SMARTPHONES IN A DIFFERENTIAL APPROACH.....	115

<i>R. Stauffer¹, R. Hohensinn^{1,3}, I. Herrera Pinzón¹, G. Moeller¹, Y. Pan¹, G. Klopotek¹, B. Soja¹, E. Brockmann², M. Rothacher¹</i>	
MODELING ATMOSPHERIC EFFECTS IN MICROWAVE SATELLITE SIGNALS	117
<i>E. Shehaj¹, A. Geiger¹, G. Moeller¹, O. Frey², L. Miotti¹, B. Soja¹, S. D'Aronco¹, J.D. Wegner^{1,3}, M. Rothacher¹</i>	
USING ATMOSPHERIC OBSERVATIONS OF MICROWAVE SATELLITE SIGNALS TO IMPROVE THE METEOROLOGICAL PRODUCTS.....	120
<i>E. Shehaj¹, A. Geiger¹, G. Moeller¹, S. Leroy², K. Cahoy³, B. Soja¹, L. Crocetti¹, M. Rothacher¹</i>	
MACHINE LEARNING-BASED PREDICTION OF ALPINE FOEHN EVENTS USING GNSS TROPOSPHERE PRODUCTS: FIRST RESULTS FOR ALTDORF, SWITZERLAND.....	122
<i>M. Aichinger-Rosenberger^{1,2}, E. Brockmann^{3,4}, L. Crocetti¹, B. Soja¹, G. Moeller¹</i>	
MPG-NET: A LOW-COST, MULTI-PURPOSE GNSS CO-LOCATION STATION NETWORK FOR ENVIRONMENTAL MONITORING	125
<i>M. Aichinger-Rosenberger^{1,2}, A. Wolf¹, C. Senn¹, R. Hohensinn^{1,3}, M.F. Glaner⁴, G. Moeller¹, B. Soja¹, M. Rothacher¹</i>	
CROWDSOURCING GNSS OBSERVATIONS FOR ATMOSPHERIC MONITORING	128
<i>G. Klopotek¹, Y. Pan¹, L. Crocetti¹, M. Awadaljeed¹, M. Rothacher¹, T. Sturn², R. Weinacker², L. See², S. Fritz², I. McCallum², V. Navarro³, B. Soja¹</i>	
REFRACTION EFFECTS ON LONG-RANGE TERRESTRIAL LASER SCANNING.....	131
<i>A. Wieser¹, E. Friedli^{1,2}</i>	
DENSE DISPLACEMENT VECTOR FIELDS FROM POINT CLOUDS	133
<i>A. Wieser¹, Z. Gojcic^{1,2}</i>	
CONTRIBUTIONS OF SWISSTOPO TO GNSS METEOROLOGY.....	135
<i>S. Lutz¹, D. Ineichen¹, S. Schaer¹, E. Brockmann¹</i>	
SWISS POSITIONING SERVICE (SWIPOS).....	138
<i>A. Villiger¹, C. Biberstein-Pedroni¹, HP. Christ¹, G. Jeiziner¹</i>	
DEEP TEMPORAL SEMI-SUPERVISED ONE-CLASS CLASSIFICATION FOR GNSS RADIO FREQUENCY INTERFERENCE DETECTION	140
<i>V. Ivanov¹, M. Scaramuzza², R.C. Wilson¹</i>	
GNSS INTERFERENCE DETECTION AND GEOLOCALIZATION FOR AVIATION APPLICATIONS.....	141
<i>H. Nasser¹, G. Berz¹, M. Gómez², A. de la Fuente², J. Fidalgo², W. Li², M. Pattinson², P. Truffer³, M. Troller³</i>	
NAVIGATION AND GUIDANCE OF PLATFORMS	143
<i>J.-C. Charlaix¹, M. Khaghani¹, G. Laupre¹, P. Longobardi¹, F. Nex¹, J. Skaloud¹</i>	
NAVIGATION SENSOR NOISE MODELS AND SENSORS CALIBRATION	144
<i>J.-C. Charlaix¹, M. Khaghani¹, G. Laupre¹, P. Longobardi¹, F. Nex¹, J. Skaloud¹</i>	
ESTIMATION METHODS FOR KINEMATIC POSITIONING	145
<i>A. Brun¹, D.A. Cucci¹, K. Mouzakidou¹, J. Skaloud¹</i>	
FUSION BETWEEN NAVIGATION AND OPTICAL SENSORS FOR PRECISE MAPPING.....	146
<i>E. Cledat¹, D.A. Cucci¹, K. Joseph-Paul¹, L.V. Jospin¹, J. Skaloud¹</i>	
REFERENCES.....	147
TABLE OF CONTENTS	149
BIBLIOGRAPHY COMMISSION 4.....	149

1 Reference Frames

Satellite Laser Ranging at Zimmerwald

T. Schildknecht¹, L. Kleint¹, P. Lauber¹, M. Prohaska¹, A. Jäggi¹

¹ *Astronomical Institute, University of Bern*

The Zimmerwald SLR station is part of the global tracking network of the International Laser Ranging (ILRS) and is providing measurements on a 24/7 basis. The SLR system is continuously being improved in terms of measurement accuracy and efficiency. Thanks to the versatility of the Zimmerwald Laser Ranging and Astrometry Telescope (ZIMLAT), laser ranging to space debris using a new high-power laser system will be possible in near future.

STANDARD ILRS SLR SERVICES

The Zimmerwald SLR station is part of the global tracking network of the International Laser Ranging (ILRS) and observes the ILRS satellites according to ILRS priorities on a 24/7 basis. Zimmerwald continues to be the most productive SLR station of the ILRS in the northern hemisphere second to Yaragadee only, a station in Australia. Current developments are focusing on the improvement of the accuracy of the delivered range measurements, both, in terms of achieving smaller observation rms, and reducing the biases. The latter includes the improvement of the calibration measurements.

Evaluations for replacing the current 100Hz laser system with a KHz laser are under way. At the same time, we should be able to shorten the pulse width of currently ~60ps by a factor of 10.

STANDARD ILRS SLR SERVICES

The Zimmerwald SLR station of the Swiss Optical Ground Station and Geodynamics observatory Zimmerwald (SwissOGS) is part of the global tracking network of the International Laser Ranging Service (ILRS) and observes the SLR satellites according to ILRS priorities on a 24/7 basis. Zimmerwald continues to be the most productive SLR station in the northern hemisphere (Figure 1.1) ((and provides a substantial contribution to the ILRS products used for geodesy and Earth sciences. The main science products to which the station is significantly contributing are the International Terrestrial Reference Frame (ITRF), a central reference point to tie the Swiss geodetic network to the ITRF, the observation of the center of mass of the system Earth, and the spatial and temporal variations of the Earth's long-wavelength gravity field. All these efforts are part of the larger context of the Global Geodetic Observing System (GGOS) of the International Association of Geodesy (IAG).

The productivity of the Zimmerwald SLR station, measured by the number of “normal points”, is excellent. Normal points are a standard ILRS product generated by averaging single-shot range data over short time intervals. Obviously, the number of individual measurements used in this procedure directly influence the precision of the normal point. Normal points from Zimmerwald contain up to 30% fewer single-shot measurements than from the best stations in this respect. This is largely due to the 100Hz repetition rate of our current laser, which is one order of magnitude lower than for the top SLR lasers stations in the ILRS. One goal of our future upgrades is the kHz domain.



Figure 1.1: Zimmerwald Satellite Laser Ranging (SLR) nighttime tracking.

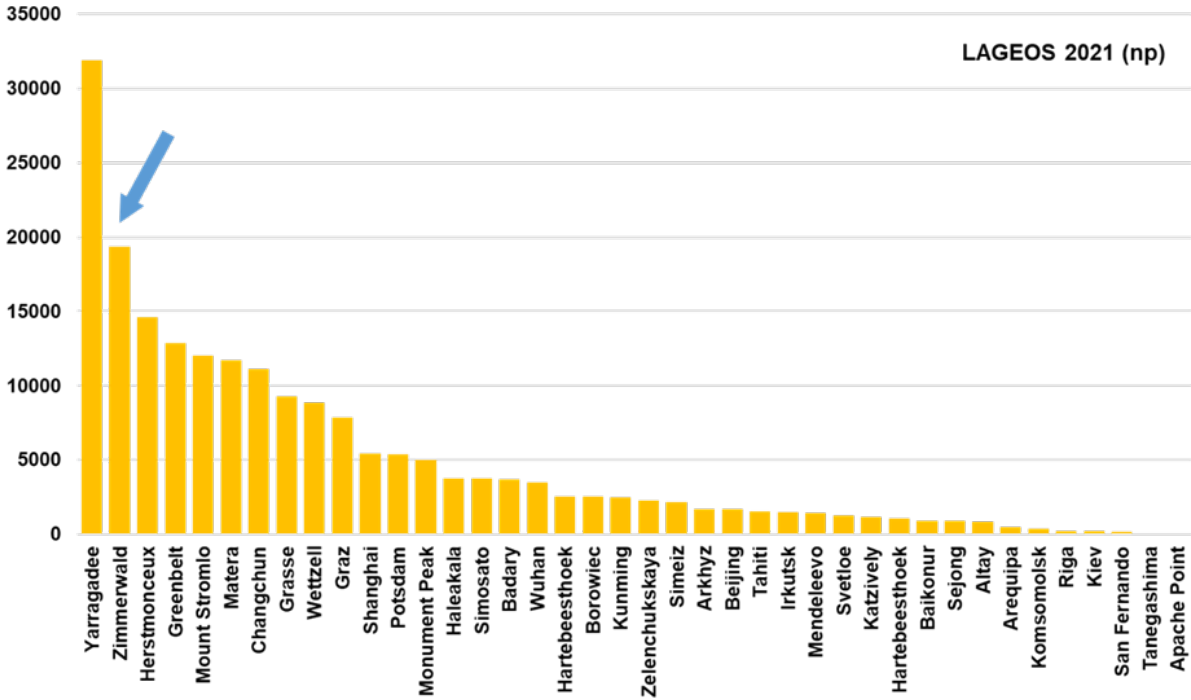


Figure 1.2: Number of SLR normal points in the ILRS for the satellite LAGEOS collected in the period from February 1, 2021 to January 31, 2022.

In order to achieve the GGOS science goals, which are asking for a long-term station coordinate stability of 1 mm and for a velocity stability of 0.1 mm/y, the accuracy and amount of SLR measurements need to be significantly improved. The current SLR system in Zimmerwald, produces range data with an accuracy of about 12 mm RMS, while the best state-of-the-art stations provide measurements with about 5 mm RMS. This performance cannot be improved further as it is entirely limited by the pulse width of 60 ps of the current laser system (60 ps correspond to 9 mm two-way range). We therefore procured a new laser system, which should allow us to improve the single observation range accuracy from 1.2 cm to 2 mm and at the same time to increase the number of measurements by a factor of 10. The new laser system has a repetition rate of 1 kHz and a pulse width of 8 ps. This laser will be installed on the tube of the ZIMLAT SLR telescope, such that the existing system located in the Coudé room may still be used in parallel to avoid a longer downtime period for the Zimmerwald SLR station.

Station Upgrades

In 2022 the existing all-sky dome of the SLR system was replaced by a larger slit-type dome. This refurbishment should substantially reduce the thermal stress of the telescope during daytime observations. This in turn will allow improving the efficiency of the automated blind tracking observations during daytime. At the same time, the air conditioning system in the laser room and the laser cooling system were replaced to provide a stable environment for the laser and the receiver electronics. As a consequence, the SLR station was not operational from March 2022 onward.

Space Debris Laser Ranging

In the area of space safety, the Zimmerwald observatory has a world-leading position in providing passive optical observation data on the current space debris environment. Orbits of objects in Low-Earth orbits (LEO) are mostly determined using radar measurements. Laser ranging is a promising technique to improve the accuracy of orbits of space debris objects in LEO by about one order of magnitude compared to traditional radar techniques. Space debris objects are not carrying retroreflectors, which prevents the use of conventional SLR systems for tracking of debris objects with cross-sections smaller than a few 10 square meters. A new high-power laser system was thus procured and the installation started in 2022. The system shall allow tracking of debris objects with diameter as small as 1 meter in LEO.

CODE Contributions to the IGS

R. Dach¹, S. Schaer^{1,2}, D. Arnold¹, M. Kalarus¹, L. Prange¹, P. Stebler¹, D. Sidorov^{1,3}, A. Villiger^{1,4}, A. Jäggi¹

¹ Astronomical Institute, University of Bern

² Federal Office of Topography swisstopo

³ now with Leica Geosystems

⁴ now with Federal Office of Topography swisstopo

The consortium Center of Orbit Determination in Europe (CODE) consists of four institutions:

- Astronomical Institute of University Bern (AIUB), Switzerland
- Federal Office of Topography swisstopo, Switzerland
- Federal Agency of Cartography and Geodesy (BKG), Germany
- Ingenieurinstitut für Astronomische und Physikalische Geodäsie at Technische Universität München (IAPG/TUM), Germany

CODE is an Analysis Center (AC) of the International GNSS Service (IGS, Johnston et al., 2017) generating operationally series of Global Navigation Satellite System (GNSS) products since 1992. Since 2003, the contributions from CODE to the IGS are based on a rigorously combined analysis of GPS and GLONASS measurements in the legacy product chains. Since September 2019 Galileo was included in the rapid and ultra-rapid processes. The final legacy processing chain finally contains Galileo since end of November 2022 based on the station network shown in Figure 1.3. The scheduling of the various processes is summarized in Figure 1.4.

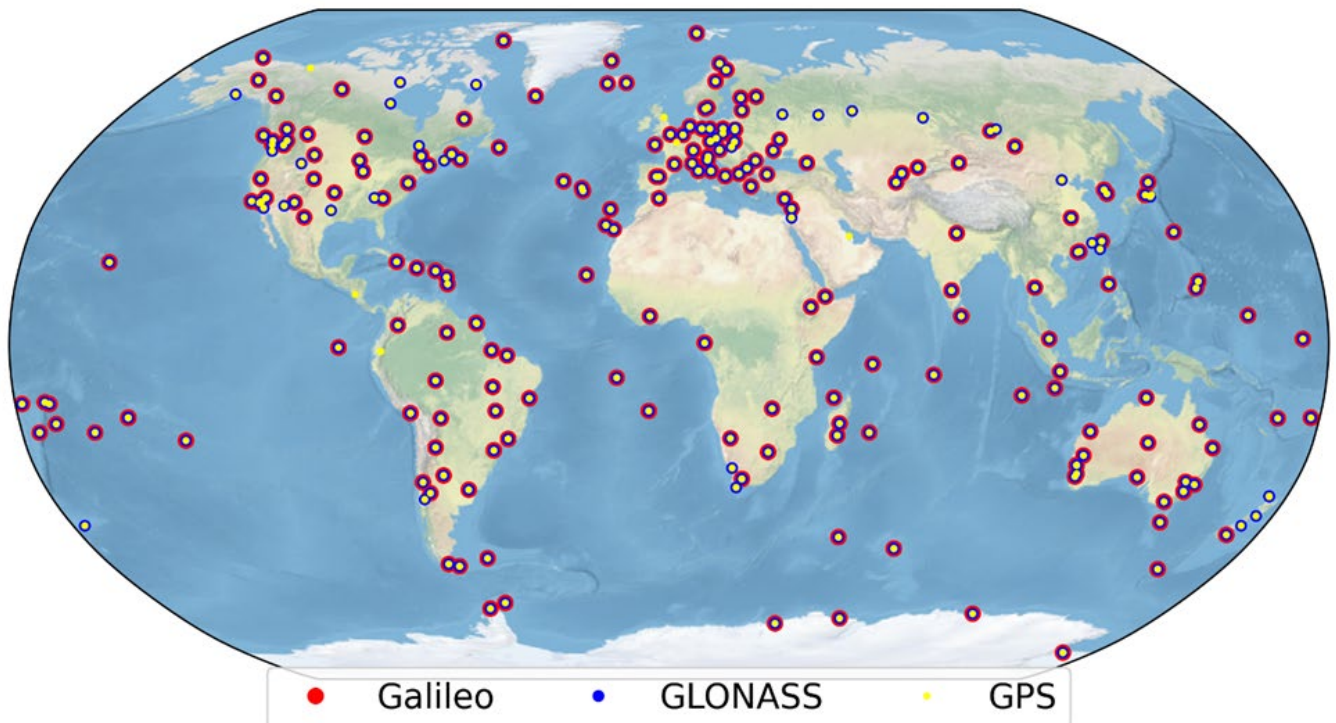


Figure 1.3: IGS network processed at CODE (status of December 2022).

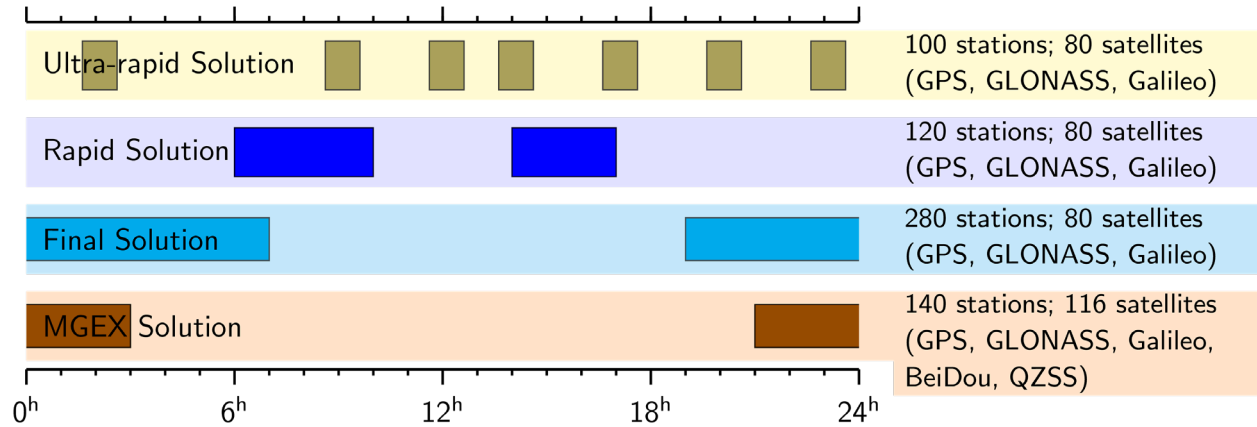


Figure 1.4: Scheduling of the various IGS-related processing at CODE analysis center.

The major products are GNSS orbits, Earth orientation parameters (EOPs), receiver station coordinates, model parameters describing the troposphere and global ionosphere maps, phase-consistent satellite and receiver clock corrections (up to a time resolution of 5 seconds), and pseudo absolute code observable specific bias (OSB, Villiger et al., 2019); related phase biases allow the ambiguity resolution in the PPP approach (Schaer et al., 2021). A complete list of all our products is available on our ftp server (http://ftp.aiub.unibe.ch/AIUB_AFTP.TXT).

We aim to deliver the best possible solutions to the IGS leading to a steady development of the processing routines and used software. Therefore, we use the development version of the Bernese GNSS Software (BSW, Dach et al., 2015), which is further developed and maintained at our institute. Because of this, we can benefit from the latest implementations and adapt the software in order to support the best possible processing strategies. A complete overview of the development steps during the covered reporting period can be obtained in the IGS technical reports (Dach et al. 2019, 2020, 2021, 2022, and 2023). The following improvements are a brief selection of the most important ones:

2018	<ul style="list-style-type: none"> • Activate a dedicated orbit model for BDS and QZSS satellites in orbit normal mode (Prange et al. 2020a) • Rapid clock product extended from GPS only to GPS/GLONASS
2019	<ul style="list-style-type: none"> • Switch to satellite-specific empirical models; activate the extended thermal radiation modelling for Galileo satellites in the MGEX solution (Sidorov et al., 2020) • Galileo activated in rapid and ultra-rapid processing including the ambiguity resolution, allowing in particular the ambiguity resolution in PPP when introducing the related phase bias products
2020	<ul style="list-style-type: none"> • Switch from FES2004 to FES2014b for station deformation corrections and gravitational effect on the satellite orbits. • Switch reference frame to IGB14 for all product lines. • Stop the 1-day solution (with the ID COF) and reactivate the 3-day solution as the primary and only operational final contribution to the IGS final series. • Reschedule the stochastic pulses to orbit midnight instead of noon/midnight GPS time. • Stop using VMF in the rapid and ultra-rapid processing because of announced rescheduling of the provision for the VMF-corrections
2021	<ul style="list-style-type: none"> • Report satellite attitude in ATT-ORBEX format in the final and MGEX solution series • Activation of BeiDou 3 constellation in MGEX solution series • Change of troposphere model (GMF1 to GPT3/GMF3 in the rapid and ultra-rapid series; VMF1 to VMF3 in the final and MGEX series)
2022	<ul style="list-style-type: none"> • Switch reference frame to IGS20 for all product lines together with a number of model changes • Include Galileo also to the final processing chain • Switch to long product filenames for published result files

As a contribution to the ITRF2020 CODE has consistently reprocessed the IGS data in order to provide:

	Orbits, ERPs, station coordinates	Clock corrections (30 s), code and phase biases	Ultra-high rate clock corrections (5 s)
GPS	since 1994	since 2000	since 2003
GLONASS	since 2002	since 2008	since 2012
Galileo	since 2013	since 2014	-- ^a

^a Product not needed because the 30 s satellite clock corrections can be linearly interpolated.

Together with the clock corrections also the phase biases are provided allowing for a PPP ambiguity resolution according to Schaer et al. (2021). In the frame of the reprocessing, consistently between all space geodetic techniques, the high-frequency pole model (from IERS2010 to Desai and Sibois, 2016) and the mean pole model (from IERS2010 to IERS2010, version 1.2.0) were changed along with a number of other model changes that are discussed in Dach et al., 2020.

In addition to our operational running legacy processing lines CODE is contributing to the MGEX pilot project of the IGS (MGEX: multi-GNSS extension, Montenbruck et al., 2017). It is intended to incorporate the new satellite systems and signals into the operational product series of the IGS. In this context the above mentioned inclusion of Galileo in the recent reprocessing and final processing was well prepared. The current status of CODE's contribution to MGEX is reported in Prange et al., 2020b. One of the recent achievements was the inclusion of the BeiDou 3 constellation in March 2021. The quality of the related products is assessed in Steigenberger et al., 2022. The development of the extension of the solution is visible in Figure 1.5 showing the processed satellites at CODE in all our IGS and MGEX contributions.

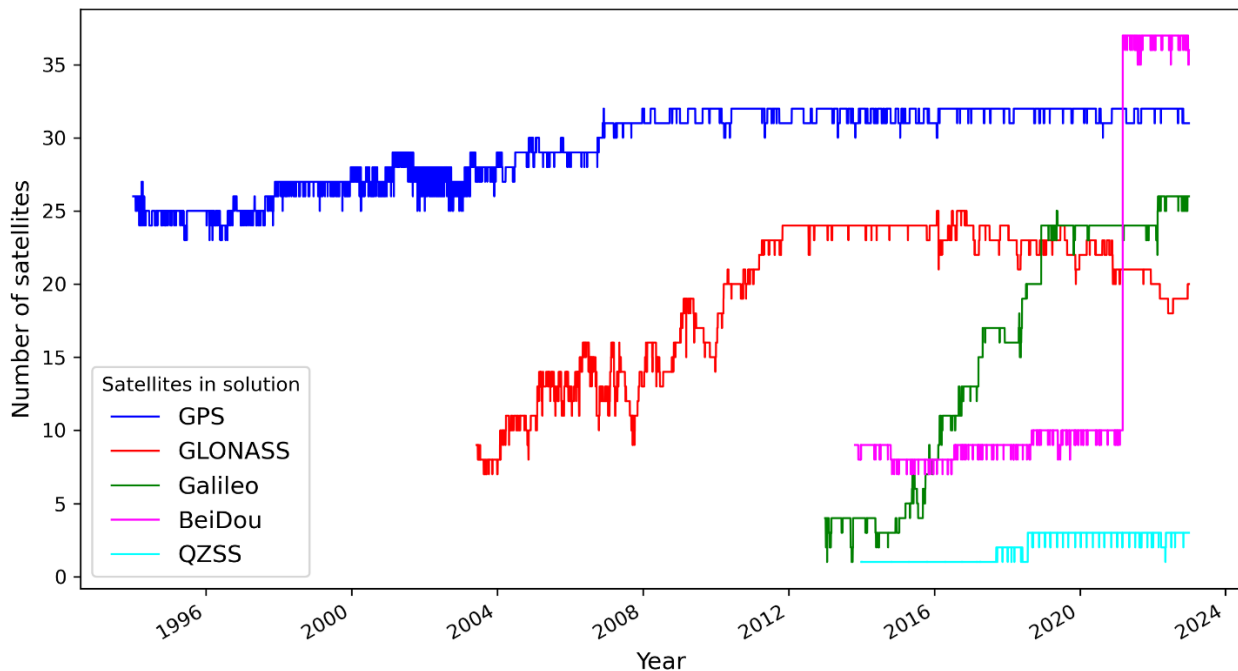


Figure 1.5: Cumulative diagram of the processed satellites at CODE: Number of satellites which have been considered and delivered in the products for IGS final solutions and the MGEX project.

EUREF Activities at CODE

S. Schaer^{1,2}, D. Arnold¹, R. Dach¹, L. Prange¹, D. Sidorov¹, P. Stebler¹, A. Sušnik^{1,3}, A. Villiger¹, A. Jäggi¹

¹*Astronomical Institute, University of Bern*

²*Federal Office of Topography swisstopo*

³*now with Leica Geosystems*

⁴*now with Federal Office of Topography swisstopo*

EUREF is an integrated component of the Subcommittee 1.3, Regional Reference Frames, of the IAG (International Association of Geodesy). A key component is the EUREF Permanent Network (EPN, Bruyninx et al., 2019, Lidberg et al. 2021), consisting of about 400 GNSS tracking stations (status March 2023). The data are analyzed in a distributed processing scheme between 17 Analysis Centers (ACs). It is worth mentioning that 15 out of 17 are using the Bernese GNSS Software (Dach et al., 2015) from version 5.2 up to the current development version at AIUB.

CODE, the Center for Orbit Determination in Europe, is one of the EUREF AC. It is a joint venture between the Astronomical Institute of the University of Bern (AIUB, Switzerland), the Swiss Federal Office of Topography (swisstopo, Wabern, Switzerland), the Federal Agency for Cartography and Geodesy (BKG, Frankfurt am Main, Germany), and the Ingenieurinstitut für Astronomische und Physikalische Geodäsie at Technische Universität München (IAPG, TUM, Munich, Germany).

CODE processes parts of the EPN network operationally using the development version of the Bernese GNSS Software package and delivers the results to the combination center. The weekly station coordinates are generated using a combined GPS/GLONASS solution. The precise orbits, used during the processing steps, are taken from CODE which are also submitted to the IGS for the final combination products. The contribution contains up to 58 stations (49 GPS/GLONASS and 9 GPS-only) as shown in Figure 1.6. The EPN network has its focus on Europe; therefore, most stations are located on the western part of the Eurasian plate. End of 2022, about 38 sites are submitted to the EPN via the SINEX format (6 GPS-only, 9 GPS-GLO, 23 GPS-GLO-GAL).

A complete redesign of the EPN contribution was developed in November 2022 (GPS week 2238) closely aligned to the RNX2SNX processing example, which was developed and provided with the latest version 5.4 of the Bernese GNSS Software package in autumn 2022. In agreement with all EPN ACs the solution is aligned to the ITRF2020/IGS20 reference frame together with the related model changes. Since the related antenna model contains also receiver antenna corrections for Galileo, CODE considers now the three systems GPS, GLONASS, and Galileo for its EPN solution. In analogy to the IGS the EPN products also use of long filenames.

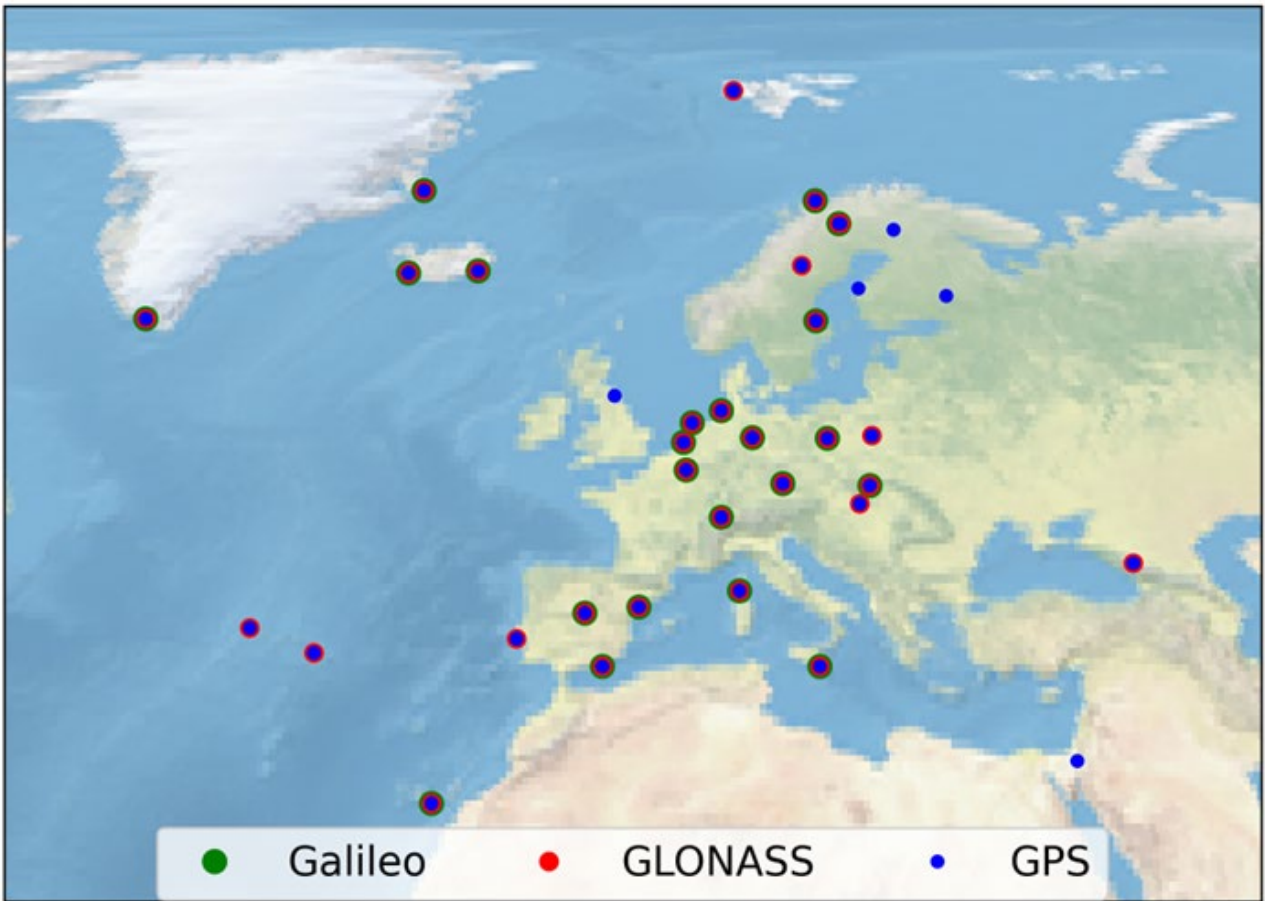


Figure 1.6: GNSS network which is processed at AIUB and contributed to the EPN network.

The Swiss Optical Ground Station and Geodynamics Observatory Zimmerwald

L. Kleint¹, T. Schildknecht¹, P. Lauber¹, M. Prohaska¹, A. Jäggi¹

¹ Astronomical Institute, University of Bern

We will present a short summary of the main activities and recent achievements of the Zimmerwald observatory.

The Astronomical Institute of the University of Bern (AIUB) operates the Swiss Optical Ground Station and Geodynamics Observatory Zimmerwald (SwissOGS). The observatory consists of five domes with astronomical telescopes and is among the leading observatories in satellite laser ranging (SLR) and space debris observations. ZIMLAT is a 1 m telescope, used for SLR and observations of light curves of space debris. Its dome and cooling system were newly upgraded in 2022. ZimMAIN is an 80 cm telescope used for surveys, light curves, and spectroscopy of space debris. ZimTWIN consists of two 40 cm telescopes on the same mount that can either be used to double the observable field of view, or to observe the same object with different filters, for example for color photometry. ZimSMART is a 20 cm telescope, which is part of the SMARTnet network, that focuses on a global monitoring of resident space objects. The fifth dome houses temporary experiments and developments, for example currently a new telescope that is being developed and tested to be deployed within SMARTnet in South America.

Satellite Laser Ranging (SLR)

In 1998, the International Laser Ranging (ILRS) was founded. The Zimmerwald SLR station has always been an integral part of this service. It is operated jointly by the Astronomical Institute of the University of Bern (AIUB) and the Swiss Federal Office of Topography (swisstopo) and supported by the Swiss Academy of Sciences (SCNAT). In 2022, a major upgrade of the infrastructure was carried out. The dome was replaced with a slit-type dome from Baader that helps to minimize the heat load of the telescope during daytime SLR observations (Figure 1.7). This included major building works and infrastructure upgrades, such as the whole laser cooling system. In addition, the installation of a new laser was started in 2022, which will allow us to measure space debris more efficiently. The new laser operates in the infrared, which is beneficial due to the lower atmospheric attenuation, and it can reach a power of 40 W.



Figure 1.7: Installation of the new 6.15 m. slit-type dome for ZIMLAT.

ZimTWIN – Observations of space debris

Survey

The Zimmerwald Twin Wide-field Instruments (ZimTWIN) consists of two ASA 16 inch f2.4 primary focus telescopes on the same mount, which were installed in September 2017. A field of View (FoV) of 2.14×2.14 degree² is available in the primary focus. By adjusting the relative pointing of the tubes, a contiguous FoV of 4.28×2.14 degree², optimal for space debris and Near Earth Objects (NEO) surveys, can be obtained. Currently, the ZimTWIN is used for surveys and for student projects, such as a master thesis on color photometry.

Automatic Tilt Control

The two ZimTWIN telescopes are located on the same mount, meaning that a manual alignment is required to either align them, or to offpoint one of the telescopes to increase the field of view. Because this is a cumbersome task, an automatic tilt-control has been developed, which can position the second telescope via motors (Figure 1.8). For the prototype design, ± 5 mm position change at each axis are possible and the total tilt between two axes should not exceed 5 mm. For ZimTWIN, a similar design is foreseen. The encoder precision per axis is $0.1 \mu\text{m}$. The system is currently in the testing phase.

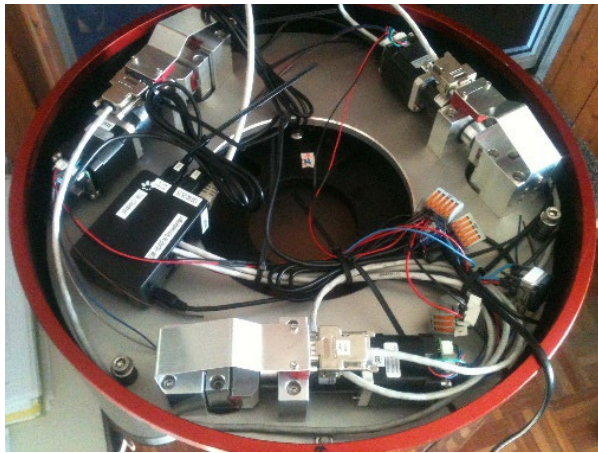


Figure 1.8: Prototype of the tilt control mechanism mounted in the mirror cell of a 40 cm telescope. The basic mechanism for ZimTWIN will be similar.

ZIMLAT – Optical Observations

During nighttime, the ZIMLAT telescope time is shared between SLR and CCD observations. The switch between observing modes is completely automatic, only photometric observations are performed manually. For CCD observations, the main targets of ZIMLAT are the faint high area to mass ratio (HAMR) space debris objects of the AIUB internal catalog. ZIMLAT is also used for space debris characterization. Several hours per night are dedicated to the acquisition of light curves. The AIUB light curve database contains more than 6187 light curves for more than 624 objects.

ZimMAIN and ZimSMART – Observations of space debris

The main purpose of the ZimSMART telescope is the discovery of space debris in the geostationary Earth orbit (GEO) region using survey observations. Its aperture enables the observation of 1 meter-size objects at GEO altitude (cut off at 16 magnitude) with an exposure time of only 8 seconds. These observations are used to build up and maintain the AIUB internal GEO catalog of space debris. ZimSMART produces ~1800 images and ~400 tracklets over 8 hours of observation time (based on March 2023 data). Technical improvements and bug-fixes of ZimSMART have led to a very stable operation.

The Zimmerwald Multiple Applications Instrument (ZimMAIN) is an 80 cm aperture Ritchey-Chrétien telescope with 0.64×0.64 degree² FoV. The telescope was installed in February 2018. The instrument is currently used for follow-up observations of the faint objects of AIUB's catalog (18-19 magnitude) and the follow-up of faint fragments from recent breakup events in GEO and highly elliptical orbits (HEO) The telescope acquires an average of ~2200 images over 9.5 hours of observation time (based on October 2018 data). ZimMAIN is also used for spectroscopic measurements of space debris in collaboration with colleagues from the Comenius University Bratislava. These measurements allow us to derive the material of space debris.

ZimNET – Status of collaboration with DLR

The Zimmerwald Network Telescope (ZimNET) is part of the SMARTnet project, a joint project between the German Aerospace Center (DLR) and the AIUB. The first ZimNET telescope (SMART-01) was deployed in South Africa and is operational since April 2017, with a service visit in 2022. The second (SMART-02) was deployed in Australia and is operational since 2019. The third ZimNET telescope is currently undergoing testing at SwissOGS and is planned to be shipped to South America in 2024. All ZimNET telescopes were assembled, tested, and validated at the SwissOGS. The ZimNET telescopes consist of two tubes on the same mount, one Dall-Kirkham (50 cm aperture) and one Newtonian 20 cm (SMART-01) or 25 cm aperture (SMART-02 and SMART-03), used for the follow-up and the discovery of space debris.

Software development

The collaboration has developed a new control software, SMARTies, which is open-source and programmed in Python. AIUB has in addition developed so-called "device-controllers", which are the interfaces between any hardware device, including mounts and optics, and SMARTies. Their design is modular and highly flexible and it makes adding a new element (e.g. focuser, camera, filter wheel) much simpler. The software upgrade is a major project, which will soon replace the current ageing software that includes difficult to understand code and discontinuation of support by companies. Upon the completion of the software development and testing, the new software will be used by all telescopes at SwissOGS.

Global Navigation Satellite Systems (GNSS)

GNSS receivers are operated at Zimmerwald by swisstopo. Two permanent GNSS receivers mounted on 9-meter masts provide data to the data centers of the International GNSS Service (IGS), to the EUREF, and to the Automated GNSS Network for Switzerland (AGNES) of swisstopo.

Unifying the three Pillars of Geodesy using Space Ties

A. Jäggi¹, E. Calero¹, L. Geisser¹, C. Kobel¹, D. Arnold¹, G. Bury¹, R. Dach¹, T. Grombein¹, M. Kalarus¹, X. Mao¹, S. Schaer¹, A. Villiger¹

¹ Astronomical Institute, University of Bern

Terrestrial Reference Frames (TRFs) are the basis to which all positions on the Earth's surface and all satellite orbits in the near Earth space have to refer to. The changes in the Earth's shape, rotation, and gravity field, the so-called "three pillars" of geodesy, provide the conceptual and observational basis for the TRFs. For today's TRF realizations, four space geodetic techniques are combined and linked by co-location sites on the Earth's surface ("Earth's shape") and by common Earth orientation parameters ("Earth rotation"). The third pillar ("Earth's gravity field") is today only contributing to the TRF determination via its associated center-of-mass. The project SPACE TIE shall pave the way to unify the "three pillars" of Geodesy in future TRF realizations by using the two satellite geodetic techniques Global Navigation Satellite Systems (GNSS) and Satellite Laser Ranging (SLR) and connecting them by co-location sites in space. These so-called space ties shall be realized on satellites of the currently existing space infrastructure, as well as on satellites due for launch in the near future. To maximize the sensitivity to the Earth's gravity field, the ultra-precise inter-satellite ranging between the dedicated GRACE/GRACE-FO satellites is envisaged to be added as a third satellite geodetic technique (see Figure 1.9).

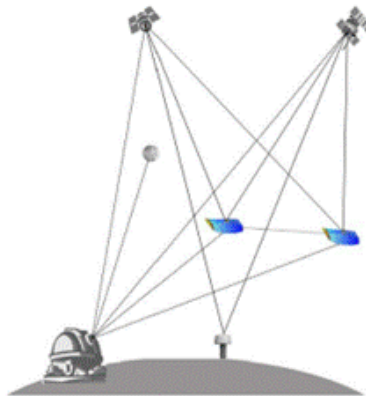


Figure 1.9: General concept of the envisaged combinations within the Space Tie project.

The Space Tie project is structured in four work packages:

The goals of WP 1 are to exploit un-differenced ambiguity resolution (Schaer et al., 2021), to set-up rigorous multi-GNSS solutions based on un-differenced GNSS observations (Calero et al., 2023), and to exploit the disclosed Galileo satellite antenna patterns to the determination of the terrestrial scale (Villiger et al., 2020). As GNSS microwave signals are the key to link all co-location platforms in SPACE TIE, WP 1 provides the foundation for all other WPs. Further activities are planned to focus on the determination of geophysical parameters, e.g., low-degree SH coefficients of the Earth's gravity field, in global GNSS solutions.

The goals of WP 2 are to exploit dynamic LEO POD (Mao et al., 2021) in order to exploit in a next step rigorously combined GNSS-LEO solutions including un-differenced ambiguity resolution. As LEO satellites are the key to access the Earth's time-variable gravity field, WP 2 provides the foundations for the following WPs. Further activities are

planned to focus on the determination of geophysical parameters, e.g. the geocenter and the terrestrial scale, in a combined GNSS-LEO using ambiguity resolution.

The goals of WP 3 are to exploit SLR full-rate data for a homogeneous formation of SLR normal points (Geisser et al., 2023b), to further reduce SLR systematic errors (Strugarek et al., 2022), to analyze geophysical parameters from SLR normal points (Geisser et al., 2023a), and to explore SLR data to LEO satellites in preparation of the envisaged GNSS-SLR co-locations on-board GNSS and LEO satellites (Strugarek et al., 2021).

The goals of WP 4 are to assess the sensitivity of the Earth's time-variable gravity field to dynamic LEO POD (Peter et al., 2022), to exploit the contribution of the GPS tracking of multiple LEO satellites to derive the Earth's time-variable gravity field (Grombein et al., 2022) as a preparation to bring together the results from WPs 1-3 to exploit the global constraint given by the Earth's gravity field. Ultimately, the K-Band inter-satellite ranging shall be added to derive a fully consistent time-variable gravity field together with the Earth's geometry and rotation.

The SPACE TIE project is receiving funding from the European Research Council (ERC) under grant no. 817919.

Differencing Strategies for SLR Observations

I. Herrera Pinzón^{1,2}, M. Rothacher¹

¹ Institute of Geodesy and Photogrammetry, ETH Zurich

² now with Astronomical Institute, University of Bern

Co-located SLR telescopes connected by a local tie, controlled by a common timing system and affected by the same atmosphere, allow the study of the size and stability of instrumental biases, the quality of the local ties, and the investigation of new processing strategies, such as single- and double-differences of SLR observations. Forming single- or double-differences provides a strategic approach to mitigate satellite- (by forming single-differences) and station-specific (by forming in addition double-differences) error sources and attain high-accuracy measurements of the short baseline. These methods enable the assessment of existing biases and the estimation of precise relative coordinates between neighboring telescopes, providing an important approach for validating local ties.

The acquisition of simultaneous SLR observations poses a practical challenge, as obtaining double-differences is practically unfeasible. While observing a common target simultaneously with both telescopes is feasible and can yield single-differences, double-differences - which require observing two satellites with both telescopes at the same time - are impossible to obtain. In light of this, the need arises to either interpolate normal points at common epochs for both satellites, or to employ quasi-simultaneous observations, wherein a time window between the observations is allowed.

Therefore, the fundamental tool to build single- and double-differences is the concept of *quasi-simultaneous* observations. We have developed an innovative approach to building differences that leverages a short SLR baseline and a custom quasi-simultaneity strategy. In practice, two observations are considered quasi-simultaneous if they lie within a specified time window. This is, range $\rho^{k_1}(t_i)$ from telescope 1 to satellite k observed at time t_i and range $\rho^{l_2}(t_j)$ from telescope 2 to satellite l at time t_j are considered quasi-simultaneous if $\|t_j - t_i\| \leq \delta t$, where δt is the so-called quasi-simultaneity, a fixed value. If t_j and t_i satisfy this condition, they are considered *quasi-simultaneous epochs*. The value of the quasi-simultaneity threshold, δt , is dependent on the quality and dynamics of the satellite orbits. Through empirical analysis, we have determined that a value of 30 minutes provides optimal results (Figure 1.10). This approach enables us to construct both, single- and double-differences, using linearised observation equations derived from the original ranges. Unlike other methods, we do not need to interpolate either the normal points or the original ranges. Instead, we rely on a continuous representation of satellite orbits, namely dynamic orbits.

The differencing methods were validated with data from the SLR short baseline at the Geodetic Observatory Wettzell, realised by the Wettzell Laser Ranging System (WLRS) and the Satellite Observing System Wettzell (SOS-W). The horizontal distance between these systems is ca. 58 m, and the difference in height is about 2.3 m. The local tie vector between the two telescopes has been determined by terrestrial measurements and is continuously compared to the SLR-derived solutions. For the scope of this work, we restricted our study to only LAGEOS and GLONASS observations, and we analysed the behaviour of the SLR differences using the available ILRS data in the 2-year time interval from 01.01.2018 to 31.12.2019. Selecting those days, where WLRS and SOS-W tracked the same satellites, yielded 402 potential sessions with data, from which 172 and 255 sessions contain sufficient GLONASS and LAGEOS data, respectively, to obtain differences.

The ENU estimates obtained with the differencing methods were subtracted from the local tie, so that the values depict the difference between the SLR estimates and the terrestrial measurements (see Table 1.1). A tendency of lower values of the formal errors in the north component is seen in the two approaches, as a result of the south–north orientation of the baseline, and the formal errors of the up component show the largest values.

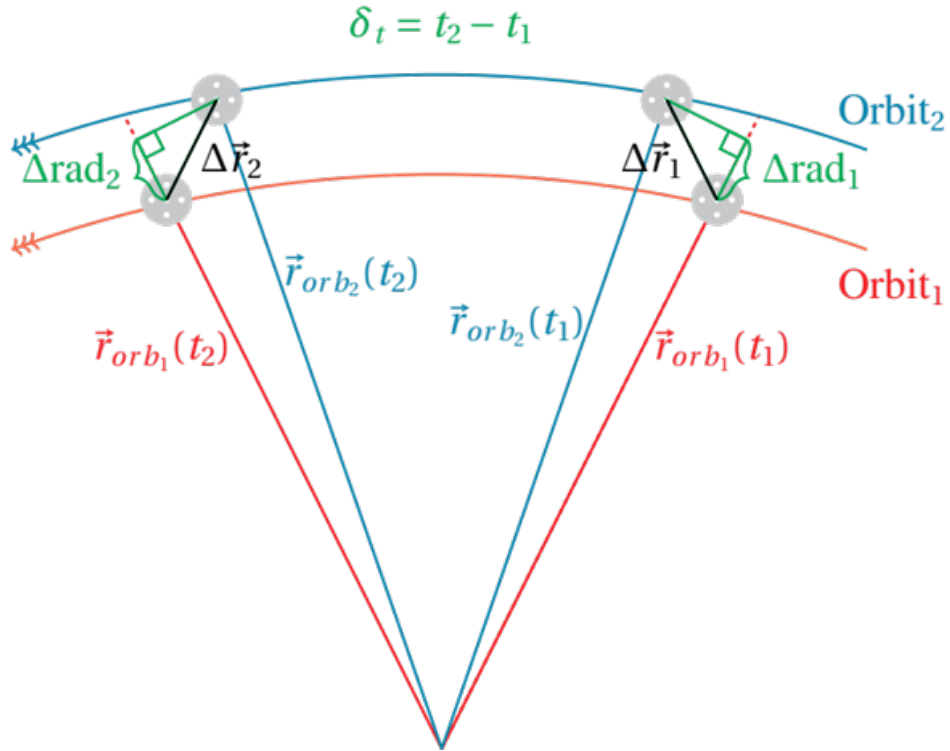


Figure 1.10: Concept for the determination of the best quasi-simultaneous threshold. Using only one satellite, two different orbit solutions (from different processing centres) are compared. First, perfectly simultaneous single-differences between the orbit solutions are formed ($\Delta \mathbf{r}_1$ and $\Delta \mathbf{r}_2$, with their corresponding radial components Δrad_1 and Δrad_2). Then, double-differences with all possible time steps are built, and the RMS value of the double-differences at a certain time step is calculated.

The estimated coordinates based on single-differences show a millimetre agreement with the local tie, with relatively low formal errors. Although these coordinates based on single-differences show a millimetre agreement with the local tie, with relatively low formal errors, possible temporal variations of the instrumental biases are still present in the adjustment and may have an impact on the final solution. To avoid these issues with the determination of instrumental biases and to reduce and mitigate the influence of other error sources, a double-difference weighted least-squares estimation was performed. Moreover, due to the short distance between the two telescopes, the influence of the troposphere on the SLR signal is expected to be the same (apart from the height difference). Therefore, with the use of double-difference observations, the tropospheric delay affecting the original observations is mitigated or strongly reduced. With the elimination of these biases, the estimation of relative coordinates, and therefore the validation of the local ties, is performed clearly more accurately. We found that the agreement of the relative coordinates and the local tie is within 1 mm for each of the ENU components, with corresponding formal errors in the sub-mm domain (Table 1.1).

	Single-Diff.		Double-Diff.	
	Value	σ	Value	σ
E [mm]	0.2	0.7	0.7	0.2
N [mm]	0.8	0.6	-0.9	0.2
U [mm]	-2.1	0.7	-0.6	0.2
GLO_b [mm]	24.0	0.5		
	0.4	0.2		
LAG_b [mm]	14.8	0.8		
	-1.3	0.5		

Table 1.1: Estimated ENU coordinate differences w.r.t the local tie, and instrumental biases estimated with single- and double-differences. All values in millimetres

Rigorous Combination of GNSS and VLBI Observations

I. Herrera Pinzón¹, M. Rothacher¹

¹ *Institute of Geodesy and Photogrammetry, ETH Zurich*

² *now with Astronomical Institute, University of Bern*

We analysed the impact of the use of site coordinate and tropospheric ties between VLBI telescopes and GNSS antennas at co-location sites during the CONT17 campaign. We performed the rigorous estimation of all parameter types common to these two techniques: station coordinates, troposphere zenith delays and gradients, and the full set of Earth Orientation Parameters (EOPs) and their rates, including their full variance-covariance information. The core element of our processing scheme is the combination of the techniques via coordinate and tropospheric ties, the latter being essential especially for the height estimates. By using and evaluating different weighting schemes to obtain a unique set of consistent parameters, we analysed coordinate repeatabilities and the behaviour of the EOPs to discuss the impact of the accuracy and the weighting of the coordinate and troposphere ties on the estimation of geodetic parameters.

The test scenario for this work was the VLBI data of the Continuous VLBI Campaign 2017 (CONT17). To complement the VLBI observations, we selected about 180 GNSS stations of the IGS network covering the same time interval, including all stations co-located with the VLBI telescopes. The integrated processing of the different techniques was done at the observation level, which provides the most rigorous and consistent solution, especially, when all the possible ties are considered. To guarantee the consistency, we performed the processing with a single piece of software capable of handling all the techniques with state-of-the-art models and identical parametrization, this is, a modified version of the Bernese GNSS Software v5.2, capable of handling VLBI data.

For the modelling of the troposphere, we used as a-priori values for the zenith hydrostatic delays and mapping functions the VMF1 model. The use of this type of modelling ensures that the zenith total delay (ZTD) difference between GNSS and VLBI at co-located stations, caused by the height difference, are modelled in advance. The residual wet delays were then estimated as one-hourly piece-wise-linear functions and the tropospheric gradients with daily resolution. An important aspect of the combination is the weighting of each technique, as the quality of the individual techniques varies considerably. This large contrast in the formal errors of each solution supports the need for an adequate inter-technique weighting. Our approach uses coordinate repeatabilities as the base of the weights, since they are directly part of the terrestrial reference frame. For the data of the CONT17 campaign, an optimal weight for the VLBI NEQs of 0.276 compared to GNSS was determined.

Then we compared the relevant estimated parameters to the single-technique solutions, and to a rigorous combination where only coordinate ties were used. First, we looked into the RMS of the coordinate repeatabilities. While the combined results of both techniques may show a decrease in the performance of the rigorous solution with respect to the GNSS solution (top plot of Figure 1.11) when separating the repeatabilities per technique, the benefits of the combined solution are more evident (bottom plot of Figure 1.11). The improvement in the repeatabilities of the GNSS stations in the rigorous solution regarding the GNSS-only solution are 22%, 24%, and 19%, for east, north and height, respectively. Similarly, the improvement regarding the VLBI-only solution amounts to 2% and 14% for the north and height component, respectively. We also observe an improvement in the coordinate repeatabilities when comparing the rigorous solution with coordinate and tropospheric ties with the rigorous solution with only coordinate ties, as expected mainly in height, with the height component of the former improving the performance by 11% (only GNSS stations), 7% (only VLBI stations), and 6% (all stations included).

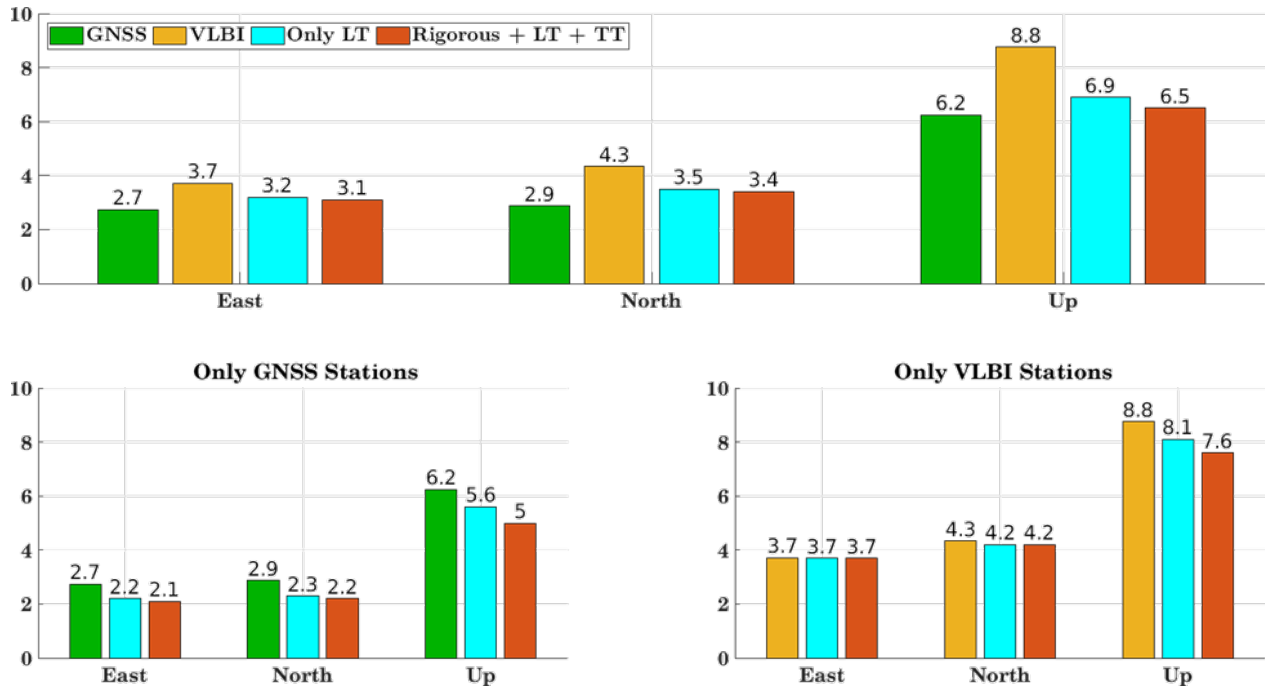


Figure 1.11: RMS of coordinate repeatabilities [mm] for the individual technique solutions, and the combined solutions over 15 days.

Additionally, the RMS of the difference of the EOPs regarding the IGS final solution is investigated, and displayed in Figure 1.12. Once again, the rigorous solution outperforms the single-technique solutions in the polar motion estimates, with an improvement of 35% and 9% regarding the GNSS-only solution, for the X and Y components, respectively, and 25% and 19% regarding the VLBI-only solution. The three solutions agree with the IGS solution at approximately the same level for the UT1-UTC, with the rigorous solution helping to improve the results in the LOD estimate: 48% and 10%, compared to the GNSS-only and VLBI-only solutions, respectively. Polar motion rates show a favourable tendency towards the rigorous solution: 20% and 2% for the rate of the X and Y component, respectively, compared to the GNSS-only solution, and 9% and 20% regarding the VLBI-only solution. The comparison of the rigorous solution with coordinate and tropospheric ties with the rigorous solution with only coordinate ties showed that both approaches yield similar results regarding the LOD estimation, with an improvement of the polar motion of 14% and 5%, for the X and Y components, respectively.

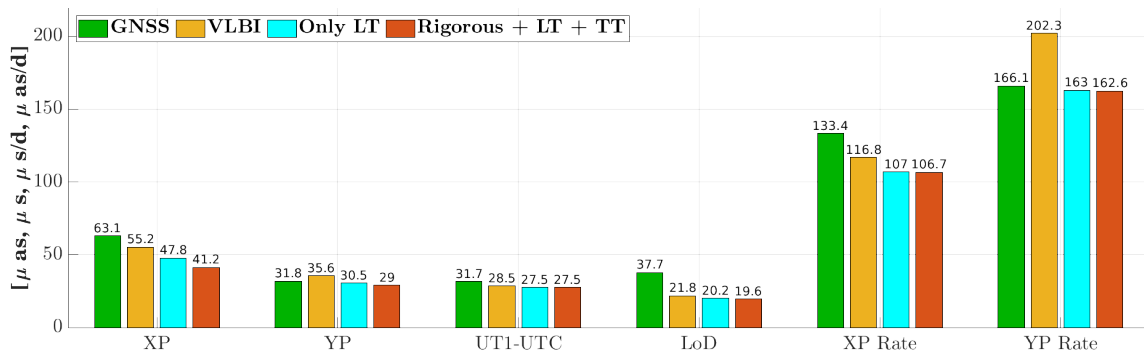


Figure 1.12: RMS of daily EOP differences to IGS for the individual technique solutions, and the combined solutions over the 15 days. Notice the different units on the left side for each parameter.

Shaping the future of VLBI Global Observing System observations at ETH Zurich

M. Schartner¹, B. Soja¹

¹ *Institute of Geodesy and Photogrammetry, ETH Zurich*

Introduction

Very Long Baseline Interferometry (VLBI) is a microwave-based space geodetic technique. By simultaneously measuring radiation from extragalactic radio sources with a global network of telescopes, differences in the arrival time of those signals can be determined via cross-correlation. These time differences can then be used to measure the coordinates of the telescopes and the observed radio sources, as well as determine Earth's orientation in space and study geophysical signals.

Due to the interferometric nature of VLBI, observations have to be coordinated between all participating telescopes. Therefore, a detailed observing plan, the so-called schedule, has to be generated and distributed. The schedule includes information regarding the participating telescopes, observed sources, frequency setup, and most importantly, the sequence of observations to be carried out. The task of generating a schedule can be seen as an advanced optimization problem: Given a list of around 100 suitable radio sources and a global network of telescopes, within 24 hours, up to 4000 scans can be observed. The task of VLBI scheduling is to find the optimal sequence of scans leading to the best possible outcome in terms of targeted geodetic parameters.

Currently, the aging VLBI network is undergoing a major upgrade, named VLBI Global Observing System (VGOS). As part of this upgrade, a new network of smaller but faster slewing telescopes is being built and changes to the observation frequency sequence are being established. The network of faster telescopes requires adaptations in the observing strategy to yield optimal results, investigated at ETH Zurich.

ETH Zurich's role within the IVS and for VGOS

ETH Zurich has taken over a leading role in organizing VLBI observations within the International VLBI Service for Geodesy and Astrometry. Together with partners in Germany and Austria, ETH is running the joint IVS operation center "DACH". During the year 2021, DACH was responsible for 205 sessions within the IVS. The number increased to 376 for the year 2022, which is over 30 % of all IVS sessions observed worldwide. During 2023, it is expected that DACH will be scheduling more than 400 sessions distributed among 14 observing programs. These sessions also include the research and development (R&D) experiments of VGOS.

The responsibility over these sessions was gained based on the success of the VLBI scheduling software VieSched++ (Schartner et al. 2019). VieSched++ was initially developed at TU Wien but is now extended and maintained at ETH Zurich. It is capable of scheduling and simulating VLBI sessions at a large scale using a variety of novel approaches, some of which are especially designed for the VGOS system.

VGOS R&D sessions

In 2022, resources for six VGOS-R&D experiments have been allocated by the IVS. An expert committee including members of ETH Zurich designed the sessions. For the generation of the observation plan, all six sessions have been assigned to ETH Zurich. From a scheduling point of view, the main novelties are a signal-to-noise-based integration time down to 5 seconds, increased sampling of the troposphere for high-frequency tropospheric zenith wet delay and gradient determination, and a better distribution of scans among sources. To meet these goals, significant extensions have been implemented into VieSched++.

With the new observation strategy, it was possible to approximately double the total number of scans within the R&D sessions compared to regular VGOS sessions. This also applies to the total number of resulting observations per session and scans per station. Figure 1.13 depicts the azimuth and elevation angles for one station at the Onsala site located in

Sweden on the left and compares it with the regular VGOS session observed one week later on the right. A clear improvement w.r.t. the number of scans and the distribution of these scans in the sky can be seen. The latter is especially important for improved estimation of the tropospheric parameters. An external study by Haas et al (2022) confirmed the superiority of the VGOS-R&D sessions by investigating the estimated zenith wet delays with a temporal resolution of 5 minutes and comparing them with independent measurements derived from co-located Global Navigation Satellite System (GNSS) stations and measurements from a co-located ground-based microwave radiometer for the Onsala site. They found a high correlation of over 0.9 for all but one station and root mean square differences of only 4-14 mm and, thus, concluded that with the VGOS-R&D sessions, it is possible to derive tropospheric parameters at such a high rate.

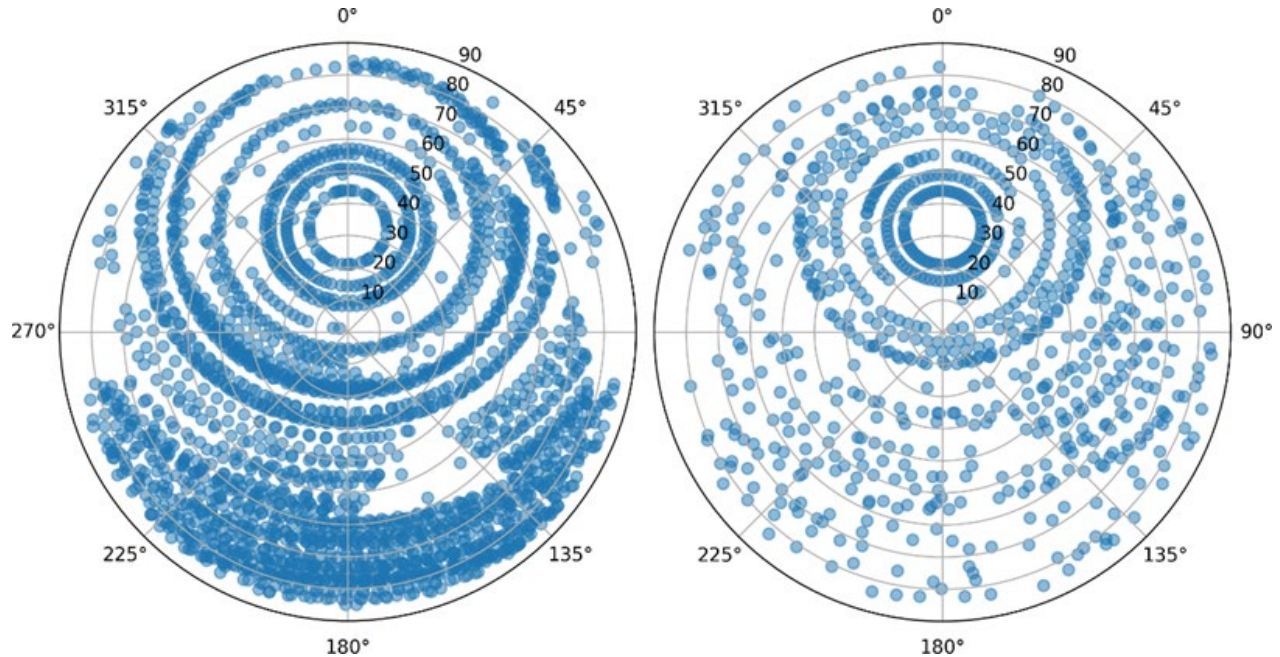


Figure 1.13: Azimuth and elevation observation angle of one Onsala site for a VGOS-R&D experiment (2022-05-12) on the left and for a standard VGOS experiment (2022-05-19) on the right.

Not all VGOS-R&D experiments have already been processed and analyzed. Therefore, it is not yet possible to draw final conclusions. However, based on the official IVS analysis reports of the already analyzed sessions, the formal errors of the estimated station coordinates of standard VGOS sessions are about 60 % larger compared to the VGOS-R&D sessions, indicating that improvements in the geodetic core products can be expected based on the new observation strategy.

Simultaneously, due to the shorter, signal-to-noise-based integration time, the required data storage could be reduced. This is especially important to speed up data transfer, one of the biggest bottlenecks in today's VGOS operation.

Analysis of Permanent GNSS Networks at swisstopo (PNAC)

S. Lutz¹, D. Ineichen¹, S. Schaer¹, E. Brockmann^{1,2}

¹ *Federal Office of Topography swisstopo*

² *now with Astronomical Institute, University of Bern*

The Automated GNSS Network of Switzerland (AGNES) is a multi-purpose reference network for national first order surveying, scientific research such as geodynamics and GNSS meteorology and serves as a base for the Swiss Positioning Service (swipos). AGNES was set up at the beginning of 1998 and reached its designated configuration of 29 stations by the end of 2001. After the enhancement of the network by GPS and GLONASS mid of 2007, totally 41 receivers are operating continuously to support the various applications. Since the first quarter of 2015 the network is capable for full multi-GNSS functionality.

The Permanent Network Analysis Center at swisstopo (PNAC) is not only analyzing the data of the AGNES stations but also of other national, European and global GNSS networks on an hourly near real-time as well as on a daily basis using the Bernese GNSS Software from the Astronomical Institute of the University of Bern.

In addition, swisstopo has been monitoring the quality of all the input observation files extensively since 2015 using G-Nut/Anubis and the BKG Ntrip Client (BNC). All available satellites, frequencies and observables are considered and the daily updated results are graphically summarized and put to the PNAC website (<http://pnac.swisstopo.admin.ch> >PNAC monitoring >Data monitoring >”swisstopo”) (see, e.g., Figure 1.14).

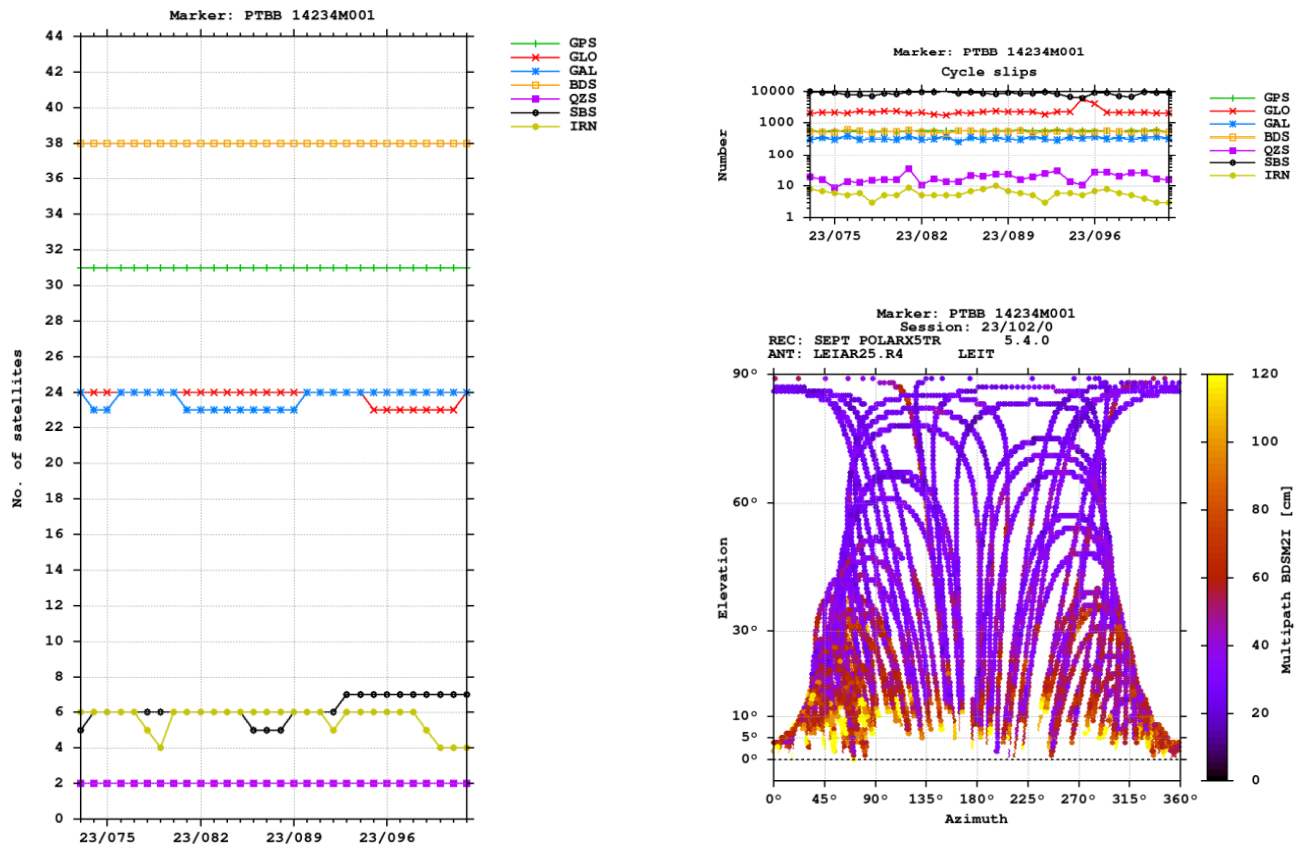


Figure 1.14: Left: Number of satellites available in the daily RINEX-3 files from station PTBB (Braunschweig, Germany). Top right: Number of cycle slips found by the Anubis QC analysis. Bottom right: Multipath for BeiDou observation code 21.

Operational network solutions

Three major processing lines are performed at swisstopo. One near real-time analysis with the data of about 200 stations every hour to monitor the station coordinates and to submit the tropospheric estimates (Zenith Total Delays) to meteorological organizations for numerical weather prediction (see Chapter “Contributions of swisstopo to GNSS Meteorology” in Commission 4). Another analysis runs every week and is based on daily RINEX observation files together with so called final orbit products from the Center for Orbit Determination in Europe (CODE) considering a subset of about 60 stations from the European Permanent Network (EPN) including the two Zimmerwald stations ZIMM and ZIM2. This solution is submitted regional product centers to support and monitor the European reference frame (EUREF). Since the beginning of 2022 all the EPN stations swisstopo is considering in this processing scheme deliver RINEX-3 files – a result also from the EUREF “Multi-GNSS” Working Group established in 2012 and chaired by Dr. E. Brockmann. The third analysis runs also every week and is based on daily observation files to primarily monitor the Swiss reference frame and to compute multi-year velocities for more than 200 stations European-wide. Figure 1.15 shows the number of GNSS satellites used in this last solution currently considering the four global constellations GPS, GLONASS, Galileo and BeiDou.

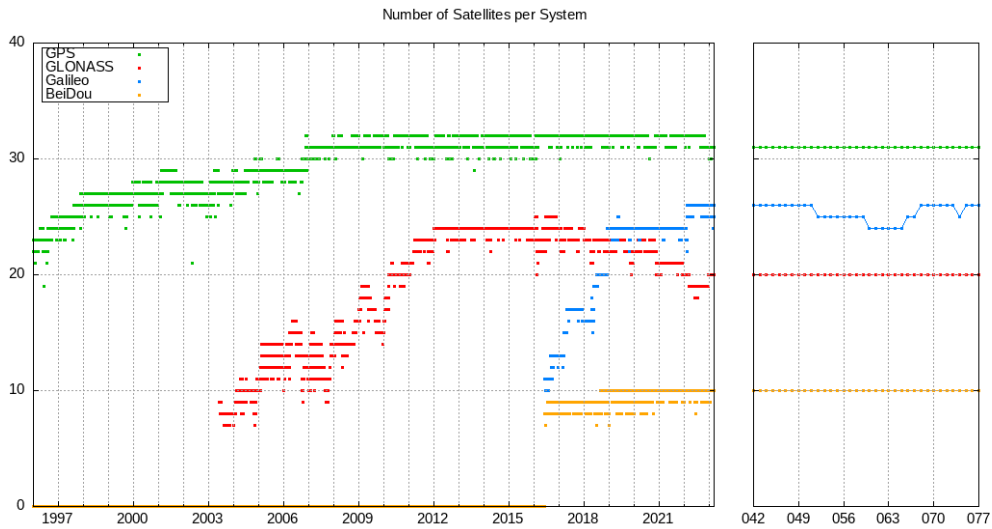


Figure 1.15: Number of satellites per system analyzed in the daily GNSS data processing at PNAC. Since 2019, more satellites of the European Galileo constellation are available compared to the Russian GLONASS system, where some active satellites can only be tracked.

The above-mentioned multi-year solution is routinely recalculated every day and the last days are supplemented with daily solutions from the near real-time processing as long as the final solutions are not yet available. In this way, the behavior of a permanent station can always be evaluated in a larger temporal context and the determined velocity field is always up to date. The available time series of the coordinates have meanwhile a length of more than 28 years, which allows the determination of velocities with accuracies of a few tenths of a millimeter/year (see Figure 1.16).

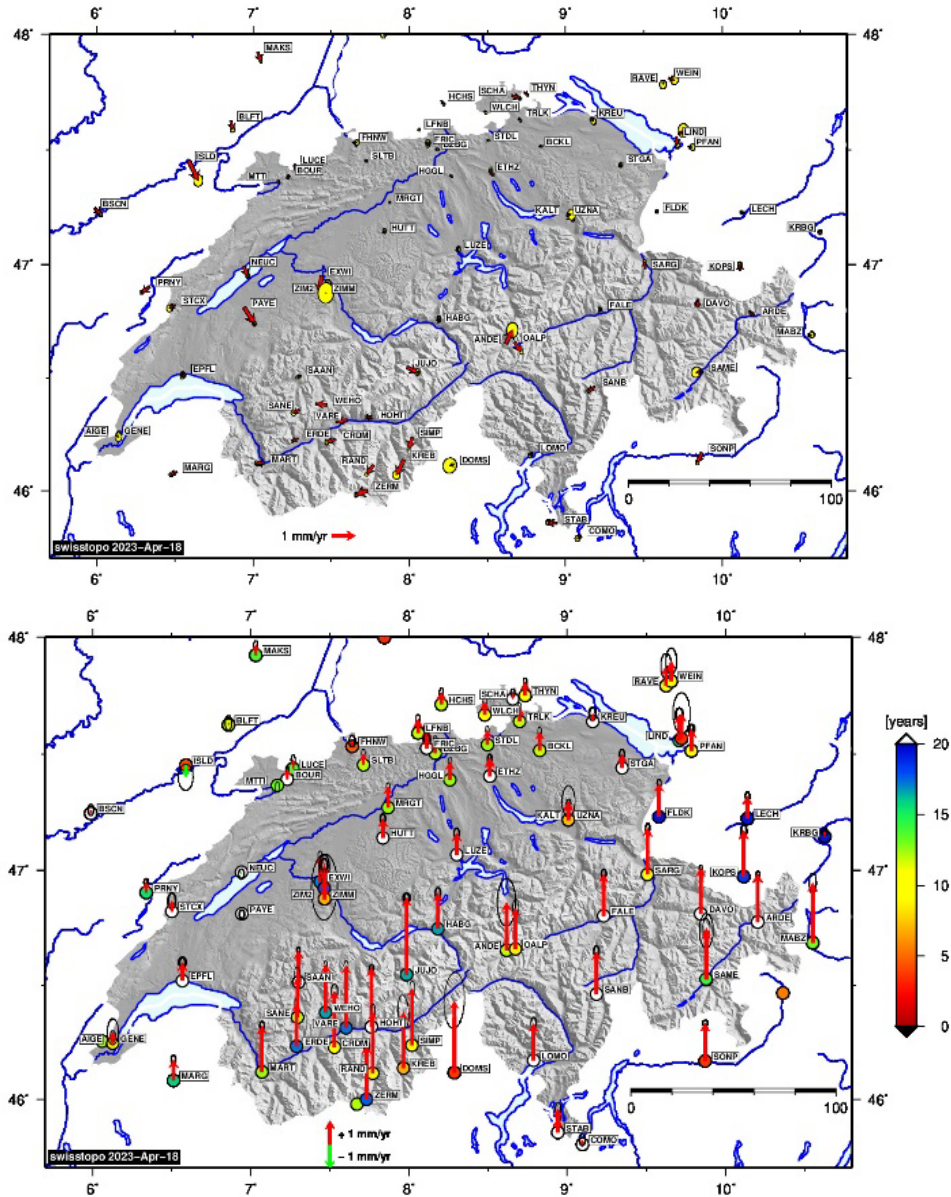


Figure 1.16: Horizontal (top) and vertical (bottom) velocity field determined with the daily updated multi-year solution of permanent GNSS stations in or near Switzerland.

For so-called double stations with short baselines, special time series are additionally computed: They are based on single frequency observations without the need of tropospheric parameter estimation. This increases the relative accuracy further, so that on sites equipped with more than one GNSS antenna a highly precise mutual control can be performed. The dual-station approach also prevents the need to change antennas too often due to, e.g., technical innovations useful for providers of positioning services, which has a negative impact on long-term series for the purpose of velocity estimation.

Long-term series of other parameters can also be viewed on the PNAC web pages, such as tropospheric parameters or the so-called intersystem translation parameters. These intersystem translation parameters give an impression of the

systematic differences between the coordinate determinations of each individual satellite navigation system used and their behavior over time.

Reference frame and model changes

In 2022, a new realization of the International Terrestrial Reference System was introduced and the products of the International GNSS Service (IGS) switched from the IGB14 to the IGS20 reference frame. This update came along with other important model changes, which were also applied in the different GNSS data analysis schemes at swisstopo (see Table 1.2).

	Hourly NRT	Daily FINAL	Daily EUREF
Fiducial stations	IGb14 -> IGS20	IGb14 -> IGS20	IGb14 -> IGS20
Satellite antenna phase center correction model	I14 -> I20	I14 -> I20	I14 -> I20
Receiver antenna phase center correction model	M14 -> igs20	C14	E14->igs20
Usage of uncalibrated (adopted) frequencies	Yes	Yes	Yes -> No
Orbits	Ultra-Rapid	MGEX	Rapid -> Final
Stochastic pulses	No	Spacing 12 hours	Spacing 12 hours -> Orbit midnight
Meanpole model	IERS2010 -> IERS2010 v1.2.0	IERS2010 -> IERS2010 v1.2.0	IERS2010 -> IERS2010 v1.2.0
Subdaily ERP model	IERS2010XY -> DESAI2016	IERS2010XY -> DESAI2016	IERS2010XY -> DESAI2016
Atmospheric tides	Yes	Yes	Yes -> No
Troposphere modelling	GPT1/GMF1	VMF1	VMF1 -> VMF3

Table 1.2: Some important model changes that were applied in the GNSS data analysis procedures at swisstopo along with the reference frame update from IGB14 to IGS20 in 2022.

Precise Point Positioning

PNAC setup an additional processing chain using the Precise Point Positioning (PPP) approach with undifferenced observations. In very close collaboration with the Astronomical Institute of the University of Bern (AIUB) and due to the enhancements of the global products of the Center for Orbit Determination in Europe (CODE), PPP is applied with ambiguity resolution for the GPS and Galileo constellations. The observations of the other global satellite systems can be used as well but without fixing the zero-difference ambiguities.

The design of the PPP engine is very flexible in terms of setting different processing options or the analysis of single stations (e.g., to compute new a priori station coordinates). A daily job runs with the rapid products of the previous day and serves as a link between the hourly near real-time solutions and the daily “final” solutions, which have a delay of about two weeks. By comparing the estimated parameters (e.g., station coordinates or troposphere parameters) of the different solution types, the identification of station problems can be further improved (see Figure 1.17).

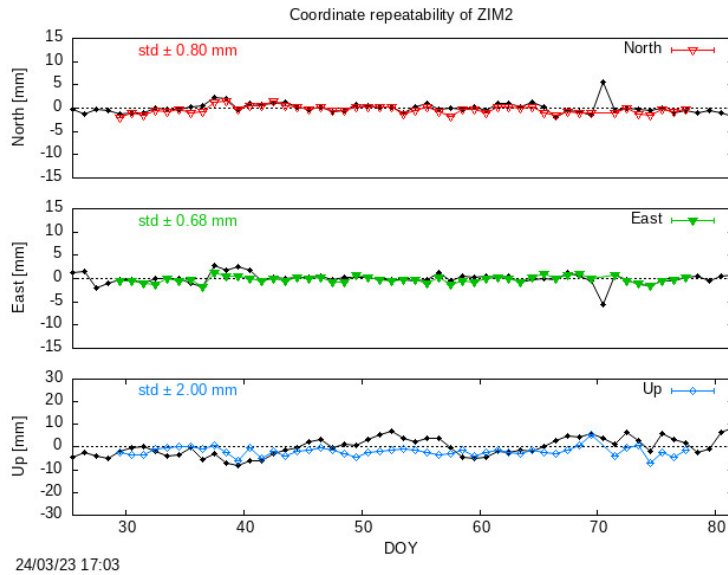


Figure 1.17: Repeatability of the daily coordinates of station ZIM2 (Zimmerwald) from the double-difference approach (red, green and blue) and from the zero-difference approach (black) without exclusion of detected outliers. The horizontal components fit very well, whereas for the height the difference in the quality mainly comes from different a priori troposphere models (VMF in the double-difference case versus GMF in the zero-difference case).

The PPP engine was also used in the frame of the ETH project “Absolute field calibration for multi-GNSS receiver antennas”. It is further possible to analyze high-rate data and to estimate, e.g., tropospheric slant delays.

GNSS2022: 5th re-observation of the national GNSS network LV95

J. Carell¹, G. Palma¹, E. Brockmann^{1,2}, S. Condamin¹, M. Mäusli¹, Ch. Theiler¹, A. Schlatter¹, T. Seiler¹, M. Smolik¹, D. Willi¹

¹ Federal Office of Topography swisstopo

² now with Astronomical Institute, University of Bern

Stable and accurate geodetic reference frames are part of a modern national infrastructure. They are the basis for precise national (official) as well as for private practical surveying and positioning, for geodynamic applications, for geographic information systems (GIS) and for cartography. The importance and need of a new, GPS based three-dimensional reference frame in Switzerland was recognized by swisstopo in the 1980ies (D. Schneider, E. Gubler and A. Wiget, 2015).

The Swiss national three-dimensional geodetic reference frame (Swiss Terrestrial Reference Frame CHTRF) is materialized by more than 200 stable points of the LV95-network and 41 continuously operating reference stations (CORS) of the automatic GNSS network “AGNES”. The concept and the realization of the “Landesvermessung 1995 (LV95)” is documented in the “swisstopo DOKU” series. The last and final report is planned to be published in 2023 (swisstopo-DOKU, 2023).

The LV95-network was established and first observed between 1989 and 1994. The three-dimensional coordinates (CHTRF95- and LV95-coordinates) of the LV95-points were published in 1995 (therefore the name “Landesvermessung 1995”). The network is periodically re-observed following a six year turn since 1998 (CHTRF98, CHTRF2004, CHTRF2010; CHTRF2016). Therefore, a new re-observation campaign of the complete network was due and conducted in 2022. The concept and organization of the 2022-campaign is described in (to be published; Carrel and Palma, 2023). Note that the campaign is called GNSS2022, in order to avoid any confusion with CHTRF2022, which designates only the reference frame from now on.

The maintenance concept guarantees the quality of the three-dimensional reference frame CHTRF / LV95 regarding

- the control of the stability of the points,
- the check of the 3D-coordinates and their uncertainty,
- the proof of the reliability and consistency of the points and their coordinates,

and it provides a meaningful density of data for the long-term determination of the velocity field of these points and stations, respectively, eventually allowing to estimate the recent kinematics of the upper crust within Switzerland and relative to its surrounding countries in Europe (Brockmann, 2018).

The following main goals of the GNSS2022 campaign can be mentioned:

- **Control of the official reference frame LV95:** The re-observation allows the proof of the quality of LV95 and the application of coordinate changes or station exchanges if necessary. The criteria for this are published in the maintenance concept of the national geodetic survey (Wiget et al. 2010a) and in its quality standards (Wiget et al. 2010b).
- **Determination of the reference frame CHTRF2022:** New re-observation of the network for the long-term monitoring of tectonic movements in Switzerland. With this 5th re-observation the time span since the first observation is growing to approx. 28 – 34 years.
- **NEOTEK2022:** Re-observation of a densified network of reference points in northern Switzerland which were specially established for Nagra (National Cooperative for the Disposal of Radioactive Waste) in 1988 and are since regularly re-observed together with the LV95-network.

The number of observed points / stations in the GNSS2022-campaign was as follows:

41	AGNES permanent stations
103	Main points (H) of LV95
105	Densification points (V) of LV95
5	additional points in NEOTEK 2022
8	CHGeoid2003 points for the combination with the geoid determination
221	Total number of (passive) reference points

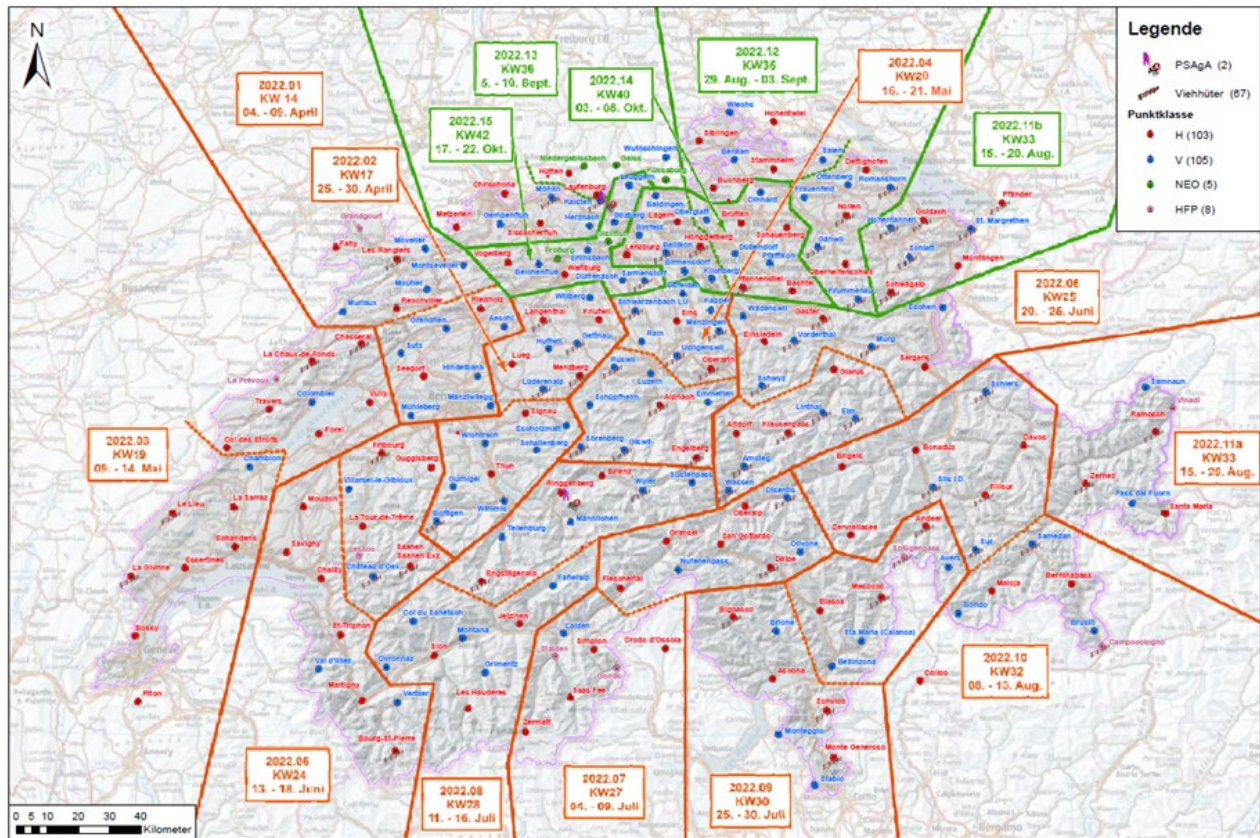


Figure 1.18: Network of reference points observed in GNSS2022 and their subdivision in weekly campaign areas.

The GNSS measurements were done using 8 swisstopo-owned Trimble NetR9 GNSS receivers with individually calibrated Trimble Zephyr Geodetic model 2 antennas. Each observer (typically 2 observers work simultaneously) had operated 4 receivers. Further statistical details and their comparison with the former campaign CHTRF2016 are given in the following table:

Indicators	CHTRF2016	GNSS2022	Difference
Number of GNSS-operators	10	10	0
Number of campaign weeks	15	16	+1
Number of GNSS receivers per week	8	8	0
Number of field-days per campaign	90	91	+1
Number of person-field-days	188	214	+26
Number of observed points (without AGNES stations)	223	221	-2
Total number of point observations	225	222	-3
Total amount of GNSS observation time [h]	9852	9690	-162
Mean observation time per point [h]	44.18	43.6	-1%
Max. / Min. observation time per point [h]	87.4 / 31.8	63.8 / 22.4	-23.6 / -9.4
Total kilometers driven by car [km]	31'139	35'465	+13%

Table 1.3: Statistics of the GNSS2022 campaign, compared with the CHTRF2016-campaign.

The final results (multi-year combination solution over all measurement epochs) is expected to be available by the end of 2023.

Measurements for the National Height System

A. Schlatter¹, U. Marti¹, D. Willi¹

¹ Federal Office of Topography swisstopo

Precise levelling within the National Height Network 2019-2022

Between 2019 and 2022 a total of 160 km (around 40 km per year) of leveling observations have been performed within the National Height Network LHN (see red lines in Figure 1.19). This is 50 km/year less than the average as between 2015 and 2018 and 90 km/year less as between 2007 and 2014. The main reason is a reduction of staff in the team responsible for the maintenance of the national height frame. In addition, more height difference was measured on some lines at the expense of line length. Usually, these measurements were carried out on lines that were leveled 40 to 50 years ago for the last time.

The main part leveled in this epoch were third observations of 1st order levelling lines:

- Landquart - Davos (2019)
- Davos – Flüelapass – Susch (2020)
- Susch – Scuol – Martina (2021; Connection to Austria)
- Martigny – Col de la Forclaz – Le Châtelard (2022; Connection to France)

Besides these line measurements, which principally serve for the realization of the two national vertical reference frames (LN02 and LHN95), geoid determination and the investigation of recent crustal movements (s. Figure 1.20), regular local maintenance works were performed in the observing period. The national height network contains today around 4'600 km of leveling lines with approximately 8'900 benchmarks.

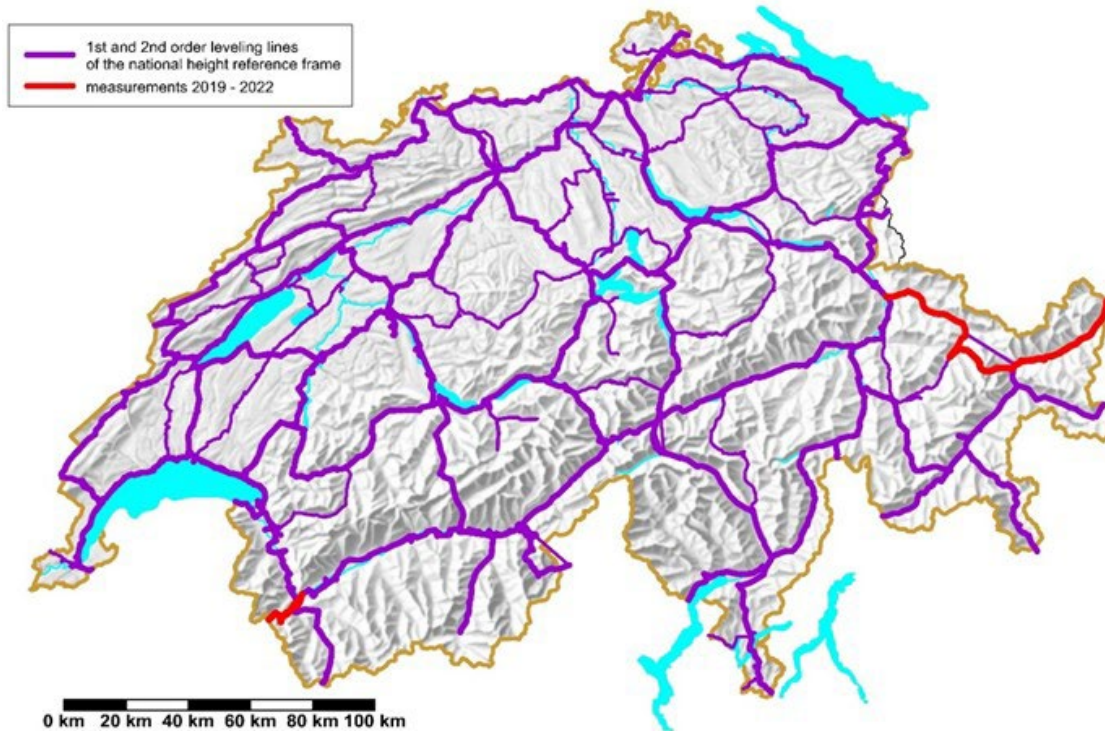


Figure 1.19: Measurements 2019 – 2022 for the National Height System LHN

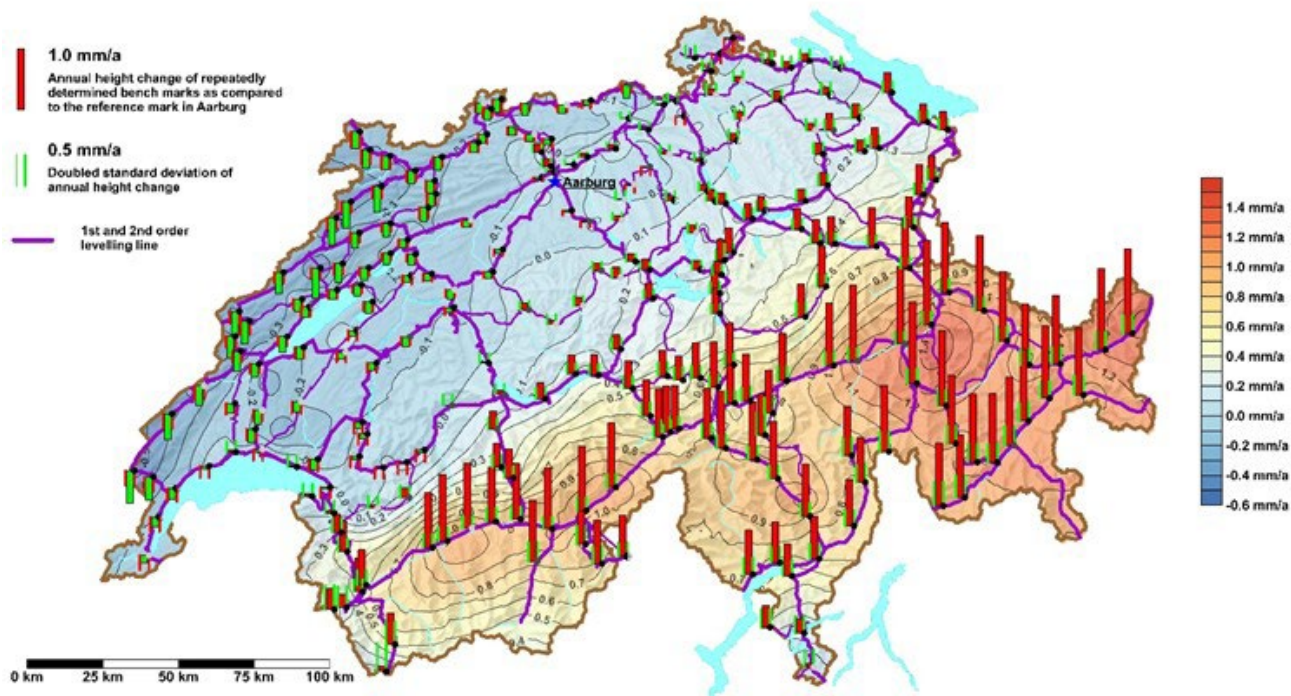


Figure 1.20: Recent Crustal Movements from Precise Levelling (Status 2022)

2020 : Anniversary 200 years of Repère Pierre du Niton

In 2020, one of Switzerland's important geodetic fundamental points celebrated its 200th anniversary. Repère Pierre du Niton (RPN), the bronze plate on an erratic boulder in the harbour basin of Geneva was originally created in 1820 as a level marker for water level measurements. As a landlocked country, Switzerland has always depended on neighbouring countries to determine sea levels. When the first French levellings arrived in Switzerland in 1860, RPN served as the fundamental point for height determinations (Schlatter 2020). This is still the case today.

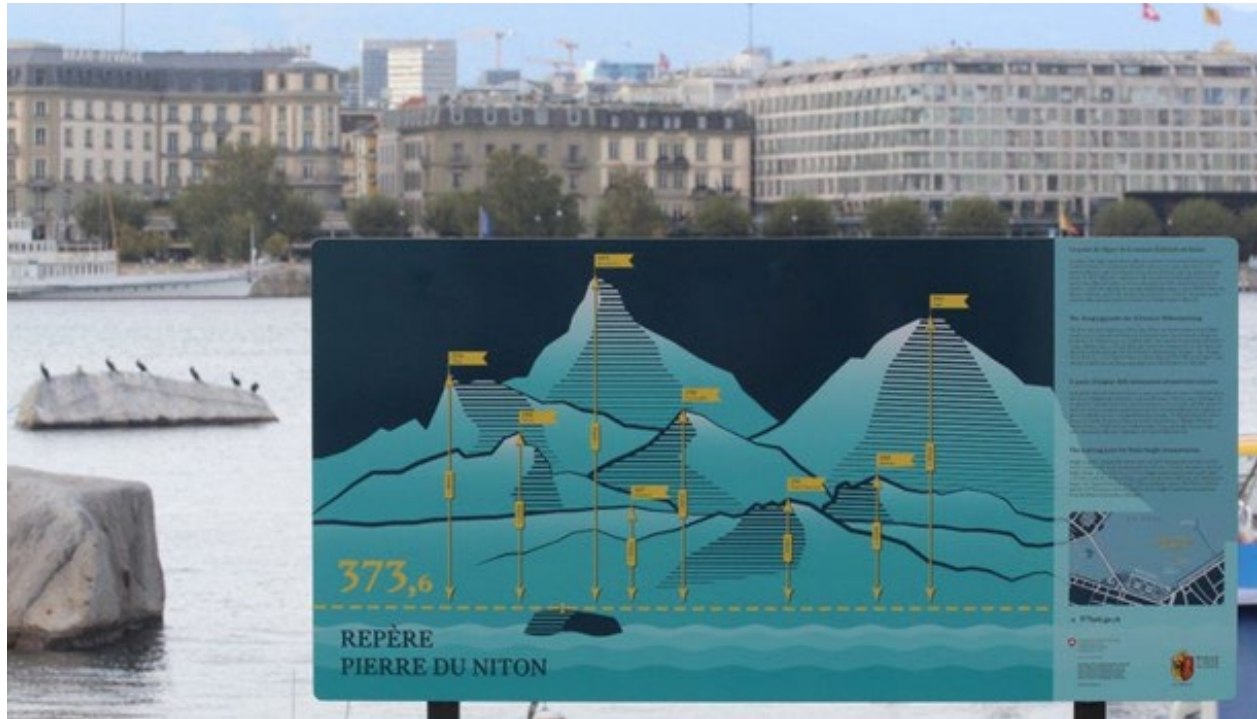


Figure 1.21: The starting point for the heights in Switzerland with the commemorative plaque on the occasion of the 200th anniversary (A. Schlatter)

Project Swiss Height System

At the beginning of the 2000s, the Federal Council decided to change the position reference system for the official cadastral survey and indirectly also of the geographic information systems in Switzerland, but to retain the old LN02 height system. In fact, the cost-benefit ratio of a change in the height reference system was too little at that time, and the fear of confusion was much greater.

More than twenty years after this decision, the "Haute Ecole d'Ingénierie et de Gestion du canton de Vaud" (HEIG-VD), in close cooperation with the Federal Office of Topography (swisstopo), is once again putting the question of the height reference up for discussion and is launching a scientific analysis of the opportunities and benefits of a possible introduction of a new height reference system in Switzerland.

In October 2022, a survey was completed on the use and management of elevation data in Switzerland and the consequences of a possible change in the elevation framework. The publication of the results is still in progress. As a first part of the study of the modernization of the Swiss height reference system and framework, swisstopo prepared a report on the fundamentals, the state of the art and the international comparison (Willi et al. 2022).

TABLE OF CONTENTS

Bibliography Commission 1

- Brockmann, E. (2018): LV95 / CHTRF2016 (Swiss Terrestrial Reference Frame 2016) Teil 2: Auswertung der GPS-Messungen 2016 und Resultate der Gesamtausgleichung 1988-2016. swisstopo Report 16-19. Bundesamt für Landestopografie swisstopo, Wabern.
- Bruyninx, C., Legrand, J., Fabian, A., Pottiaux E., GNSS metadata and data validation in the EUREF Permanent Network, GPS Solut (2019) 23: 106. DOI:10.1007/s10291-019-0880-9.
- Carrel, J., Palma, G. (2023): LV95 / CHTRF2022 (Swiss Terrestrial Reference Frame 2016) Teil 1: Messkonzept und Messkampagnen vom April bis Oktober 2022 im Landesnetz LV95. swisstopo Report. Bundesamt für Landestopografie swisstopo, Wabern.
- Calero-Rodríguez, E., A. Villiger, S. Schaer, R. Dach, A. Jäggi (2023): Between-satellite ambiguity resolution based on preliminary GNSS orbit and clock information using a globally applied ambiguity clustering strategy. GPS Solutions, 27, 125, DOI:10.1007/s10291-023-01435-3.
- Cordelli, E., Schlatter, P., Schildknecht, T. (2018). Simultaneous multi-filter photometric characterization of space debris at the Swiss Optical Ground Station and Geodynamics Observatory Zimmerwald. Advanced Maui Optical and Space Surveillance Technologies Conference (AMOS) 2018, Wailea, Hawaii, USA, September 11-14.
- Cordelli, E., Lauber, P., Prohaska, M., Rodriguez, J., Schlatter, P., Schildknecht, T. (2019). Recent Developments at the Swiss Optical Ground Station and Geodynamics Observatory Zimmerwald. 1st ESA NEO and Debris Detection Conference 2019, ESA/ESOC, Darmstadt, Germany, January 22-24.
- Dach, R., Lutz, S. Walser, P. Fridez, P. (Eds); 2015: Bernese GNSS Software Version 5.2. User manual, Astronomical Institute, University of Bern, Bern Open Publishing. DOI:10.7892/boris.72297; ISBN: 978-3-906813-05-9.
- Dach, R., S. Schaer, D. Arnold, L. Prange, D. Sidorov, A. Sušnik, P. Stebler, A. Villiger, A. Jäggi, G. Beutler, E. Brockmann, D. Ineichen, S. Lutz, U. Wild, M. Nicodet, J. Dostal, D. Thaller, W. Söhne, J. Bouman, I. Selmke, U. Hugentobler; 2019: Center of Orbit Determination in Europe: IGS Technical Report 2018. International GNSS Service: Technical Report 2018; edited by A. Villiger and R. Dach (AIUB), IGS Central Bureau and University of Bern, Bern Open Publishing, pp 31-46, July 2019, DOI:10.7892/boris.130408.
- Dach, R., S. Schaer, D. Arnold, L. Prange, D. Sidorov, P. Stebler, A. Villiger, A. Jäggi, G. Beutler, E. Brockmann, D. Ineichen, S. Lutz, U. Wild, M. Nicodet, J. Dostal, D. Thaller, W. Söhne, J. Bouman, I. Selmke, U. Hugentobler; 2020: Center of Orbit Determination in Europe: IGS Technical Report 2019. International GNSS Service: Technical Report 2019; edited by A. Villiger and R. Dach (AIUB), IGS Central Bureau and University of Bern, Bern Open Publishing, pp 39-56, May 2020, DOI:10.7892/boris.144003.
- Dach, R., S. Schaer, D. Arnold, M. Kalarus, L. Prange, S. Sidorov, P. Stebler, A. Villiger, A. Jäggi, G. Beutler, E. Brockmann, D. Ineichen, S. Lutz, U. Wild, M. Nicodet, D. Thaller, J. Dostal, W. Söhne, J. Bouman, I. Selmke, U. Hugentobler; 2021: Center of Orbit Determination in Europe (CODE): IGS Technical Report 2020. IGS Central Bureau and University of Bern, Bern Open Publishing, pp 49-66, June 2021, DOI:10.48350/156425.
- Dach, R., I. Selmke, A. Villiger, D. Arnold, L. Prange, S. Schaer, D. Sidorov, P. Stebler, A. Jäggi, and U. Hugentobler (2021). Review of Recent GNSS Modelling Improvements Based on CODEs Repro3 Contribution. Advances in Space Research, 68(3):1263–1280, DOI:10.1016/j.asr.2021.04.046.
- Dach, R., S. Schaer, D. Arnold, M. Kalarus, L. Prange, P. Stebler, A. Villiger, A. Jäggi, E. Brockmann, D. Ineichen, S. Lutz, U. Wild, M. Nicodet, D. Thaller, L. Lengert, J. Dostal, W. W. Söhne, J. Bouman, I. Selmke, U. Hugentobler; 2022: Center of Orbit Determination in Europe (CODE): IGS Technical Report 2021. IGS Central Bureau and University of Bern, Bern Open Publishing, pp 45-60, August 2022, DOI:10.48350/169536.
- Dach, R., S. Schaer, D. Arnold, M. Kalarus, L. Prange, P. Stebler, A. Villiger, A. Jäggi, E. Brockmann, D. Ineichen, S. Lutz, D. Willi, M. Nicodet, D. Thaller, L. Klemm, A. Rülke, W. Söhne, J. Bouman, U. Hugentobler; 2023: Center for Orbit Determination in Europe (CODE) Analysis Center Technical Report 2022. IGS Central Bureau and University of Bern, Bern Open Publishing, pp 45-64, May 2023. DOI:10.48350/17929

- Diehl, T., Madritsch, H., Schnellmann, M., Spillmann, T., Brockmann, E., Wiemer, S. (2023): Seismotectonic evidence for present-day transtensional reactivation of the slowly deforming Hegau-Bodensee Graben in the northern foreland of the Central Alps. In *Tectonophysics* 846.
- Desai, S. D. and A. E. Sibois (2016). Evaluating predicted diurnal and semidiurnal tidal variations in polar motion with GPS-based observations. *Journal of Geophysical Research*, 121(7): 5237–5256, DOI:10.1002/2016JB013125.
- Geisser, L., U. Meyer, D. Arnold, A. Jäggi (2023a): Contribution of LARES SLR Data to Co-estimated Earth Geopotential Coefficients. In: *International Association of Geodesy Symposia*. Springer, Berlin, Heidelberg, DOI:10.1007/1345_2022_185, in press.
- Geisser, L., T. Schildknecht, U. Meyer, D. Arnold, A. Jäggi (2023b): Homogeneous formation of SLR Normal Point data at AIUB. In *Proceedings of the 22nd International Workshop on Laser Ranging*, November 7-11, 2022, Guadalajara, Spain, in press.
- Grombein, T., M. Lasser, D. Arnold, U. Meyer, A. Jäggi (2022): Determination and combination of monthly gravity field time series from kinematic orbits of GRACE, GRACE-FO and Swarm. In: *IAG Symposia*, Springer, Berlin, Heidelberg, DOI:10.1007/1345_2022_163, in press.
- Haas, R., Johansson, J., Elgered, G., Diamantidis, P.K., Nilsson, T. (2023): Assessment of Parameters Describing the Signal Delay in the Neutral Atmosphere Derived from VGOS Observations, *IVS General Meeting proceedings NASA/TP-20210021389*
- Herrera-Pinzón, I. D. and M. Rothacher (2019). Double-Differences of SLR-Observations for Parameter Estimation: The Wettzell Case. *Frontiers of Geodetic Science*; Conference Location: Stuttgart, Germany; Conference Date: September 17-19, 2019; Presentation on 19 September 2019.
- Herrera-Pinzón, I. D. and M. Rothacher (2020). A Study on Rigorous Combination of GNSS and VLBI Observations. *EGU General Assembly 2020*; Conference Location: Online; Conference Date: May 4-8, 2020; Presentation on May 6, 2020. Göttingen. DOI:10.3929/ethz-b-000528214.
- Herrera-Pinzón, I. D., M. Rothacher, and S. Riepl (2021). “Differencing strategies for SLR observations at the Wettzell observatory”. In: *Journal of Geodesy* 96.4. issn:1432-1394. DOI:10.1007/s00190-021-01588-4.
- Herrera-Pinzón, I. D. and M. Rothacher (2021). A Study on Differencing Approaches for SLR Observations. *Scientific Assembly of the International Association of Geodesy (IAG 2021)*; Conference Location: Beijing, China; Conference Date: June 28 - July 2, 2021; Poster abstract. Poster presented on June 28, 2021. Beijing.
- Herrera-Pinzón, I. D. and M. Rothacher (2021b). Towards Inter-Technique Co-Location of GNSS and VLBI Observations. *EGU General Assembly 2021*; Conference Location: Online; Conference Date: April 19-30, 2021; Presentation on April 4, 2021. Göttingen. DOI:10.3929/ethz-b-000528210.
- Herrera-Pinzón, I. D. and M. Rothacher (2022). Local And Tropospheric Tie Analysis at Fundamental Sites in the CONT17 Campaign. *EGU General Assembly 2022*, Vienna, Austria, 23–27 May 2022. DOI:10.5194/egusphere-egu22-9240.
- Herrera-Pinzón, I. D. and M. Rothacher (2023). “Impact of Local- and Tropospheric Ties for the Rigorous Combination of GNSS and VLBI”. In: *Proceedings of the IAG International Symposium on Reference Frames for Applications in Geosciences (REFAG 2022)*. In Press.
- Johnston, G., Riddell, A., Hausler, G. (2017). The International GNSS Service. In Teunissen, Peter J.G., & Montenbruck, O. (Eds.), *Springer Handbook of Global Navigation Satellite Systems* (1st ed., pp. 967-982). Cham, Switzerland: Springer International Publishing, DOI:10.1007/978-3-319-42928-1
- Lauber P., T. Schildknecht, SLR-System Upgrade and Experiments at Zimmerwald, *Proceedings of 22nd International Workshop on Laser Ranging*, Yebes, Spain, 2022.
- Lidberg M., Bruyninx C., Brockmann E., Dach R., Kenyeres A., Kollo K., Legrand J., Liwosz T., Rosa Pacione R., Sacher M., Söhne W., Völkens C., Altamimi Z., Caporali A., Poutanen M. (2021), Scientific goals and strategic actions of EUREF in a changing landscape, *Session Regional reference frames and networks at IAG general Assembly 2021*, Jun 28-Jul 2, 2021, Beijing, China.

- Mao, X., D. Arnold, V. Girardin, A. Villiger, A. Jäggi (2021): Dynamic GPS-based LEO orbit determination with 1 cm precision using the Bernese GNSS Software. *Advances in Space Research*, 67, 788-805, DOI: 10.1016/j.asr.2020.10.012.
- Montenbruck O., P. Steigenberger, L. Prange, Z. Deng, Q. Zhao, F. Perosanz, I. Romero, C. Noll, A. Stürze, G. Weber, R. Schmid, K. MacLeod, S. Schaer (2017) The Multi-GNSS Experiment (MGEX) of the International GNSS Service (IGS) – Achievements, Prospects and Challenges, *Advances in Space Research* 59(7):1671-1697, DOI:10.1016/j.asr.2017.01.011.
- Müller, H. R., Garrard, R., Brockmann, E., Spillmann, T. et al. (2022): Nagra's permanent GNSS network for geodynamic monitoring in the sub-millimeter range: site selection, installation and first measurement results. In *Swiss Bulletin for Applied Geology*, Vol. 27(2).
- Peter, H., U. Meyer, M. Lasser, A. Jäggi (2022): COST-G gravity field models for precise orbit determination of Low Earth Orbiting Satellites. *Advances in Space Research*, 69, 4155-4168, DOI:10.1016/j.asr.2022.04.005.
- Petrachenko, B., Schartner, M., Xu, M., (2023): VGOS Technology R&D Sessions, IVS General Meeting proceedings NASA/TP-20210021389
- Prange, L., G. Beutler, R. Dach, D. Arnold, S. Schaer, A. Jäggi; 2020a: An empirical solar radiation pressure model for satellites moving in the orbit-normal mode. *Advances in Space Research*, Vol 65, Issue 1, pp 235-250, Jan 1st, 2020. DOI:10.1016/j.asr.2019.07.031.
- Prange, L., A. Villiger, D. Sidorov, S. Schaer, G. Beutler, R. Dach, A. Jäggi; 2020b: Overview of CODE's MGEX solution with the focus on Galileo. *Advances in Space Research*, Vol 66, Issue 12, pp 2786-2798, DOI:10.1016/j.asr.2020.04.038.
- Rodriguez, J., T. Schildknecht, Daylight Measurement Acquisition of Defunct Resident Space Objects Combining Active and Passive Electro-Optical Systems. *IEEE Transactions on geoscience and remote sensing*, 60, 2022.
- Rodriguez, J., E. Cordelli, T. Schildknecht, The stare and chase observation strategy at the Swiss Optical Ground Station and Geodynamics Observatory Zimmerwald: From concept to implementation, *Acta Astronautica* 189, pp 352 - 367, 2021.
- Schaer, S., A. Villiger, D. Arnold, R. Dach, L. Prange, A. Jäggi (2021): The CODE ambiguity-fixed clock and phase bias analysis products: generation, properties, and performance. *Journal of Geodesy*, Vol. 95 (81), DOI:10.1007/s00190-021-01521-9.
- Schartner, M., Böhm, J. (2019): VieSched++: A new VLBI scheduling software for geodesy and astrometry, *PASP*, 131(1002), ab1820, DOI:10.1088/1538-3873/ab1820
- Schartner, M., Plötz, C., Soja, B. (2021): Automated VLBI scheduling using AI-based parameter optimization, *J Geod* 95, 58, DOI:10.1007/s00190-021-01512-w
- Schartner, M., Kern, L., Nothnagel, A., Böhm, J., Soja, B. (2021): Optimal VLBI baseline geometry for UT1-UTC Intensive observations, *J Geod* 95, 75, DOI:10.1007/s00190-021-01530-8
- Schartner, M., Plötz, C., Soja, B. (2022): Improvements and comparison of VLBI INT2 and INT3 session performance, *J Geod* 96, 26, DOI:10.1007/s00190-022-01621-0
- Schartner, M., Collioud, A., Charlot, P., Xu, M.H., Soja, B. (2023): Bridging astronomical, astrometric and geodetic scheduling for VGOS, *J Geod* 97, 17 (2023), DOI:10.1007/s00190-023-01706-4
- Schlatter A., 2020: 200 Jahre Repère Pierre du Niton. Über das Niveau der Schweiz. In: *Die auf dem Messtisch*. 175 Jahre Dufourkarte, Bundesamt für Landestopografie swisstopo, pp. 127-149, DOI:10.24894/978-3-7965-4216-9.
- Schneider D., Gubler, E., Wiget, A. (2015): Meilensteine der Geschichte und Entwicklung der Schweizerischen Landesvermessung. *Geomatik Schweiz* 11/2015, p. 462 – 483.
- Sidorov, D., R. Dach, B. Polle, L. Prange, A. Jäggi; 2020: Adopting the Empirical CODE Orbit Model to Galileo satellites. *Advances in Space Research*, Vol 66, Issue 12, pp 2799-2811, DOI:10.1016/j.asr.2020.05.028.

- Steigenberger, P., Z. Deng, J. Guo, L. Prange, S. Song, Oliver Montenbruck (2022): BeiDou-3 orbit and clock quality of the IGS Multi-GNSS Pilot Project. *Advances in Space Research*, Vol. 71(1), pp. 355-368, DOI:10.1016/j.asr.2022.08.058.
- Strugarek, D., K. Sośnica, D. Arnold, A. Jäggi, R. Zajdel, G. Bury (2021): Determination of SLR station coordinates based on LEO, LARES, LAGEOS, and Galileo satellites. *Earth, Planets and Space*, 73, 87, DOI:10.1186/s40623-021-01397-1.
- Strugarek, D., K. Sośnica, D. Arnold, A. Jäggi, R. Zajdel, G. Bury (2022): Satellite laser ranging to GNSS-based Swarm orbits with handling of systematic errors. *GPS Solutions* 26, 104, DOI:10.1007/s10291-022-01289-1.
- Rodriguez, J., E. Cordelli, T. Schildknecht, The stare and chase observation strategy at the Swiss Optical Ground Station and Geodynamics Observatory Zimmerwald: From concept to implementation. *Acta Astronautica*, 189, 352-367, 2021.
- Rodriguez, J., P. Lauber, T. Schildknecht, Novel Data Analysis Strategy at the SwissOGS Zimmerwald. *Proceedings of 22nd International Workshop on Laser Ranging*, Yebe, Spain, 2022.
- swisstopo-DOKU Reihe [bzw. „Berichte aus der L+T“] (1995-2023): Teile 1 – 15 zum Aufbau der neuen Landesvermessung der Schweiz 'LV95'. Bundesamt für Landestopografie swisstopo, Wabern.
- Vananti, A., D. Guthruf, Y. Lu, T. Schildknecht, Estimation of reflective properties from light curves of a H2A rocket body. *Proceedings of 8th European Conference on Space Debris (Virtual Conference)*, 2021.
- Villiger, A., R. Dach, S. Schaer, L. Prange, F. Zimmermann, H. Kuhlmann, G. Wübbena, M. Schmitz, G. Beutler, A. Jäggi (2020): GNSS scale determination using calibrated receiver and Galileo satellite antenna patterns. *Journal of Geodesy*, 94, 93, DOI:10.1007/s00190-020-01417-0.
- Villiger, A., S. Schaer, R. Dach, L. Prange, A. Sušnik, A. Jäggi (2019). Determination of GNSS pseudo-absolute code biases and their long-term combination. *Journal of Geodesy*, 93, pp. 1487-1500, DOI:10.1007/s00190-019-01262-w.
- Wiget, A., Brockmann, E., Kistler, M., Marti, U., Schlatter, A., Vogel, B., Wild, U. (2010a): Nachführungskonzept für die geodätische Landesvermessung. swisstopo Report 09-14, Bundesamt für Landestopografie, Wabern.
- Wiget, A., Andrey, D., Brockmann, E., Ineichen, D., Kistler, D., Marti, U., Schlatter, A., Vogel, B., Wild, U. (2010b): Qualitätsstandards der Landesvermessung. Indikatoren, Standards und Messgrößen für die Produkte der geodätischen Landesvermessung. swisstopo Report 10-11 (also available in french), Bundesamt für Landestopografie, Wabern.
- Willi, D., Lutz, S., Brockmann, E. (2020): Absolute field calibration for multi-GNSS receiver antennas at ETH Zürich. In *GPS Solutions*, Vol. 24(1).
- Willi D., A. Schlatter, U. Marti, S. Guillaume, 2022: Neues Schweizer Höhensystem. Studie zur Modernisierung des Schweizer Höhebezugssystems und -rahmens. Teil I – Grundlagen, Sten der Technik und internationaler Vergleich. swisstopo Report 22-07, Bundesamt für Landestopografie swisstopo, Wabern.

2 Gravity Field

Absolute and Relative Gravity Measurements

U. Marti¹, H. Baumann²

¹ Federal Office of Topography swisstopo

² Federal Institute of Metrology METAS

Absolute Measurements

The backbone of the Swiss Gravity Network (Landesschwerenetz, LSN) is formed by around 10 absolute gravity stations (Figure 2.1), which are repeatedly observed with a Micro-g LaCoste FG5x. Usually, the instrument (#209) of METAS is used. In 2019, the stations in Lausanne, Zurich and Zimmerwald were observed. In 2020, no observations were possible. In 2021, the observed stations were Zimmerwald, Mont Terri, Andermatt and Monte Ceneri. And in 2022, the observations took place in Basel, Chur and Grindelwald. In 2021, IGN (France) made an absolute measurement in Basel with a Micro-g LaCoste A10.

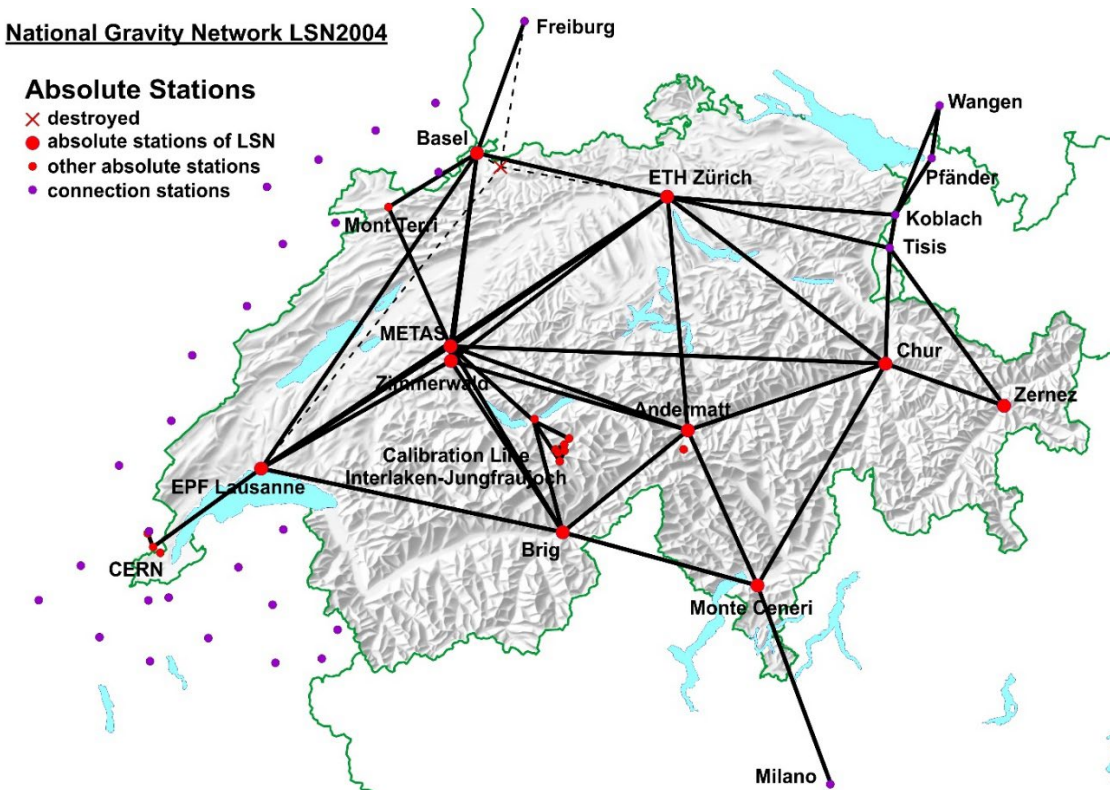


Figure 2.1: Absolute gravity stations (Zero Order Network of the LSN) in Switzerland and connection points to neighboring countries.

Besides of these measurements, absolute measurements are performed regularly (usually each month) in the METAS laboratory. Today, on most stations, 2-3 absolute measurements are available and all results are stored in the absolute gravity database of BKG and BGI (<https://agrav.bkg.bund.de>, currently in maintenance).

Relative Measurements for the LSN

Besides of the absolute stations (zero order network), the national gravity base network (LSN) is densified by about 500 relative stations (orders 1 – 3). Each year, around 2 weeks are invested for measurements in this network. Usually,

Scintrex CG-5 and CG-6 instruments are used. Figure 2.2 shows the LSN up to order 2 (out of 3) and the relative measurements performed between 2019 and 2022.

National Gravity Network LSN2004
relative measurements

December 2022

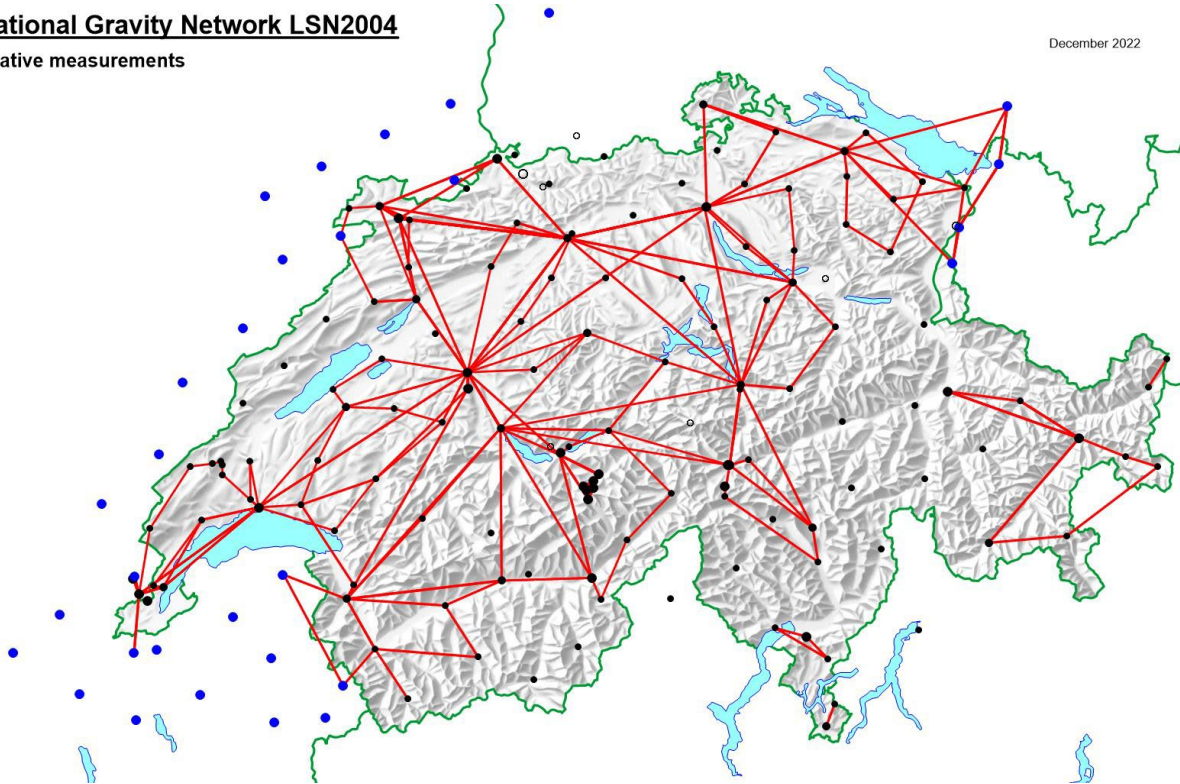


Figure 2.2: Points of the LSN (order 0 - 2) and the relative measurements performed in 2019-2022.

All the absolute and relative measurements of the LSN are evaluated in a common adjustment. In general, the RMS of the adjusted gravity value of an absolute station is better than 3 μGal , and the RMS of relative stations is better than 8 μGal . All the site descriptions and adjusted gravity values can be downloaded at the geoportal of the Swiss Confederation (<https://map.geo.admin.ch/>, layer “Gravimetric Base Network”).

On the calibration line Interlaken – Jungfrauoch, campaigns took place in 2020 and in 2022. The main purpose of the 2020 campaign was the calibration of the newly acquired CG-6 of swisstopo and in 2022, the new CG-6 of the University of Lausanne was calibrated for the first time.

Gravity measurements along the levelling lines

Along the levelling lines, gravity measurements are usually performed in the same year, as the levelling measurements. In flat areas, gravimetric measurements are performed about each km. In the mountains, the gravimetric measurements take place every 20-30 meters in height difference (gravity difference < 10 mGal). These measurements are used for the calculation of geopotential numbers, orthometric and normal heights.

Since 2018, gravity measurements are available along all of our 1st and 2nd order levelling lines (see Figure 2-3). The next goal is to replace all the old measurements of the 1950ies (green points in Figure 2.3). A big part of this goal could already be reached with the measurements of 2019 – 2022.

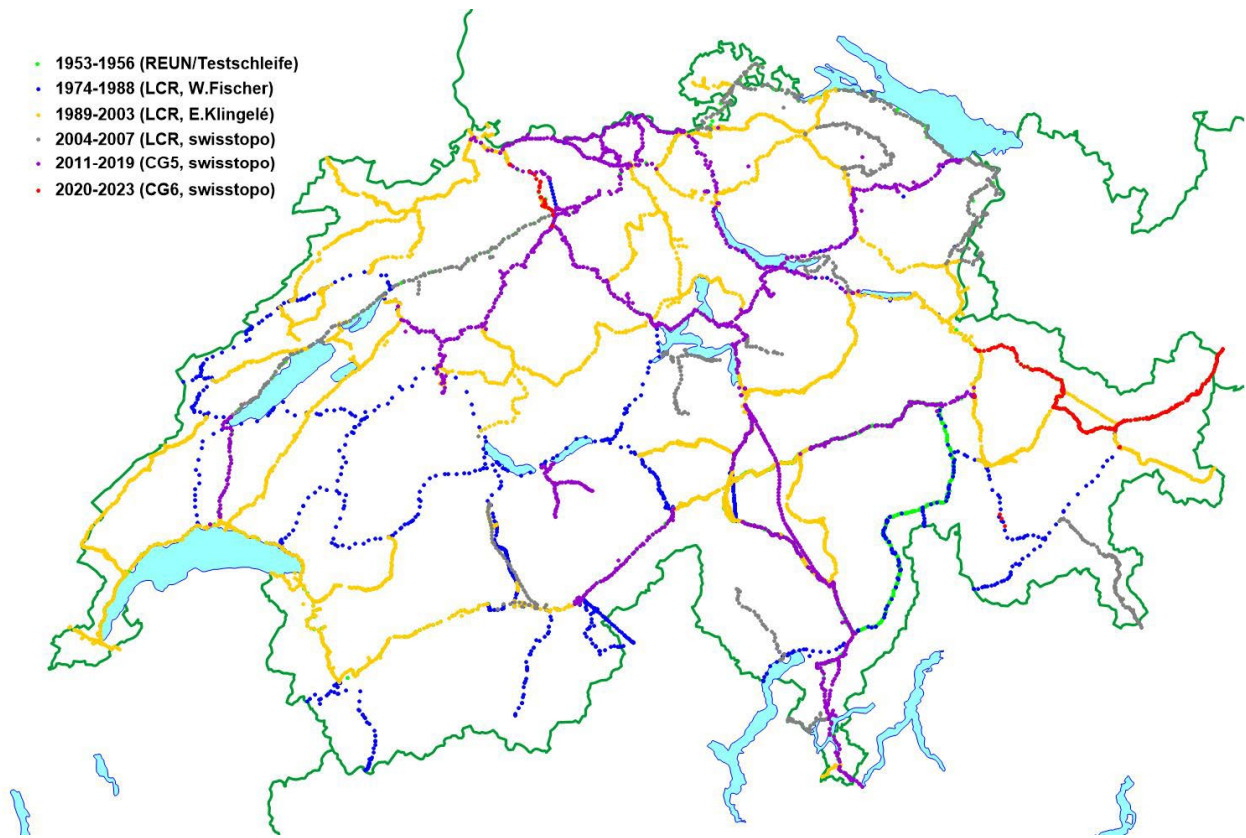


Figure 2.3: Gravity measurements along the levelling lines

Gravity measurements for geophysical projects and geoid determination

Swisstopo collects all the gravity measurements performed in Switzerland and maintains the national gravity database. These data are freely available on request and are mostly used for geophysical research and for geoid determination. The current state of the dataset is shown in Figure 2.4. Most of these points were collected by the University of Lausanne for the production of the Bouguer anomalies maps 1:100'000. Many points are as well the result of free data exchange with all our neighboring countries.

Some recent projects (2019-2022) for the densification of the dataset are the following:

- A geophysical project to model the quaternary structure in the region of Berne (University of Berne)
- A project to model the rock structure in the Bedretto valley (ETH Zurich)
- A profile above the Gotthard base tunnel to model the geology (University of Lausanne)
- Filling a data gap in the Stockhorn region (Bernese Oberland) for geoid modelling (swisstopo)
- A profile along the Julier pass for geoid investigations (ETH Zurich)
- Measurements in Northern Italy for the modelling of the Ivrea body (University of Lausanne)
- Filling a data gap for geoid modelling north-west of Annecy (France) (CERN)

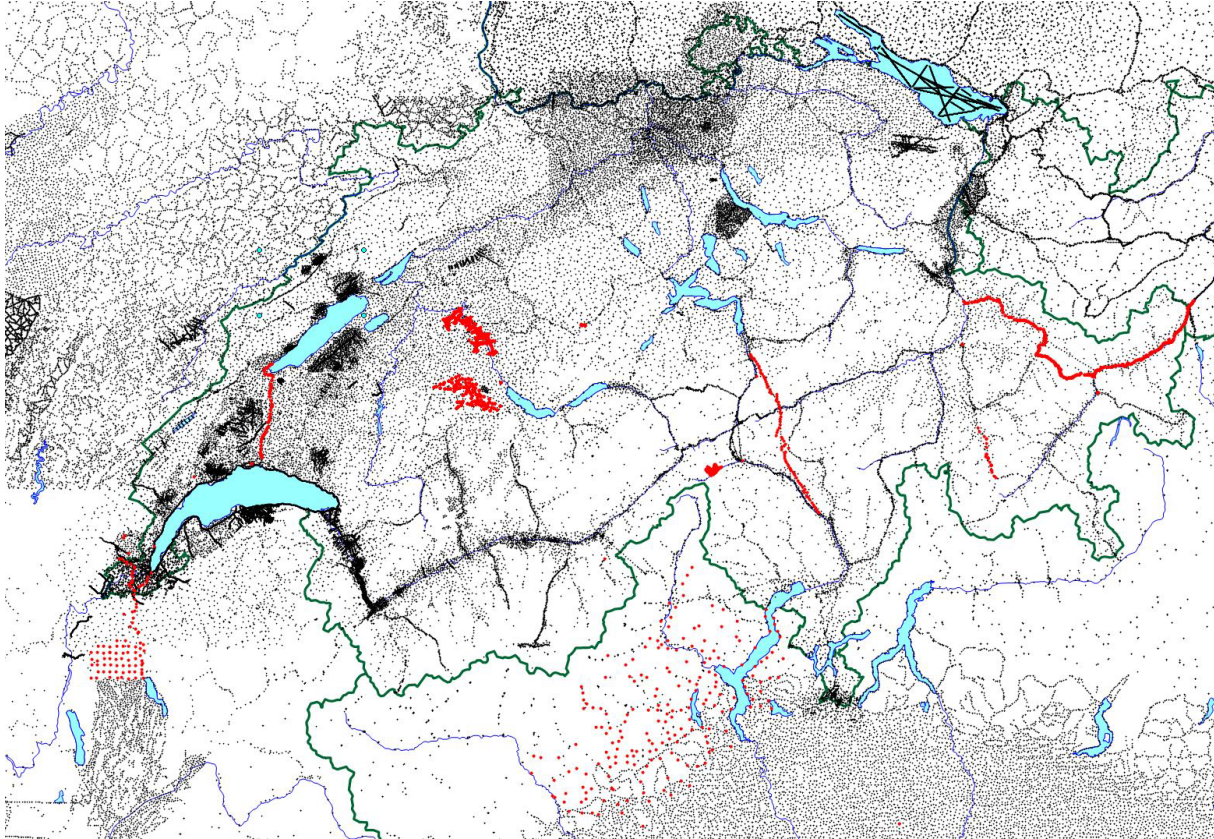


Figure 2.4: Swiss gravity database and measurements performed in 2019-2022 (in red)

Deviations of the Vertical measurements in Switzerland

D. Willi¹, J. Carell¹, U. Marti¹, S. Guillaume², S. Brossi³

¹ *Federal Office of Topography, swisstopo*

² *University of Applied Science Yverdon*

³ *mylab elektronik GmbH Bubikon*

Deflections of the vertical (DoV) measurements have a century long tradition in Switzerland. Until the advent of digital measurement technologies, the measurements were slow and tedious. Since the beginning of the 21st century, the use of charge-coupled device (CCD) sensors in zenith cameras has revolutionized the measurement of DoV (Hirt et al. 2010). The latest Swiss instrument is the Compact Digital Astrometric Camera (CODIAC), which was developed at ETH Zürich (Guillaume 2015). The camera and its components are depicted in Figure 2.5. The core of the system is the optical system composed of the telescope, the focuser and the CCD sensor with its mechanical shutter. Another key feature of CODIAC is the redundancy in the inclinometers. The zenith camera is equipped with two one-axis inclinometers of the Wyler type and two one-axis inclinometers of the Lippmann type. Therefore, two independent solutions can be computed. This is of particular interest, as both inclinometer types use different measurement principles and have different instrumental responses to small movements of the camera during the measurements. Not only is the averaged solution more robust, but the two inclinometer solutions also give an indication of precision.

Both CODIAC prototypes (the only two existing systems) were taken into service at swisstopo in 2019. The first productive campaign was conducted in 2020 with the measurement of some 30 DoV (see Figure 2.6). The measurement sites were selected in order to fill gaps in the existing DoV dataset. In future, it is planned to perform yearly a few weeks of measurements, in order to densify and update this dataset and to maintain the two instruments in operational condition. The DoV dataset is a precious input for geoid determination and validation. It is worthwhile noting that these measurements were the first productive measurements with CODIAC in Switzerland.

Commissioning of the cameras turned out to be more difficult than originally expected. Even though the cameras are very well designed and very well build, a certain level of experience is necessary to operate them in rough field conditions, on different heights, with varying temperature and by night. The processing pipeline had to be set-up at swisstopo and refined, in order to be integrated in swisstopo's IT-infrastructure.

Throughout 2021, the CODIAC zenith camera was used to measure an Astro-geodetic profile in the CERN region. More details on the Astro-geodetic profile are found in the corresponding article of the present report. The camera proved to be extremely reliable during this month-long measurement campaign. The whole profile could be acquired in one season, despite an unusual cloudy summer and despite travel restriction due to the SARS-CoV-2 pandemic (the profile is located on both sides of the Swiss-French border).

Other than CODIAC, the QDaedalus system was used to acquire DoV in Switzerland. QDaedalus is a theodolite-based system for astronomic observations. A more detailed description of the system is found for instance in Albayrak et al. (2022). In June 2021 an astrogeodetic profile was measured on the northern side of the Julierpass (Albayrak et al. 2021). It consists of 14 DoV acquired with QDaedalus and 2 DoV acquired with CODIAC.

Beside productive measurements, the CODIAC twin instruments are an unprecedented opportunity to investigate the precision of the measurements and the error sources. As a first test, parallel measurements with both instruments were performed during several nights in Zimmerwald. A first surprising result was an important drift in the east-west component of the measured deflections, whereas the north-south component showed a high stability (see Figure 2.7). A measurement of the shutter opening and closing delay under laboratory conditions revealed that the mechanical shutter opens and closes with a delay of up to 55 ms at temperatures below 10° C. Because of the Earth rotation of roughly 15 degrees per hour and at mid latitudes, a delay of 1 ms causes a bias of 0.01 arcsec in the Eta (east-west) component of the DoV.

In order to fix this timing issue, swisstopo launched an upgrade project for both zenith cameras, together with mylab elektronik GmbH. Nowadays, complementary metal-oxide-semiconductor (CMOS) imaging sensors with electronical global shutters fulfilling the requirements for astronomical observations are available. A first test observation with the CODIAC zenith camera was very promising. In the coming months, the CCD sensor will therefore be replaced by an CMOS sensor with an electronical shutter, making the mechanical shutter obsolete and increasing the timing accuracy of the images by several orders of magnitude. The updated instruments are expected to have the same accuracy on both components (Xi and Eta), making them one of the most accurate, if not the most accurate, zenith camera system ever built.



- Telescope with condensation shield
- Inclinometer «Wyller»
- CCD-sensor with shutter and focuser
- Inclinometer «Lippmann»
- Tuning screw for the inclinometer
- Servomotor
- Upper turntable
- Nylon foot
- Controller for the lower turntable
- Lower turntable step motor
- Base plate with turntable

Figure 2.5: Main parts of the digital zenith camera CODIAC (this camera is CODIAC “red”).

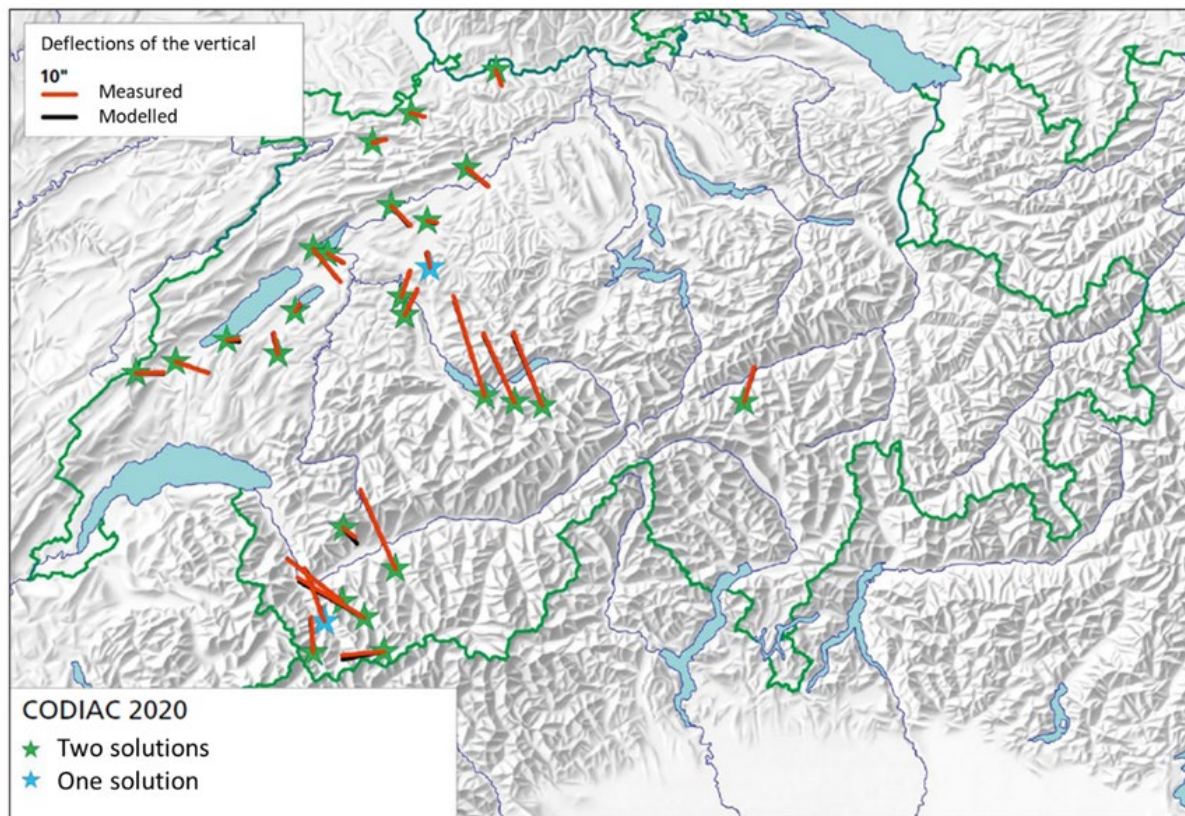


Figure 2.6: Results of the 2020 DoV campaign in Switzerland.

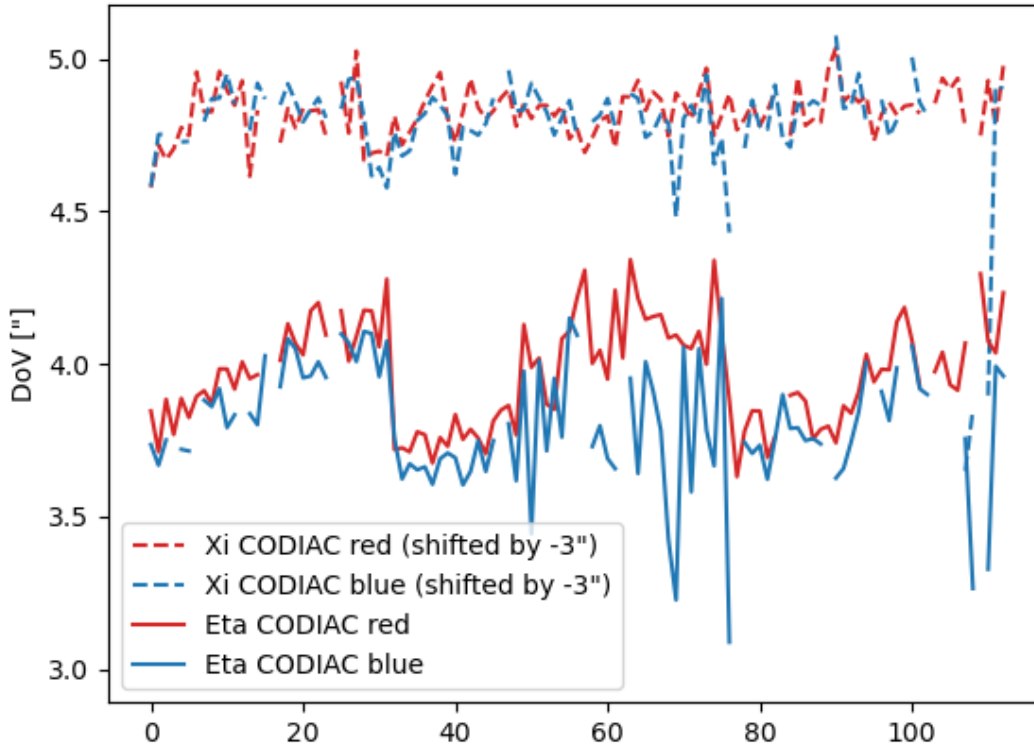


Figure 2.7: Measured DoV with both CODIAC systems (called “red” and “blue” because of the colours of the cameras) in Zimmerwald over three nights. The x-axis is the index over all measurements. The Xi (north-south) component is depicted on top, the Eta (east-west) component on bottom. The Eta component would be expected to have a very similar behaviour to the Xi component, which is obviously not the case. This effect can be explained by an opening and closing delay in the mechanical shutter of the CCD sensor.

Geoid Determination

U. Marti¹

¹ Federal Office of Topography, swisstopo

The activities for geoid determination were concentrated on two international projects. The determination of a DACH-geoid (“D-A-CH” stands for Germany, Austria and Switzerland) was a collaboration of swisstopo, BKG (Germany) and BEV (Austria). In a pilot study, a geoid model was calculated for the wider area of lake Constance. BKG and the TU Graz delivered independent solutions for the gravimetric quasigeoid. The differences of the two models in the core region was better than 5 cm, except for edge regions with missing data (Figure 2.8). The comparison with GNSS/levelling as well showed differences of usually smaller than 5 cm. A further goal of the project was the harmonization of datasets at the national borders and to provide transformation procedures for the national height systems with an accuracy of better than 1 cm. This resulted in a preliminary transformation service that was installed on the BKG website.

The main problems that remained in the determination of the geoid models are the treatment of the harmonic reduction in the calculation of the residual terrain correction and the correct modelling of the geoid to quasigeoid separation.

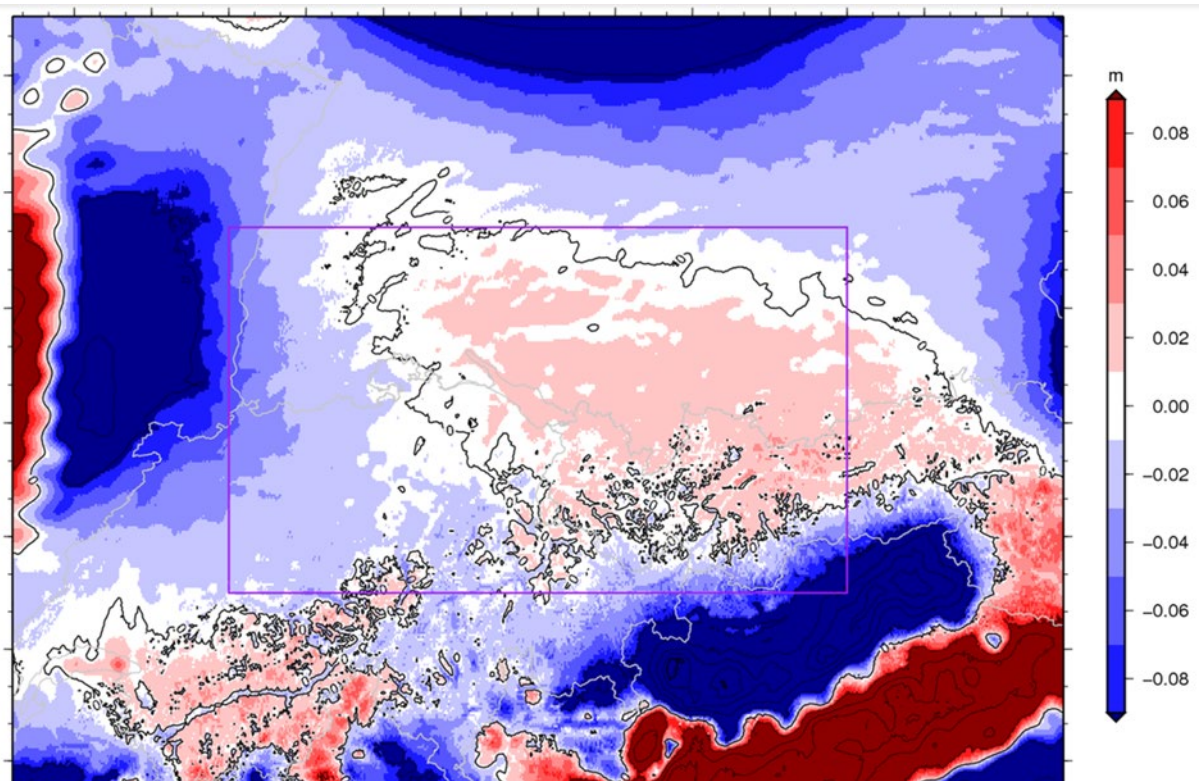


Figure 2.8: Differences of the BKG solution (FFT) minus TUG of the DACH geoid (after the elimination of an offset of 2 cm) (figure by BKG).

After the presentation of the results in the test area, it was decided to enlarge the project to the entire Alpine area. This led to a new Project “European Alpine Geoid” (EAlpG) and it was necessary to include more participating partners from France, Italy, Slovenia, Czechia, Slovakia and Hungary. A memorandum of Understanding for the participation and the free data exchange was signed by all partners in 2022. As a starting gravity dataset, the results of the AlpArray project (Zahorec et al. 2021) can be used. Besides of geoid and quasigeoid determination, the goal is again to provide

tools for height transformations between the national height systems and the European system EVRS (Figure 2.9). The first phase of this project was to collect the existing datasets (gravity, GNSS/levelling, Deflections of the vertical, DTMs).

Differences EVRF2019 (mean tide) – national height

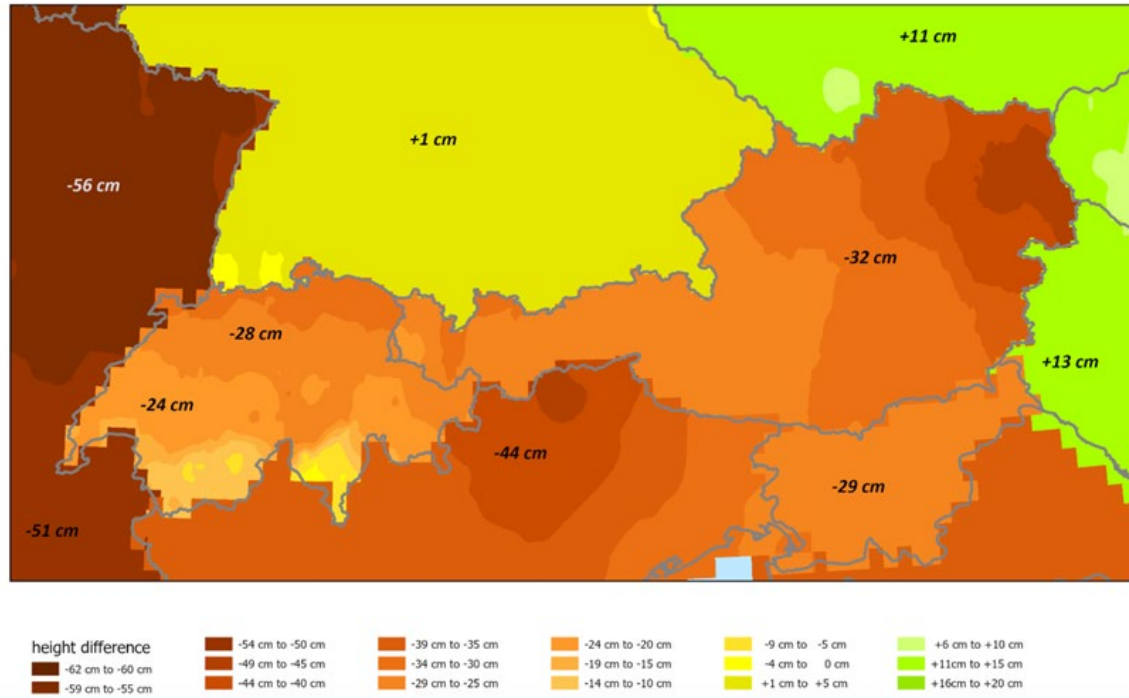


Figure 2.9: Height differences between EVRF2019 and National heights

The Swiss data was prepared at the end of 2022. Especially, the generation of a new GNSS/levelling dataset has to be mentioned (shown in Figure 2.10). A new complete adjustment of the Swiss levelling network (LHN) including all the data until 2022 was performed and the results of the GNSS campaign 2016 was used. Unfortunately, the results of the GNSS campaign 2022 could not be integrated yet. Nevertheless, this update allowed the integration of about 15 new GNSS-levelling stations – without counting the stations measured for the CERN profile.



Figure 2.10: GNSS-levelling stations of Switzerland

The geoid calculation software at swisstopo (QUAWIRK) was revised. Especially the gravity reduction and interpolation part were widely extended. The integration of the high resolution 2m-DTM (SwissAlti3D) and the correct treatment of the bathymetric models of Swiss lakes were reached.

Geoid validation dataset from profile measurement campaigns for the FCC at CERN

J.A. Koch¹, D. Willi², U. Marti², B. Soja¹, M. Rothacher¹

¹ *Institute of Geodesy and Photogrammetry, ETH Zurich*

² *Federal Office of Topography swisstopo*

The Large Hadron Collider (LHC), the biggest collider of its type, is reaching its conclusion by 2040. In the scope of initial studies for a post-LHC particle accelerator, the design and feasibility of the Future Circular Collider (FCC) at CERN, with a circumference of around 100 km, are studied until 2025/26. In the FCC-Geodesy project, which belongs to these initial studies, the reference network on the surface and in the tunnel is under development and a new high-precision geoid model for the significantly larger FCC area will be computed. The alignment of the magnets and thrusters in the tunnel requires a high-precision geoid with a precision of 30 μm over 225 m. Therefore, we established a 50 km long validation profile for the assessment of existing and more precise geoid models to be derived in the future for the region. This profile runs in a North-South direction through the area of interest and crosses the French-Swiss border twice. In several measurement campaigns in 2021 and 2022, measurements at a spacing of approximately 1 km along the profile were carried out collecting:

1. Astro-geodetic deflections of the vertical (DoV) with the CODIAC zenith camera with a spacing of 800 m,
2. spirit leveling for height determination, integrating available Swiss and French leveling results,
3. corresponding gravimetric measurements for the gravity adjustment, and
4. GNSS measurements during two sessions of about 24 hours on 36 semi-permanent points.

GNSS Observations

In October and December 2021, two measurement campaigns were carried out along the geodetic profile crossing the FCC area (see Figure 2.11). The measurements were conducted by personnel from CERN, ETH Zurich, and HEIG-VD. A total of 36 survey markers, located in the vicinity of the existing leveling benchmarks, which are part of the Swiss and French leveling network, were observed. Each point was observed during two independent sessions of 24 hours, with two different instrumental setups, using different antenna heights and different antenna and receiver types and manufacturers. The GNSS data was processed at ETH Zurich with the Bernese GNSS software developed by the Astronomical Institute of the University of Bern, resulting in state-of-the-art high accuracy 3D coordinates for every marker. The goal was to compute ellipsoidal heights of every leveling benchmark as accurately as possible, to derive the geoid-ellipsoid separation.

The initial results in January 2022 showed that the mean RMSE of the residuals of the coordinates in the Up component is 17.6 mm, thus the coordinates deviate by around 35 mm, since this is the deviation from a weighted average coordinate for each site. These discrepancies are too significant to use this set of coordinates as ground truth for the validation of the accuracy of geoid solutions to be computed in the further progress of this project. The most probable cause for the unexpectedly high deviations was found in the IGS antenna phase center offset and variation pattern of the Trimble R8 RTK-GNSS antenna. An antenna calibration, called ETHCal, was conducted on the rooftop of ETH Zurich using a robot of KUKA robotics, which is programmed for GNSS antenna calibrations, and an in-house analysis software. A clear difference between the results was discovered, especially for the ionosphere-free linear combination (L3), which was used in the GNSS processing chain to minimize the impact of the ionosphere on the coordinates. Using the new ETHCal calibration lowered the average RMSE of the residuals to 8.8 mm, and an additional antenna offset estimation for the Trimble R8 RTK-GNSS antenna in the Bernese GNSS software lowered the remaining RMSE of the residuals to 7.1 mm.

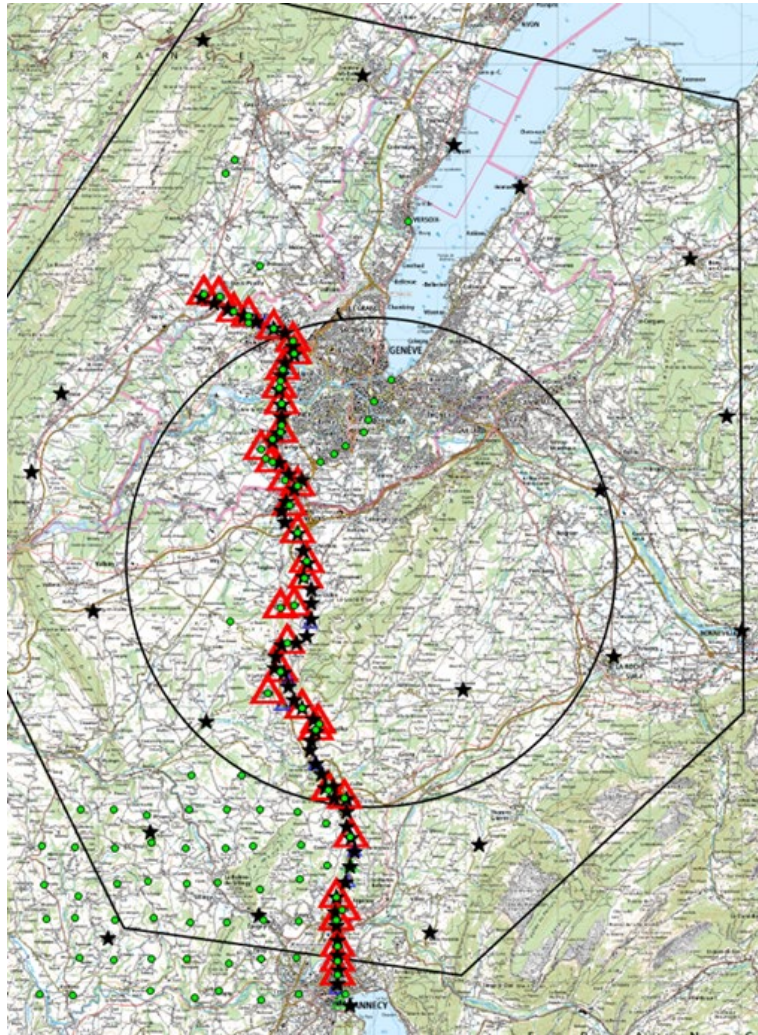


Figure 2.11: Location of the measurements along the profile. The black circle represents the approximate location of the FCC and the black polygon shows the wider area of interest of the project. Red triangles: GNSS-levelling points, green dots: relative gravimetry, black stars: DoV stations

Leveling and Gravimetric Observations

For the validation of geoid solutions with GNSS/leveling, measurements of GNSS, geodetic leveling and gravimetry must be available at the same locations. Since it was not possible to re-measure the whole leveling line, we had to rely on existing leveling data and only short paths between the GNSS/leveling station and the height benchmark were newly measured in May 2021. It was conducted by CERN with support of swisstopo and aimed at connecting the French and Swiss vertical networks on both sides of the border, from Saint-Julien-en-Genevois to Bernex. The purpose of these measurements was to remove a potential referencing bias between the systems, since each materialized network is separately maintained by its own national institute, i.e., IGN in France and swisstopo in Switzerland.

By fixing the height of the starting point in Bernex to its official value in the Swiss Height System, the differences to the heights of the benchmarks along the line until Lully can be calculated. All differences were below 1 mm, except for the benchmarks at a bridge in Lully, which deviated by 1.1 cm and 1.8 cm. Even the very old benchmarks in Certoux and Perly showed only minor differences of 1 and -3 mm, respectively.

A comparison of the official Swiss heights in Bernex with the official French heights shows an offset of 32.03 cm. In St. Julien, the mean difference is 31.2 cm. Since the points in Bernex are only connected to the French leveling network by GNSS/leveling, the offset determined from the comparison in St. Julien should be used as reference for future studies.

In April 2022, gravity measurements along the whole profile were performed by swisstopo using the Scintrex CG-6 (#248). The absolute gravity value at the Swiss National Gravity Network (LSN) station Prévessin in the CERN area was used as reference. No measurements had to be eliminated, since the vibrations that occurred sometimes at sites close to principal roads did not impact the results significantly. The adjustment of the data was done using swisstopo's program GRAVNET, which is used for the adjustment of the national gravity network of Switzerland too.

Astro-geodetic Observations

The measurements of the DoVs were conducted with the zenith camera CODIAC developed at ETH Zurich and now in use at swisstopo. In 15 nights, 61 stations were acquired with an average spacing of 791 m between adjacent stations along the profile.

The DoV processing was carried out with the software AURIGA, which uses the sky images acquired with CODIAC and the inclinometer measurements. The GNSS measurements obtained on board of CODIAC are only used to provide a precise time stamp for all observations. For the final computation of the DoVs, the geodetic positions were acquired using RTK-GNSS measurements relying on the swipos positioning service. The DoVs' results show a very good internal consistency.

The geoid profile solutions shown in Figure 2.12 have been obtained by least-squares collocation with correlation lengths between 1250 m and 2500 m, which were shown in a pre-study to lead to the most plausible, thus best, results. It must be noted, that DoVs do not provide absolute information, since only the slope of the geoid can be determined but no absolute values. Therefore, all solutions are fixed to zero geoid respectively quasi-geoid height at the beginning of the profile. The negative slope in the first part of the profile is very well modelled by the French and Swiss geoid models (RAF20 and CHGeo04, respectively), but the two global models (EGM2008 and XGM2019e) show some deficiencies, especially the EGM2008 model. In the second half of the profile a strong deviation of CHGeo04 is visible. This was to be expected since the Swiss geoid is fitted to the area of Switzerland and the full Southern part of the profile is on French territory. The difference between GNSS/leveling and the various geoid solutions derived from DoV shows only very small differences with respect to each other. The differences of the DoV solutions to the GNSS/leveling are within +4.5 cm and -2 cm for all models and no clear trend can be detected.

Conclusion and outlook

This geoid validation profile has an unprecedented density of measurements (especially DoVs) in this area and will serve as a fundament for the validation of any geoid model computed in the future. As the independent validation for geoid models is typically difficult to achieve, this work can be considered a crucial milestone in the establishment of very high accuracy geodetic references for the CERN-FCC project.

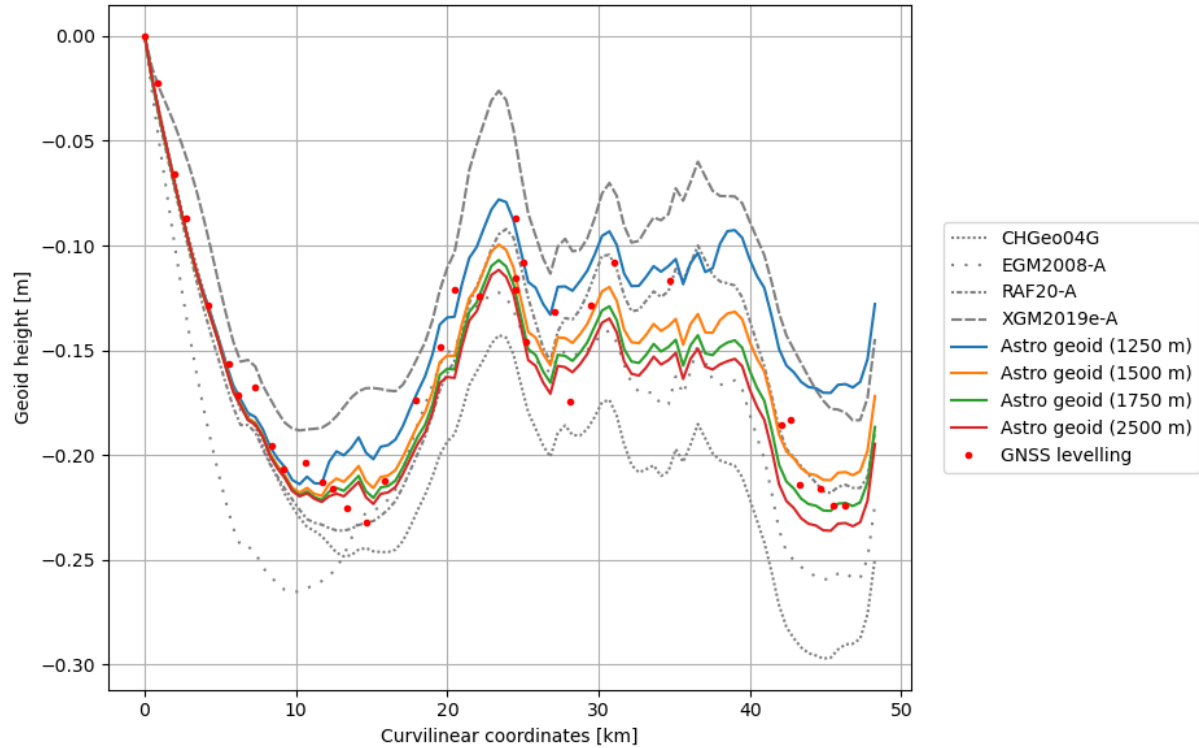


Figure 2.12: Geoid profiles obtained from Astro-geodetic observations with least-squares collocation using different correlation lengths between 1250 m (Astro geoid (1250 m)) and 2500 m (Astro geoid (2500 m)) compared with Swiss (CHGeo04G), French (RAF20-A) and global geoid models (EGM2008-A and XGM2019e-A) and with the GNSS-Levelling solution. All geoid models are offset to equal on the first value of the profile.

Combination Service for Time-Variable Gravity Fields (COST-G)

U. Meyer¹, M. Lasser¹, A. Jäggi¹

¹ Astronomical Institute, University of Bern

The Combination Service for Time-variable Gravity fields (COST-G), initiated by AIUB in the frame of the H2020 project EGSIM (see Swiss Nat. Report 2015-19, pp. 111-112) and transformed into a product center of the International Gravity Field Service (IGFS) under the umbrella of the IAG in 2019 (see Swiss Nat. Report 2015-19, pp. 113-114), continued its success story. With support by the H2020 project Global Gravity-based Groundwater product (G3P), successor to EGSIM under the lead of GFZ, the range of COST-G products (Meyer et al., 2020a; Teixeira da Encarnacao et al., 2019, 2020) has been complemented by the combination of monthly gravity fields derived from data of the GRACE-FO satellite mission (Meyer et al., 2020b,c). Since November 2020 the GRACE-FO combinations are generated on a regular basis and are distributed via the International Center for Global Earth models (ICGEM).

The COST-G combination scheme, developed for the monthly solutions derived from GRACE data, turned out to be not optimal for the GRACE-FO gravity fields. Differences in the high-order spherical harmonic (SH) coefficients, which are poorly determined from the along-track ranging observations (main observable of GRACE and GRACE-FO), led to a down-weighting of the ITSGGrace_operational time-series, not in accordance with the very favorable noise behavior of ITGS (Figure 2.13, bottom). By the exclusion of the high-order SH coefficients from the variance component estimation (VCE), applied for the COST-G combination on the solution level, relative weights much more consistent with the noise assessment could be achieved (Figure 2.13, top). The combined gravity fields based on the new weighting scheme outperform even the best of the individual contributions (Figure 2.13, bottom) and have been used for the derivation of the G3P groundwater product. With the availability of new time-series RL06.1 of monthly gravity fields from the GRACE-FO Science Data System (SDS), the official COST-G GRACE-FO combination is being continued as RL02 (Meyer et al., 2022b), exploiting the G3P-weighting scheme and the new AIUB time-series GRACE-FO RL02 and SDS RL06.1.

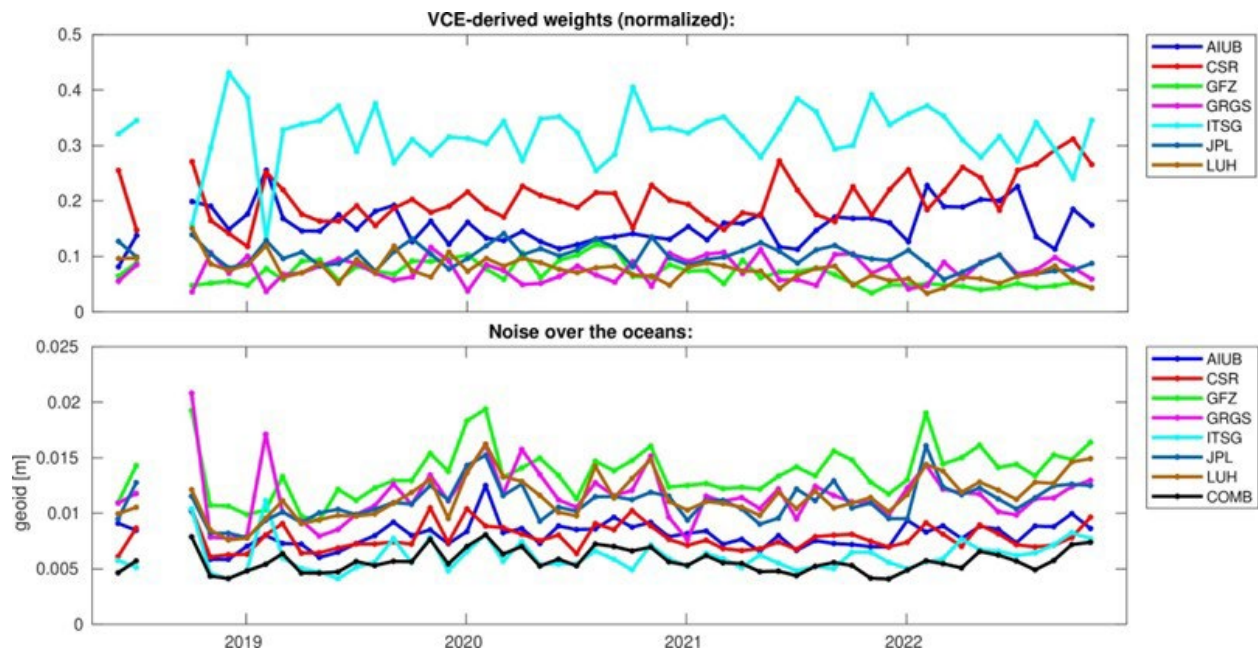


Figure 2.13: Relative weights (top) and noise assessment (bottom) of the monthly GRACE-FO gravity fields.

To formalize the extension of COST-G, a benchmark test was set up for the orbit and gravity field determination (Lasser et al., 2020) and the Institute of Geodesy of the Leibniz University Hannover (LUH) was accepted as a new GRACE-FO analysis center (AC) of COST-G, after successfully passing the test. Also a number of Chinese GRACE ACs announced their interest to join COST-G. A first validation of the Chinese time-series of monthly GRACE gravity fields yielded very promising results (Meyer et al., 2021) and an extension of the COST-G GRACE combination, including time-series from the Huazhong University of Science and Technology (HUST), the School of Geospatial Engineering and Science at the Sun Yat-sen University (APM), the Southern University of Science and Technology (SUS) and the Tongji University, Shanghai is under preparation (Figure 2.14, Meyer et al., 2022a).

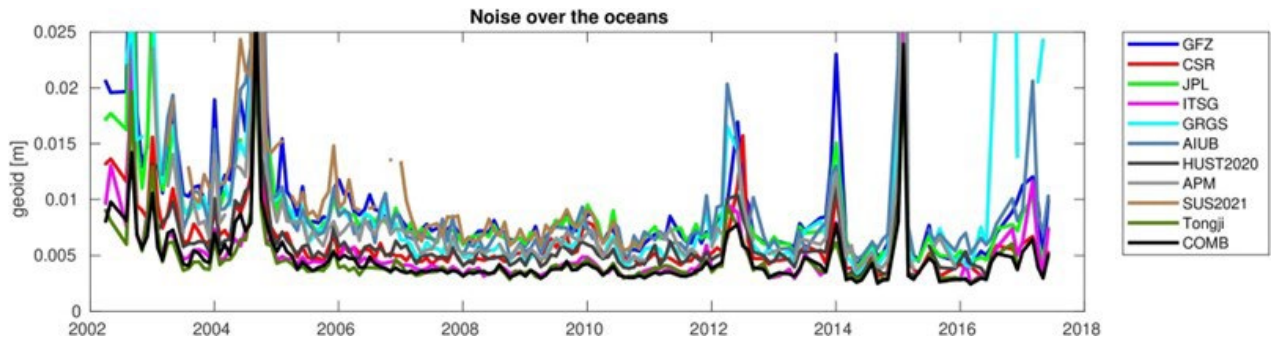


Figure 2.14: Test GRACE combination including four additional time-series from Chinese ACs.

The Earth's gravity field is the major force acting on satellites, with Low Earth Orbiters (LEOs) being sensitive also to the time-variations of the gravity field. Consequently, the monthly COST-G gravity fields are of interest for the precise orbit determination (POD) of LEOs. But the latency of 2-3 months prevents the direct use of the monthly gravity fields in operational LEO POD. In response to the user needs from the POD community a fitted signal model (FSM) was developed as a new COST-G product (Peter et al., 2022). Based on the monthly COST-G GRACE-FO combinations secular trends in the SH coefficients and periodic variations with annual and semiannual periods are determined and updated quarterly, always incorporating the newest GRACE-FO results.

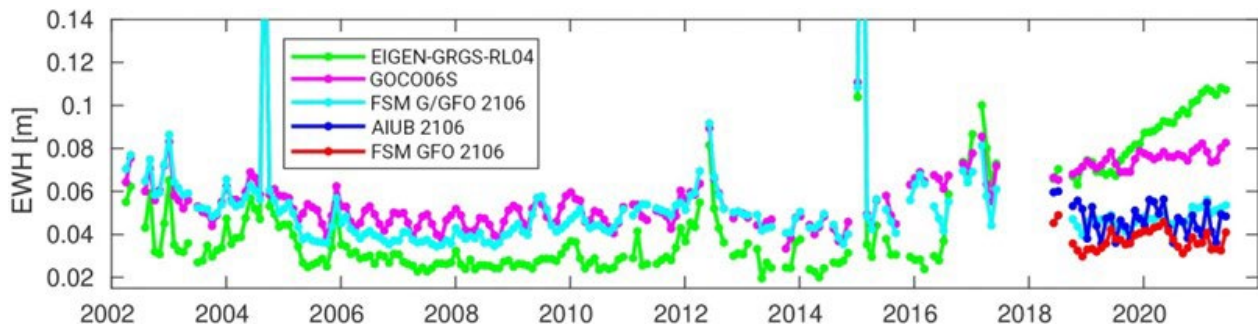


Figure 2.15: Monthly RMS of EWH differences (smoothed by a 300 km Gauss filter) to the GRACE and GRACE-FO gravity fields 04/2002 - 12/2022 over land areas.

In Figure 2.15 the COST-G FSM for the GRACE-FO period (red) is validated by direct comparison to the monthly gravity fields over the continents, where the major mass variations take place. For comparison the gravity models GOCO06S (magenta, Kvas et al., 2021), where time variations were co-estimated together with the static SH coefficients from a combination of GRACE, CHAMP, and satellite laser ranging (SLR) observations, EIGEN-GRGS-RL04 (green), where the time-variable part was fitted in yearly batches to the monthly GRGS gravity fields of the

GRACE period, and a FSM consisting of a single set of trend and periodic parameters fitted to the GRACE and GRACE-FO monthly COST-G gravity fields (cyan) are also evaluated. Obviously, a single set of trend and periodic parameters cannot describe the time-variations with the same accuracy like the multi-set fit of the EIGEN-GRGS model, which is currently the standard model for altimetry satellite POD, while for the GRACE-FO period the degradation of the GOCO06S and EIGEN-GRGS models due to the extrapolation is clearly visible. To also study the co-estimation of time-variations, which from a theoretical point would be preferable to the a posteriori fit of monthly solutions, a high-resolution static GRACE-FO gravity field with time-variable coefficients up to degree 96, comparable to the monthly gravity fields, was computed at AIUB (blue), but the validation revealed a slight overestimation of the semi-annual variation, probably caused by over-parametrization. Meanwhile, the COST-G GRACE-FO FSM was successfully tested for the POD of geodetic SLR satellites (Meyer et al., 2022b) and is considered for the routine POD of the International Laser Ranging Service (ILRS) and by the Copernicus POD Service.

Noise Modelling for GRACE Follow-On Observables in the Celestial Mechanics Approach

M. Lasser¹, U. Meyer¹, A. Jäggi¹

¹ *Astronomical Institute, University of Bern*

A key to understanding the dynamic system Earth in its current state is the continuous observation of its time-variable gravity field. The satellite missions Gravity Recovery And Climate Experiment [GRACE, Tapley et al., 2004] and its successor GRACE Follow-On [Landerer et al., 2020] take an exceptional position in sensing these time-variable components because of their unique observing concept [Wolff, 1969], which is based on ultra precise measurements of distance changes between a pair of satellites separated by a few hundred kilometres. These observations, together with a GPS-based positioning system and some auxiliary measurements, e.g., of the satellites' attitude and of onboard accelerometers, allow for a modelling of the Earth's gravity field, typically on a basis of monthly snapshots.

One of the key components of any model is the accurate specification of its quality. The correct characterisation of noise in the data helps to retain the full signal content and separates signal from noise through a modelling of the latter - provided that the signal component is also adequately modelled. In temporal gravity field modelling from GRACE Follow-On data, one has to cope with several noise sources, which are contaminating not only the measurements itself but also the observation equations via mis-modellings in the underlying background force models. When employing the Celestial Mechanics Approach [CMA, Beutler, 2005], developed at the Astronomical Institute of the University of Bern (AIUB), for gravity field modelling from satellite data a Least-Squares Adjustment (LSQA) is performed to compute monthly models of the Earth's gravity field. However, as a consequence of the various contaminations with noise, the jointly estimated formal errors usually do not reflect the error level that could be expected but provides much lower error estimates.

Addressing the problem of noise contamination from the point of the GRACE Follow-On satellite mission's observations, we incorporate noise models derived from post-fit residuals of an initial joint orbit and gravity field estimation into the CMA, following the approach from Ellmer [2018]. The derivation and application of empirical noise models obtained from post-fit residuals between the final GRACE Follow-On orbits, that are co-estimated together with the gravity field, and the observations, expressed in position residuals to the kinematic positions and in the inter-satellite link range-rate residuals, considers the post-fit residuals \hat{e} to be an univariate time series, hence, only being correlated over time. We assume that a (weak) stationary process underlies and characterises the stochastic behaviour of the residuals. As a consequence, a covariance function computed by auto-correlation fully describes this process. Such a covariance function for a certain time interval Δt_k may be estimated by

$$\hat{C}_{rr}(\Delta t_k) = \frac{1}{N} \sum_{n=1}^{N-k} \hat{e}(t_{n+k})\hat{e}(t_n) \quad \text{with} \quad k \in \{0, \dots, K\} \quad (1)$$

where K defines the maximum lag [see e.g., Etten, 2005]. A covariance matrix based on the covariance function may be set up with Eq. 2, which leads to a symmetric matrix in Toeplitz structure

$$\hat{C}_{ee}^{rr} = \begin{bmatrix} \hat{C}_{rr}(\Delta t_0) & \hat{C}_{rr}(\Delta t_1) & \hat{C}_{rr}(\Delta t_2) & \cdots & \hat{C}_{rr}(\Delta t_K) \\ \hat{C}_{rr}(\Delta t_1) & \hat{C}_{rr}(\Delta t_0) & \hat{C}_{rr}(\Delta t_1) & \cdots & \hat{C}_{rr}(\Delta t_{K-1}) \\ \hat{C}_{rr}(\Delta t_2) & \hat{C}_{rr}(\Delta t_1) & \hat{C}_{rr}(\Delta t_0) & \cdots & \hat{C}_{rr}(\Delta t_{K-2}) \\ \vdots & \vdots & \vdots & \ddots & \vdots \\ \hat{C}_{rr}(\Delta t_K) & \hat{C}_{rr}(\Delta t_{K-1}) & \hat{C}_{rr}(\Delta t_{K-2}) & \cdots & \hat{C}_{rr}(\Delta t_0) \end{bmatrix} \quad (2)$$

The relation between the covariance matrix set up in Eq. 2 and the weight matrix P introduced into the LSQA may be established by

$$P \triangleq \sigma_0^2 (\hat{C}_{ee}^{rr})^{-1}. \quad (3)$$

The dependency on the a priori gravity field is mitigated to the extent possible by estimating an independent gravity field solution first and by computing the covariance function from post-fit residuals. The interdependency between the orbit parametrisation and the shape of the residuals, however, strongly impacts the basic assumption of stationarity. Any parameter set up to compensate for remaining signal in the system (be it noise or sought-after gravity field signal) leads to a flatter spectrum of the residuals and a smaller amount of noise to be compensated by the empirically determined covariances which are only accounting for (stationary) stochastic noise on the level of observation weighting. Thus, it is advisable to treat systematic and non-stationary signal either with co-estimated parameters and/or an accurate a priori stochastic model [see e.g., Ellmer, 2018, Kvas and Mayer-Gürr, 2019].

In our processing we consider a correlation length of three hours which is about two orbital revolutions of the satellites and an empirical model is derived for kinematic positions K-band range-rate (KBRR) observations. The empirical noise models shift the magnitude of the formal errors to a more 'realistic' level and change their shape when being compared to the solution without empirical noise modelling (labelled as *op*), now featuring the resonance orders (see Figure 2.16b) and closely follow the difference degree amplitudes in the mid-degrees (Figure 2.16a). The small bend in the high degrees is an indication that more information from the high degrees of the static background gravity field went into the solution with empirical noise modelling than in the classical solution without empirical noise modelling.

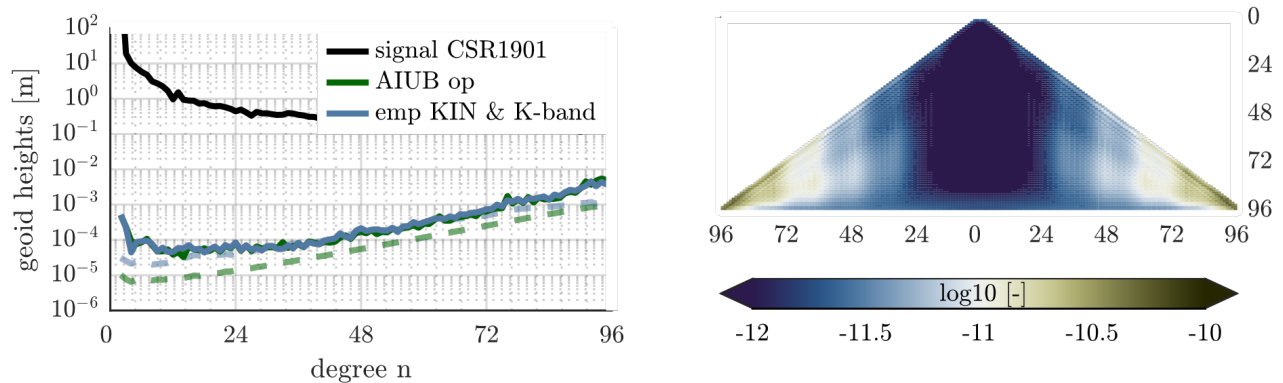


Figure 2.16: Difference degree amplitudes for January 2019 with respect to a solution from CSR for the same month for a solution without (*op*) and with empirical noise modelling (*emp*). The formal errors of the latter become much more realistic when being compared with the reference of CSR. Triangle of coefficients for the formal errors of a solution with empirical noise modelling for kinematic positions and KBRR (*b*), where the stripe pattern due to the resonance orders became visible.

Applying the empirical modelling for longer time spans shows that the RMS over the oceans, a means which should reflect the quality of the solution since little-to-no variations are to be expected, can be significantly lowered (Figure 2.17), indicating that this modelling technique is capable of absorbing noise. The other two solutions from the CSR [Center for Space Research, Save, 2019] at The University of Texas at Austin and the TUG [Technical University of Graz, Mayer-Gürr et al., 2018] may serve as a reference for this quality indicator. The latter also applies a sophisticated empirical noise modelling approach from post-fit residuals, see Ellmer [2018], whereas the CSR solutions are commonly used as gold standard for temporal gravity fields from GRACE and GRACE Follow-On. Our solutions with empirical noise modelling perform very well with this metric, being 87.5% of the time lower than the ones from CSR. Thus, we conclude that adapting the stochastic model of the observations based on the information contained in the post-fit residuals is beneficial to suppress noise leaking into monthly gravity field solution from GRACE Follow-On data.

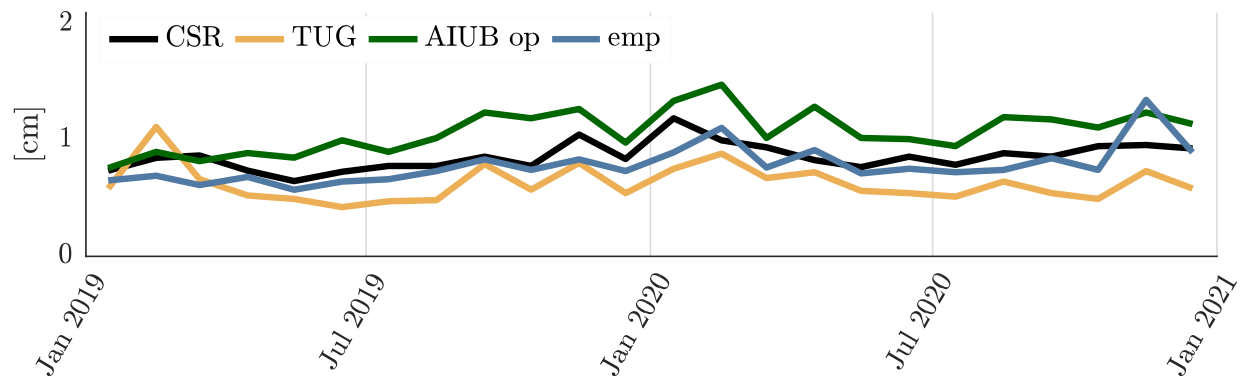


Figure 2.17: RMS over the oceans for two years of GRACE Follow-On comparing the TUG and CSR solutions to a solution from AIUB without (op) and with empirical noise modelling (emp) based on the post-fit residuals.

AIUB contribution to the Global Gravity-based Groundwater Product (G3P)

A. Jäggi¹, N. Darbeheshti¹, M. Lasser¹, U. Meyer¹, A. Güntner²

¹ Astronomical Institute, University of Bern

² GeoForschungsZentrum Potsdam

Groundwater is one of the most important freshwater resources for mankind and for ecosystems. Assessing groundwater resources and developing sustainable water management plans based on this resource is a major field of activity for science, water authorities and consultancies worldwide. Due to its fundamental role in the Earth's water and energy cycles, groundwater has been declared as an Essential Climate Variable (ECV) by the Global Climate Observing System (GCOS). The G3P consortium combines key expertise from science and industry across Europe that optimally allows to capitalize from the unique capability of GRACE and GRACE-FO satellite gravimetry as the only remote sensing technology to monitor subsurface mass variations, addressed as Terrestrial Water Storage (TWS) variations. Groundwater storage change for large areas may then be obtained from TWS variations by subtracting the different storage compartments of the water cycle (Figure 2.18) provided by the portfolio of the Copernicus Services.

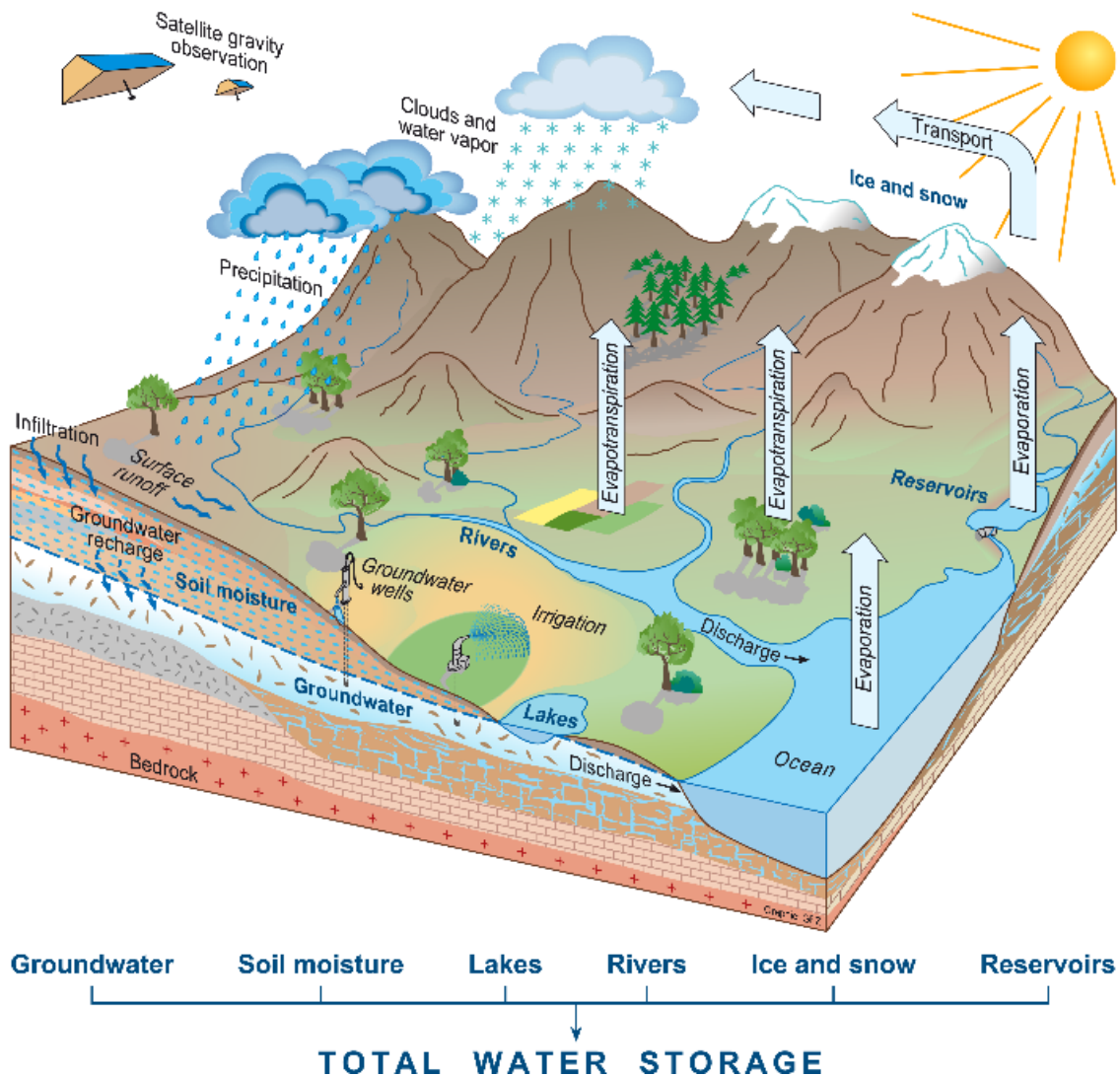


Figure 2.18: General Water storage in the vicinity of the Earth's surface (Copyright GFZ).

The Astronomical Institute of the University of Bern (AIUB) led work package 2 of the G3P project, which aimed at providing global TWS maps. This required the project partners GeoForschungsZentrum Potsdam (GFZ), Technische Universität Graz (TUG) and AIUB to compute monthly gravity fields of the Earth from observations of the GRACE and GRACE-FO satellite missions. Specifically, AIUB has provided improved GRACE monthly fields from the last years (2011-2017) observations of the GRACE mission, which are difficult to process due to numerous instrument artifacts. In addition, it has computed a completely revised time series of monthly gravity field solutions for the GRACE-FO mission period (as of June 2018), based on empirical error modeling and now benefiting from automated screening methods based on it.

The monthly gravity fields from all analysis centers were validated and combined as part of the Combination Service for Time-variable Gravity fields (COST-G), also led by AIUB. The combined global gravity field models form the basis of the monthly maps of the TWS calculated from them, from which the target groundwater was derived by reducing the compartments such as surface water, glacier ice, snow cover and soil moisture, which were also quantified within the G3P project. In addition to the individual elements of the hydrological cycle, the uncertainties of the individual compartments, which are important for further interpretation, were also determined. The resulting monthly groundwater storage anomaly (GWSA) maps are available with a spatial resolution of 0.5 degrees in NetCDF format via the GravIS portal for the international user community: <http://gravis.gfz-potsdam.de/gws>. The gain in accuracy achieved by revising the satellite gravimetric observations and combining them can be seen in the improvement in the signal-to-noise ratio for the Earth's large river basins (Figure 2.19).

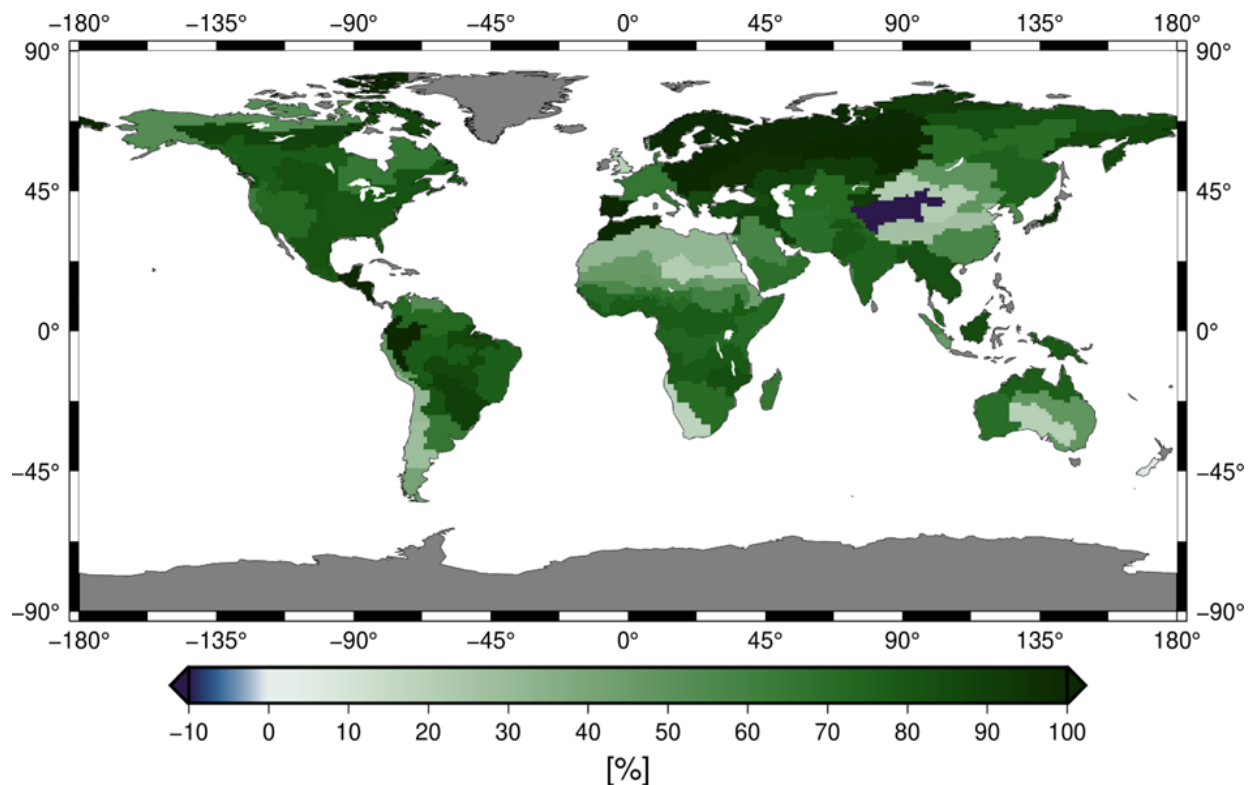


Figure 2.19: Improvement of signal-to-noise ratios (in percent) in large river basins.

Simulation Study for Geodetic Parameter Recovery at Europa and Callisto

W. Desprats¹, D. Arnold¹, A. Jäggi¹

¹ *Astronomical Institute, University of Bern*

There is an extensive interest in the Jovian moons exploration as reflected by planned missions to visit them, e.g., JUICE, Europa Clipper, Tianwen-4 (China National Space Administration), or mission proposals such as the Joint Europa Mission (Blanc et al. 2020) and MAGIC (Magnetics, Altimetry, Gravity, and Imaging of Callisto). Recovering geodetic parameters such as gravity field, k_2 tidal Love number, and rotation and orientation parameters allows to constrain internal structure models of the Galilean moons, including the characterization of potential subsurface oceans.

Using a development version of the Bernese GNSS Software (BSW, Dach et al., 2015), we have performed closed-loop simulations of realistic range-rate (2-way Doppler) and accelerometer data of high-inclination and low-altitude orbiters around Callisto and Europa, which we then have used for the recovery of the spacecraft orbits and of the geodetic parameters of the two Galilean moons. We have considered Repetitive Ground Track Orbits (RGTO) between 100km and 200km for mission durations of 3 months, allowing for a proper definition of the ground track coverage on the surface of each moon.

Influence of Low Orbit Design

Because external constraints from mission design can influence the choice of potential science orbits, a careful analysis of the suitability of certain orbits for the recovery of global geodetic parameters is essential. In the case of Europa, we have systematically compared solutions based on different input orbital parameters and we have quantified their impact on the gravity field recovery process, which is of great importance for future mission designs.

We studied the influence of the altitude and of the inclination of the orbit, but also the distribution of ground tracks and the orientation of the orbital plane with respect to the Earth direction (characterized by the angle β_{Earth}). Figure 2.20 shows the benefit of an edge-on orbit (with low β_{Earth}) for the low-degrees of the gravity field, but higher β_{Earth} angles improve the ground coverage (thus the higher degrees) at the expense of gravity signal global sensitivity.

Our best-case scenario shows that the gravity field can be estimated up to degree and order 72 after 3 months in a circular polar orbit at 100 km over Europa's surface (Desprats et al, 2023).

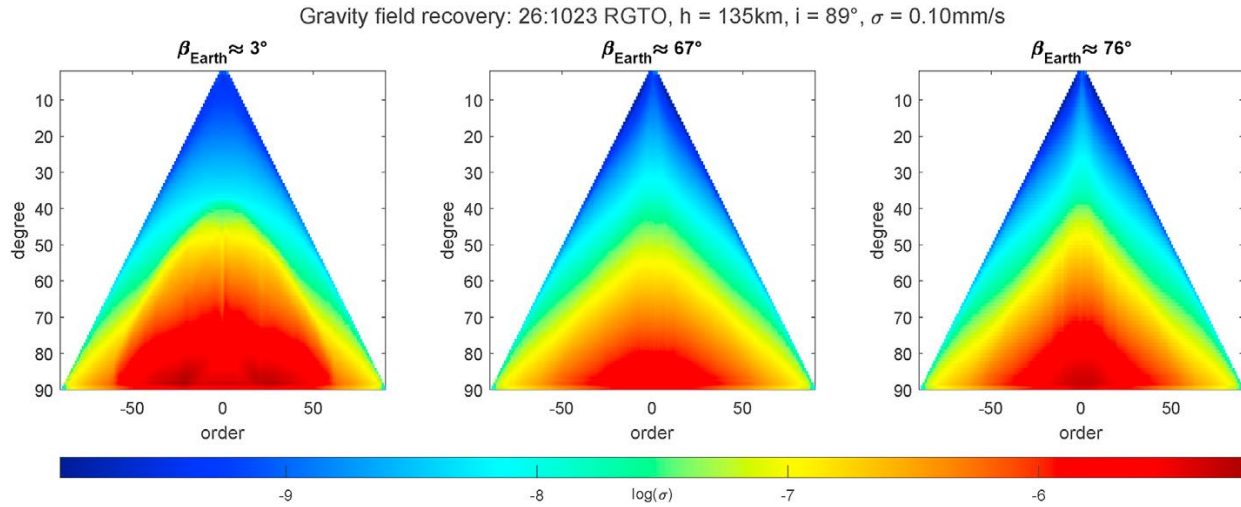


Figure 2.20: Formal errors of Europa's gravity field harmonics for different orientations of the orbital plane with respect to the Earth.

Gravity field recovery strategies

The gravity fields of the Galilean moons have been recovered only up to degree and order 2 from Galileo flybys (Anderson et al, 1998, 2001). The estimation of coefficients up to degree and order 90 can be challenging using only so limited a priori information. We propose and evaluate two strategies to estimate a full gravity field solution starting from only d/o 2. We either use pseudo-stochastic pulses (i.e., instantaneous velocity changes) to cope with the large model deficiencies, or co-estimate low-degree gravity field coefficients and orbit parameters to bootstrap the estimation process.

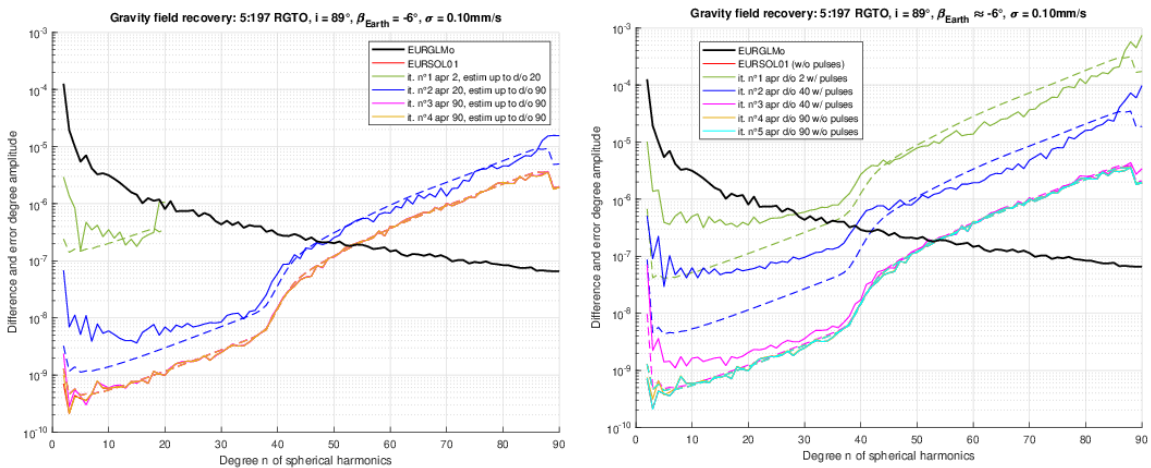


Figure 2.21: Difference degree amplitudes w.r.t. EURGLMo (synthetic Europa gravity field) of solutions iterated from d/o only using pseudo-stochastic pulses, loosely constrained at first (left) or co-estimating the low-degree coefficients with the other orbital parameters in the first iteration (right).

These processes require several iterations, but in both cases, final gravity field solutions are very close to the solution EURSOL01, when a true gravity field is considered as a priori (see Figure 2.21).

Non-gravitational acceleration mitigation

Non-gravitational accelerations (NGA) can be difficult to model. In the case of Callisto, we have considered solar and planetary radiation pressure which for a JUICE-like orbit would reach up to 15nm/s^2 . We have evaluated several ways to mitigate the mismodeling of these non-gravitational accelerations:

- Using realistic accelerometer data (white noise and biases in 3 directions)
- Pseudo-stochastic pulses (every 80min = $\frac{1}{2}$ orbital period)
- 1 Cycle-Per-Revolution acceleration in 3 directions and one bias in cross-track direction

Pseudo-stochastic pulses are very efficient to reduce the Doppler residuals, but they have a negative impact on the orbit (see Figure 2.22) and on the low degree of the gravity field. Empirical accelerations are a good compromise in case no accelerometer data is available. In both cases, the estimation of biases (10nm/s^2 for state-of-the-art accelerometer) proved to be challenging. This can be explained by the low magnitude of the considered NGA, and we had to consider constant biases every Callisto day = 16,7 Earth days.

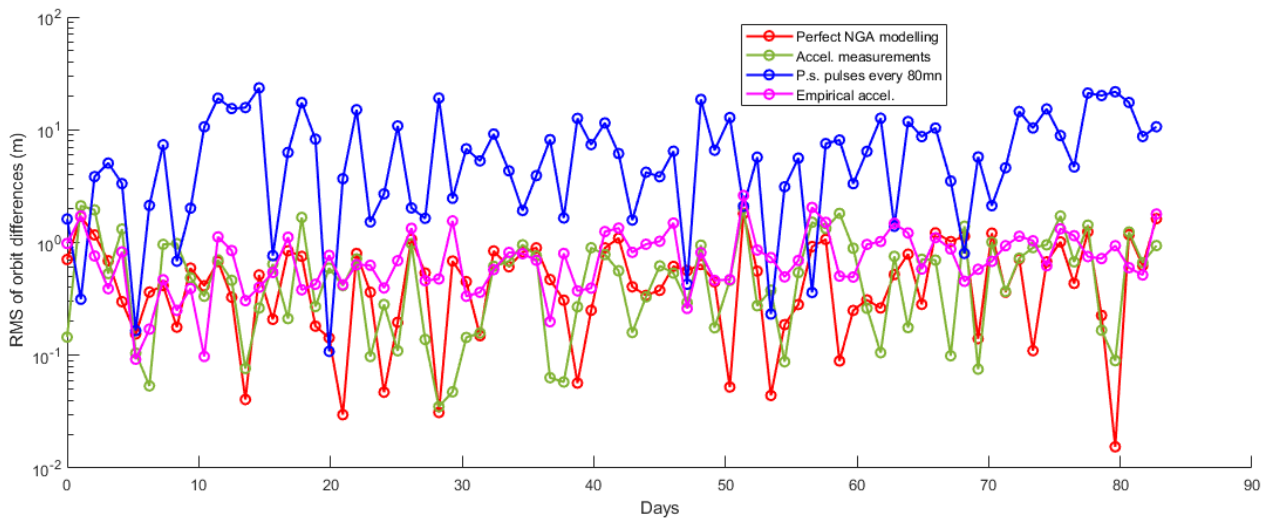


Figure 2.22: RMS of orbit differences for several mitigation strategies around Callisto.

Orientation and Rotation parameters estimation

In addition to the gravity field, we have investigated to estimate orientation and rotation parameters of planetary bodies (e.g., Callisto) from Doppler data only. Table 2.1 summarizes the accuracy to which we could recover these parameters from a $200 \times 200\text{km}$ polar orbit, using 2-way Doppler data from the Chinese Deep Space Network (one station operating in X-band and the two other operating in Ka-band).

	Nominal value	Difference
k_2 Love number	0.3	$3.7 \cdot 10^{-4}$
Right Ascension of the pole	268.7 deg	0.15 mdeg
Declination of the pole	64.83 deg	0.015 mdeg
Angular velocity	21.57 deg/day	0.13 μ deg/day
Main longitudinal libration amplitude	0 deg	13 μ deg
\bar{C}_{20}	$-1.462 \cdot 10^{-5}$	$2.97 \cdot 10^{-9}$
\bar{C}_{22}	$-1.580 \cdot 10^{-5}$	$5.33 \cdot 10^{-9}$

Table 2.1: Subset of unconstrained estimated geodetic parameters of Callisto.

TABLE OF CONTENTS

Bibliography Commission 2

- Albayrak, M., Willi, D., Guillaume, S., Herrera Pinzón, I., Müller, L., Marti, U., Hirt, Ch. (2021): Validation of GGMplus and CHGeo2004 Using Observed Deflection of the Vertical Data from QDaedalus and CODIAC Systems in the Mountainous Terrain of the Surses Region, Switzerland. AGU Fall Meeting 2021, New Orleans, Louisiana, USA.
- Albayrak, M., Willi, D., Guillaume, S. (2022): Field comparison of the total station-based QDaedalus and the zenith telescope-based CODIAC astrogeodetic systems for measurements of the deflection of the vertical. *Survey Review* 55(390): 247-259.
- Anderson, J., Schubert, G., Jacobson, R., Lau, E., Moore, W., Sjogren, W. (1998): Europa's Differentiated Internal Structure: Inferences from Four Galileo Encounters. *Science*, 281(5385), 2019-2022.
- Anderson, J., Jacobson, R., McElrath, T., Moore, W., Schubert, G., Thomas, P. (2001): Shape, mean radius, gravity field, and interior structure of Callisto. *Icarus*, 153(1):157–161.
- Bandou D., Schlunegger, F., Kissling, E., Marti, U., Schwenk, M., Schläfi, P., Douillet, G., Mair, D. (2021): Three-dimensional gravity modelling of a Quaternary overdeepening fill in the Bern area of Switzerland discloses two stages of glacial carving. *Nature. Scientific Reports* Vol. 12 pp 1-14. DOI:10.1038/s41598-022-04830-x.
- Beutler, G. (2005): *Methods of Celestial Mechanics*. Springer, Berlin-Heidelberg, Germany. ISBN 978-3642-10529-6.
- Blanc, M., Prieto-Ballesteros, O., André, N., Gómez-Elvira, J., Jones, G., Sterken, V., ... , Wurz, P. (2020): Joint Europa Mission (JEM): a multi-scale study of Europa to characterize its habitability and search for extant life. *Planetary and Space Science*, 193, 104960.
- Dach, R., Lutz, S., Walser, P., Fridez, P., editors (2015): *Bernese GNSS Software, Version 5.2*. Astronomical Institute, University of Bern, Bern, Switzerland, ISBN 978-3-906813-05-9. DOI:10.7892/boris.72297. User manual.
- Desprats, W., Bertone, S., Arnold, D., Jäggi, A., Blanc, M. (2023): Influence of low orbit design and strategies for gravity field recovery of Europa. *Planetary and Space Science*, 105631, DOI:10.1016/j.pss.2022.105631
- Ellmer, M. (2018): *Contributions to GRACE Gravity Field Recovery: Improvements in Dynamic Orbit Integration Stochastic Modelling of the Antenna Offset Correction, and Co-Estimation of Satellite Orientations*. PhD thesis, Graz University of Technology, In Monographic Series TU Graz, number 1, Verlag der Technischen Universität Graz, Graz, Austria.
- v. Etten, W. (2005): *Introduction to Random Signals and Noise*. John Wiley & Sons, New York, NY, USA. ISBN 978-0-470-02411-9. 1
- Guillaume, S. (2015): *Determination of a Precise Gravity Field for the CLIC Feasibility Studies*. *Geodätisch-geophysikalische Arbeiten in der Schweiz*, Volume 94. Swiss Geodetic Commission, Zurich. ISBN 978-3-908440-40-6.
- Güntner, A., Sharifi, E., Behzadpour, S., Boergens, E., Dahle, C., Darbeheshti, N.; Dobsław, H., Dorigo, W., Dussailant, I., Flechtner, F., Haas, J., Jäggi, A., Kidd, R., Kosmale, M., Kvas, A., Luojus, K., Mayer-Gürr, T., Meyer, U., Pasik, A., Paul, F., Pedinotti, V., Preimesberger, W., Ruz Vargas, C., Vayre, M., Zemp, M. (2023): *Global Gravity-based Groundwater Product (G3P)*. V. 1.11. GFZ Data Services, DOI:10.5880/G3P.2023.001.
- Hirt, C., Bürki, B., Somieski, A., Seeber, G. (2010): Modern Determination of vertical deflections using digital zenith cameras. *Journal Surveying Engineering* 136(1), Feb 2010, 1-12. DOI:10.1061/_ASCE_SU.1943-5428.0000009.
- Koch, J., Marti, U., Rothacher, M., Willi, D. (2022); High-precision Profile for Geoid Validation in the FCC Region at CERN. Poster presentation at GGHS 2022 Symposium, Austin, 12-14 September, <https://www.csr.utexas.edu/gghs2022/gghs-2022-program/posters/>, <https://www.researchcollection.ethz.ch/handle/20.500.11850/571609>.

- Koch, J., Rothacher, M., Marti, U., Willi, D. (2022): Gravity field modeling. Presentation at FCC Week, May 30 – June 3, Paris, <https://indico.cern.ch/event/1064327/contributions/4883205/>
- Kvas, A., Brockmann, J.M., Krauss, S., Schubert, T., Gruber, T., Meyer, U., Mayer-Gürr, T., Schuh, W.-D., Jäggi, A., Pail, R. (2021): GOCCO06s – a satellite-only global gravity field model. *Earth Syst. Sci. Data* 13, 99–118, DOI:10.5194/essd-13-99-2021
- Kvas, A., Mayer-Gürr, T. (2019): Grace gravity field recovery with background model uncertainties. *Journal of Geodesy*, 93(12):2543–2552, 2019. ISSN 1432-1394. DOI:10.1007/s00190-019-01314-1. 2
- Landerer, F.W., Flechtner, F.M., Save, H., Webb, F. H., Bandikova, T., Bertiger, W.I., Bettadpur, S.V., Byun, S.H., Dahle, C., Dobslaw, H., Fahnestock, E., Harvey, N., Kang, Z., Kruizinga, G.L.H., Loomis, B.D., McCullough, C., Murböck, M., Nagel, P., Paik, M., Pie, N., Poole, S., Strelakov, D., Tamisiea, M.E., Wang, F., Watkins, M.M., Wen, H.-Y., Wiese, D.N., Yuan, D.-N. (2020): Extending the Global Mass Change Data Record: GRACE Follow-On Instrument and Science Data Performance. *Geophysical Research Letters*, 47(12). DOI:10.1029/2020GL088306.
- Lasser, M., Meyer, U., Jäggi, A., Mayer-Gürr, T., Kvas, A., Neumayer, K.H., Dahle, C., Flechtner, F., Lemoine, J.-M., Koch, I., Weigelt, M., Flury, J. (2020): Benchmark data for verifying background model implementations in orbit and gravity field determination software. *Adv Geosci* 55, 1-11, DOI:10.5194/adgeo-55-1-2020
- Marti U., Condamine, S. (2020): Kalibrierung Gravimeter CG-6, inkl. Messung Kalibrierlinie Interlaken-Jungfrauoch. Swisstopo-Report 20-11.
- Marti, U. (2022): Gravimetric Calibration Line Interlaken – Jungfrauoch: Campaign 2022. Swisstopo-Report 22-04.
- Mayer-Gürr, T., Behzadpur, S., Ellmer, M., Kvas, A., Klinger, B., Strasser, S., Zehentner, N. (2018): ITSGGrace2018 - Monthly, Daily and Static Gravity Field Solutions from GRACE. GFZ Data Services, dataset. DOI:10.5880/ICGEM.2018.003.
- Meyer, U., Jaeggi, A., Dahle, C., Flechtner, F., Kvas, A., Behzadpour, S., Mayer-Gürr, T., Lemoine, J.-M., Bourgoigne, S. (2020a): International Combination Service for Time-variable Gravity Fields (COST-G) Monthly GRACE Series. V. 01. GFZ Data Services, DOI:10.5880/ICGEM.COST-G.001
- Meyer, U., Lasser, M., Jäggi, A., Flechtner, F., Dahle, C., Mayer-Gürr, T., Kvas, A., Lemoine, J.-M. Bourgoigne, S., Koch, I., Groh, A., Förste, C., Eicker, A., Meyssignac, B. (2020b): Combination Service for Time-variable Gravity Fields (COST-G) – GRACE-FO operational combination. GSTM2020, October 27-29, Potsdam, Germany (online).
- Meyer, U., Lasser, M., Jäggi, A., Dahle, C., Flechtner, F., Kvas, A., Behzadpour, S., Mayer-Gürr, T., Lemoine, J.-M., Koch, I., Flury, J., Bourgoigne, S. (2020c): International Combination Service for Time-variable Gravity Fields (COST-G) Monthly GRACE-FO Series. GFZ Data Services, DOI:10.5880/ICGEM.COST-G.002.
- Meyer, U., Lasser, M., Jäggi, A., Flechtner, F., Dahle, C., Boergens, E., Förste, C., Mayer-Gürr, T., Kvas, A., Behzadpour, S., Lemoine, J.-M., Bourgoigne, S., Koch, I., Flury, J., Groh, A., Eicker, A., Meyssignac, B., Zhou, H., Yan, Z., Chen, Q., Guo, X., Wang, C., Feng W. (2021): Combination Service for Time-variable Gravity Fields: operational GRACE-FO combination and validation of Chinese GRACE time-series. EGU General Assembly, 19-30 Apr. 2021, online.
- Meyer, U., Lasser, M., Darbeheshti, N., Jäggi, A., Flechtner, F., Dahle, C., Förste, C., Güntner, A., Mayer-Gürr, T., Kvas, A., S. Behzadpour, S., Lemoine, J.-M., Koch, I., Flury, J., Bourgoigne, S., Feng W. (2022a): COST-G: towards a new GRACE and GRACE-FO combination. GRACE Science Team Meeting, Oct 18-20, 2022, Potsdam, DOI:10.5194/gstm2022-75.
- Meyer, U., Geisser, L., Dach, R., Thaller, D., Jäggi, A. (2022b): COST-G gravity field models: application in SLR orbit determination. 22nd International Workshop on Laser Ranging. Yebe, Spain. November 7-11, 2022.
- Peter, H., Meyer, U., Lasser, M., Jäggi, A. (2022): COST-G gravity field models for precise orbit determination of Low Earth Orbiting Satellites. *Advances in Space Research* 69(12), 41554168, DOI:10.1016/j.asr.2022.04.005.

- Rothacher, M., Koch, J. (2022): A new gravity field model for the FCC region. Presentation at Colloquium “Zukünftiger Teilchenbeschleuniger am CERN: Herausforderung für die Geodäsie”, swisstopo, Wabern, 28.1.
- Save, H. (2019): CSR Level-2 Processing Standards Document For Level-2 Product Release 06. Processing Standards Document. The University of Texas at Austin, Austin, TX, USA.
- Scarponi, M., Hetényi, G., Baron, L., Marti U. (2022): A gravimetric assessment of the Gotthard Base Tunnel geological model: insights from a novel gravity terrain-adaptation correction and rock physics data. *Swiss Journal of Geosciences* (2022) 115:22. DOI:10.1186/s00015-022-00422-z.
- Tapley, B.D., Bettadpur, S., Watkins, M.M., Reigber, C. (2004): The gravity recovery and climate experiment: Mission overview and early results. *Geophysical Research Letters*, 31(9). DOI:10.1029/2004GL019920.
- Teixeira da Encarnação, J., Visser, P., Jaeggi, A., Bezdek, A., Mayer-Gürr, T., Shum, C.K., Arnold, D., Doornbos, E., Elmer, M., Guo, J., van den IJssel, J., Iorfida, E., Klokocnik, J., Krauss, S., Mao, X., Meyer, U., Sebera, J., Zhang, C., Zhang, Y., Dahle, C. (2019): Multi-approach Gravity Field Models from Swarm GPS data. GFZ Data Services, DOI:10.5880/ICGEM.2019.006
- Teixeira da Encarnação, J., Visser, P., Arnold, D., Bezdek, A., Doornbos, E., Ellmer, M., Guo, J., Van den IJssel, J., Iorfida, E., Jäggi, A., Klokocnik, J., Krauss, S., Mao, X., Mayer-Gürr, T., Meyer, U., Sebera, J., Shum, C.K., Zhang, C., Zhang, Y., Dahle, C. (2020): Description of the multiapproach gravity field models from Swarm GPS data. *Earth System Science Data* 12(2), 1385-1417, Copernicus Publications, DOI:10.5194/essd-12-1385-2020
- Willi D., Carrel, J. (2021): CODIAC Shutter Kalibration: Kalibration des Shutter-Delays der beiden CODIAC-Zenitkameras. Swisstopo-Report 21-08.
- Willi, D., Koch, J., Weyer, B., Carrel, J., Marti, U. (2022): Astrogeodätisches Profil am CERN. *Cadastre* (40), p. 16-18, <https://www.cadastre.ch/de/services/revue.detail.publication.html/cadastre-internet/de/publications/revue/cadastre-40-2022-de.pdf.html>
- Willi, D., Schlatter, A., Marti, U., Guillaume, S. (2022): Nouveau Système altimétrique Suisse (fr). Neues Schweizer Höhensystem (de). Swisstopo-Report 22-07.
- Wolff, M. (1969): Direct measurements of the Earth's gravitational potential using a satellite pair. *Journal of Geophysical Research*, 74(22):5295–5300. DOI:10.1029/JB074i022p05295.
- Zahorec, P., Papco, J., Pašteka, R., Bielik, M., Bonvalot, S., Braitenberg, C., Ebbing, J., Gabriel, G., Gosar, A., Grand, A., Götze, H.J., Hetényi, G., Holzrichter, N., Kissling, E., Marti, U., Meurers, B., Mrlina, J., Nogová, E., Pastorutti, A., Salaun, C., Scarponi, M., Sebera, J., Seoane, L., Skiba, P., Szücs, E., Varga, M. (2021): The first pan-Alpine surface-gravity database, a modern compilation that crosses frontiers. *Earth Syst. Sci. Data*, 13, 2165–2209, 2021. DOI:10.5194/essd-13-2165-2021.

3 Earth Rotation and Geodynamics

Alpine Metrology Lab for the monitoring of station movements in the Matter Valley

G. Moeller¹, T. Medic¹, M. Aichinger-Rosenberger², L. Schmid¹, A. Wieser¹, M. Rothacher¹

¹ Institute of Geodesy and Photogrammetry, ETH Zurich

² University Corporation for Atmospheric Research, USA

In response to the growing significance of monitoring geologically active areas, such as landslides, we established the Alpine Metrology Lab (AML) to study and enhance geomonitoring technologies. Our focus has been on utilizing permanent Global Navigation Satellite Systems (GNSS) and Terrestrial Laser Scanning (TLS) to validate and improve the interpretation of Interferometric Synthetic Aperture Radar (InSAR) observations. This report presents our initial findings regarding the cross-validation of mass movements observed through permanent GNSS and long-range TLS.

Figure 3.1 presents the region of interest (ROI) and our measurement setup. The study is centered on the orographic right side of the Matter Valley situated in Canton Valais, Switzerland, with a specific focus on the region below the mountain peaks of Breithorn (3176 m) and Gugla (3376 m), where the mean slope angle is around 30 degrees. The multitude of mass movements observed in this area is of significant interest due to their potential to cause damage to infrastructure and adversely affect living conditions in the region.

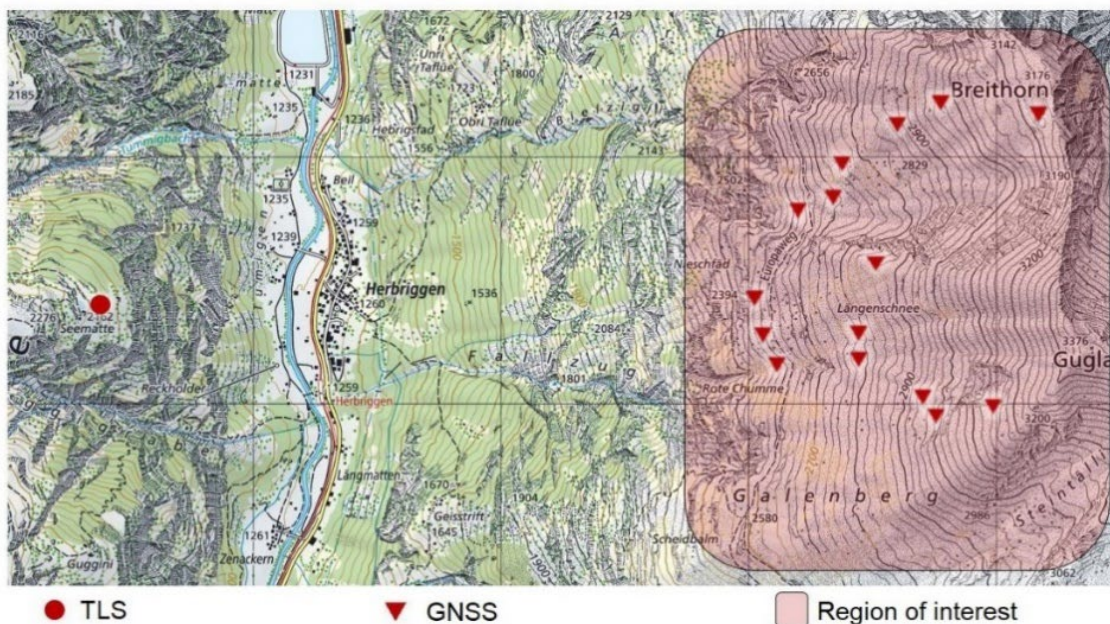


Figure 3.1: Map indicating the region of interest and the measurement locations. (Kartendaten: geo.admin.ch, © swisstopo).

Figure 3.2 illustrates the deformation estimates obtained from Terrestrial Laser Scanning (TLS) for two different time periods: a two-year span from August 2019 to July 2021 (top), and a shorter two-month duration from July to September 2021 (bottom). The color-coded point clouds represent the magnitude of vectors connecting corresponding points in two measurement epochs, indicating estimated mass movements. The accumulated uncertainty arising from (1) atmospheric influences, (2) measurement uncertainty, (3) laser footprint size and surface roughness, as well as (4) data processing uncertainty, including point cloud registration and (5) detection of corresponding points, was found to be in the order of a few decimeters. Consequently, for this report, areas with detected displacement magnitudes below 0.4 m were considered stable and are shown in gray in Figure 3.2

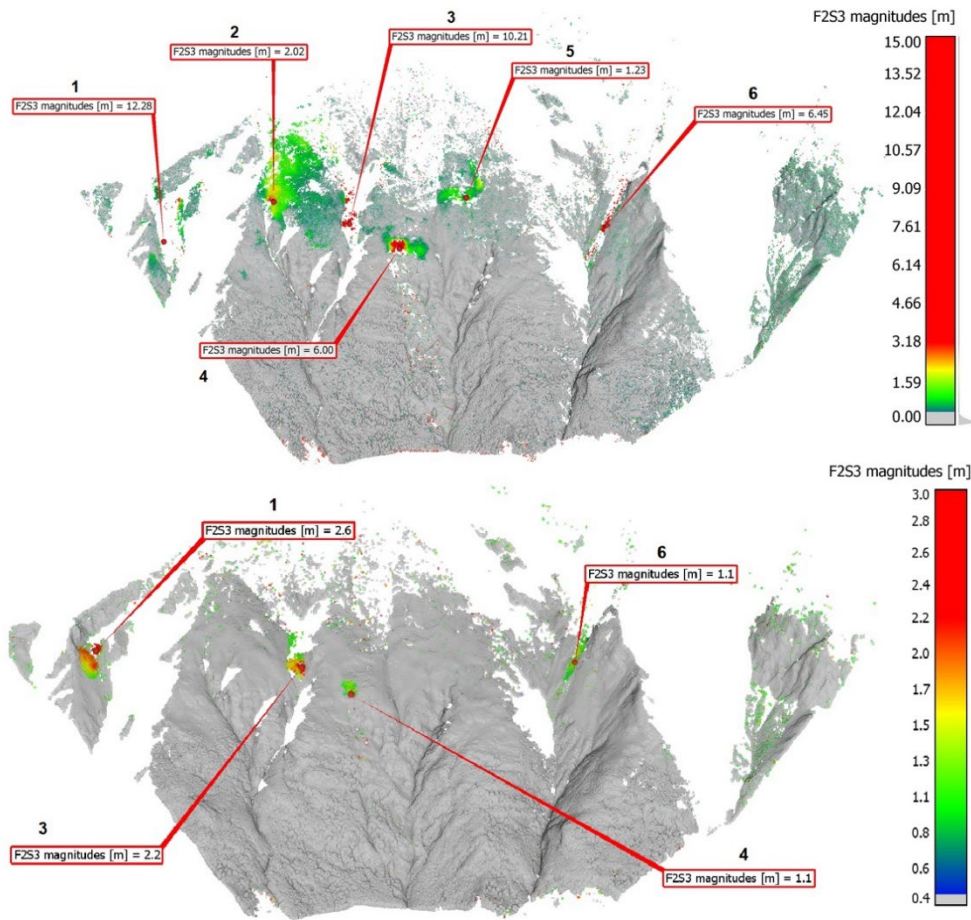


Figure 3.2: Mass-movement magnitudes estimated by the F2S3 algorithm: Sep 2019 vs. Jul 2021 (top) and Jul 2021 vs. Sep 2021 (bottom).

Our findings demonstrate that long-range TLS can be used for remote sensing of mass movements over large areas, if the displacements exceed 0.4 meters. We have identified this as the sensitivity threshold of the implemented workflow. The permanent GNSS network installed provides the reference values of mass movement magnitudes, with an uncertainty of approximately 2 to 4 millimeters, exposing slight systematic biases in the TLS data. This finding necessitates further investigation in order to employ both measurement methods for validating InSAR measurements.

Rotational Sensors, Accelerometers and GNSS for Strong Ground Motion

Y. Rossi^{1,2}, K. Tatsis³, M. Awadaljeed¹, K. Arbogast¹, R. Hohensinn¹, J. Clinton², E. Chatzi³, M. Rothacher¹

¹ Institute of Geodesy and Photogrammetry, ETH Zurich

² Swiss Seismological Service, ETH Zurich

³ Institute of Structural Engineering, ETH Zurich

Ground motion recordings obtained from monitoring stations in the near field of an earthquake source are often unreliable, especially in the case of very large earthquakes. State-of-the-art monitoring stations utilize strong motion sensors measuring acceleration. However, the frequency bandwidth of seismic motion excited by such earthquakes is broad, and classic seismic instrumentation alone cannot accurately measure it. Accelerometers, in particular, have difficulty recording low frequencies and permanent displacements. Additionally, these measurements are further compromised by rotations due to a leakage of the gravitational acceleration into the horizontal axes and due to a misorientation of the sensor in the local system. The presence of Coriolis, Centrifugal and Euler forces may also induce errors, but their quantification is challenging as the distance to the point of rotation is not always clear in a seismic wave field. The errors resulting from rotations and the low-frequency inaccuracies are further exacerbated by the double integration required to obtain displacement.

In recent years, Global Navigation Satellite System (GNSS) technology has emerged as a valuable tool for accurately measuring both dynamic and permanent displacement in the near field of large earthquakes. The combination of GNSS positions with acceleration for seismic applications allows for a more precise determination of the ground motion with higher resolution than relying on seismic-only solutions (Bock et al., 2011; Melgar et al., 2013; Geng et al., 2013; Shu et al., 2018; Dahmen et al., 2020). With new rotation sensors emerging in the last years such as the blueSeis-3A fiber optic gyroscope from exail (former iXblue), it is now possible to measure the rotations and incorporate them into sensor fusion methods. In our approach, we use a linear Kalman filter to combine GNSS positions with accelerometer data as well as a tilt and misorientation correction to account for rotation. While a similar filter has been tested by (Geng et al., 2019) to correct only for rotation-error in the accelerations, we also correct for the GNSS antenna column tilt. This enables us to accurately reproduce real-time, rotation-free and broadband displacement and velocities.

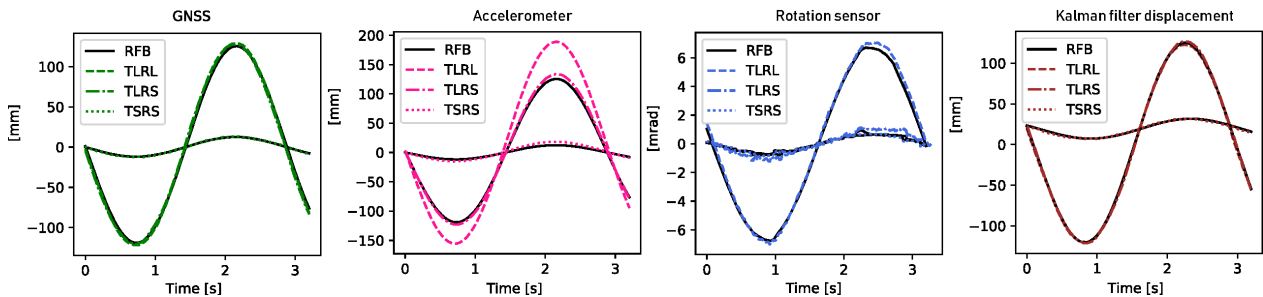


Figure 3.3: Adapted from Figure 9 in (Rossi et al., 2021). Earthquake-like motion performed on a robot arm, measured by GNSS instrumentation, accelerometer, rotational sensor and combined in a Kalman filter. RFB: robot feedback self-recording. TLRL: translation large, rotation small. TSRS: translation small rotation small.

The linear Kalman filter was applied to experimental data from a controlled robot experiment. The experiment based on a 6C robot arm that could perform earthquake-like motions while carrying different types of instruments i.e., GNSS antenna, accelerometer and rotational sensor (Rossi et al., 2021). The combined solution always outperformed any single instrument solution, as demonstrated by the results of three different experiments with varying translation to rotation ratios (i.e., TLRL, TLRs, TSRS) shown in Figure 3.3. The Kalman filter combination was able to retrieve the robot self-recording best.

Subsequently, the sensor fusion was further developed to include the rotation correction within the Kalman filter, rendering the process non-linear and requiring the use of the Unscented Kalman filter. We collected data using the

same triple instrumentation (rotation sensor, GNSS and accelerometer) deployed on a flexible footbridge, excited by jumping, twisting and running (Rossi et al., 2023). In addition to the broadband displacement and velocity estimated by the linear Kalman filter, the Unscented Kalman filter also estimates angles as shown in Figure 3.4. In Figure 3.4 the two Kalman filter implementations are compared to the rotation-corrected observations from GNSS and accelerometer and the rotation sensor. The high frequency observations are retained through the contribution of the accelerometer, while the long-term displacements are determined through the GNSS positions. The estimated timeseries of displacement and velocity were no longer distorted by rotation errors, and even the co-seismic rotation was estimated. Such a monitoring station has the potential of providing clean translation and rotation information in the near field of large earthquakes.

In conclusion, the combination of GNSS positions, accelerometers, and rotational sensors using Kalman filters has shown great promise in providing reliable information on the 6C ground motion during seismic events.

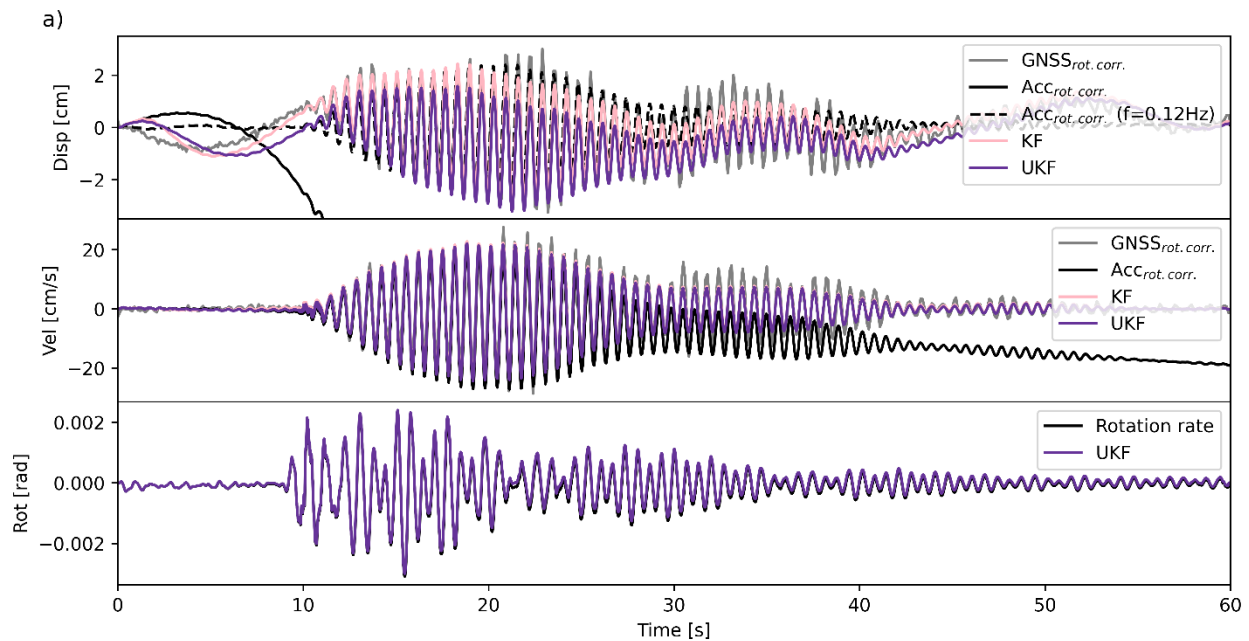


Figure 3.4: Adapted from Figure in (Rossi et al., 2023). Comparison of the KF and UKF state estimates with the rotation-corrected observations - GNSS, accelerometer and rotation sensor. From top to bottom the panels show displacement, velocity and angles time series of the East axis. The accelerations were integrated to displacement and velocity for comparison - for the displacement time series the filtered and unfiltered integrations are shown.

Operational prediction of Earth orientation parameters with machine learning

M. Kiani Shahvandi¹, M. Schartner¹, J. Gou¹, B. Soja¹

¹ *Institute of Geodesy and Photogrammetry, ETH Zurich*

Earth orientation parameters (EOPs) present the variations in the orientation of rotation axis and the rotation rate of the Earth. There are five EOPs, namely, polar motion (two components denoted by x_p , y_p), dUT1 (difference between universal time UT1 and coordinated universal time UTC), length of day (LOD), and nutation (denoted by dX , dY). These are important parameters that connect coordinates in the terrestrial system to the celestial system. They are therefore important in applications such as spacecraft navigation and orientation of deep space telescopes. Nowadays, EOPs are determined through various space-geodetic techniques such as Global Navigation Satellite System (GNSS) and Very Long Baseline Interferometry (VLBI). Various institutions have undertaken the task of providing EOPs, including the official solution of the International Earth Rotation and Reference Systems Service (IERS), Jet Propulsion Laboratory (JPL), and SYstèmes de Référence Temps-Espace (SYRTE). However, there is a latency of up to several weeks by which the so-called final EOP series are provided. Some applications such as spacecraft navigation require instantaneous information about the EOPs, thus making the prediction of EOPs an indispensable task in the field of geodesy.

Methodology to predict EOPs

The Space Geodesy group at ETH Zurich has undertaken the task of providing reliable daily predictions of all the five EOPs. The methodology is based on a variety of machine learning architectures devised and implemented for this purpose. These include, among others, Neural Ordinary Differential Equations (Neural ODEs), Long Short-Term Memory (LSTM), encoder-decoder LSTM, quantum LSTM, and attention-based residual LSTM autoencoder stacking. The predictions are made in three different time horizons: ultra-short term (up to 10 days to the future), short term (up to 30 days to the future), and medium term (up to 367 days ahead). The algorithms are trained daily and mainly on the IERS final EOP 14 C04 series, combined with the Effective Angular Momentum (EAM) analysis and forecasts provided by GFZ German Research Centre for Geosciences. In the prediction phase, however, the inputs to the algorithms are the rapid EOP series of IERS, JPL, and SYRTE, thus presenting different prediction solutions. A simple comparison between the prediction performance of the different input series (Figure 3.5, for x_p and y_p) reveals that using EOP series of JPL is preferable. The predictions are made publicly available at the Geodetic Prediction Center (GPC) <https://gpc.ethz.ch/EOP/>. The summary of all the methods and their characterizations, server for downloading the predictions, and some prediction performance assessments are presented on the webpage.

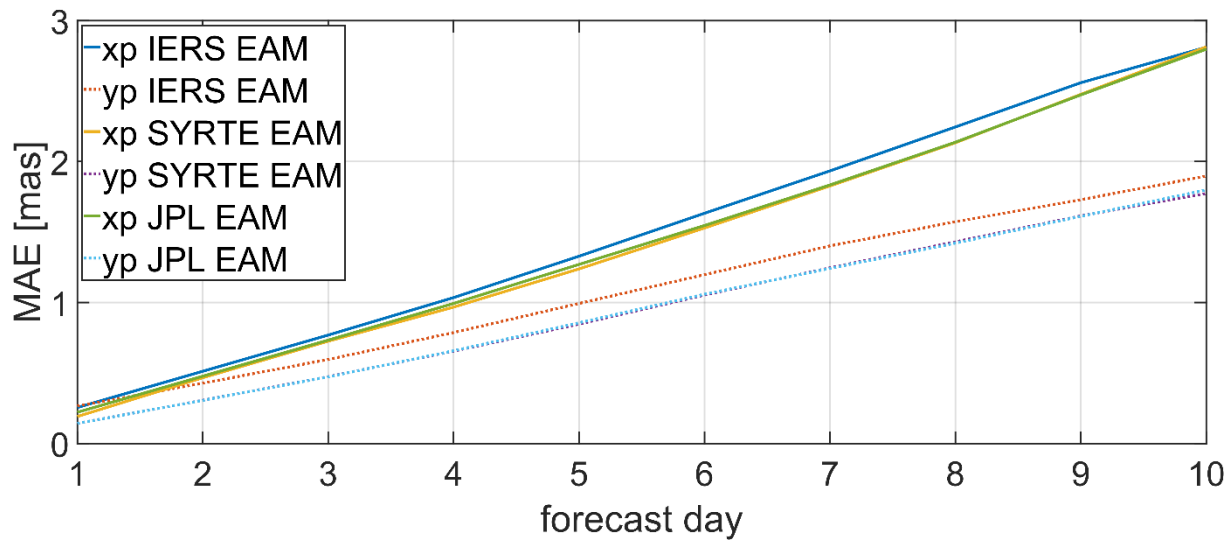


Figure 3.5: Prediction performance assessment in terms of mean absolute error (MAE) for polar motion (x_p , y_p) using the IERS, SYRTE, and JPL rapid EOPs. EAM functions are used as additional features. The unit is milliseconds of arc [mas].

Forecasting EAM

As variations in EOPs are driven by geophysical phenomena, the Space Geodesy group at ETH Zurich also provides forecasts of EAM functions, which are the source of excitations and variability in EOPs. All the four types of EAM are analyzed, i.e., Atmospheric Angular Momentum (AAM), Oceanic Angular Momentum (OAM), Hydrological Angular Momentum (HAM), and Sea-Level Angular Momentum (SLAM). The forecasts are up to 14 days ahead, longer than those of other institutions and thus enabling higher accuracy prediction of EOPs. Neural ODEs are used as the mathematical algorithm to provide the forecasts. In Figure 3.6, the prediction accuracy in terms of the prediction horizon, as well as a comparison to the prediction performance of the forecasts provided by GFZ, are shown. The results are for AAM and only the z-component (AAMz), but similar improvements can be observed in other components as well. AAMz is fundamental to atmospheric studies and its connection to LOD. Thus, improvements in this component can enable more accurate LOD predictions. It is worth mentioning that EAM functions are important geophysical quantities per se, representing the high-frequency mass redistribution in atmosphere, ocean, hydrology, and sea level. The forecasts can thus show potential for important applications such as climate research and oceanography, among others. The predictions are publicly available in the EAM section of the GPC <https://gpc.ethz.ch/EAM/>. Similar to EOPs, the webpage contains assessments of the prediction performance.

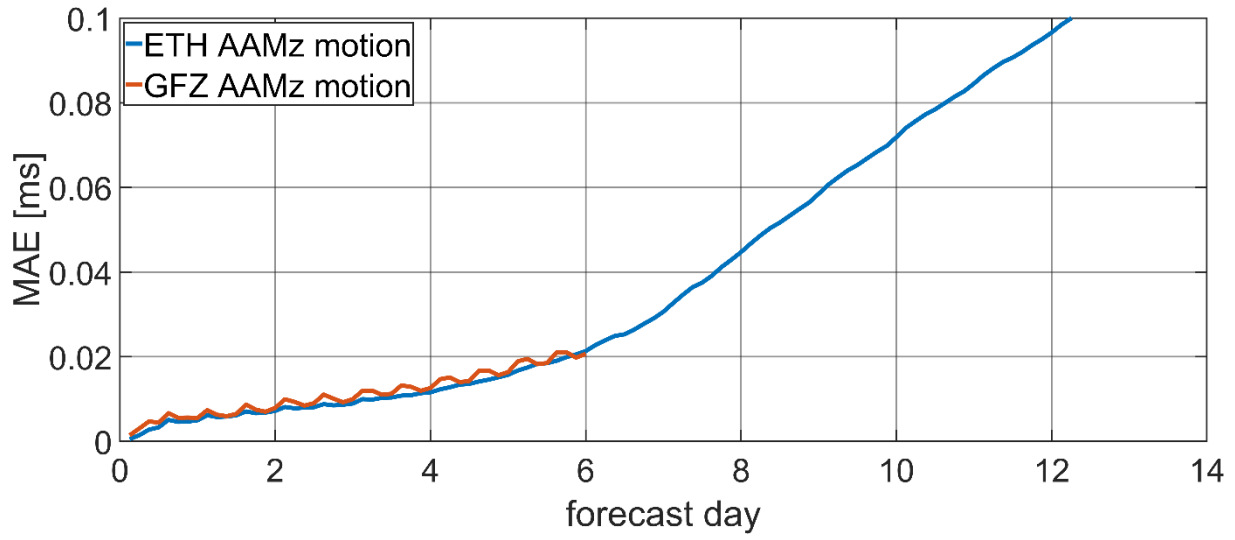


Figure 3.6: Prediction performance assessment of EAM in terms of MAE in milliseconds [ms]. Shown are the results of ETH Zurich and GFZ for the motion term of AAM in z direction.

TABLE OF CONTENTS

Bibliography Commission 3

- Bock Y., D. Melgar, B. W. Crowell, “Real-Time Strong-Motion Broadband Displacements from Collocated GPS and Accelerometers,” *Bulletin of the Seismological Society of America*, vol. 101, pp. 2904–2925, 12 2011.
- Dahmen, N., R. Hohensinn, and J. Clinton, “Comparison and Combination of GNSS and Strong-Motion Observations: A Case Study of the 2016 Mw 7.0 Kumamoto Earthquake,” *Bulletin of the Seismological Society of America*, vol. 110, pp. 2647–2660, 12 2020.
- Geng, J., Y. Bock, D. Melgar, B. W. Crowell, and J. S. Haase, “A new seismogeodetic approach applied to GPS and accelerometer observations of the 2012 Brawley seismic swarm: Implications for earthquake early warning,” *Geochemistry, Geophysics, Geosystems*, vol. 14, pp. 2124–2142, 7 2013.
- Geng, J., Q. Wen, Q. Chen, and H. Chang, “Six-Degree-of-Freedom Broadband Seismogeodesy by Combining Collocated High-Rate GNSS, Accelerometers, and Gyroscopes,” *Geophysical Research Letters*, vol. 46, pp. 708–716, 1 2019.
- Gou, J, Kiani Shahvandi M, Hohensinn R, Soja B, (2021) Ultra-short-term prediction of LOD using LSTM neural networks. Submitted.
- Kiani Shahvandi M, Schartner M, Soja B, (2022) Neural ODE Differential Learning and Its Application in Polar Motion Prediction. *Journal of Geophysical Research: Solid Earth*, 127(11). DOI:10.1029/2022JB024775.
- Kiani Shahvandi M, Soja B, (2022) Inclusion of data uncertainty in machine learning and its application in geodetic data science, with case studies for the prediction of Earth orientation parameters and GNSS station coordinate time series. *Advances in Space Research*, 70(3). DOI:10.1016/j.asr.2022.05.042.
- Kiani Shahvandi M, Gou J, Schartner M, Soja B, (2022) Data driven approaches for the prediction of Earth's effective angular momentum functions. *IEEE International Geoscience and Remote Sensing Symposium*. DOI:10.1109/IGARSS46834.2022.9883545.
- Kiani Shahvandi M, Soja B, (2022) Small geodetic datasets and deep networks: attention-based residual LSTM autoencoder stacking for geodetic time series. *International Conference on Machine Learning, Optimization, and Data Science*. DOI:10.1007/978-3-030-95467-3_22.
- Kiani Shahvandi M, Soja B, (2021) Modified deep transformers for GNSS time series prediction. *IEEE International Geoscience and Remote Sensing Symposium*. DOI:10.1109/IGARSS47720.2021.9554764.
- Melgar, D., Y. Bock, D. Sanchez, and B. W. Crowell, “On robust and reliable automated baseline corrections for strong motion seismology,” *Journal of Geophysical Research: Solid Earth*, vol. 118, no. 3, pp. 1177–1187, 2013.
- Moeller, G., Medic, T., Aichinger-Rosenberger, M., Schmid, L., Wieser, A., Rothacher, M. (2023): Alpine Metrology Lab: Geomonitoring Using Long-Range TLS and Permanent GNSS. In: Wieser, A. (Ed.) *Ingenieurvermessung 23 - Beiträge zum 20. Internationalen Ingenieurvermessungskurs*, Zürich, April 11.-14, Wichmann Verlag, 107-113.
- Rossi, Y., K. Tatsis, M. Awadaljeed, K. Arbogast, E. Chatzi, M. Rothacher, and J. Clinton, “Kalman Filter-Based Fusion of Collocated Acceleration, GNSS and Rotation Data for 6C Motion Tracking,” *Sensors*, vol. 21, p. 1543, 2 2021.
- Rossi, Y., K. Tatsis, R. Hohensinn, J. Clinton, M. Rothacher, and E. Chatzi, “Unscented Kalman Filter based fusion of acceleration, GNSS and rotational sensor demonstrated on a flexible foot bridge.,” *planned Journal of Geophysical Research*, 2023.
- Shu, Y., R. Fang, J. Geng, Q. Zhao, and J. Liu, “Broadband Velocities and Displacements From Integrated GPS and Accelerometer Data for High-Rate Seismogeodesy,” *Geophysical Research Letters*, vol. 45, pp. 8939–8948, 9 2018.

4 Positioning and Applications

Bernese GNSS Software

R. Dach¹, P. Fridez¹, D. Arnold¹, E. Calero¹, N. Darbeheshti¹, W. Desprats¹, C. Gattano¹, L. Geisser¹, T. Grombein¹, M. Kalarus¹, C. Kobel¹, M. Lasser¹, X. Mao¹, U. Meyer¹, L. Prange¹, S. Schaer¹, L. Schreiter¹, D. Sidorov¹, P. Stebler¹, A. Villiger¹, A. Jäggi¹

¹ Astronomical Institute, University of Bern

The Bernese GNSS Software (BSW, Dach et al., 2015) is the backbone for all activities of the satellite geodesy research group at AIUB: high performance processing of measurements, obtained by GNSS (Global Navigation Satellite Systems) and SLR (Satellite Laser Ranging), precise orbit determination for GNSS as well as Low Earth Orbiting satellites (LEOs), and even gravity field determination. There are developments started to extend the functionality towards VLBI (Very Long baseline Interferometry).

The software is also applied in the context of operational processing schemes, e.g., in the context of CODE (Center for Orbit Determination in Europe) since more than 25 years. CODE is a consortium of four institutions, namely the Astronomical Institute of University of Bern (AIUB, Switzerland), the Swiss Federal Office of Topography (swisstopo, Switzerland), the Bundesamt für Kartographie und Geodäsie (BKG, Germany), and the Ingenieurinstitut für Astronomische und Physikalische Geodäsie, Technische Universität München (IAPG/TUM, Germany). CODE's main functions are its activities as an Analysis Center (AC) of the International GNSS Service (IGS, Dach et al. 2023a), AC of the European Permanent Network (EPN, Dach et al. 2023b), and as an Associated AC of the International Laser Ranging Service (ILRS, e.g., Meyer 2020).

The BSW is a high performance, high accuracy GNSS and SLR post-processing software package primarily used in the space-geodetic community. It is supported,

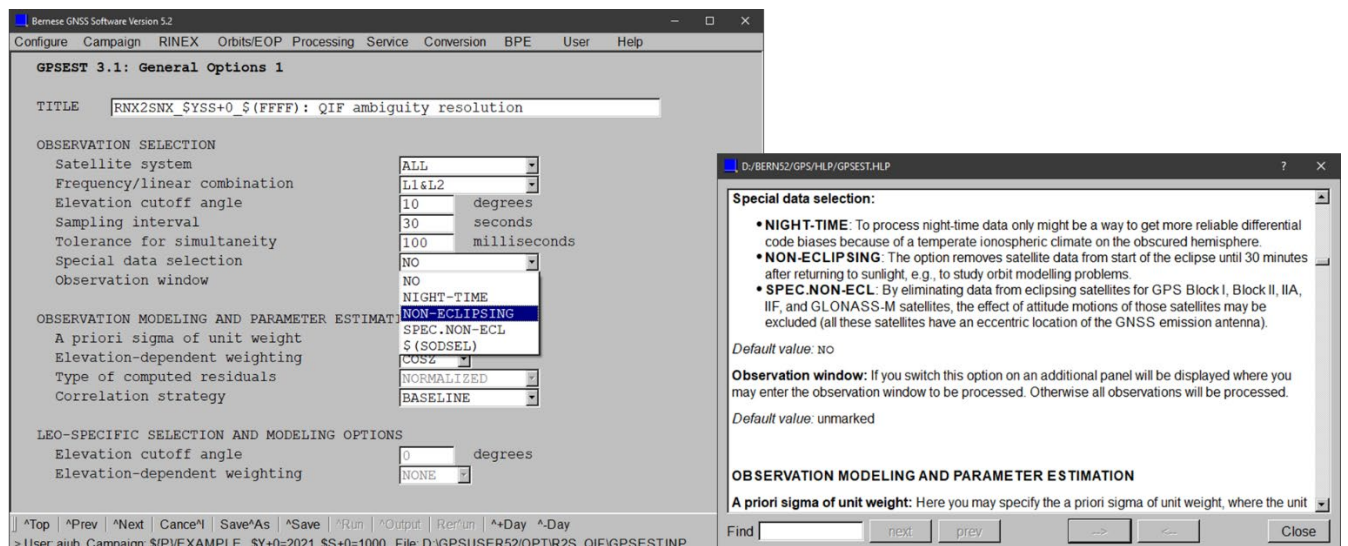


Figure 4.1: Example for the graphical user interface and online-Help function of the BSW.

maintained, and regularly updated by AIUB, considering the latest recommendations and models (e.g., according to the IGS standards and IERS Conventions, Petit and Luzum, 2010) as well as technological advancements (e.g., new satellite systems and observables), offering the user a maximum of flexibility in customizing processing strategies and

options. The BSW comes with a user-friendly interface, an online help system and an extensive user manual. The so-called Bernese Processing Engine (BPE) allows for automated processing, which is especially useful for large network processing and reprocessing efforts. Nowadays the BSW consists of more than 100 programs and about 1300 modules and subroutines written according to the Fortran 2003 standard, is platform-independent, and is used by several hundred customers throughout the world (see Figure 4.2).

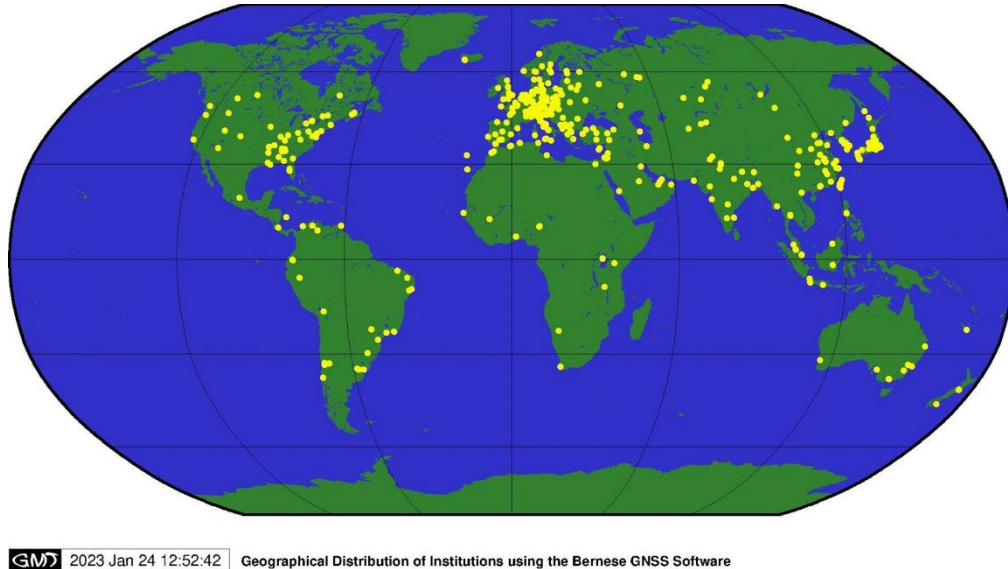


Figure 4.2: Worldwide distribution of the Bernese GNSS Software users as of January 2023.

Since the release of the version 5.2 of the BSW in 2012, 12 maintenance releases have been made available to the users. These updates not only correct software bugs, but also implement improvements based on our own research activities and developments in the area of GNSS, thus keeping the BSW version 5.2 as an efficient and useful tool for GNSS data analysis.

At the EUREF symposium 2022 the availability of a new version 5.4 was announced where the distribution to the use community started in September 2022. Many new developments in improvements, in particular regarding multi-GNSS data processing and orbit modelling, have been included. Key elements of the new version are:

- Multi-GNSS capability,
- Enhanced satellite orbit modelling,
- Ambiguity resolution for PPP,
- Support of latest IGS/IERS conventions and file formats.

A summary is available in the updated flyer characterizing the software (see Figure 4.3).

Bernese GNSS Software

The Bernese GNSS Software established a tradition as a high performance, high accuracy, and highly flexible reference multi-GNSS (currently GPS, GLONASS, Galileo, BeiDou, and QZSS) post-processing package. State-of-the-art modeling, detailed control over all relevant processing options, powerful tools for automatization, the adherence to up-to-date, internationally adopted standards, and the inherent flexibility due to a highly modular design are characteristics of the Bernese GNSS Software.

Features and Highlights

- Available on UNIX/Linux, Mac, and Windows platforms
- **User-friendly GUI**
- Built-in HTML-based **help system**
- Multi-session parallel processing for **reprocessing** activities
- **Ready-to-use BPE** examples for different applications:
 - PPP (Precise Point Positioning)
 - RINEX-to-SINEX (double-difference network processing)
 - Clock determination (zero-difference network processing)
 - Ionosphere model determination
 - LEO precise orbit determination based on GPS-data
 - SLR validation of GNSS or LEO orbits

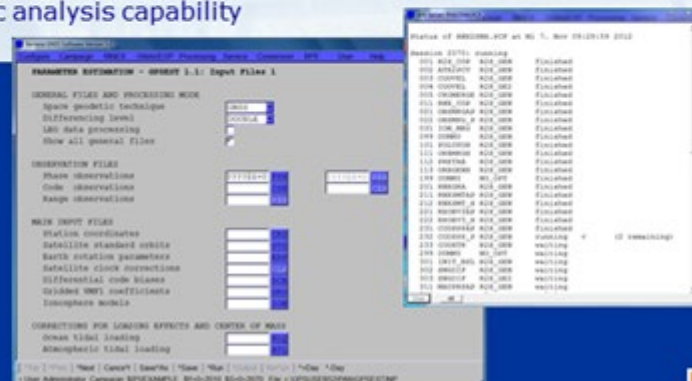
All examples are designed for **combined multi-GNSS** processing. Some of them are prepared for an **hourly processing scheme**.

- Program for automated coordinate **time series analysis** (FODITS)
- **Ambiguity resolution** also for PPP
- Extended orbit modelling capability for GNSS and LEO satellites
- **Multi-GNSS processing support** advanced observation-type specific bias handling based on RINEX3/4 specifications
- GNSS- and frequency-specific receiver and satellite antenna models
- Compliance with latest **IERS and IGS conventions**
- Real kinematic analysis capability

Contact

Astronomical Institute
University of Bern
Sidlerstrasse 5
CH-3012 Bern
Switzerland

bernese@aiub.unibe.ch



Visit our website: www.bernese.unibe.ch

Figure 4.3: Flyer on the BSW

Selected products from the CODE analysis center

R. Dach¹, S. Schaer^{1,2}, D. Arnold¹, M. Kalarus¹, L. Prange¹, P. Stebler¹, D. Sidorov^{1,3}, A. Villiger^{1,4}, A. Jäggi¹

¹ *Astronomical Institute, University of Bern*

² *Federal Office of Topography swisstopo*

³ *now with Leica Geosystems*

⁴ *now with Federal Office of Topography swisstopo*

The Center of Orbit Determination in Europe (CODE) is a joint venture between

- Astronomical Institute of University Bern (AIUB), Switzerland
- Federal Office of Topography (swisstopo), Switzerland
- Federal Agency of Cartography and Geodesy (BKG), Germany
- Ingenieurinstitut für Astronomische und Physikalische Geodäsie at Technische Universität München (IAPG/TUM), Germany

It acts among others as a global Analysis Center (AC) of the International GNSS Service (IGS, Johnston et al., 2017) generating operationally series of Global Navigation Satellite System (GNSS) products since 1992. In the data analysis various products based on a rigorous multi-GNSS processing scheme. The operational solution series consider GPS since 1994; GLONASS since May 2003; and Galileo since November 2022 (in the rapid series already since September 2019).

The main products from CODE are the GNSS satellite orbits and station coordinates that are computed at daily basis with different latencies (see Dach et al., 2023). Nevertheless, numerous other products are generated where a few of them are closer introduced in the subsequent paragraphs.

Earth Rotation Parameters

The orbits of GNSS-satellites realize a quasi-inertial reference system, so that the analysis of tracking data from the global network of the IGS allows it to estimate Earth rotation parameters (ERPs). As a result x and y positions and daily rates of the Earth's rotation axis in an Earth-fixed frame (polar motion) and rates thereof as well as excess length of day (LOD) are obtained.

In 2015, software and (final) processing was further developed and prepared for the capability to set up EOPs satellite-respectively GNSS-wise (described by Scaramuzza et al., 2017). By this expanded parameter setup, studies on the basis of NEQ results become feasible in assessing EOP differences specific to individual satellite systems, satellite planes, satellite groups (or blocks), etc. This setup was for instance used to assess the impact of the updated high-frequency pole model in the recent IGS reprocessing (see Dach et al., 2021).

Today, a time series of more than 25 years is available from CODE. Figure 4.4 (left figure) shows the Chandler wobble of the Earth's rotation axis since July 1993. The accuracy of the daily values compared to other techniques is a few 0.1 mas.

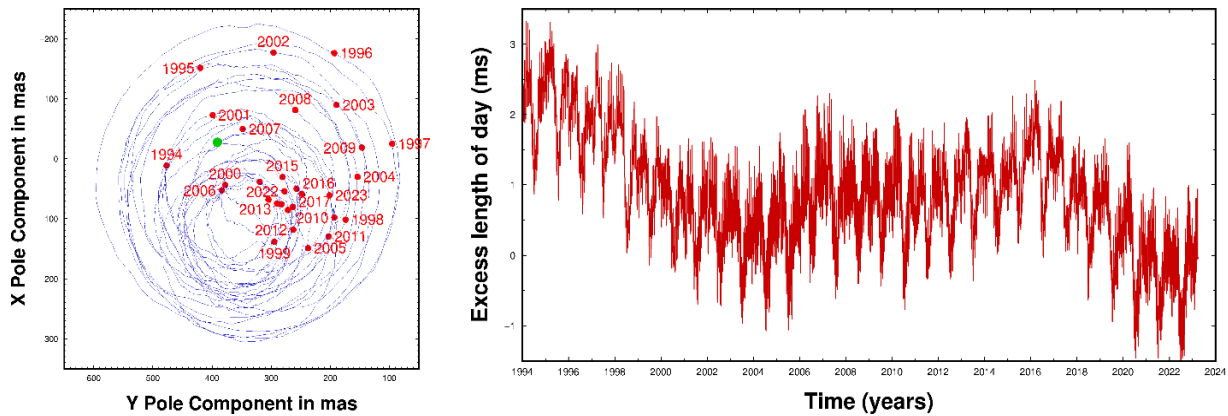


Figure 4.4: Polar motion (left) and excess length of day (right) derived from GNSS observations from the operational CODE final solution from July 1993 until March 2023

Ionosphere monitoring

CODE has been extracting information of the total electron content (TEC) from the IGS tracking data since 1995. Since June 1998, related global ionosphere maps (GIM) have been generated in IONEX (Ionosphere Exchange) format and provided to the IGS to support various applications, e.g., dealing with the ionosphere induced short-term signal disturbances or strong horizontal gradients. As it can be seen in Figure 4.5 the maximum TEC follows the Sun during a day.

In addition to this primary IONEX product, which is a product of the final analysis line, also corresponding rapid and predicted GIMs are generated at CODE on an operational basis. All GIM products are made available in form of IONEX and as ionosphere files in the internal format of the Bernese GNSS Software (Dach et al. 2015). Since July 2000, CODE has additionally been providing RINEX-formatted Klobuchar-style ionosphere coefficients (best fitting CODE's IONEX data).

The time series of global mean TEC values extracted from the GIMs produced by CODE covers, nearly 30 years, more than two and a half (11-year) solar cycles. Daily averaged mean TEC values, namely the zero-degree coefficients of the spherical harmonic expansion used to represent the global TEC, are shown in Figure 4.6. Annual and semi-annual variations are visible. The ionospheric signal also includes very pronounced 27-day variations, caused by distinctive groups of sunspots co-rotating with the Sun.

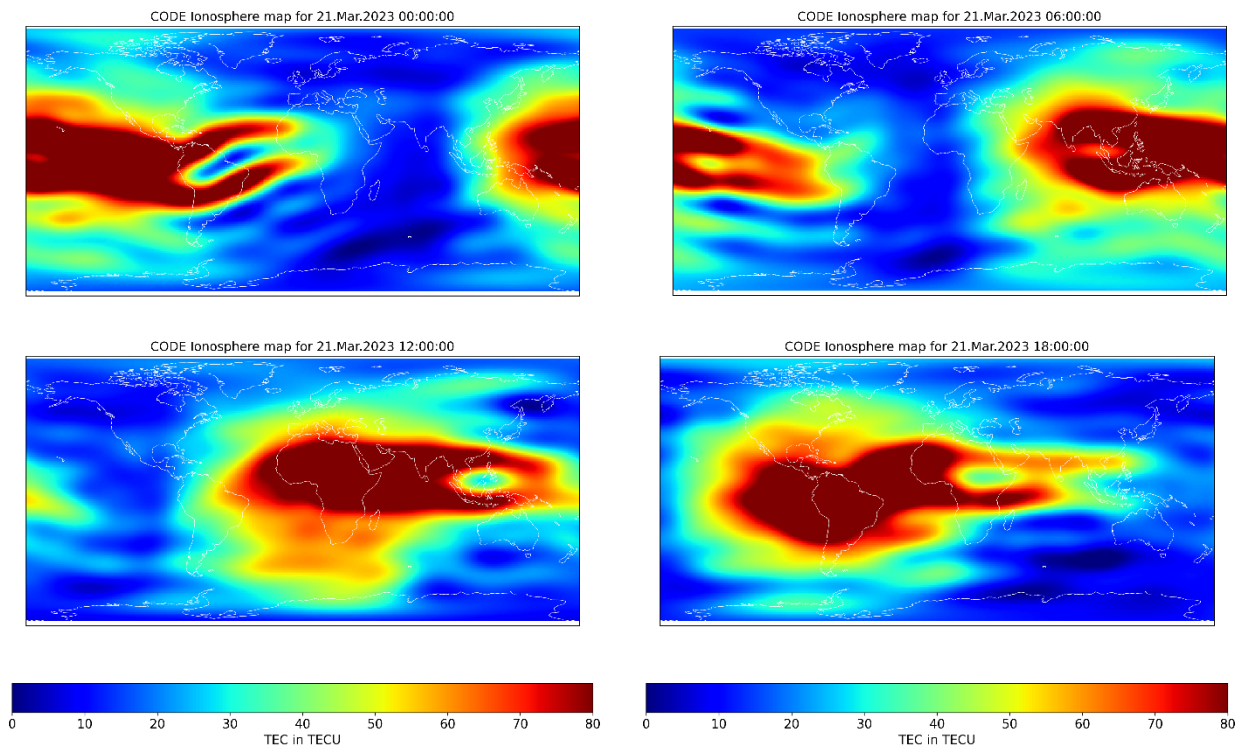


Figure 4.5: GIM models for one day in March 2023.

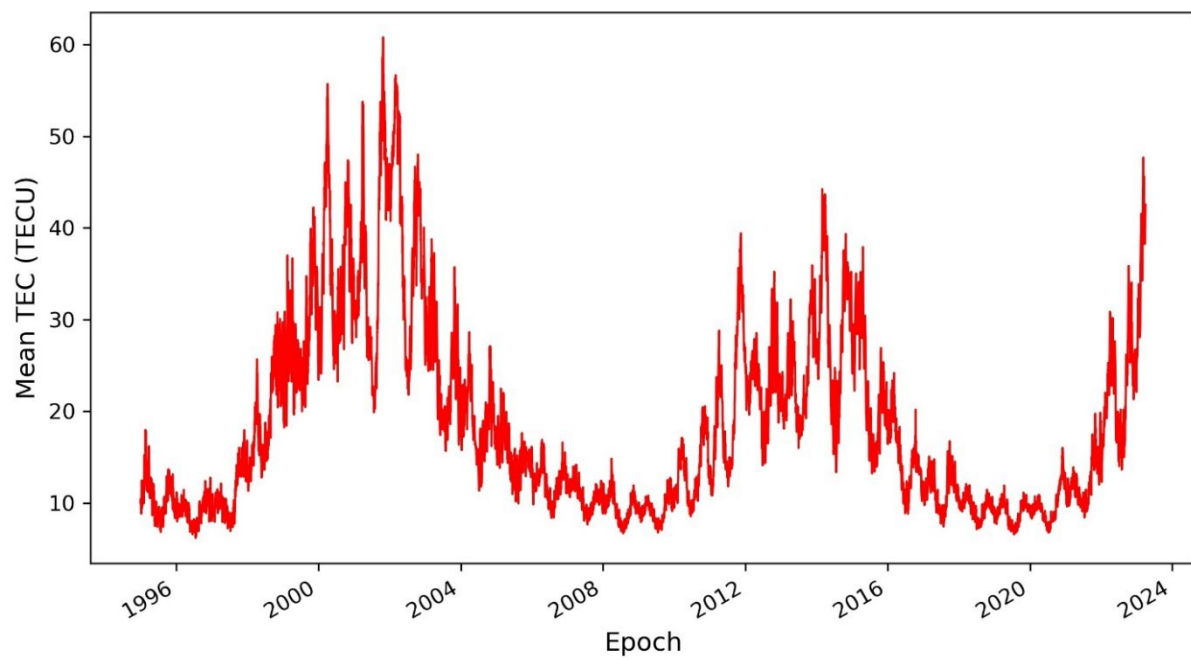


Figure 4.6: Development of mean TEC values derived from GNSS observations from the operational CODE final solution from January 1995 until March 2023.

Troposphere monitoring

The composition of the troposphere is effecting the GNSS signal propagation. This is usually considered by mapping the effect from the so-called zenith path delay. The hydrostatic part is typically introduced with a model whereas the wet part is estimated as parameters. The total sum from both components is shown as a time series for three selected stations from the most recent reprocessing series in Figure 4.7.

The figure gives some first-level confidence about the obtained parameters, e.g., the station at the equator (Kourou) shows the biggest scatter because of the humid environment whereas the station in Antarctica (Scott Base) has the lowest scatter because of the dry air. The phase of the annual signal is swapped between the stations on the Northern (Zimmerwald) and Southern (Scott Base) hemisphere.

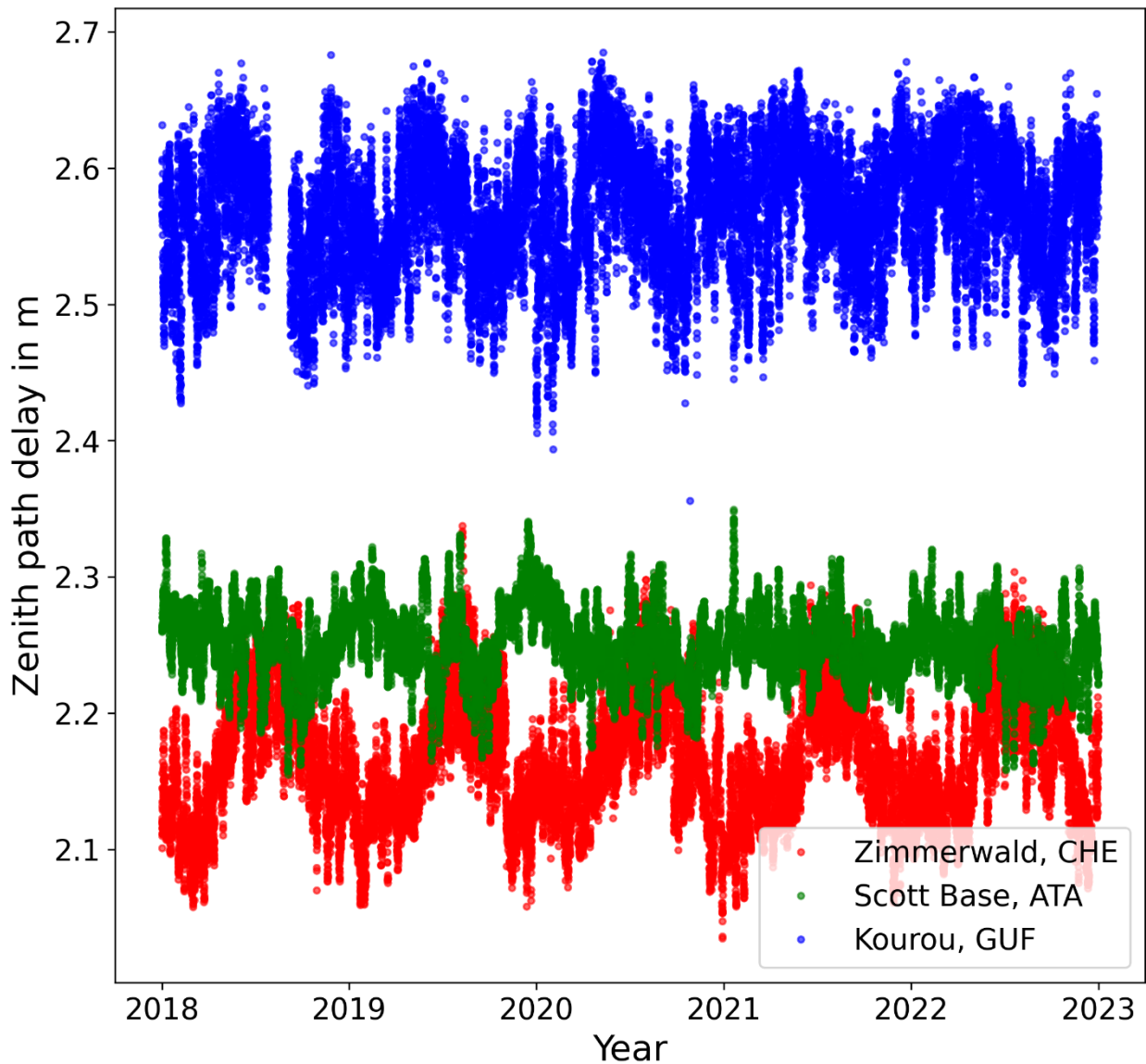


Figure 4.7: Troposphere zenith path delays for three selected stations as obtained from GNSS data.

The troposphere parameters as obtained in the operational processing at CODE are submitted to the IGS product centers as well. In December 2020 the rapid and ultra-rapid processing chain was switched to GPT/GMF troposphere model because this can be applied with external data. In this way the operational processing was made more robust. In July 2021 the new VMF3/GMF3 versions of the troposphere models (Landskron and Böhm, 2018) have been enabled to benefit from the higher resolution of the coefficients. Finally yet importantly, in January 2023, the troposphere product from CODE got a revision that the zenith path delays are computed in a station-wise processing scheme using the PPP method (precise point positioning). This allows to increase the number of stations in the product and to increase the resolution of the estimated parameters from two hours to hourly. At the same time the new troposphere SINEX result format (version 2.00, Pacione and Douša, 2020) was introduced.

AIUB contribution to the Copernicus POD Service

D. Arnold¹, C. Kobel¹, X. Mao¹, A. Jäggi¹

¹ *Astronomical Institute, University of Bern*

ESA's Sentinel satellites constitute the space segment for the Earth observation program Copernicus (Aschbacher and Milagro-Pérez, 2012) of the European Union. Currently (as of March 2023) in Low Earth orbit are the satellites Sentinel-1A (for radar imaging, Sentinel-1B was decommissioned in 2022 after a satellite anomaly in December 2021), Sentinel-2A and -2B (for multi-spectral high-resolution imaging), Sentinel-3A and -3B (for radar altimetry as well as sea and land temperature and color measurements), Sentinel-5P (for air pollution monitoring) and Sentinel-6A (for radar altimetry).

The AIUB is involved in the Global Navigation Satellite System (GNSS)-based precise orbit determination (POD) of all of these Sentinel satellites – apart from Sentinel-5P – as a member of the Copernicus POD Quality Working Group (CPOD QWG, Fernández et al., 2014). Numerous different members of the QWG produce independent precise orbit solutions of the Sentinel satellites for the quarterly Regular Service Reviews (RSRs), in the frame of which the official orbit solutions are validated by inter-comparison to the individual and combined orbit solutions. The orbits are combined as a weighted mean of the individual orbit solutions, where the weights are derived from the distance w.r.t. a simple arithmetic mean combination. Alternative combination strategies using Variance Component Estimation have been analyzed and proposed by Kobel et al. (2019). For each RSR AIUB delivers two different orbit solutions computed with the Bernese GNSS Software: A baseline solution without usage of explicit non-gravitational force models and based on a rather reduced-dynamic orbit parametrization, as well as a second solution, where state-of-the-art models are employed for the modeling of air drag, direct solar radiation pressure and Earth radiation pressure (Mao et al., 2021), allowing for an orbit parametrization with a much more dynamical stiffness. Since RSR #14 (covering the time span 27 January – 18 May 2019) the AIUB Sentinel orbit solutions benefit from single-receiver GNSS carrier phase ambiguity resolution by means of the Center for Orbit Determination in Europe (CODE) ambiguity-fixed clock and observable-specific signal bias products (Schaer et al., 2021).

The satellite Sentinel-6A (launched on 21 November 2020) is the first of the Sentinel fleet which, besides GPS, also tracks signals from the European GNSS Galileo for POD. At AIUB (and other member institutes of the QWG) this data is successfully processed using the CODE Rapid product line (Dach et al., 2020a, containing Galileo). With the switch from ITRF2014 to ITRF2020 on 27 November 2022 also the CODE Final product line (Dach et al., 2020b) contains Galileo and can be used for the Sentinel-6A POD. In the figure below, the solution labeled “AIUB” corresponds to the baseline reduced-dynamic AIUB solution, while “AING” refers to the solution with more dynamic stiffness. It can be seen that the AING solution performs well, yielding among the smallest 3D orbit differences. This is confirmed by convincingly small Satellite Laser Ranging (SLR) residuals of 8.2 mm RMS over the entire year, which is among the best performance.

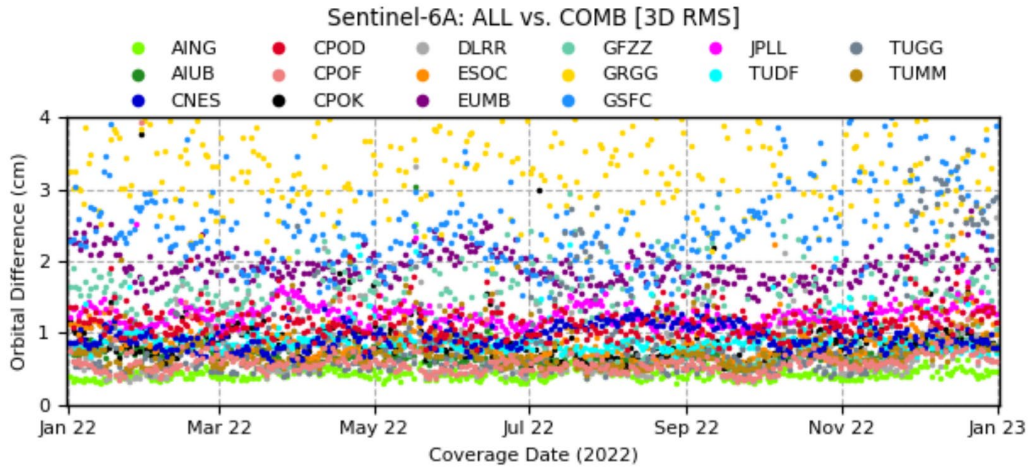


Figure 4.8: Sentinel-6A orbit comparison conducted in the frame of RSR #27, covering the entire year 2022. Daily 3D RMS values w.r.t. combined solutions are shown.

In 2021 AIUB contributed to the Sentinel-1 reprocessing campaign (Fernández et al., 2022) in the course of which the complete orbit time series (starting on 7 April 2014 for Sentinel-1A and on 28 April 2016 for Sentinel-1B, until end of 2020) were reprocessed. This reprocessing became necessary due to multiple improvements in the Sentinel-1 POD (e.g., antenna reference point updates) over the last years. CODE reprocessed the GNSS final products for the time span of the campaign using the reference frame IGB14 (Villiger et al., 2020) as part of the IGS repro3 effort. These products were used by all contributing QWG members (including AIUB) for the Sentinel-1 reprocessing, enabling also single-receiver ambiguity resolution for the entire time span.

On 21-23 June 2022, the 11th meeting of the CPOD QWG took place at the University of Bern, organized by AIUB. Three years after the last in-person meeting at DLR in Oberpfaffenhofen, followed by two virtual meetings due to the Covid pandemic, the QWG members could meet in person again. During three days many presentations and lively discussions were used to exchange on the current status of the different Sentinel missions, on recent progress, problems and questions in particular related to precise orbit determination of the Sentinel satellites and on future developments and challenges.

Analysis and Quality Assessment of LEO GPS Data for Geophysical and Ionospheric Applications

L. Schreiter¹, D. Arnold¹, A. Jäggi¹

¹ Astronomical Institute, University of Bern

Introduction

GPS signals traveling to receivers located in low earth orbit experience significant code delay and phase advance due to free electrons in the ionosphere and plasmasphere. Given the availability of two frequencies, these effects can be largely eliminated using the ionosphere-free linear combination or extracted to measure the integrated electron density along the line-of-sight (slant TEC) by using the geometry-free linear combination. The conducted work focuses on two aspects. First, the receiver's internal tracking of GPS signals, because it was observed in early phases of the study that severe variations of the slant TEC may cause tracking issues and thus cause biased positions. And secondly, the slant TEC information derived from different low earth orbiting (LEO) satellites are used to estimate the three-dimensional electron density distribution from LEO altitude to GPS altitude.

Ionospheric impacts on GPS tracking

The first part is conducted for the Swarm satellite missions. For this mission information about the receiver tracking was provided by RUAG. The L2 phase measurements are tracked by a third-order Digital Phase Lock tracking loop with a relatively long integration time of 100 ms. Together with the tracking loop coefficients, we conduct simulations to derive the response of the loop to ionospheric stimuli. To simulate the effect of the equatorial ionization anomaly, where the largest differences between kinematic and reduced dynamic orbit were observed, we use a cosine-shaped pulse to simulate one ionization peak (see Figure 4.3). Even though this is just an approximation, a similar pattern compared to the phase residuals of the orbit determination is observed. To invert the loop filter, we make use of the transfer function. Therefore, the signal is transferred into frequency space using Fast Fourier Transform (FFT), where the inversion of the loop-specific transfer function is trivial. It should be noted, that a full reconstruction requires 10 Hz data. This is not the case for Swarm, where only 1 Hz data is available. As can be deduced from the amplitude of the transfer function (see Figure 4.4), the strongest deviation occurs at periods between 10 and 30 s.

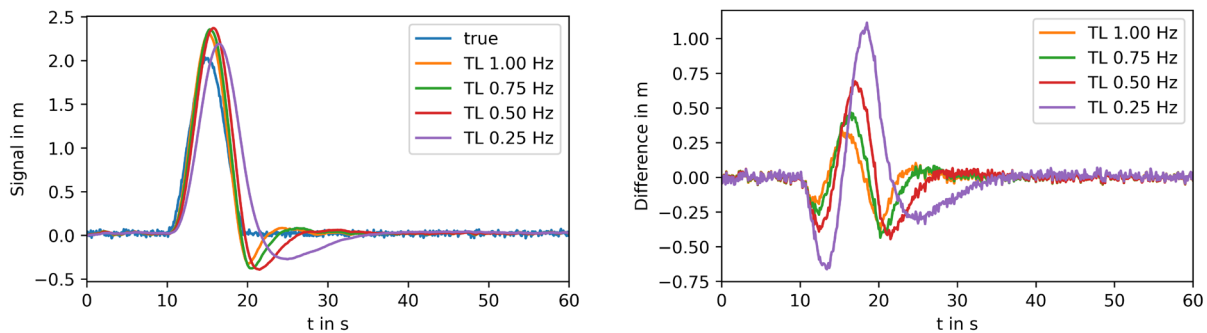


Figure 4.9: Tracking loop simulations for the different L2 bandwidths of the Swarm receiver. The input and output signals are shown on the left, and the differences to the true signal are shown on the right for the 2nd of July 2019, between 03:00 h and 06:00 UTC.

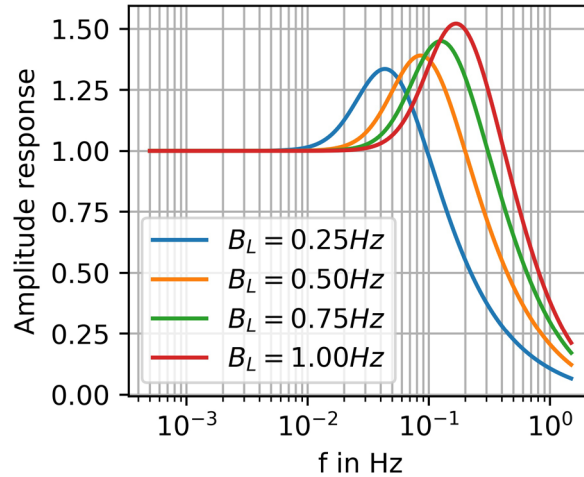


Figure 4.10: Amplitude response for the Swarm tracking loop implementation for the different bandwidths used.

Reconstruction of the topside ionosphere

In the second part of our study, a fleet of LEO satellites, consisting of Swarm A/B/C, GRACE-FO, Sentinel 1 A/B, Sentinel 2 A/B, and Sentinel 3 A/B, was used to estimate the electron density distribution of the topside ionosphere and plasmasphere. An Epstein Layer approach is used to model the altitudinal development. The global representation of the key parameters, i.e., peak height, peak electron density, and scale height, is realized by spherical harmonics, whereas the reference coordinate system is magnetic latitude and magnetic local time. To connect the slant TEC observations with the electron density we make use of numerical integration by applying Gauss-Legendre quadrature. In processing slant TEC, usually the low noise phase measurements are used. They only provide a relative slant TEC, which can be assumed to be as precise as 0.1 TECU. However, to obtain an absolute value leveling is required. Usually, code measurements are used for leveling. The relatively large code noise and the estimation of the receiver-specific differential code bias lead to an uncertainty of approximately 3 TECU. Since some observations are of this quality level, the resulting uncertainty is considered too large. Therefore, the offsets between absolute and relative slant TEC are adjusted during the model estimation. Even though the resolution is just 3 h and degree and order 5 for the spherical harmonics some basic features of the TEC maps and the electron density distribution could be reproduced, for example, the ionization peak early afternoon in low latitudes (Figure 4.5).

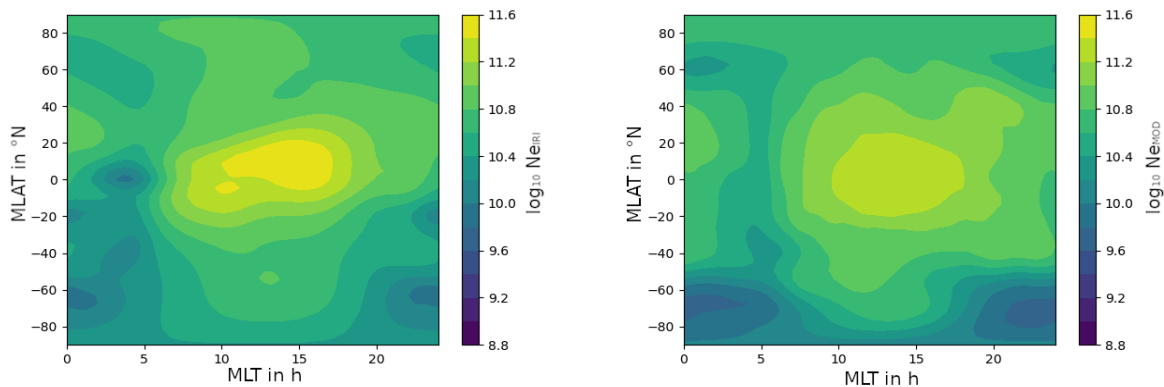


Figure 4.11: Electron density in magnetic latitude and local time at 500 km for the IRI model (left) and the derived model (right).

Real-time navigation solutions of low-cost off-the-shelf GNSS receivers on board the Astrocast satellites

L. Müller¹, M. Rothacher¹, K. Chen¹, G. Moeller¹, B. Soja¹, L. Lopez²

¹ Institute of Geodesy and Photogrammetry, ETH Zurich

² Astrocast SA, 1022 Chavannes-près-Renens

As more and more nanosatellites are launched into space, real-time orbit determination and time synchronization using the Global Navigation Satellite System (GNSS) becomes increasingly important. For CubeSat missions, low-cost commercial off-the-shelf GNSS receivers are the means of choice, adapted to the small size and weight of these satellites, as well as to the requirements for low power consumption and inexpensive components. To demonstrate the performance of low-cost GNSS receivers in space, a small single-frequency multi-GNSS payload board has been developed at the Institute of Geodesy and Photogrammetry of ETH Zürich. This payload has been deployed onboard three-unit CubeSats, which are part of a nanosatellite constellation for Internet of Things applications, developed and operated by the Swiss company Astrocast.

Figure 4.6a depicts an Astrocast CubeSat and the main components of the GNSS payload. The positioning module consists of four single-frequency multi-GNSS receivers (u-blox M8T), which are connected to two differently located GNSS antennas. In addition, the Astrocast satellites feature a laser retroreflector to enable satellite laser ranging, which can be used as an independent method for orbit validation.

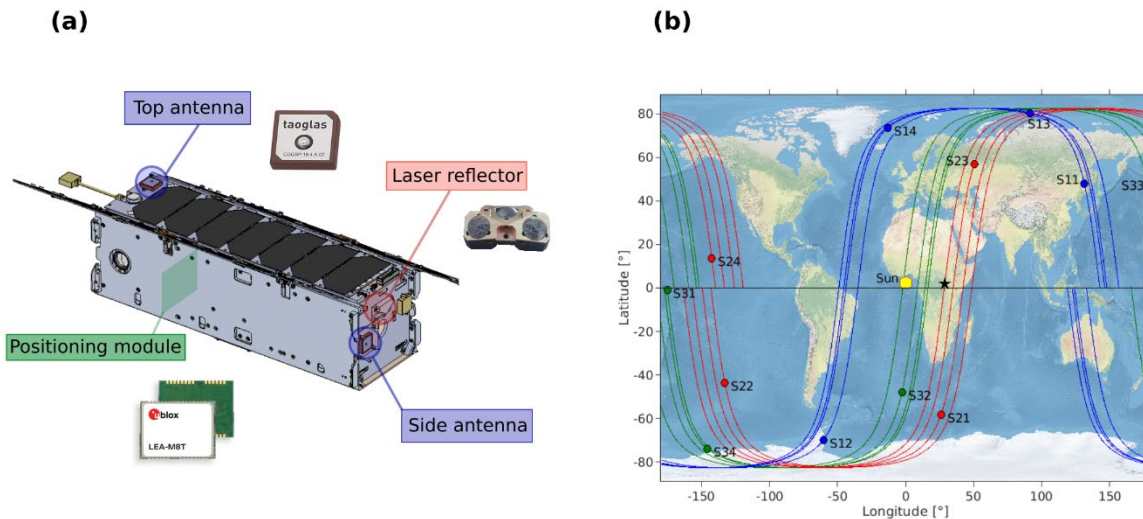


Figure 4.12: Overview of the Astrocast space segment. (a) Astrocast satellite and payload components used for orbit determination. (b) ground-tracks and positions for the Astrocast plane-1, -2, and -3 satellites, named S11-S14, S21-S24 and S31-S34, respectively, on 27 March 2023, 12:00 UTC. The black star marks the expected position of the total electron content (TEC) maximum, which is approximately 30° east of the position of the Sun.

We analyse the on-board GNSS navigation solutions (NAVSOL) from twelve Astrocast CubeSats, which are distributed over three orbital planes, launched on 25 January 2021, 1 July 2021 and 1 December 2022, respectively (Figure 4.6b). The orbits are near-circular and sun-synchronous with a satellite altitude of about 550 km and an orbital

period of 96 minutes. We assess the quality of the NAVSOL from the Astrocassat satellites by fitting a reduced-dynamic orbit using the Bernese GNSS software version 5.2 (Dach et al. 2015). A diagram with orbit-fit residuals is presented in the references. Overall, we have identified the following three effects that significantly affect the quality of the NAVSOL.

(1) The orbit-fit residuals consistently show a positive radial offset for all satellites (8 m to 26 m), which is caused by ionospheric refraction. Overall, the radial offset and the standard deviation are somewhat larger for the plane-2 and plane-3 satellites than for the plane-1 satellites. This is because the plane-2 and -3 satellites get closer to the TEC maximum and are therefore more strongly affected by ionospheric refraction. Looking at the temporal variations, all plane-1 satellites exhibit a similar pattern in the radial residuals. In addition, a long-term increase of the residuals can be observed across all satellites. These temporal variations could be related to general fluctuations and the long-term increase of solar activity during the study period (SWPC, 2023). Simulations with a GNSS signal simulator on ground showed that GNSS signals coming from negative elevations are significantly more affected by ionospheric refraction than signals from positive elevations (Müller et al., 2021). Since the elevation cut-off angle for the NAVSOL computation onboard the Astrocassat satellites is set to -25° , the radial offset is mostly caused by GNSS signals from negative elevations.

(2) Unlike the plane-1 satellites, the plane-2 and -3 satellites exhibit abrupt changes in the magnitude of the orbit fit residuals, which coincide with a switch of the active antenna. Müller et al. (2023) shows that these differences in the quality of the NAVSOL mainly depends on the location of the antenna onboard the satellite. We therefore suggest that the differences in the NAVSOL quality between different antennas are caused by interference of the GNSS signals with signals from other satellite components located in the vicinity of the respective GNSS antenna. Another possible cause, which would be related to the antenna location, is signal attenuation during the transmission from the GNSS antenna to the receiver, depending, e.g., on the cable length. Furthermore, the soldering and tuning of the GNSS antennas are also potential factors that can cause differences in the antenna performance.

(3) The comparison of NAVSOL positions and velocities as well as simulations with a GNSS signal generator show a once-per-revolution periodicity with amplitudes of 2 m and 5 cm/s in the position and velocity, respectively (Müller et al., 2021). This effect is not present in a single-point positioning (SPP) solution using simulated GNSS code observations. We therefore assume that the once-per-revolution periodicity is due to the fact that the Kalman filter used in the real-time navigation algorithm of the M8T receivers operates in an Earth-centered, Earth-fixed system, but does not account for the associated centrifugal and Coriolis accelerations (Montenbruck et al., 2022).

The presented in-flight data from the Astrocassat constellation satellites provide valuable insights into the performance of low-cost GNSS receivers in space, both in terms of temporal variations and differences between satellites and orbital planes. Based on our analysis, we are able to draw conclusions on both software and hardware adaptations for future nanosatellite missions with low-cost GNSS receivers. These include an appropriate elevation-dependent weighting of GNSS observations, improving the dynamic model used in the real-time navigation algorithm, and rearranging antennas or other components of the satellite in order to minimize interferences. With these improvements, real-time CubeSat orbit determination to within a few meters becomes possible with minimal costs and resources.

A high-precision commercial off-the-shelf GNSS payload board for nanosatellite orbit determination and timing

G. Moeller¹, F. Sonnenberg¹, A. Wolf¹, B. Soja¹, M. Rothacher¹

¹Institute of Geodesy and Photogrammetry, ETH Zurich

Accurate satellite orbits are a prerequisite for numerous Earth observation missions, enabling precise measurement of changes in gravity field, surface properties, or atmospheric conditions. Although commercial off-the-shelf GNSS technology has demonstrated utility in terrestrial applications, its suitability for space applications, particularly in small satellites, remains uncertain. To address this gap, we developed a GNSS payload board that meets the integration requirements for nanosatellites in terms of power consumption, size, communication interfaces, and data transfer.

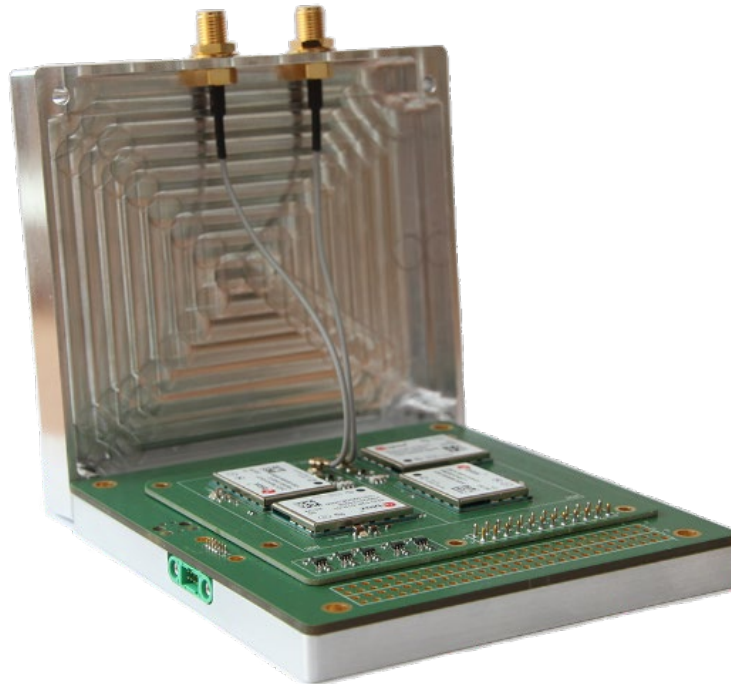


Figure 4.13: The GNSS payload board, specifically designed for nanosatellites, is composed of three main components: a receiver board featuring four modified u-blox ZED-F9P receivers, along with signal filters, splitters, and amplifiers; a main board for onboard computing; and an optional aluminum case for enhanced implementation and shielding.

The GNSS receiver serves as the central component of the board, utilizing four modified u-blox ZED-F9P modules as the baseline. This compact, dual-frequency, multi-GNSS chip, with a dimension of 17 x 22 x 2.4 mm, exhibits a low power consumption of about 0.2 W. Signal reception tests have been conducted with two passive GNSS antennas: the cubesat GNSS antenna from the Fraunhofer Institute in Germany and the taoglas GPSF.36.A patch antenna. Subsequently, orbit simulation tests were carried out in collaboration with the Environmental Engineering Institute (IIE) at the École Polytechnique Fédérale de Lausanne and the Institute of Navigation at University of Stuttgart, utilizing the Spirent GS8000 and GSS9000 signal generators to simulate the dynamics of a low Earth orbit. Different force models were applied to the initial orbital parameters to simulate practical GPS and Galileo dual-frequency observations for various tracking scenarios. A comparison between the simulated orbit and a post-processed code- and

carrier phase-solution showed high precision and solution stability, with an agreement at the level of 1-2 m and 2-3 cm, respectively.

The first prototype of the GNSS payload board was released in summer 2022 and is currently subjected to intensive testing for integration into the Precursor (<http://precursor.space/>), Outpost (<https://outpost.space>) and CHESS (<https://chessmission.ch>) nanosatellites.

Low-Cost GNSS and Real-Time PPP: Assessing the Precision of the u-blox ZED-F9P for Kinematic Monitoring Applications

R. Hohensinn¹, R. Stauffer¹, M.F. Glaner², I.D. Herrera Pinzón¹, E. Vuadens¹, Y. Rossi^{1,3}, J. Clinton³, M. Rothacher¹

¹ Institute of Geodesy and Photogrammetry, ETH Zurich

² Department of Geodesy and Geoinformation, TU Wien

³ Swiss Seismological Service (SED), ETH Zurich

With the availability of low-cost, mass-market dual-frequency GNSS (Global Navigation Satellite System) receivers and antennas, standalone processing methods such as Precise Point Positioning (PPP) are no longer restricted to geodetic-grade GNSS equipment only. However, with cheaper equipment, data quality is expected to degrade. We assessed the quality of a particular piece of low-cost GNSS equipment for real-time PPP and high-rate dynamic monitoring applications, such as strong-motion seismology. We assembled the u-blox ZED-F9P chip in a small and light-weight data logger. With observational data from static experiments - which are processed under kinematic conditions - we assess the precision and stability of the displacement estimates. We tested the impact of different multi-band antenna types, including geodetic medium-grade helical-type (JAVAD GrAnt-G3T), as well as a low-cost helical (ArduSimple AS-ANT2B-CAL) and a patch-type (u-blox ANN-MB) antenna (Figure 4.8). Besides static tests for the assessment of displacement precision, strong-motion dynamic ground movements are simulated with a robot arm. For cross-validation, we collected measurements with a JAVAD SIGMA G3T geodetic-grade receiver. It was shown that, even with low-cost GNSS equipment, it is possible to obtain a precision of one centimetre (component-wise, see Figure 4.9), and that the low-cost equipment performs similar to geodetic-grade equipment (Hohensinn et al, 2022). We conclude that these devices provide an excellent basis for the densification of existing GNSS monitoring networks, as needed for strong-motion seismology and earthquake-early-warning.

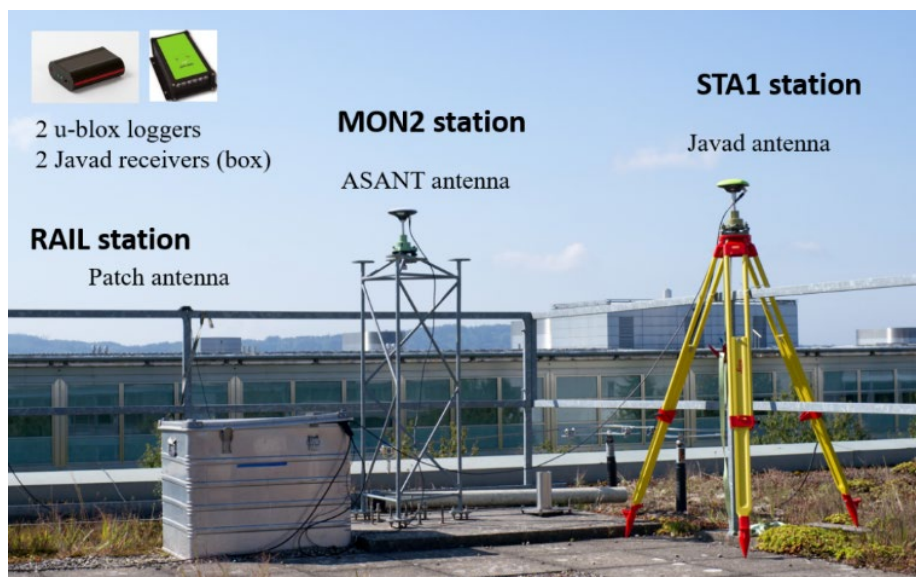


Figure 4.14: Experimental setup for the test of the u-blox receiver with two different types of low-cost antennas (left, stations RAIL and MON2), against geodetic grade equipment (right, station STA1).

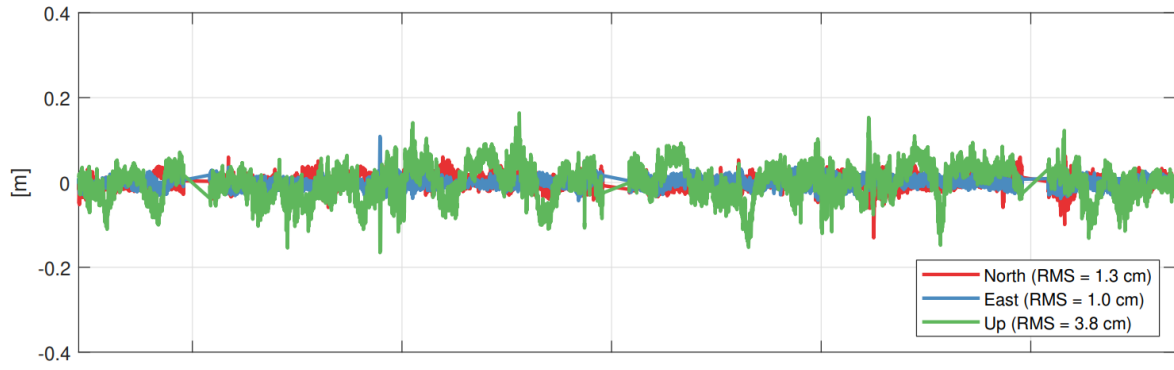


Figure 4.15: Real-time PPP results for a low-cost GNSS instrumentation (MON2 station)

Sensing small-scale structures in the lower atmosphere with tomographic principles

G. Moeller¹, E. Shehaj¹, W. Zhang^{1,2}

¹ *Institute of Geodesy and Photogrammetry, ETH Zurich*

² *Now at: School of Environment and Spatial Informatics, China University of Mining and Technology*

This report provides a summary of ETH Zurich's contributions to the activities of the IAG working group on tropospheric tomography from 2019 to 2023 and highlights some of the major achievements. The working group was established in December 2019 with the objective of bringing together researchers and professionals engaged in the study of tomography-based concepts for sensing the neutral atmosphere (Moeller, 2020). These concepts involve the use of space-geodetic and complementary observation techniques that are sensitive to the distribution of water vapor in the lower atmosphere.

While geodetic GNSS networks currently serve as the foundation for troposphere tomography studies, we investigated in the study of further refinements including local densifications, more flexible tomography models, and advanced processing strategies for sensor fusion. The primary goal of these investigations was to achieve a tomography model with very high spatial and temporal resolution. ETH Zurich contributed to this activities by the overall coordination of the working group activities and in particular by research in the following fields:

- Sensor fusion based on tomographic principles, including the establishment of a benchmark campaign for algorithm testing and validation.
- Development of dynamical tomography models that can adapt to varying input data, such as continuous-time image reconstruction and trade-off between model resolution and variance size.
- Advanced ray-tracing algorithms for reconstructing atmospheric signal paths for both ground-based and space-based (e.g., radio occultation) observations.
- Exploration and promotion of tomography applications.

The subsequent sections briefly outline two of the major achievements:

A collocation framework to retrieve tropospheric delays from a combination of GNSS and InSAR

This research contributes to advancing the spatio-temporal mapping of tropospheric delays by integrating delays derived from GNSS and InSAR measurements. Therefore, a collocation framework was introduced (see Shehaj, 2020a and 2020b) that combines and retrieves zenith and relative slant tropospheric delays, aiming to enhance the accuracy of atmospheric water vapor estimation. We examined the effectiveness of this combination approach by comparing the results of collocation with refractivity fields obtained in the alpine region of Switzerland during August 2016 using classical tomography techniques, see Shehaj (2023). Our results show that collocation and tomography agree at the level of a few ppm, with a maximum difference of 5 ppm, particularly in the lower layers, over a two-week period, see *Figure 4.10*. Despite underestimating refractivity compared to the ground truth, collocation, e.g. consistently detects the higher water vapor content during the arrival of a weather front and thus, provides significant 3D information about the current atmospheric state.

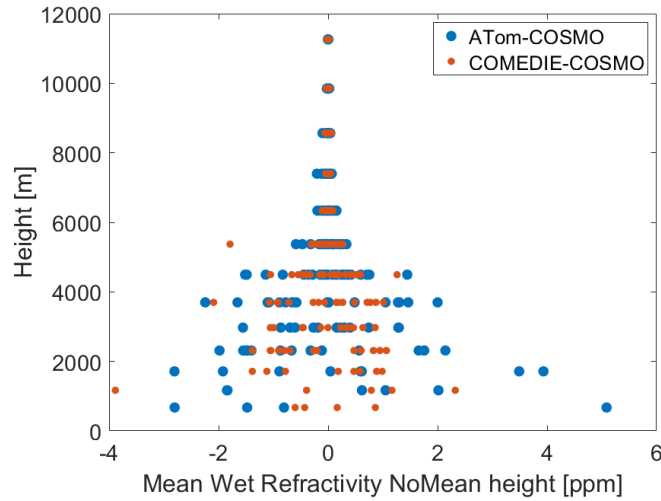


Figure 4.16: Tomography and collocation differences to COSMO-1 numerical weather model-derived refractivities, as a function of height, averaged over two weeks in 2016.

Nanosatellites: The next big chapter in atmospheric tomography

Nanosatellite technology has opened up new opportunities in the field of Earth observation. In the coming decade, we can expect the emergence of large satellite constellations consisting of hundreds, or even thousands, of satellites in low earth orbit. Many of these satellites will be equipped with cost-effective sensors like GNSS receivers, suitable for atmospheric monitoring. Our approach is to applied tomographic principles to the dense observations generated by nanosatellite formations for sensing small-scale structures in the lower atmosphere with high spatio-temporal resolution. For more comprehensive information regarding the approach, additional details can be found in the publication by Moeller (2023). Figure 4.11 highlights the underlying observation concept.

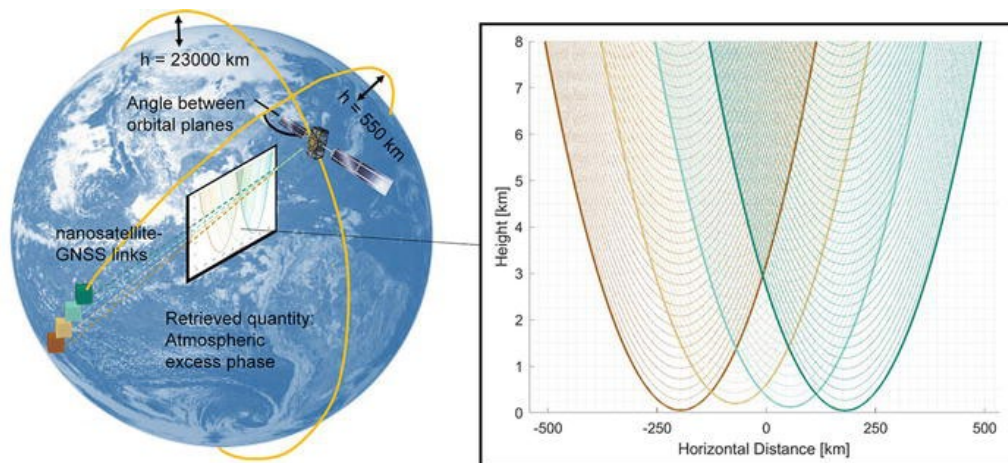


Figure 4.17: Left: The observation geometry for one GNSS satellite simultaneous observed by four nanosatellites in a string-of-pearls formation. Right: The resulting radio occultation signal paths. Source: Moeller (2023).

Figure 4.12 displays the refractivity fields obtained from an end-to-end simulation using the observation geometry presented in Figure 4.11 as baseline. The plot in the upper left corner illustrates the a priori field, which serves as the initial smooth refractivity field for initializing the tomography solution. The upper right plot presents the actual tomography solution. By comparing it with the reference field shown in the lower left plot, we can evaluate the tomography approach's ability to reconstruct the refractivity field. The lower right plot depicts the differences between the two models.

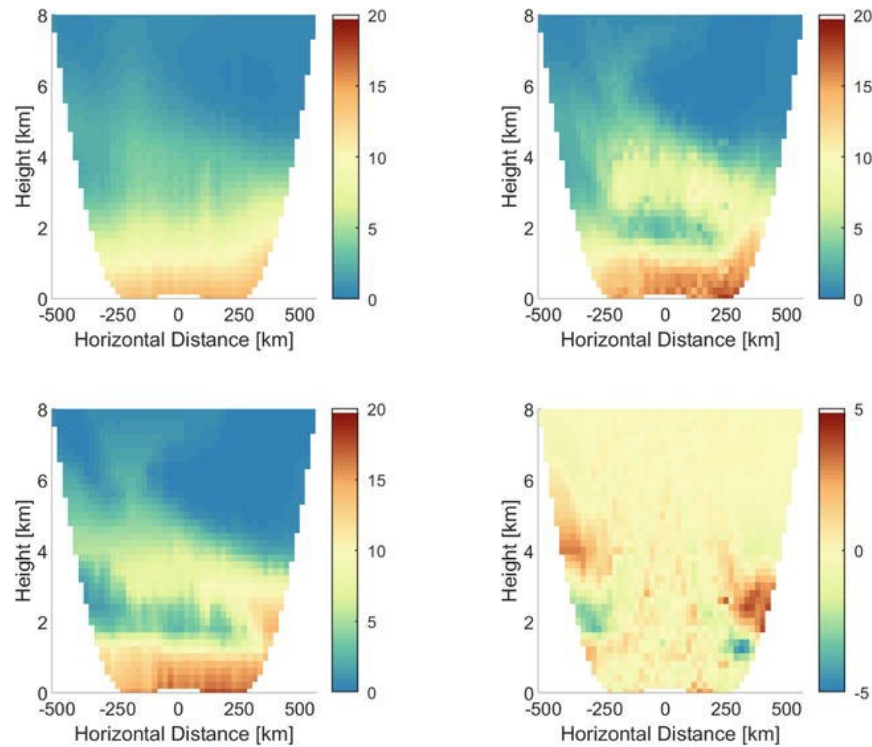


Figure 4.18: Top left: Smooth refractivity field used to initialize the tomography solution. Top right: Estimated refractivity field (tomography solution). Bottom left: Reference refractivity field. Bottom right: Closed-loop validation (tomography solution minus reference field) to assess the performance of the tomography approach. Source: Moeller (2023)

In general, the best tomography solution is achieved within the horizontal range of [-250 km, 250 km]. This range corresponds to the area where multiple observations overlap, leading to increased stability in the resolution of atmospheric structures. Within this core domain of the tomography model an RMSE of 0.5ppm (9.6%) is obtained. Applied to real measurements, this advancement holds promising potential for further breakthroughs in atmospheric science, enhancing our understanding of the Earth's atmosphere.

Absolute phase center calibration of low-cost GNSS patch antennas

G. Moeller¹, N. Ryther¹, A. Brown¹, M. Rothacher¹

¹ Institute of Geodesy and Photogrammetry, ETH Zurich

The Institute of Geodesy and Photogrammetry (IGP) at ETH Zurich has developed a robot system for the absolute calibration of GNSS antennas. The core of the system is a KUKA AGILUS KR 6 R900 sixx industrial robot with six axes (KUKA 2018). The robot's operation procedures were initially established by Willi (2019) and subsequently enhanced by Moeller (2021) for calibrating low-cost GNSS antennas and smartphones.

The motivation behind calibrating non-geodetic antennas is diverse, ranging from attitude determination on nanosatellites to ambiguity resolution in precise point positioning and environmental monitoring. One such example is the use of smartphone-based GNSS measurements for monitoring the atmospheric state.

To validate the robot system, a collaborative effort between ETH Zurich and the University of Bonn was undertaken in 2021 to calibrate the Tallysmann VP6035F antenna. Figure 1 on the left illustrates the Phase Center Variations (PCVs) resulting from the Tallysmann antenna calibration at ETH using a spherical harmonics parameterization of degree and order eight. On the right side of Figure 4.13, the differences in the best-fit Phase Center Corrections (PCCs) for the GPS L1 signal between the University of Bonn and ETH Zurich calibration facilities are shown, based on the same antenna. The root mean square (RMS) of the differences between the best-fit PCCs is 0.3 mm, with a bias of 0.0 mm. Considering a phase noise of approximately 1 mm for the GPS L1 signal, this level of agreement is remarkable and demonstrates the strong concordance between the two GNSS antenna calibration facilities.

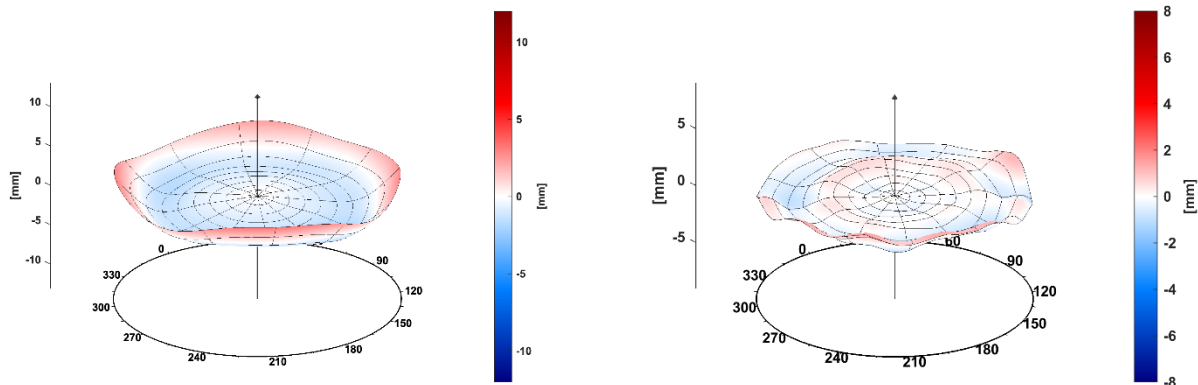


Figure 4.19: Results from the validation campaign of the robot system. Left: Phase Center Variations (PCVs) for the Tallysmann VP6035F antenna calibrated at ETH Zurich. Right: Differences of the GPS L1 best-fit Phase Center Corrections (PCCs) between the calibrations from University of Bonn and ETH Zurich.

To calibrate low-cost patch antennas or omnidirectional linearly polarized smartphone GNSS antennas, certain modifications were implemented in the calibration procedure:

- **Antenna Mounting:** Since low-cost antennas typically lack a standard 5/8" thread, a new antenna mounting system was devised to ensure a well-defined and stable antenna position during the calibration campaign. In some cases, a full ground plate design was employed to minimize multipath effects on the calibration results.
- **Antenna Reference Point (ARP):** Low-cost GNSS antennas typically lack a clearly defined reference point. Hence, an ARP was marked and measured on each calibrated antenna using a Leica Absolute Tracker AT960 with a measurement uncertainty of 15-30 μm . Knowing the exact position of the antenna ARP in the robot coordinate system allowed us to determine the GNSS antenna phase center correction with respect to this mechanical reference point.

- **Signal Reception:** To facilitate proper GNSS signal reception during the calibration campaign, a Low Noise Amplifier (LNA) was inserted between the GNSS antenna and receiver. This helped to increase the Carrier-to-Noise Density (C/N0), reducing phase noise, the occurrence of outages, and cycle slips in the carrier phase time series.
- **Rotational Sequence:** In certain cases, particularly with smartphone GNSS antennas, the calibration procedure's speed had to be reduced to maintain an acceptable level of cycle slips.
- **Sampling Rate:** In the case of smartphone antennas, GNSS signals were recorded using the internal GNSS receiver, limiting the sampling rate to a maximum of 1 Hz. In the typical calibration procedure, GNSS data is recorded at 20 Hz, necessitating a longer duration at each pose before moving on to the next calibration pose.

Using the refined calibration procedure, a series of low-cost antennas were successfully calibrated. Figure 4.14 provides an overview of three antennas analyzed in the initial calibration campaign.

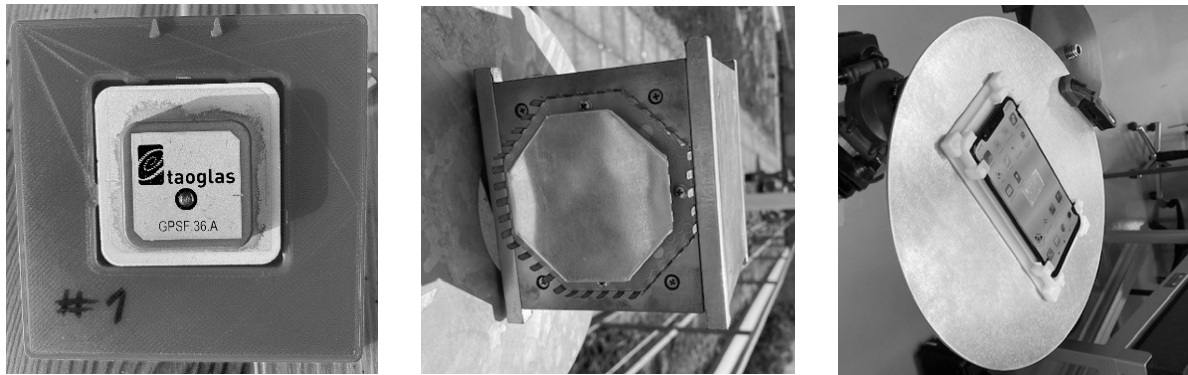


Figure 4.20: Calibrated low-cost GNSS antennas. Left: Taoglas GPSF.36.A passive patch antenna. Middle: CubeSat GNSS antenna from the Fraunhofer Institute for Integrated Circuits (IIS). Right: Xiaomi Mi8 with the integrated omnidirectional linearly polarized but dual-frequency multi-GNSS antenna.

Table 4.1: provides a comprehensive summary of the acquired GPS L1 Phase Center Offsets (PCOs) and Phase Center Variations (PCVs) for the GNSS antennas presented in Figure 2, focusing on the GPS L1 frequency. presents a summary of the obtained Phase Center Offsets (PCOs) and Phase Center Variations (PCVs) for the GPS L1 frequency.

Antenna/Device	PCO in N, E, U [mm]	PCV min / max [mm]	σ residuals
Taoglas GPSF.36.A	[-2.5, -1.1, -11.2]	[-4.3 / 5.1]	2.0 mm
CubeSat GNSS antenna	[-1.4, 0.0, 2.9]	[-4.6 / 5.5]	2.4 mm
Xiaomi Mi8	[6.5, -6.1, 16.1]	[-43.0 / 44.0]	15.1 mm

Table 4.1: provides a comprehensive summary of the acquired GPS L1 Phase Center Offsets (PCOs) and Phase Center Variations (PCVs) for the GNSS antennas presented in Figure 2, focusing on the GPS L1 frequency.

Figure 4.15: GPS L1 Phase Center Variations for the three GNSS antennas: Taoglas GPSF.36.A (left), CubeSat GNSS antenna from the Fraunhofer Institute for Integrated Circuits (middle), and the Xiaomi Mi8 with the integrated omnidirectional linearly polarized GNSS antenna (right).displays the Phase Center Variations (PCVs) for the three antennas, with distinct color bar scales for each.

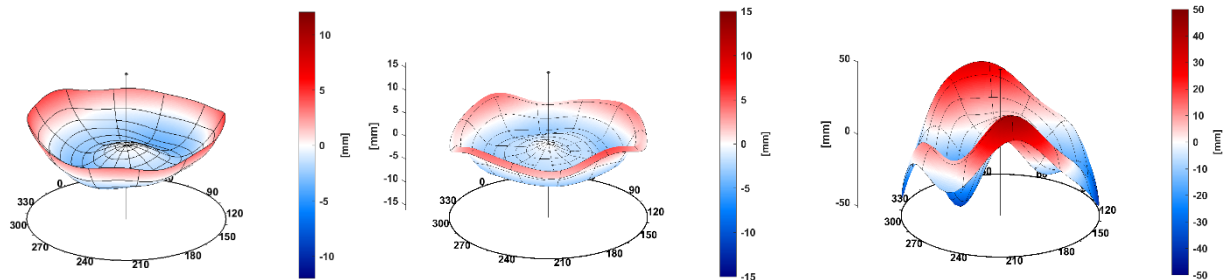


Figure 4.21: GPS L1 Phase Center Variations for the three GNSS antennas: Taoglas GPSF.36.A (left), CubeSat GNSS antenna from the Fraunhofer Institute for Integrated Circuits (middle), and the Xiaomi Mi8 with the integrated omnidirectional linearly polarized GNSS antenna (right).

The findings demonstrate the feasibility of calibrating low-cost patch antennas. The phase residuals' standard deviation at 2 mm is approximately twice as high as that of geodetic antennas, but it remains acceptable considering the range of phase center variations. The calibration results for smartphone antennas are ten times larger than those for patch antennas, indicating a need for calibration, particularly when ambiguity resolution is anticipated. The substantial standard deviation of phase residuals suggests that certain challenges in calibrating smartphones have yet to be addressed, highlighting the importance of further investigation.

Estimation of Tropospheric Parameters with GNSS Smartphones in a Differential Approach

R. Stauffer¹, R. Hohensinn^{1,3}, I. Herrera Pinzón¹, G. Moeller¹, Y. Pan¹, G. Kłopotek¹, B. Soja¹, E. Brockmann², M. Rothacher¹

¹ Institute of Geodesy and Photogrammetry, ETH Zurich

² Swiss Federal Office of Topography swisstopo, Bern

³ International Space Science Institute (ISSI), Bern

With the introduction of the operating system Android 7 Nougat in the year 2016, it became possible to access GNSS code and carrier phase observations. These observations can be processed with the state-of-the-art GNSS processing software packages, which allows an in-depth evaluation of the smartphone's GNSS performance. The availability of carrier phase observations enables sub-decimeter-level positioning. A few years ago, smartphones wearing dual-frequency GNSS chipsets hit the mass market. In Stauffer et al, 2023 we investigated the capability of such a device for the estimation of tropospheric delays. Static measurements carried out over the period of two weeks are performed using a Google Pixel 4 XL smartphone (Figure 4.10). The measurements are processed using relative positioning methods, where a Continuously Operating Reference Station acts as a base. The estimated differential zenith tropospheric wet delay (dZWD) obtained for the smartphone are then combined with absolute values computed at the reference station, in order to obtain time series of zenith total delay (ZTD). Using this method, we demonstrate that high-precision ZTDs can be successfully determined from smartphone GNSS observations (Figure 4.11). When comparing the estimated tropospheric delays with those determined at a nearby geodetic receiver to assess the accuracy of the acquired time series of ZTD, differences in the range of few millimeters to a centimeter are visible. We examine the impact of various error sources, such as antenna phase center variations and residual effects of the ionosphere. Given that the obtained accuracies are at the level of a centimeter and below, the suggested method shows the potential to resolve small-scale tropospheric structures in near real-time, and thus, could be an interesting data source for numerical weather prediction models or related GNSS crowdsourcing projects.



Figure 4.22: Experimental setup for the test of the Google Pixel 4XL for tropospheric studies. For the tests, the smartphone was covered by a radome.

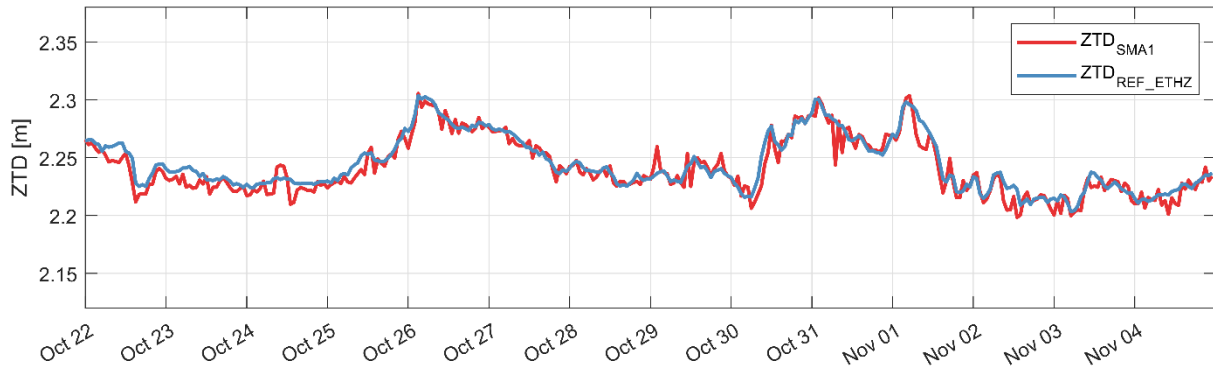


Figure 4.23: Results for the tropospheric estimation of the smartphone station (SMA1) against a geodetic-grade reference solution

Modeling atmospheric effects in microwave satellite signals

E. Shehaj¹, A. Geiger¹, G. Moeller¹, O. Frey², L. Miotti¹, B. Soja¹, S. D'Aronco¹, J.D. Wegner^{1,3}, M. Rothacher¹

¹ Institute of Geodesy and Photogrammetry, ETH Zurich

² Institute of Environmental Engineering, ETH Zurich

³ Institute for Computational Science, University of Zurich

Microwave signals of space geodetic techniques are sensitive to the constituents along the propagation ray, especially the effects of high spatio-temporal variations of atmospheric water vapor are difficult to model. Unmodeled tropospheric delays deteriorate the accuracy of remote sensing and geodetic techniques. For high-precision applications, these delays are typically estimated during the processing of the measurements. For example, in Global Navigation Satellite Systems (GNSS) the so-called zenith total delay (ZTD) is estimated together with the other unknown parameters.

In a first study, we tried to answer the question whether tropospheric path delays retrieved at GNSS permanent stations can support the processing of Interferometric Synthetic Aperture Radar (InSAR). For this purpose we assessed the consistency and differences among GNSS and InSAR datasets to better understand the ability of these microwave techniques for sensing small-scale structures in the lower atmosphere. We also utilized numerical weather model (NWM) data from the COSMO-2 model (deployed by meteoswiss) to evaluate the tropospheric fields derived by microwave techniques. Figure 4.12 displays the time series of relative delays from the 3 techniques for 28 InSAR acquisitions. From the analysis of 28 maps of ddSTDs from GNSS and InSAR (persistent scatterer interferometry PSI) in this work, for many maps GNSS was suited to facilitate the PSI processing. We also saw maps where the large-scale variations are quite different, however, although for some maps the large-scale variations seem very different, when the ddSTDs vary within a small interval (such as 10 mm), we expect GNSS to still help isolate the tropospheric phase contribution in the PSI processing. GNSS delays have a standard deviation of ~ 4 mm compared to NWM data, about $\sim 13\%$ of the SAR wavelength (3 cm). If we consider as reference the NWM, we show a quantitative argument that GNSS is suitable to model the tropospheric fields. Much more complications should be considered in reality, for instance that actual deviations can go up to 3 sigmas.

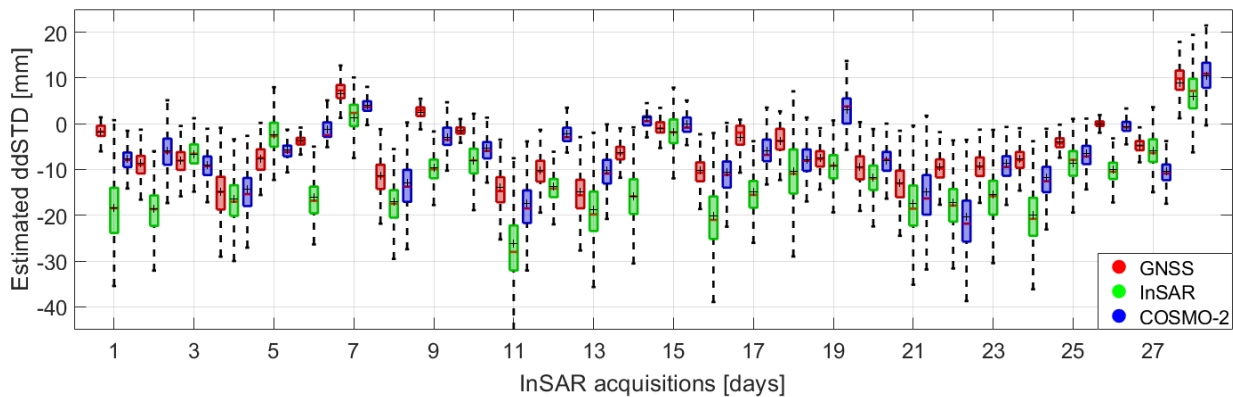


Figure 4.24: GNSS, InSAR/PSI and COSMO-2 estimated ddSTDs time series, for 28 SAR acquisition days. This is a quantile plot where the whisker corresponds to 99.3% coverage in case of a normal distribution ('+' and '-' in the box represent the mean and the median respectively).

In another study we use machine learning (ML) to model tropospheric delays in satellite signals. More concretely we used ground based meteorological parameters from the SwissMetNet network to model ZTDs estimated at 72 permanent GNSS stations in Switzerland. We used data from 2008 until 2018 where the first 10 years were used to

model the implicit relation of meteorological data and zenith delays and the last year to test the performance of the model. In addition, we performed a comparison of the ML predicted delays with the Saastamoinen model, where we initially interpolated the meteorological observations at the GNSS sites and therefore we calculated the ZTD with the empirical formula. Figure 4.13 displays the monthly root mean square error for the predicted ZTDs, for year 2018, at the 72 GNSS permanent stations. The machine learning algorithms (Random Forest (RF) and Neural Networks (NN)) both outperformed the empirical Saastamoinen model. From the statistics we noticed that the ML predicted delays are unbiased (average over all stations for all epochs), while the Saastamoinen model exhibited a few mm bias (3.4 mm). The standard deviation of the Saastamoinen model was 20.9 mm and the one of the NN (RF) model 16.1 (16.7) mm.

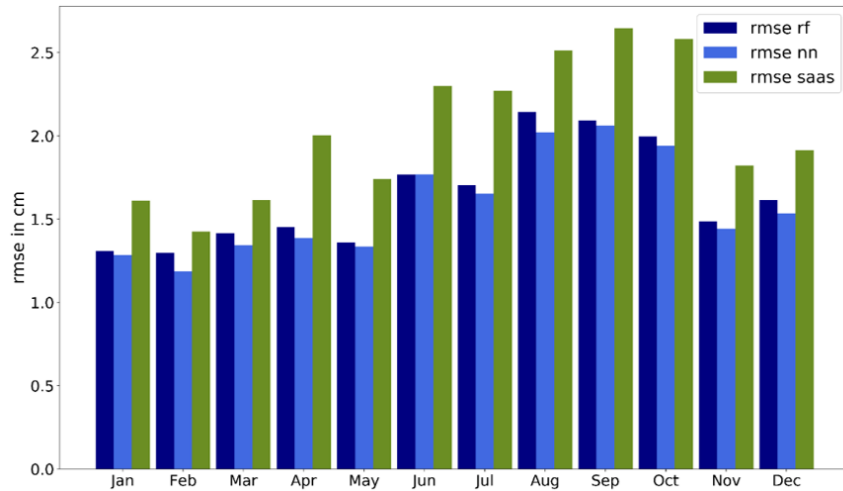


Figure 4.25: Monthly rmse of random forest, neural network and the Saastamoinen model.

In a further research, we aimed to predict the ZTDs at untrained locations. We noticed that while the ML models (NN the best performance) could predict accurately the ZTDs at the trained stations, they could not predict well at untrained locations. Indeed, when we removed some of the stations from the training process (years 2008-2017), the statistics of the predictions at these stations (year 2018) worsened considerably, especially in terms of bias. To resolve this issue and be able to predict high-resolution tropospheric fields we proposed a combination of machine learning and collocation. We make use of machine learning to predict time series of zenith total delays at trained locations and therefore we use least-squares collocation to spatially interpolate the ML predicted delays. To verify our algorithm, sequentially, we removed each of the GNSS data from the training process in ML. Then, we predicted ZTDs for year 2018 for the remaining GNSS stations and finally used these ML-predicted delays to interpolate to the excluded station. Therefore, we compared the ML+Collocation time series of the excluded station (for year 2018) with the GNSS estimated delays. Figure 4.14 displays the geographic RMS error for each of the GNSS stations. We point out that similar distribution and range of the root mean square error (1-2 cm) was achieved when the station was not excluded from the ML process and the time series were predicted using the ML trained model. Therefore, the combination of the two algorithms exploits their temporal and spatial synergies.

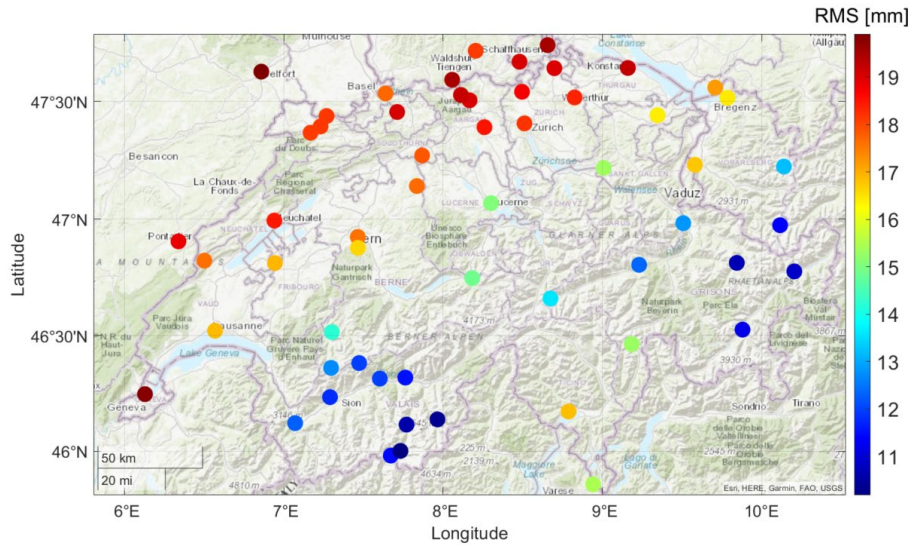


Figure 4.26: Root mean square errors for the combination predictions, for all the GNSS network, for the year 2018.

Using atmospheric observations of microwave satellite signals to improve the meteorological products

E. Shehaj¹, A. Geiger¹, G. Moeller¹, S. Leroy², K. Cahoy³, B. Soja¹, L. Crocetti¹, M. Rothacher¹

¹ Institute of Geodesy and Photogrammetry, ETH Zurich

² Atmospheric and Environmental Research (AER), USA

³ STAR lab, AeroAstro, MIT, USA

We performed a study where we evaluated the collocation capabilities to model refractivity fields from GNSS delays, based on theoretical considerations and experimentally. We compared the refractivity fields retrieved by means of collocation to fields based on GNSS tomography. From an analysis of formal errors, we could report the importance of the a-priori field in tomography and very different formal errors matrices for the two methods. For different simulated 2D networks, collocation formal errors (generally) performed a smooth change with respect to height, while for tomography the formal error changes strongly amongst neighboring voxels. From a 3D+time solution of collocation and tomography, based on synthetic (NWM-based) slant and zenith delays, we computed the differences between the two techniques, displayed in Figure 4.15. Their agreement is at the level of few ppm for low altitudes. At high altitudes the fields from the two methods are very similar. We noticed that, aided by the a-priori field applied, tomography is less prone to biases. However, collocation can better model the relative variations of the refractivity for voxels located at the same height. Finally, we applied both methods to detect an incoming weather front, in 2013 over Switzerland. We could report that both methods could sense the weather front and they perform better in case of GNSS networks which stations have a well-distributed altitude range.

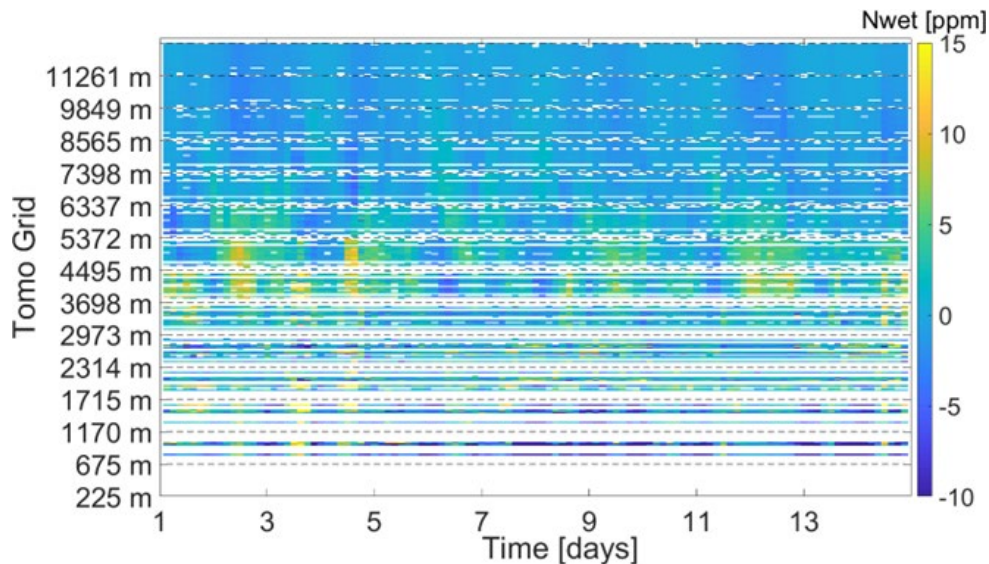


Figure 4.27: Tomography and collocation wet refractivity difference.

We applied ML to GNSS radio occultations (RO) to produce maps of RO-based refractivity. The ML maps were compared to RO gridded products by Bayesian interpolation (BI), a state-of-the-art method used to map RO data, and we noticed better results with the ML approach. Furthermore, we used ML to map residuals of BI, and therefore producing final RO mapped products by adding the BI interpolated values. This loosely coupled combination of BI and ML, namely BI&ML, resulted in the best results. Figure 4.16 displays the residuals of BI and BI&ML for a test dataset at 15 km, where we can notice a much lower number of high value residuals for BI&ML. Furthermore, the gridded refractivity fields were projected into spherical harmonics to assess their horizontal resolution. At 2 km height

we report an improvement from degree 8 for BI-only to degree 14 for BI&ML. In addition, the temporal resolution is improved, where ML (and BI&ML) can map at few hours resolution, compared to at least 3 days of observations needed from BI. Finally, we performed preliminary tests, where RO observations were mapped into gridded products with the scope to detect an atmospheric river. We could show in simulation mode that, while a constellation of 12 or 24 satellites can sense the river structure at a general level, a constellation of 48 satellites can capture its intensity and timespan very accurately.

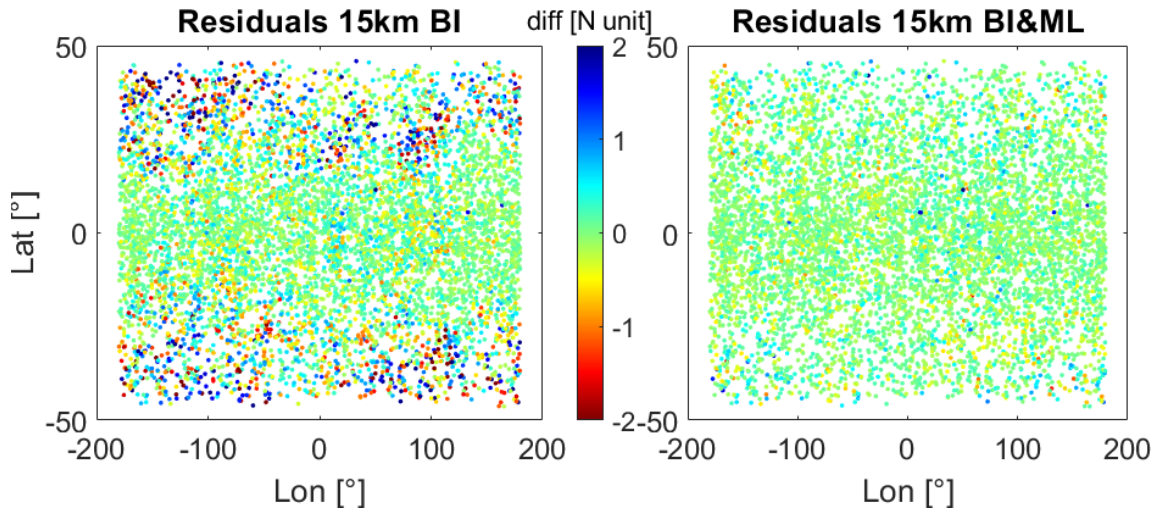


Figure 4.28: Residuals of BI and combined BI/ML at 15 km.

Machine learning-based prediction of Alpine foehn events using GNSS troposphere products: first results for Altdorf, Switzerland

M. Aichinger-Rosenberger^{1,2}, E. Brockmann^{3,4}, L. Crocetti¹, B. Soja¹, G. Moeller¹

¹ Institute of Geodesy and Photogrammetrie, ETH Zurich

² Now at: COSMIC Program, University Corporation for Atmospheric Research, Boulder, CO

³ Swiss Federal Office of Topography swisstopo, Bern

⁴ Now at: Astronomical Institute, University Bern

Foehn winds are associated with significant humidity gradients between two sides of a mountain range. Therefore, tropospheric estimates from GNSS are also affected by their occurrence. Time series of e.g. Zenith Wet Delay (ZWD) reveal characteristic features like distinctive minima and maxima as well as a significant decrease in the correlation between stations north and south of the main Alpine ridge. This is showcased in Figure 4.17 for stations KALT (north, blue) and LOMO (south, red).

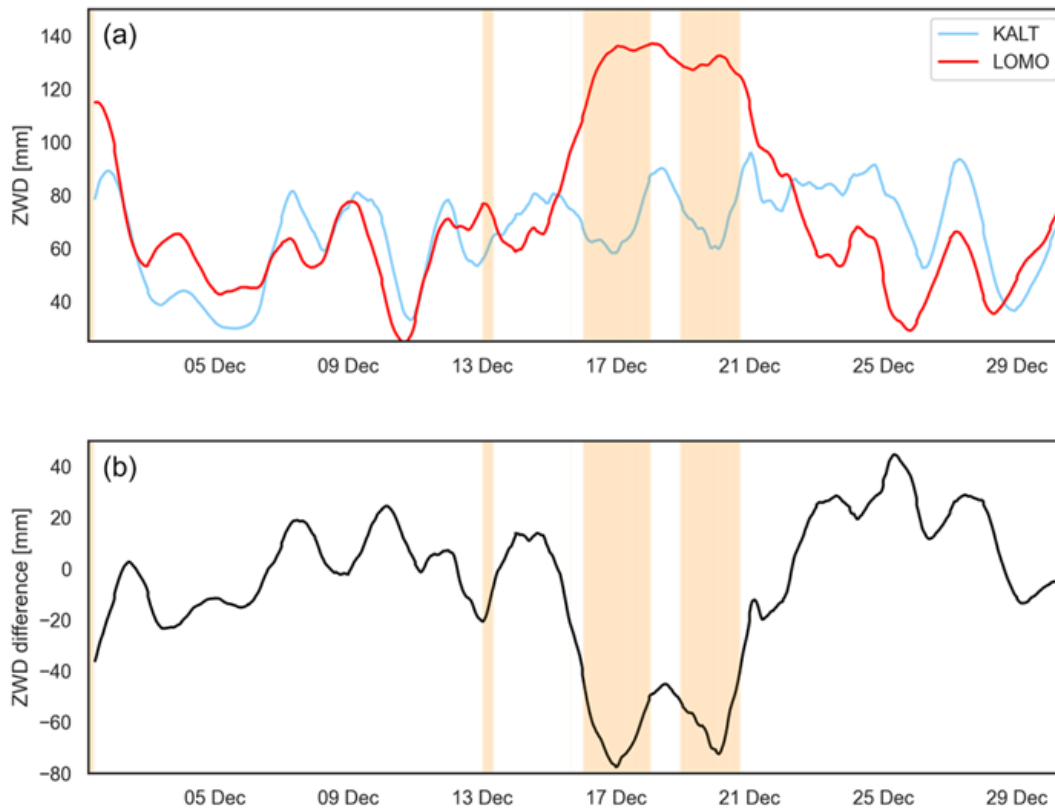


Figure 4.29: Time series of promising foehn predictors for December 2019. (a): ZWD (12 h moving-averaged for visualization) from stations KALT (north of Alpine ridge, blue) and LOMO (south of Alpine ridge, red), (b): ZWD difference between KALT and LOMO (b)

As it gets challenging to analyze these signatures for long time series, we tested the application of machine learning (ML) algorithms for this task. The study published in Aichinger-Rosenberger et.al (2022) investigates the detection and prediction of foehn events at the meteorological observation site Altdorf, by means of GNSS troposphere products and ML. Data from the Automated GNSS Network Switzerland (AGNES) and various GNSS sites from neighboring countries as well as records of an operational foehn index (FI, as ground truth) have been used to investigate the performance of several different classification algorithms based on appropriate statistical metrics. Gradient-boosting (GB) and Support-Vector-Classifier (SVC) were found to be the best performing algorithms during an extensive cross-validation procedure. They were tested in four dedicated experiments using different feature setups, each containing a different combination of stations and parameters used. As an example, Figure 4.18 shows meteorological observations such as (a) temperature (red), humidity (green) (b) and wind speed (black)/direction (grey) as well as prediction algorithm and FI results (c) for a particular foehn event in December 2019.

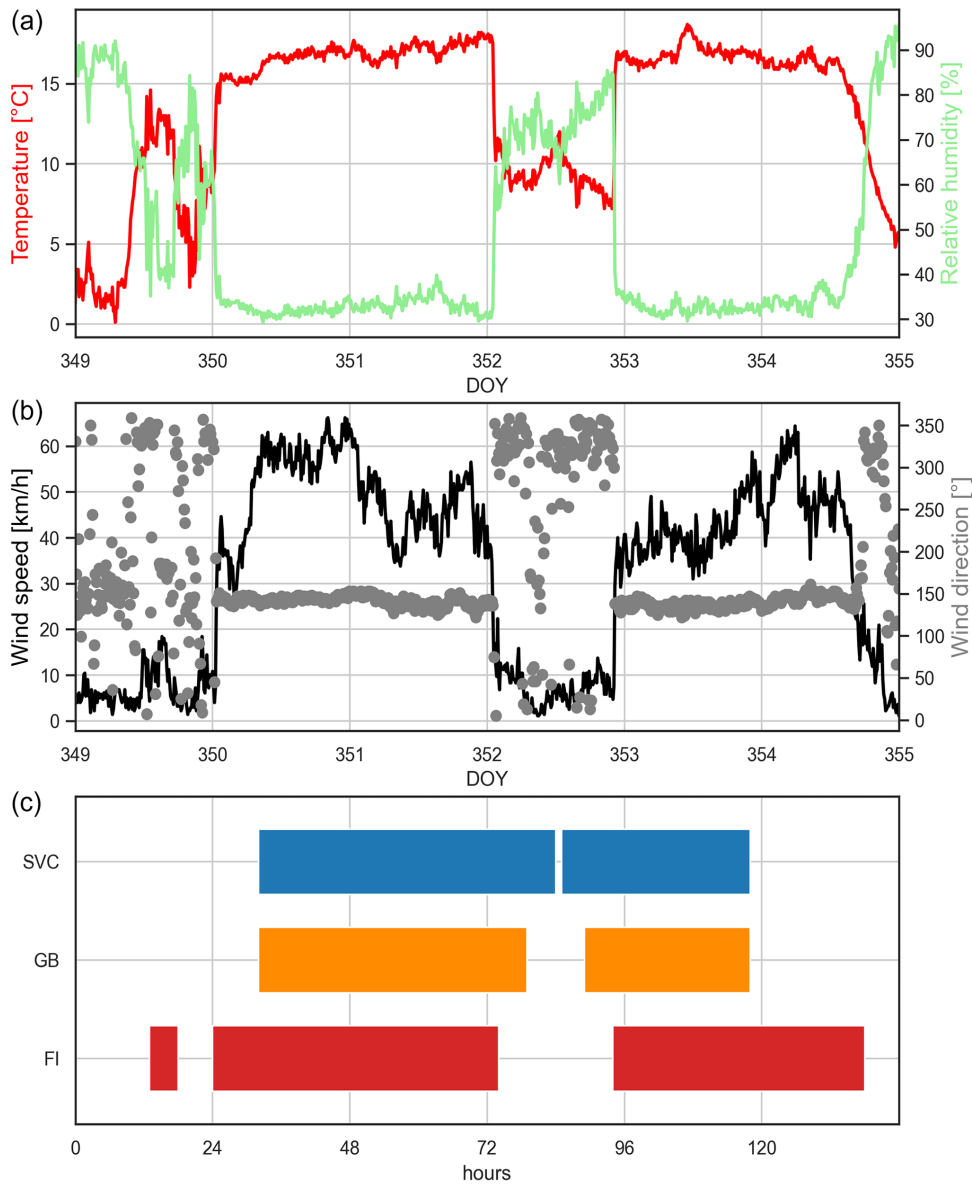


Figure 4.30: Time series of meteorological observations (a: temperature (red) and relative humidity (green), (b): wind speed (black) and direction (grey)); (c): classification results of SVC (blue) and GB (orange) and the reference FI index (red)

Overall results of the study are promising, especially when reprocessed GNSS products are utilized and the densest station setup is used. Detection- and alarm-based measures reach values between 66 %–80 % for both tested algorithms and thus are comparable to those from a reference study (Sprenger et. al (2017)), which uses data from meteorological stations and numerical weather prediction. For operational prediction, limitations due to the availability and quality of GNSS products in near-real time (NRT) exist. However, these might be mitigated to a significant extent by provision of additional NRT products (e.g. atmospheric gradients) and improved data processing in the future. Finally, results also outline benefits when including geographically relevant stations (e.g. high-altitude stations) in the utilized datasets.

MPG-NET: A low-cost, multi-purpose GNSS co-location station network for environmental monitoring

M. Aichinger-Rosenberger^{1,2}, A. Wolf¹, C. Senn¹, R. Hohensinn^{1,3}, M.F. Glaner⁴, G. Moeller¹, B. Soja¹, M. Rothacher¹

¹ *Institute of Geodesy and Photogrammetry, ETH Zurich*

² *Now at: COSMIC Program, University Corporation for Atmospheric Research, Boulder, CO*

³ *Now at: International Space Science Institute, Bern*

⁴ *Research Unit Higher Geodesy, Department of Geodesy and Geoinformation, Technical University of Vienna*

Over the last years, the quality of low-cost dual-frequency GNSS equipment has made significant improvements, which enable its usage in high-precision applications such as troposphere monitoring. At ETH Zurich, efforts have been made to introduce MPG-NET, a low-cost, multi-purpose GNSS station network for environmental monitoring. The project has been initiated in cooperation with the Federal Office of Meteorology and Climatology of Switzerland (MeteoSwiss), and is aiming to equip meteorological observation sites all over Switzerland with low-cost GNSS sensors. Therefore, a specific GNSS station setup has been developed and deployed at the SwissMetNet (SMN) station Zurich-Affoltern/Reckenholz (REH), which serves as a prototype site for the network. At the moment, seven out of ten planned pilot stations are already equipped. Figure 4.19 shows the installed setup at the prototype site (left side) and provides a look at the data logging system deployed at the newly installed MPG-NET station in Ulrichen, Valais area (right side). The actual GNSS setup consists of a u-blox ZED-F9P receiver module and low-cost helix antenna, capable of recording dual-frequency, multi-GNSS observations. The logging system is composed of a Raspberry Pi 4 and an LTE modem and antenna used for data transfer. Costs for the whole setup are approximately 1000 CHF per site. For all stations, 1Hz data is logged and processed in static Precise Point Positioning (PPP) mode using the Bernese GNSS Software 5.2 (Dach et. al, 2015) for a post-processing solution (PP) which uses final orbit and clock products from the Center for Orbit Determination in Europe (CODE). In addition, a quasi real-time (RT) solution is produced using the raPPPid software (Glaner, 2022), which utilizes real-time orbit and clock stream from the Centre National d'Etudes Spatiales (CNES).



Figure 4.31: Left: Full MPG-NET prototype setup installed at the SMN-site Zurich-Affoltern (REH). Right: Interior of the box containing the main parts of the MPG-NET data logging system.

First processing results for two product types are presented in Figure 4.20 and Figure 4.21. Figure 4.20 shows the validation of Zenith Total Delay (ZTD) from the PP (orange) and the RT solution (green) using ZTD derived from the COSMO-1 numerical weather prediction (NWP) model (black) for a three-week period in July 2022 (01.-21.07.2022).

In addition, precipitation amounts observed at the site are shown in blue. Results reveal a good agreement between the ray-traced ZTD and the GNSS-derived solutions, although distinctive biases (10-13 mm) and standard deviations (13-19 mm) are still present for both ZTD solutions.

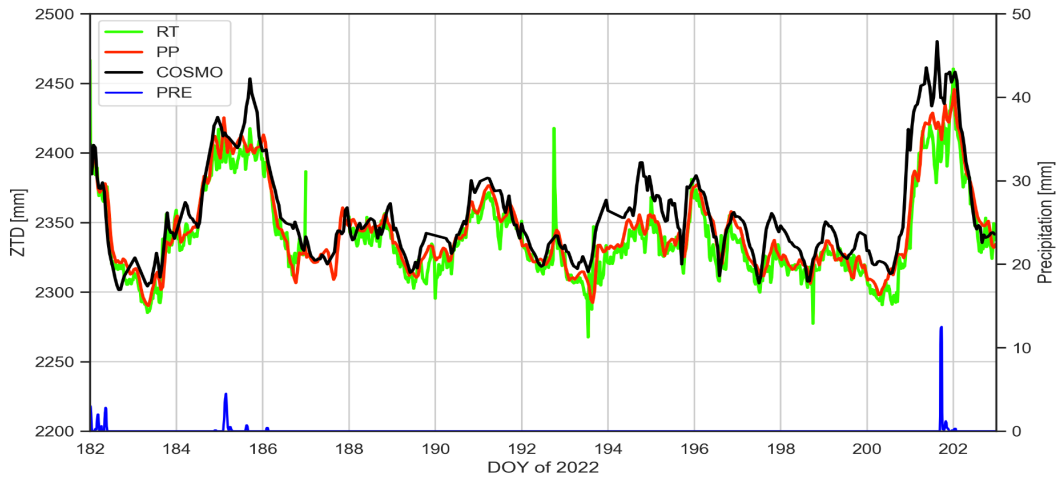


Figure 4.32: Comparison of the RT (green) and PP (orange) ZTD solutions with ray-traced ZTD from COSMO-1 (black) for the period 01.07.-07.07.2022 at the prototype site REH. In addition, precipitation events (PRE) are indicated in blue.

As an additional product type, estimates of soil moisture (Volumetric Water Content (VWC)) have been derived, using the technique of GNSS Interferometric Reflectometry (GNSS-IR, Larson et. al (2008)). Figure 4.21 shows results for a three-month period (June-August 2022, green) derived using the gnss-refl software package (Roesler and Larson, 2018) as well as a reference data set measured by an in-situ sensor (black), which is provided by the Land-Climate-Dynamics group at ETH Zurich. In general, results are very promising as the main trends observed by GNSS are consistent with the reference data set and the sensitivity to precipitation events (shown in blue) is high. Still, there is a significant bias and time lag between the two time series, but most of it can be explained by the different characteristics of the two observation types compared. The in-situ measurements are taken at 10 cm soil depth, whereas GNSS estimates are representing the VWC in the layer nearest to the surface. This also explains parts of the higher variability in GPS VWC estimates which can be observed in Figure 4.21.

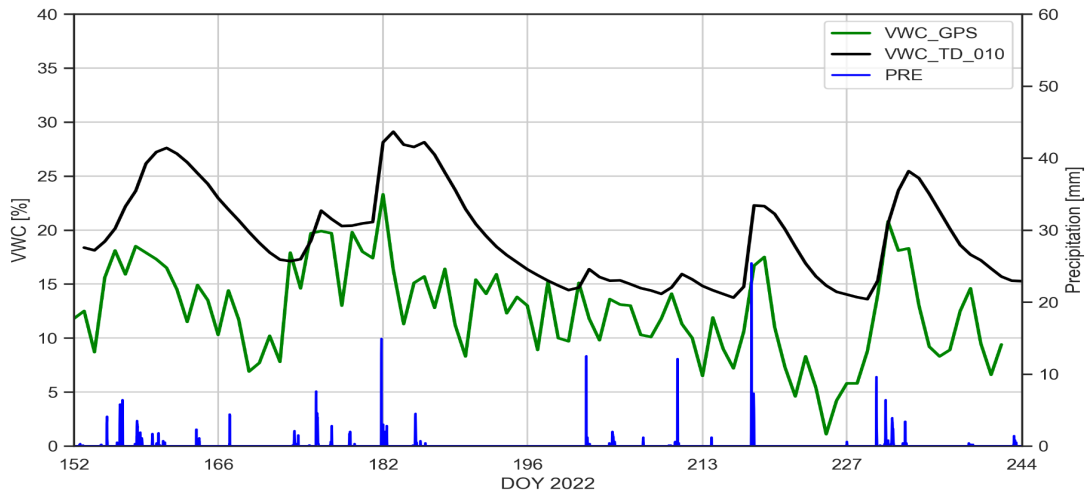


Figure 4.33: Time series of VWC at prototype site REH, derived from GPS-SNR (VWC GPS, green) and the SwissSMEX in-situ soil moisture sensor (VWC TD 10, black) for the period of 01.06 - 01.09.2022. In addition, precipitation amounts measured at the site are visualized in blue.

Overall, results for both product types are promising and further improvements in the processing schemes might still enhance their quality. Future plans for the network include an extension of products to snow parameters (height and snow-water-equivalent) as well as their operational provision to the scientific community on a dedicated online database. More detailed information on MPG-NET and initial results from the prototype station can be found in Aichinger-Rosenberger et. al (2023).

Crowdsourcing GNSS Observations For Atmospheric Monitoring

G. Kłopotek¹, Y. Pan¹, L. Crocetti¹, M. Awadaljeed¹, M. Rothacher¹, T. Sturn², R. Weinacker², L. See², S. Fritz², I. McCallum², V. Navarro³, B. Soja¹

¹ Institute of Geodesy and Photogrammetry, ETH Zurich

² International Institute for Applied Systems Analysis (IIASA), Laxenburg, Austria

³ European Space Agency (ESA), European Space Astronomy Centre (ESAC), Madrid, Spain

The CAMALIOT Project

Application of Machine Learning Technology for GNSS IoT data fusion (CAMALIOT) was an ESA NAVISP Element 1 project (NAVISP-EL1-038.2) with activities covering the acquisition of GNSS observations from the modern generation of smartphones and the development of the dedicated cloud-native software regarding GNSS processing and Machine Learning (ML) at scale based on both conventional and crowdsourced GNSS observations as well as auxiliary data sets and models related to the troposphere and ionosphere. CAMALIOT was commissioned by the European Space Agency (ESA) and led by Benedikt Soja, professor of Space Geodesy at the Department of Civil, Environmental and Geomatic Engineering at ETH Zürich in collaboration with the International Institute for Applied Systems Analysis (IIASA) in Austria.

Selected use cases were implemented in order to identify singularities and correlations across GNSS-related domains with the use of ML. The project concerned different aspects including collection of raw Internet-of-Things (IoT) GNSS data, development of methods for an efficient and automated processing of such observations, and demonstration of their suitability for scientific applications including the determination and prediction of atmospheric parameters (Soja et al., 2022).

Android Application

To cope with large amounts of GNSS data of heterogeneous type and quality, new processing methods were developed that are highly automated, scalable, and robust (Kłopotek et al., 2022). For this purpose, specific ML algorithms were also designed, trained, and validated. Two scientific use cases were studied. The first one focused on the determination of tropospheric parameters to support weather forecasts on Earth (Navarro et al., 2021; Crocetti et al., 2023), whereas the second one concerned the monitoring of space weather, important for satellite operations and communication. Information related to the crowdsourcing GNSS observations is given in the subsequent sections.

In order to secure smartphone GNSS community data, consortium members from IIASA developed an Android application, available on Google Play Store, which has been deployed and assessed throughout the course of the project. This was complemented with the establishment of the dedicated website: <https://www.camaliot.org>. The target audience in this case were researchers working in the area of GNSS and in general volunteers that were interested in improving weather forecasts. The collected observations are then submitted to the back-end by the interested and registered application users. The application provides also the possibility to convert the collected data into RINEX (ver. 3) files.

Crowdsourcing Campaigns

Based on the concept of citizen science, the first campaign was launched on 17 March 2022 and ran until 31 July 2022. In total 12,837 people uploaded 109.7 billion measurements (the number of satellite-specific and epoch-specific observations) to the CAMALIOT server. Twenty prizes were advertised during the campaign including a dual-frequency mobile phone (top prize), Amazon vouchers (prizes 2 to 5), and 15 goodie bags containing branded goods from IIASA, ESA and two sponsors (VITO and Sinergise). Additional features were added to the mobile app and the CAMALIOT website during the first campaign as a result of either the response to user feedback or to provide information/feedback to users as an incentive to keep participating or join the campaign. As the first campaign was

successful and there was an interest to continue the data collection via the application, an autumn campaign was launched, starting 1 August 2022 and running until end of November 2022. Since then, the collection of GNSS data via the CamalioT Android application continues without additional incentives such as prize draws.

Quantity of the Collected GNSS Observations

The daily quantity and volume of the observations as collected with the use of the application instances and submitted to the CAMALIOT server is shown in Figure 4.34. As the crowdsourced observations were collected in an uncontrolled manner, the size of the incoming files initially varied significantly until the so-called continuous mode was introduced to control the data flow in this regard and achieve quasi-continuous and stable data ingestion at the server side. The application working in continuous mode submits the data to the server in an automatic fashion, after collecting observations within a specified time window (specified by the user) while not disturbing or stopping the data collection process itself.

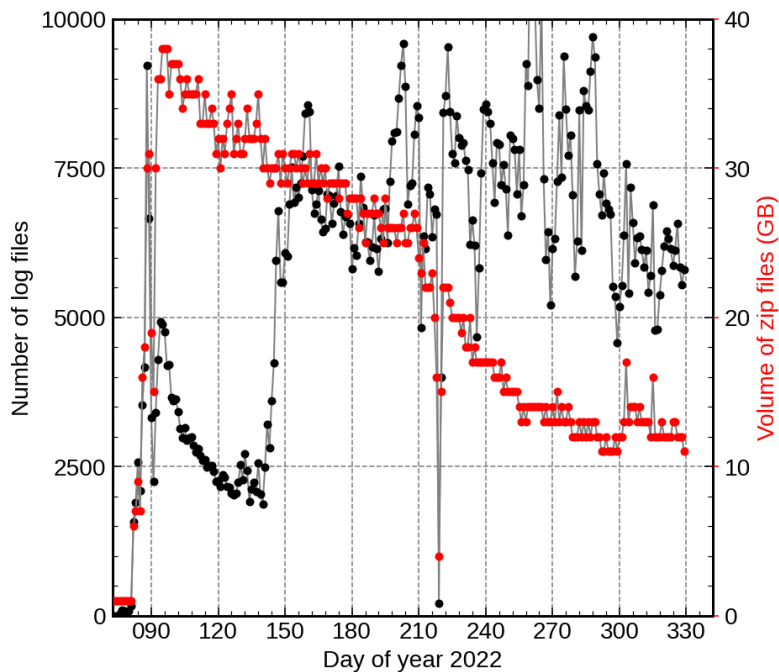


Figure 4.34: The quantity and size of the community data collected as zip archives throughout the course of the activity with the use of the developed CamalioT Android application. The number of log files corresponds to the quantity of the compressed text files (CSV files containing raw GNSS observations) that were uploaded by the registered users. The crowdsourcing campaigns concern days 76-334 (inclusive). The visible change in the number of collected files, occurring around day 140 of the year, is associated with the introduction of the continuous mode for the application.

The incoming observations were recorded with the use of different smartphones and from various parts of the globe. The distribution of the crowdsourced GNSS observations is shown below.

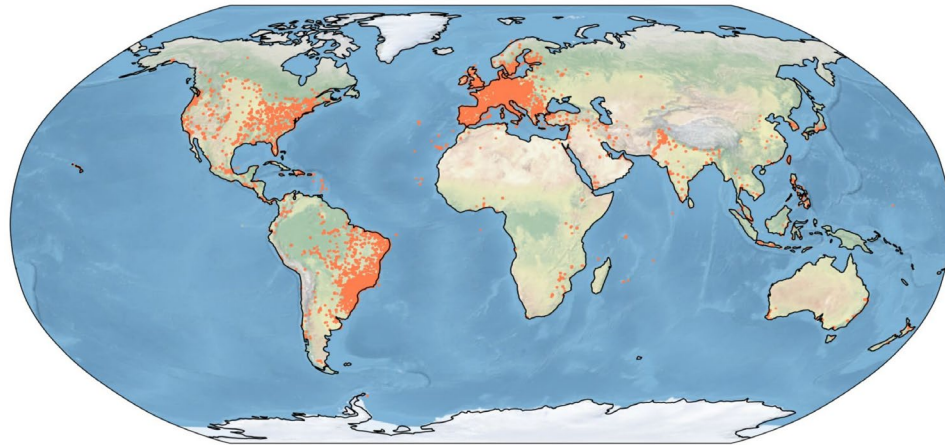


Figure 4.35: Preliminary GNSS Processing Results

Vertical total electron content (VTEC) and Zenith Total Delay (ZTD) were retrieved and uploaded to the CAMALIOT server via the developed Android application. Ionospheric delays in the form of satellite-specific slant total electron content (STEC) are derived through the method commonly referred to as carrier-to-code leveling (CCL) by forming a geometry-free linear combination of dual-frequency observations (L1 and L5 bands).

Refraction effects on long-range terrestrial laser scanning

A. Wieser¹, E. Friedli^{1,2}

¹ Institute of Geodesy and Photogrammetry, ETH Zurich

² Now with: Axpo Power AG, Baden

Monitoring of surface changes, particularly of displacements, is essential for managing risks associated with natural hazards. Established geodetic techniques like totalstation- or GNSS-based network measurements often form the backbone of related monitoring solutions by providing relative displacements between artificially materialized individual points with high and well-known accuracy. However, remote sensing techniques like photogrammetry, laser scanning and radar interferometry are able to provide areal coverage i.e., measurements relating to a dense field of non-materialized points, and can thus complement or even replace point-wise techniques. Widespread practical application to monitoring is still limited by challenges related, among others, to the mitigation of atmospheric effects.

In this context, we have studied the effects of refraction on long-range (LR) terrestrial laser scanning (TLS), see Friedli et al. (2019). An application example is the epoch-wise TLS measurement and deformation analysis of a mountain slope from a sufficiently stable location on the opposite slope, at a distance of several hundred meters or more. In a variety of such applications, we have observed stripe-wise apparent displacements of the scanned surfaces with the stripes converging towards the laser scanner (see Figure 4.23, top right, for an example). Such stripes can be produced by uncompensated tilt changes of the scanner during the scan, e.g., related to a tripod not sufficiently fixed at the ground, by time varying mechanical/electronic deviations in the scanner, or by time varying atmospheric effects.

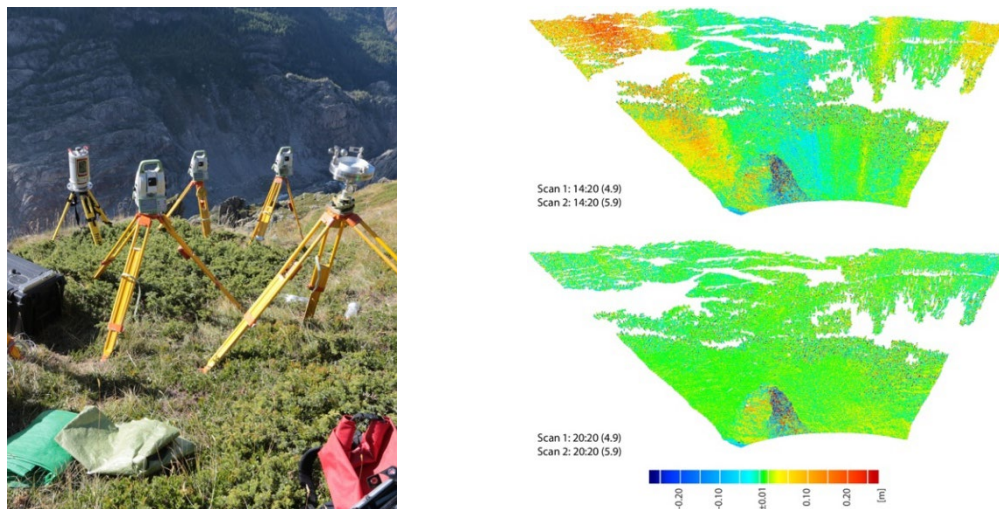


Figure 4.36: Experimental setup opposite Moosfluh landslide, next to Aletsch glacier, for investigating atmospheric effects on LR-TLS (left); calculated displacements of this landslide over 24 hours between September 4 and 5, 2018, around noon (right, top; with artefacts) and after sunset (right, bottom; without artefacts) (Source: Friedli, 2020).

Using numerical simulations and extensive outdoor experiments (see Figure 4.23, left) we were able to corroborate that these deformation artefacts in our data were mainly caused by atmospheric refraction. The variations of the density and chemical composition of the air perpendicular the signal propagation paths (line-of-sight, LOS) from the scanner to the monitored surface and back induce curvature into the LOS. This can be quantified and modeled numerically through the gradient of the refractive index. For the optical wavelengths used in laser scanning the gradient of the refractive index is dominated by the gradients of

temperature and of barometric pressure, which both vary with location and time. The temporal change means that the curvature of the LOS changes over time and thus the laser beam, even if emitted in the same spatial direction from the scanner, will be reflected from different areas at the monitored surface at different points in time. Depending on the topography, distance and location of the scanner, this effect may be negligible or may cause deviations exceeding the scanner’s potential accuracy by far.

One can show that this temporal variability of the LOS is primarily caused by changes of the temperature gradient and that such changes close to the scanner have the biggest impact. In the case shown in Figure 4.23, the temperature gradient along the LOS close to the scanner was heavily affected by wind and by rapid changes of solar radiation due to clouds. This explains the stripe-wise artifacts in the scans. While it is not possible to determine the required meteorological parameters with sufficient accuracy for forward modeling the ray curvature and thus peripheral correction of the point clouds, it may be possible to find a data driven mitigation approach exploiting spatio-temporal smoothness assumptions. This is left for future work. Through the experimental studies we were able to confirm that the diurnal cycles of temperature gradients known from the literature for flat terrain can also be found in a qualitatively similar pattern on mountain slopes. In particular, we identified the time within the first approximately two hours after the sun has disappeared behind the topographic horizon as the time of the day with (i) the smallest absolute value of the temperature gradient, and (ii) the smallest temporal variability of this gradient (see Figure 4.24). Our research indicated that the negative impact of atmospheric refraction on TLS-based deformation analysis can indeed be mitigated efficiently by using only epochs obtained during such times.

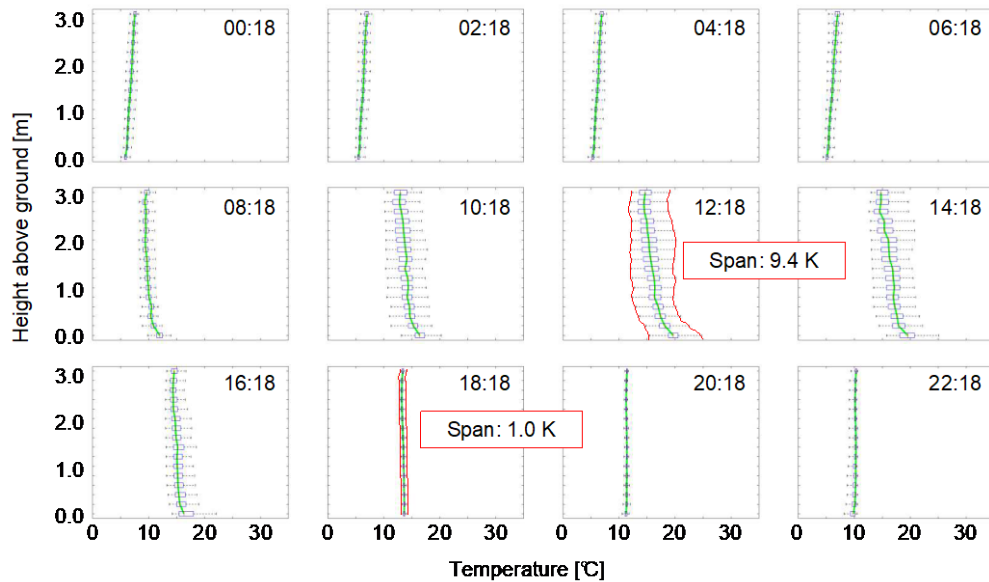


Figure 4.37: Temperature close to the ground within a time window of 23 min (scan duration) every 2 hrs for the setup from Fig. 1, left. The green lines mark the median values for the specific time window, the boxes the 25th and 75th percentiles, and the whiskers the extreme values of each period; smallest and largest variability marked in red (Source: Friedli, 2020).

Dense displacement vector fields from point clouds

A. Wieser¹, Z. Gojcic^{1,2}

¹ Institute of Geodesy and Photogrammetry, ETH Zurich

² Now with: NVIDIA Artificial Intelligence Lab

3D point clouds represent the surface geometry of the covered scenes at the time of data acquisition. Repeating acquisitions at different times facilitates change detection and deformation analysis. Established pointwise monitoring technologies typically rely on determining coordinate differences of carefully chosen and artificially marked or stabilized points, e.g., using monitoring pillars or benchmarks. 3D point clouds instead facilitate areal monitoring using remote sensing and are thus potentially more economic and more informative. However, it is not straightforward to establish the correspondences between points or areas from different point clouds. In particular, this is difficult to achieve automatically.

Established deformation analysis tools for point clouds often rely on quantifying the distance between each point of the test point cloud and its nearest neighbor in the reference point cloud, possibly restricting this search to a predetermined direction (e.g., vertically) or to the direction perpendicular to the local neighborhood in one of the two point clouds. These tools therefore fail to indicate the real 3D displacements of surface elements between the measurement epochs and are particularly insensitive to displacement components along the surface.

We have developed a deep-learning-based approach to establish 3D correspondences between points from pairs of point clouds. The approach is agnostic to the point cloud source, i.e., applicable to point clouds obtained from terrestrial, UAV-borne or airborne laser scanning as well as from photogrammetric approaches including structure from motion. Furthermore, we were able to adapt the basic approach to seemingly different applications like point cloud registration, deformation analysis and 3D scene flow through the incorporation of global, local, or instance-wise rigidity assumptions, see Gojcic (2021).

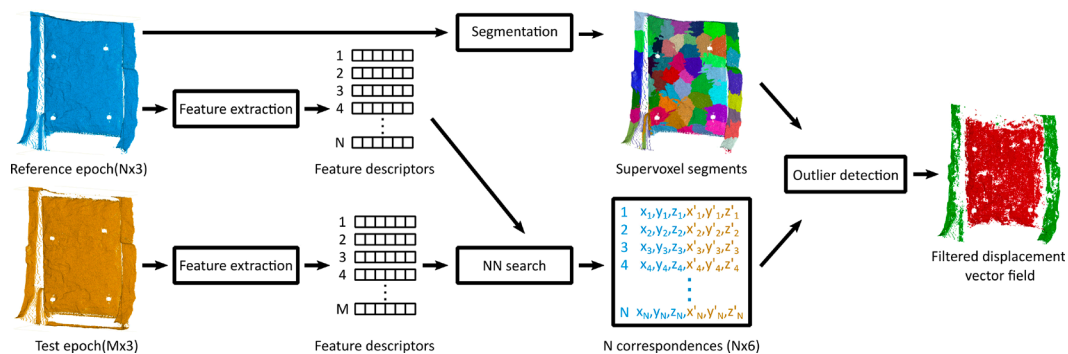


Figure 4.38: Schematic representation of the workflow for estimating 3d displacement vectors between two epochs using F2S3 (Gojcic et al., 2020).

The common core of the approach for all these application cases is the search for correspondences in a feature space instead of in 3D space. Evaluating the geometry of the point cloud in the neighborhood of each analyzed point, we assign a feature vector to the point. The starting assumption was that corresponding points should have nearly the same feature vector in different epochs if the features are well chosen while non-corresponding points should have different ones. In Gojcic et al. (2019) we introduced a learned feature descriptor fulfilling these criteria very well.

Subsequently, we have embedded the correspondence search in feature space into a workflow tailored for deformation analysis, where the tentative correspondences (between nearest points in feature space) were filtered for outliers using the assumption that neighboring areas on the same objects or surfaces typically experience similar displacements. This was achieved by a super-voxel segmentation of the reference point cloud and jointly assessing all tentative displacement vectors originating within the same super voxel (see Figure 4.25, and Gojcic et al. 2020). Finally, the algorithm could be embedded into a workflow facilitating the processing of nearly arbitrarily large point cloud pairs based on a tiling process, separate processing of the tiles sequentially or in parallel, and recombination of the results (see Figure 4.26, and Gojcic et al. 2021).

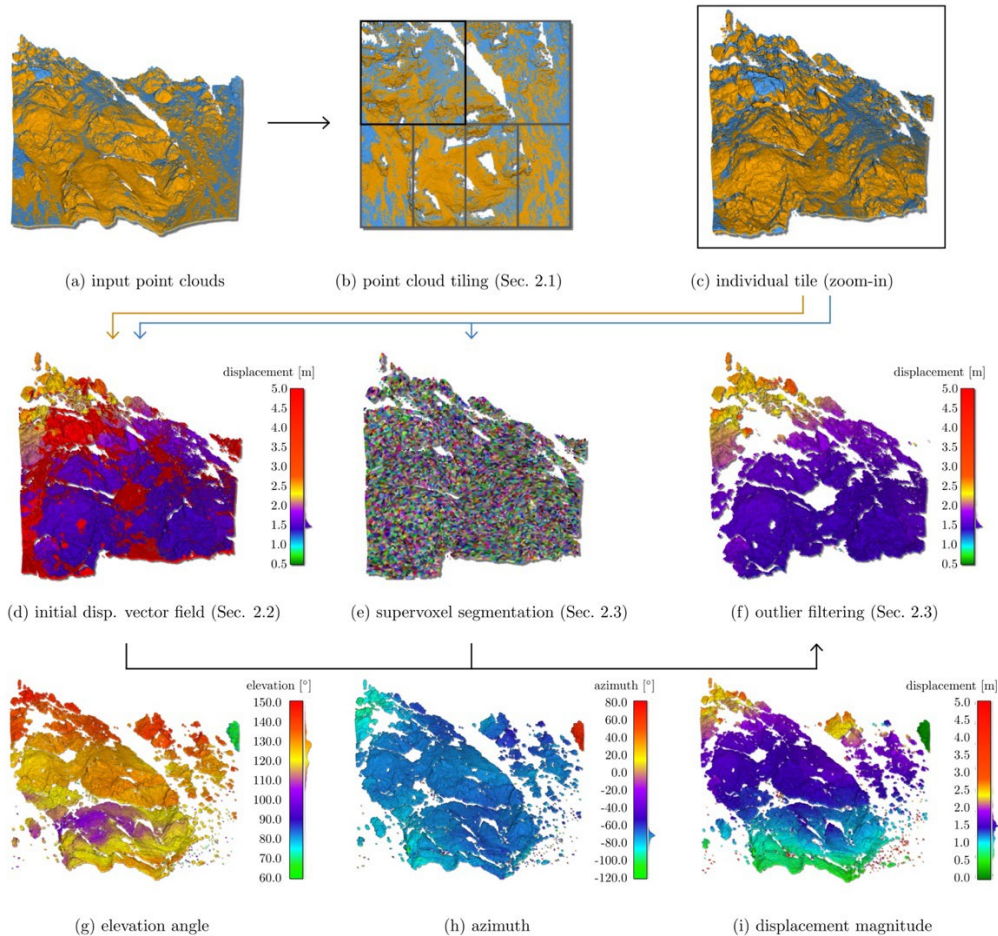


Figure 4.39: Workflow of the proposed point cloud-based deformation analysis method (Gojcic et al., 2021).

Qualitative and quantitative evaluations of the algorithm on a variety of monitoring use cases including a lab setup and real-world landslide areas, indicated that for suitable scenes the algorithm assigns final 3D displacement vectors to a significant fraction of the points in the point cloud (e.g., to about 50% of the points) even in case of predominant displacements along the surface, and that the displacement magnitudes deviated from (sparse) ground truth data with an RMSE on the order of only about 30% of the point spacing in the point cloud, suggesting that the accuracy of the algorithm's output is limited primarily by the point cloud resolution, see Gojcic et al. (2020, 2021) and Gojcic (2021).

Contributions of swisstopo to GNSS Meteorology

S. Lutz¹, D. Ineichen¹, S. Schaer¹, E. Brockmann¹

¹ Federal Office of Topography swisstopo

Since 1999, swisstopo has been active in different projects covering the area of GNSS meteorology. For instance, swisstopo delivers the zenith total path delay estimates from the operational hourly post-processing near real-time GNSS analysis, as well as from the real-time processing done in the software of the Swiss Positioning Service swipos, to the network of European National Meteorological and Hydrological Services (EUMETNET), which supports, for example, numerical weather prediction models.

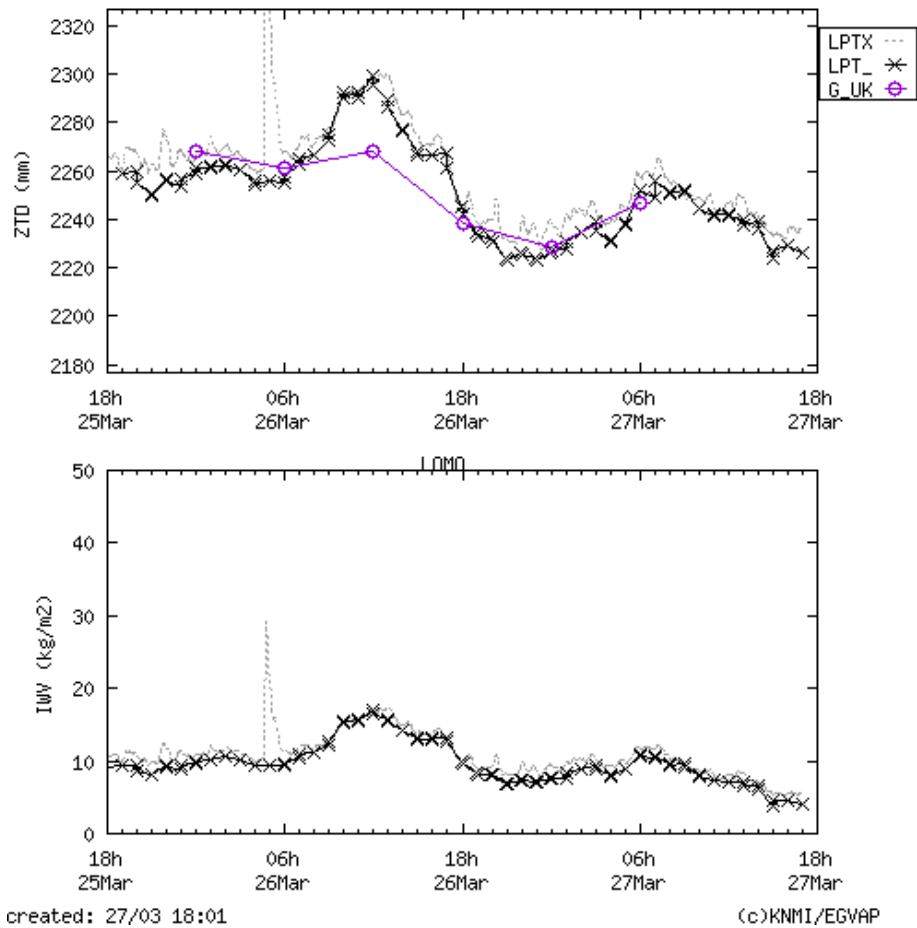


Figure 4.40: swisstopo's contributions to EUMETNET from the hourly near real-time analysis (LPT_) as well as from the real time processing (LPTX). Here station LOMO (Locarno Monti). Both solutions fit quite well, but the post-processing results are usually a bit more robust with less or pre-eliminated "outliers". See also http://egvap-validations.publ.knmi.cloud/processing_center_LPT.html.

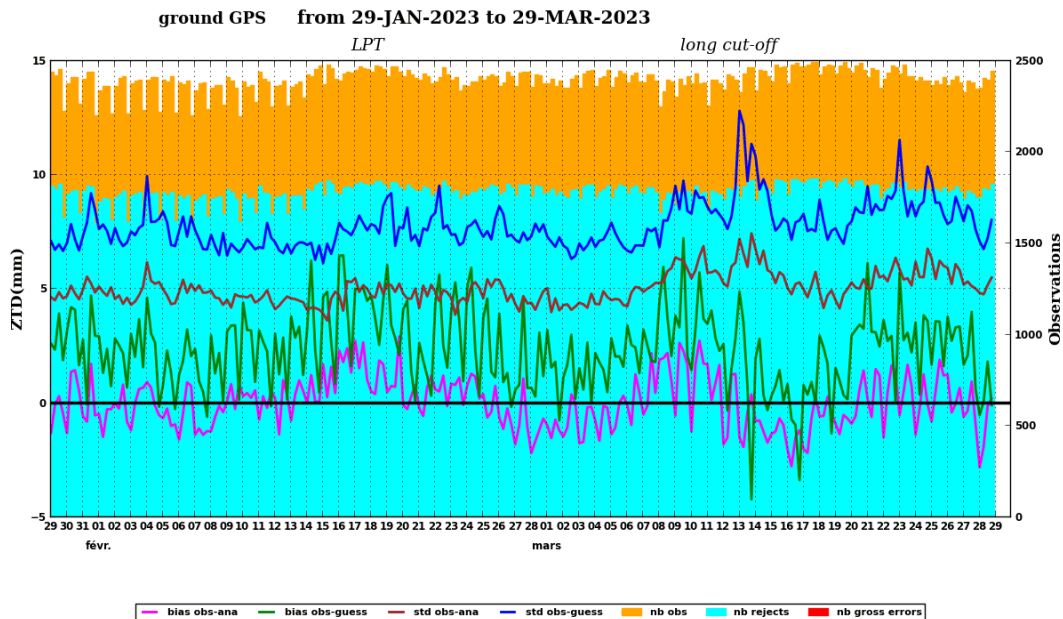


Figure 4.41: Statistical properties of swisstopo's post-processed near real-time ZTD submissions used in the numerical weather prediction analysis at Meteo France. In the time-span shown covering February and March 2023, no big data gaps and no gross errors can be identified. The overall bias is around 0 mm with a standard deviation of 5mm. See also <http://www.meteo.fr/special/minisites/monitoring/SATELLITE/ZTD/groundgps.html>

Because the ultra-rapid orbit products from the Center for Orbit Determination in Europe (CODE) switched from a two-system (GPS and GLONASS) to a three-system solution (GPS, GLONASS and Galileo) in 2019, swisstopo's near real-time troposphere estimates are derived since then from GPS, GLONASS and Galileo observations, if available. At the end of 2019, many individual receiver antenna phase center correction models for GPS and GLONASS were replaced with the type-mean model used for the third IGS reprocessing campaign. At the end of 2022 this type-mean model was replaced with the official igs20 model, which includes correction terms also for the Galileo frequencies.

Beside the near real-time contributions, swisstopo is also monitoring the long-term trends of the tropospheric parameters, which might be interesting for climate research. The results from the last reprocessing effort are regularly complemented with the estimates of the daily GNSS data analysis. For many stations, more than 20 years of zenith total delay parameters are available now.

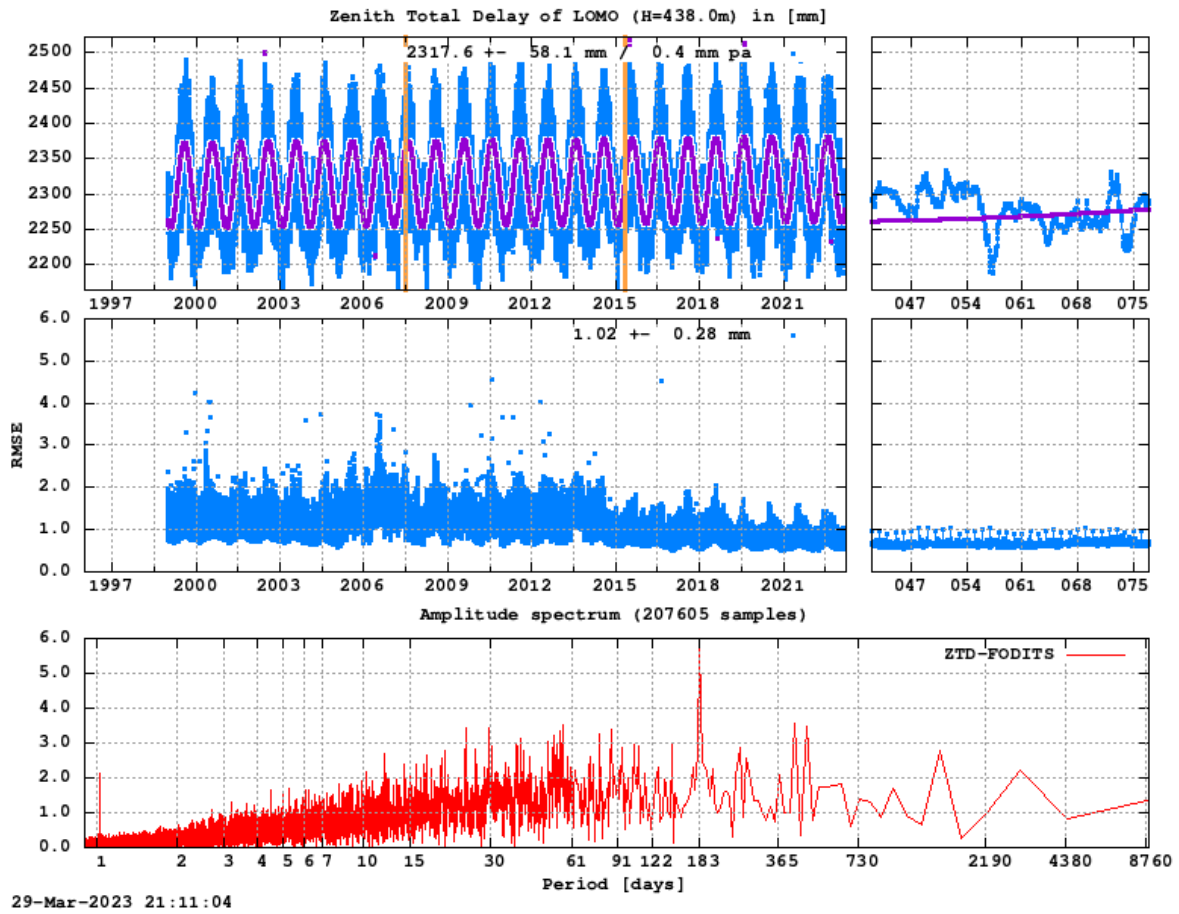


Figure 4.42: Zenith total delay parameter (ZTD) and its RMS error from the GNSS data analysis of station LOMO (Locarno Monti). The vertical lines in the upper subplot indicate antenna changes. A small positive trend of 0.4 mm per year can be detected. In the lower subplot, the amplitude spectrum of the ZTD time series minus the linear trend and the most dominant yearly signal (basically winter/summer) shows another significant period of 183 days (i.e., twice a year), which could be due to local weather conditions. See also <http://pnac.swisstopo.admin.ch> >AGNES status / time series.

Swiss Positioning Service (swipos)

A. Villiger¹, C. Biberstein-Pedroni¹, HP. Christ¹, G. Jeiziner¹

¹ Swiss Federal Office of Topography

The Swiss Positioning Service (swipos) is a real-time correction service for GNSS-RTK applications covering all systems. The main focus area of the service is on the state territory of Switzerland and its backbone is the Automated GNSS Network Switzerland (AGNES) which provides 31 evenly distributed stations over Switzerland. Incorporating additional sites from partner institutions close to the Swiss border ensures the service quality not only within the country but also close to the boundary regions.

The main purpose of the swipos Service is to ensure the access to the Swiss reference system using real-time kinematic applications (RTK). This is currently achieved by offering two different services (also known as mountpoints) including a multi-GNSS mountpoint and a legacy mountpoint which includes only GPS and GLONASS. While swipos was extended to multi-GNSS over the last period, the Beidou support remained restricted as the Beidou 3 satellites are not supported. This will be addressed in the next years to support all satellite system without restrictions. In 2016 a new reference system was introduced replacing the old LV03 system. Until 2021 swipos offered access points for the old LV03 and the new LV95 reference system. Early 2021 the access points for LV03 were suspended as they became obsolete.

The operating system was running seamlessly over the last years. The main focus was set on the transition of the running platform from the Begasoft service to amazon cloud computing (AWS).

The VRS service itself is provided by the Trimble Pivot Platform which is regularly updated. In 2020 the software was updated to 4.5 and early 2022 to the current active version 4.7.1.

Since 2020 another focus was set to increase the monitoring capabilities for the provided services to the customers. For this purpose, an additional network of monitoring stations was installed to monitor the service availability and quality assessment as seen by the users. The monitoring receivers and antennas are installed permanently and send their positions based on RTK solutions using the swipos service regularly to a centralized monitoring platform. This allows to observe the availability and quality assessment of the VRS service as seen by the customers.

To ensure the quality of the service, the maintenance and monitoring of the AGNES network is essential. If the AGNES network is disturbed it has a direct impact on swipos. In the last years, the main issues were snow on the antennas in winter, dirt within the antenna which required manual cleaning, and the detection and repairing of faulty equipment. In the last years this was only needed for the station Ste. Croix where the antenna had to be changed and on the ETH2 station, where the receiver had to be repaired.

In the last 4 years the number of licensed customers continued to grow until 2021 and reached its maximum with about 3623 customers (see Figure 4.30). In 2022 the number of licenses slightly decreased. The main reasons were the cancellation of no longer used licenses and increased activities of other GNSS-RTK service providers. The old DDPS Ordinance on the Fees of the Federal Office of Topography (GebV-swisstopo) was revised during 2022 and 2023 bringing simplifications in the pricing models of the swipos services and bringing prices down to market level. The new GebV-swisstopo was introduced as of 1. April 2023.

The swipos service was used more than 3 million times in 2022 leading to a total of almost 70'000 days of requested corrections. It is worth mentioning that the use cases are more and more moving from traditional surveying to construction work, precision farming, and positioning of drones.

As expected, the main areas of usage are correlated with the populated areas. Figure 4.31 shows the location where the users were active when they ordered the correction signals. Nevertheless, even though the main areas are close to the urban regions the service is also needed for works in the country side and mountain regions.

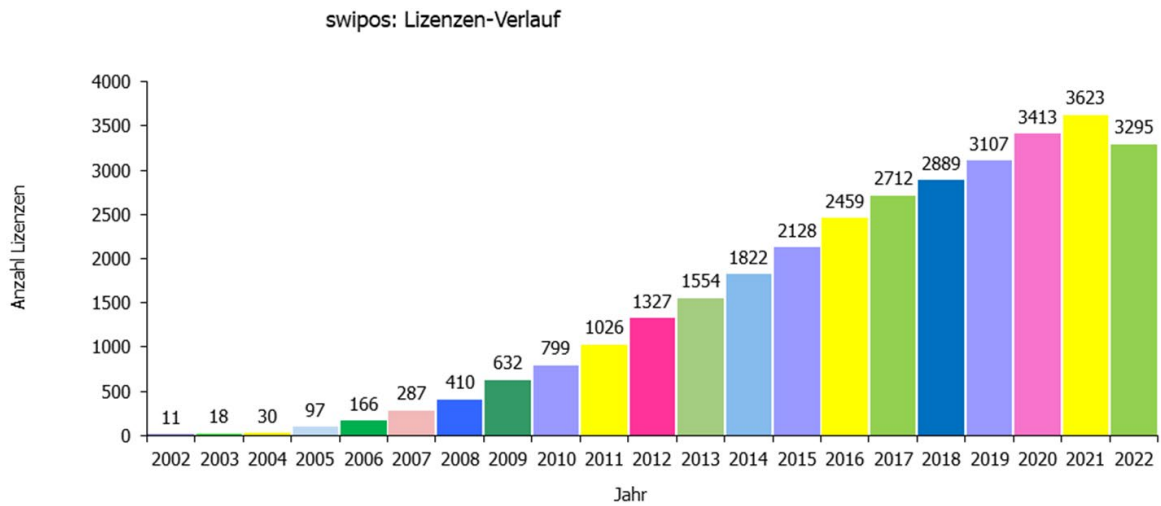


Figure 4.43: Number of active licensed customers

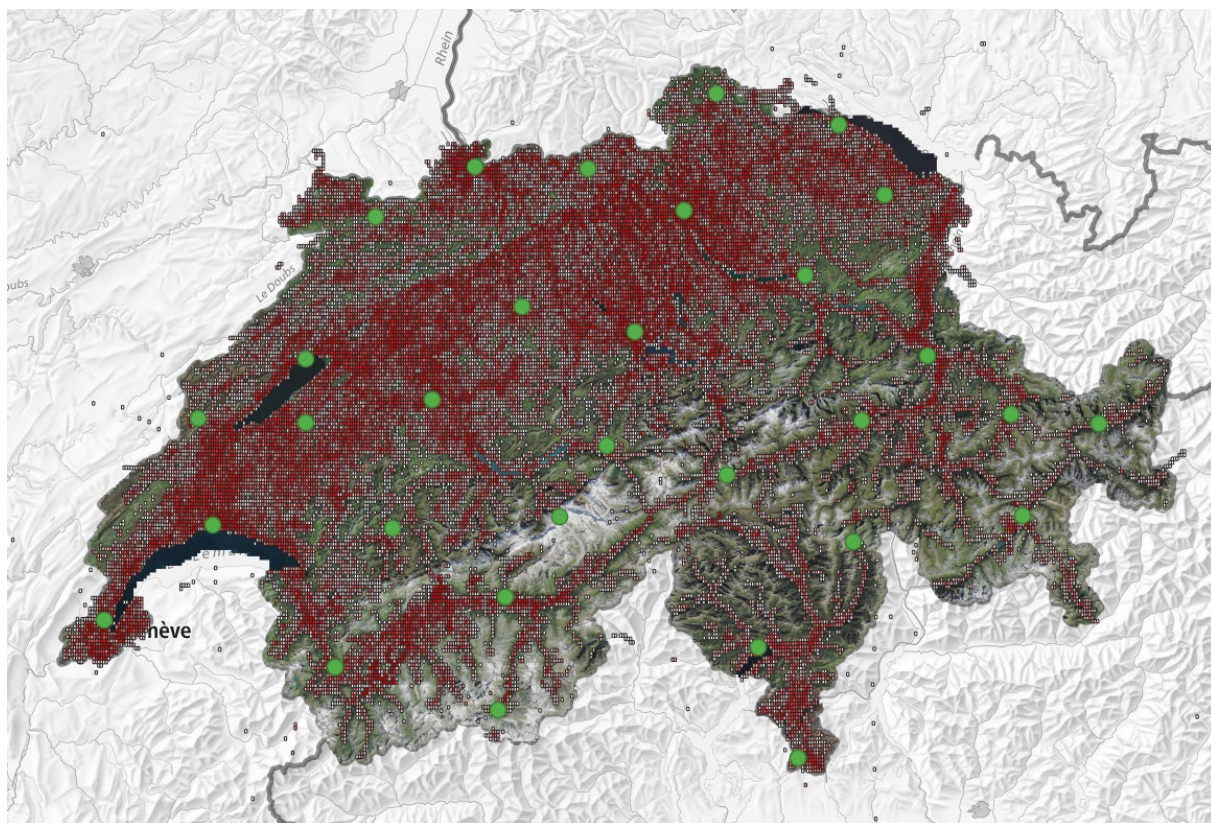


Figure 4.44: Distribution of the customer sessions in 2022

Deep Temporal Semi-Supervised One-Class Classification for GNSS Radio Frequency Interference Detection

V. Ivanov¹, M. Scaramuzza², R.C. Wilson¹

¹ University of York, United Kingdom

² Skyguide, Swiss Air Navigation Services, Switzerland

A new deep learning approach has been developed for the near real-time detection of Global Navigation Satellite System (GNSS) Radio Frequency Interference (RFI) events. It is based on a large amount of data of Global Positioning System (GPS) and Attitude and Heading Reference System (AHRS) recorded on-board of several helicopters during many years. The approach enables detection of GNSS RFI in the absence of total GPS failure i.e. while the receiver is still able to determine a position, which means RFI sources with low power or at larger distance can be detected. It has been demonstrated for the first time how deep one-class classification can be used to detect GNSS RFI. Furthermore, thanks to the unique dataset from Swiss Air Force and Helicopter Emergency and Medical Service operator (REGA), preprocessed by Swiss Air Navigation Services Ltd. (Skyguide), this is the first work which demonstrates application of deep learning for GNSS RFI detection on real-world large scale aircraft data collected onboard and containing flight recordings impacted by real jamming. The work also enables the application of variety of cutting-edge deep learning techniques to the field of GNSS RFI detection by connecting it to deep one-class classification. The approach is very general and can be applied to other systems apart of GPS as well. The experimental results indicate that the method successfully detects GNSS RFI with 83.5% accuracy. Extensive empirical studies demonstrate that the proposed method outperforms strong machine learning and rule-based baselines.

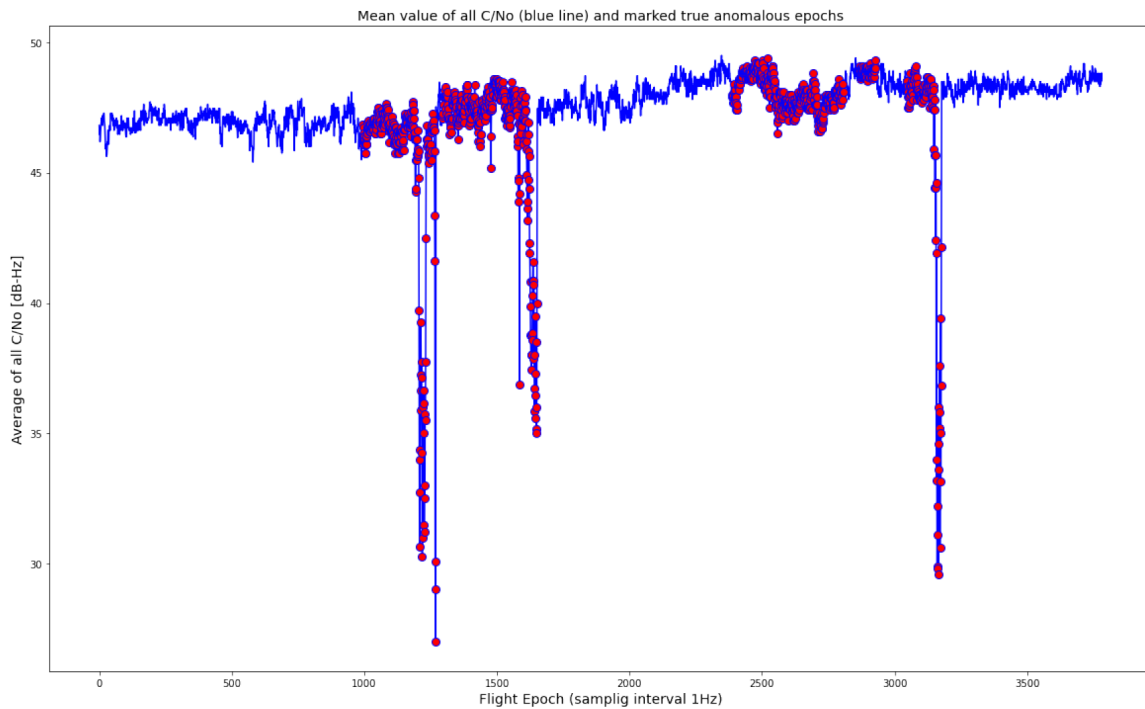


Figure 4.45: Mean value of all C/No (blue line) and marked true anomalous epochs (red dots) detected by the deep learning approach.

GNSS Interference Detection and Geolocalization for Aviation Applications

H. Nasser¹, G. Berz¹, M. Gómez², A. de la Fuente², J. Fidalgo², W. Li², M. Pattinson², P. Truffer³, M. Troller³

¹ *EUROCONTROL*

² *GMV, Spain & GMV-NSL, United Kingdom*

³ *Skyguide, Swiss Air Navigation Services*

GNSS is the primary enabler for Performance Based Navigation (PBN) and Automatic Dependent Surveillance Broadcast (ADS-B) applications and is becoming an increasingly essential technology used in air navigation. GNSS outputs are also used in various other Communication, Navigation and Surveillance (CNS) applications. Unfortunately, in some regions, Radio Frequency Interferences (RFI) affecting aviation has become a widespread challenge. EUROCONTROL monitors GNSS RFI impact through a number of means, including pilot reports and ADS-B data. Thanks to alternative CNS capabilities, these situations can generally be managed. Nonetheless, EUROCONTROL is investigating how GNSS RFI impact zones can be detected and how this information can be used by operational centers to improve the management of air traffic when subject to GNSS RFI.

EUROCONTROL has conducted a GNSS Receiver Interference Testing (GRIT) study with a GMV-led consortium to better understand the behavior of currently fielded aircraft GNSS receivers when subject to RFI. Skyguide participated in the test campaign with simulations conducted with three receivers commonly used in aviation. The objective of the testing was to see how receiver observables could be used to help detect RFI. Based on the simulation results, a set of RFI detection techniques have been defined and tested against different types of RFI, including CW, chirp and Noise-like jammers. The proposed techniques focused on the use of C/N0 derived metrics: detection of RFI based on the entropy of the C/N0 mean, Classification of RFI versus non-RFI events using Support Vector Machine method and Random Sample Consensus method applied to C/N0 versus elevation. These methods will be further explained in the paper [15] and their performances will be discussed in terms of detection, complexity and possible ways of improvement. Finally, a dataset was generated to obtain receiver tracking profiles with a simulated RFI source to see how ADS-B data can be used to detect and localize the RFI source.

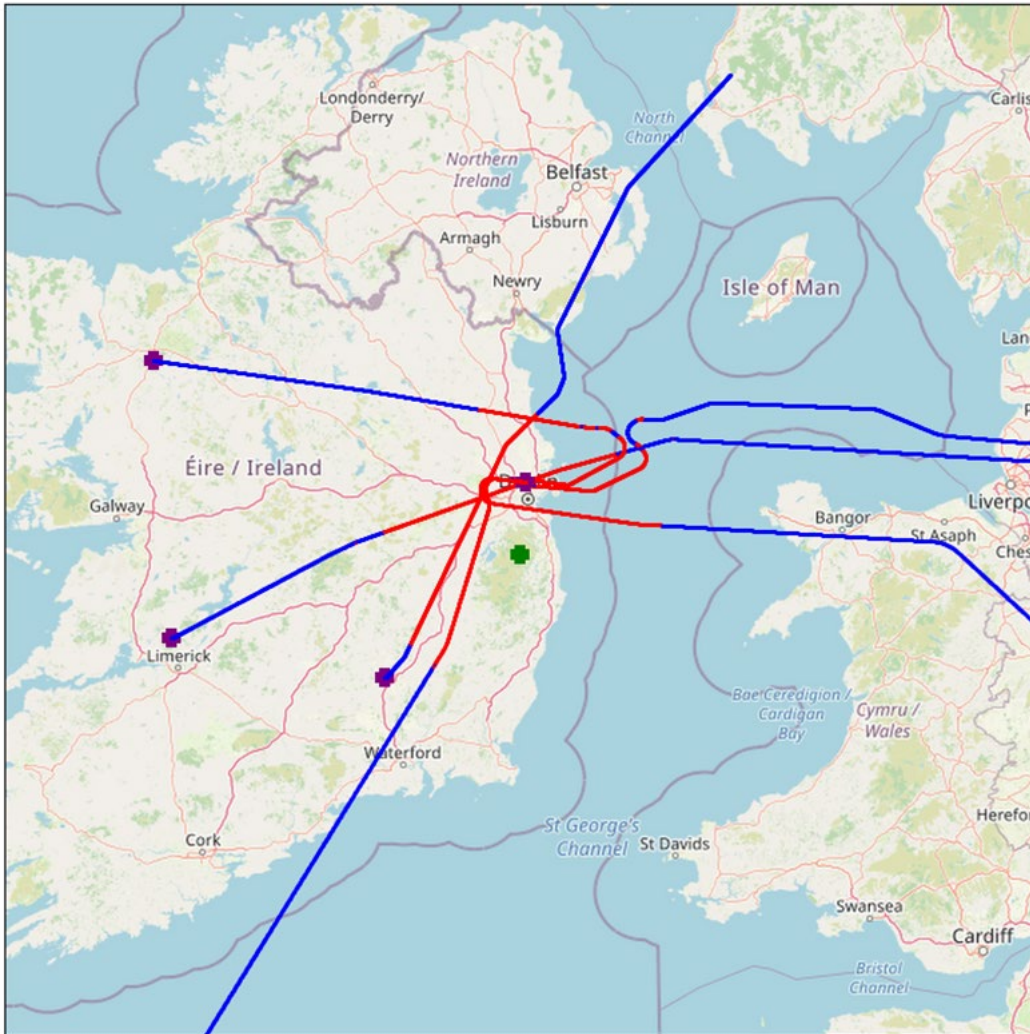


Figure 4.46: A/C trajectories. Blue: aircraft trajectory. Red: aircraft trajectory with Jammer / Signal ratio >15dB. Green: RFI location.

Navigation and guidance of platforms

J.-C. Charlaix¹, M. Khaghani¹, G. Laupre¹, P. Longobardi¹, F. Nex¹, J. Skaloud¹

¹ Ecole Polytechnique Fédérale de Lausanne, EPFL

This research focuses on the improvement of safety in navigation of small drones, notably on extending their capacity to stay within a planned trajectory in case the reception of GNSS signal gets disturbed. In such a situation the drone trajectory relies on autonomous (dead reckoning) navigation that employ interoceptive sensors such as inertial measurement unit (IMU) and barometer. We show that that the inherit drift of inertial navigation can be substantially mitigated when constraining the motion of the drone by a mathematical model that specifies all aerodynamical forces and moments. The respective contributions to the presented research concentrate on investigating: i) the sensitivity of synchronization between autopilot commands and sensory data, ii) the capacity of performing self-calibration of model coefficients, iii) the conception of model structure between different type of drones (e.g. conventional aircraft shape, flying -delta-wing), iv) other aspects and the evaluation of navigation performance.

References: [1], [2], [3], [4], [5] (Excel table [53-57])

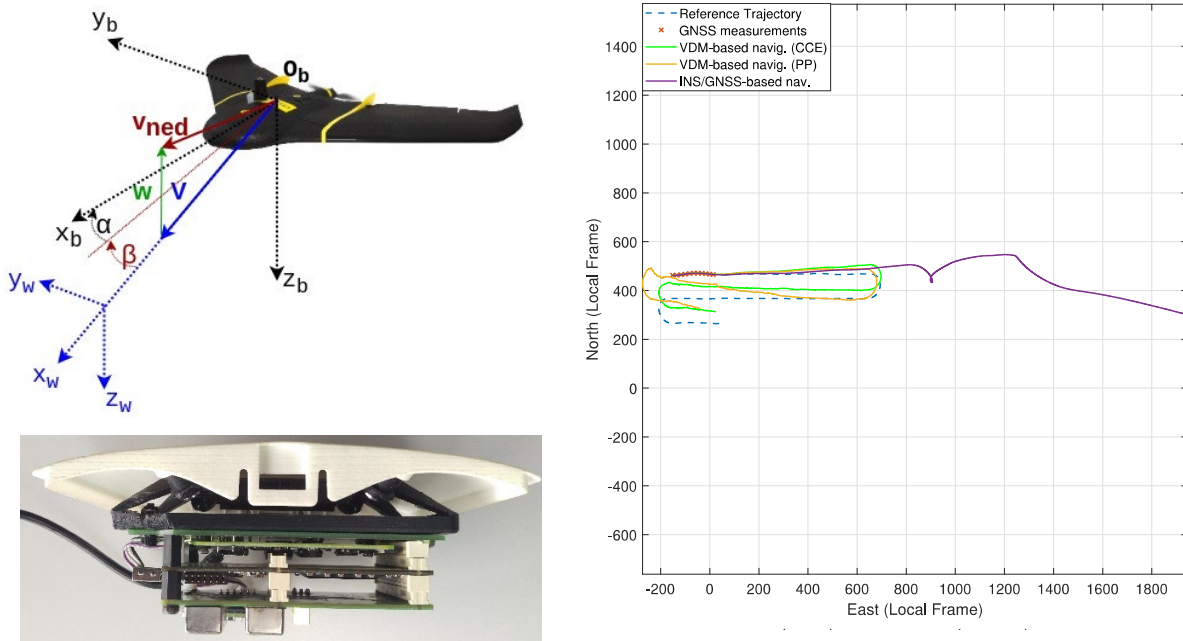


Figure 4.47: After [5] - Left: experimental commercial drone eBeeX (top) depicting relation between body (b)-frame and wind (w)-frame via air-speed vector (V) with custom payload (bottom) carrying two IMUs. Right: Comparison of reference (blue) and autonomous (i.e. without GNSS) navigation of this drone over 2 minutes using inertial (purple) and model-based navigation with approximate (yellow) and fine-tuned (green) calibration of aerodynamic coefficients.

Navigation sensor noise models and sensors calibration

J.-C. Charlaix¹, M. Khaghani¹, G. Laupre¹, P. Longobardi¹, F. Nex¹, J. Skaloud¹

¹ Ecole Polytechnique Fédérale de Lausanne, EPFL

This research improves the stochastic characterization and calibration of small inertial sensors that are used in many geodetic, surveying, mapping and navigation instrumentation (e.g. GNSS receivers on poles, surveying drones, cameras, laser-scanners etc.). Indeed, the identification of correct noise characteristic is an essential pre-requisite for correctly fusing observations from such sensors with other devices. Nevertheless, the identification become challenging when several stochastic processes are superposed. In this case the classical approaches like the regression of Allan variance (AV) or power spectral density (PSD) fail due to the difficulty of separating the error processes in the spectral domain. The following research contributions are on one side related to the modeling of these errors by wavelet moment-matching (called Generalized Method of Wavelets Moments - GMWM) and evaluating the impact on the quality of sensor integration; on the other side, on mitigating their deterministic part by special procedures. The latter aspect is useful when the deterministic errors are difficult to observe through normal sensor fusion, for instance, when the observation period is of a short duration.

References [6], [7], [8] (in Excel table [58 – 60])

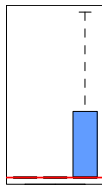


Figure 4.48: Comparison of stochastic parameter estimation between the proposed (GMWM), reference (ARMAV) and traditional Allan Variance Slope Method (AVSM).

Estimation methods for kinematic positioning

A. Brun¹, D.A. Cucci¹, K. Mouzakidou¹, J. Skaloud¹

¹ Ecole Polytechnique Fédérale de Lausanne, EPFL

The estimation in kinematic positioning is usually based on state-space modelling and some form of Bayesian filtering. Although this approach is very efficient computationally and therefore very popular in real-time operations, it is suboptimal in other aspects. For instance, it is more difficult to identify faulty observations or to introduce spatial (non-temporal) constraints between the estimated parameters. This research advances the sensor fusion via a network approach, within which all temporal and spatial conditions are formulated concurrently and all observations are adjusted altogether at once including the differential quantities as those coming at high-rate from inertial sensors. The research is focusing on overcoming challenges related to the resolution and stability of a large system (millions of parameters) and on the introduction of spatial constraints through active optical sensors such as lidar. Albeit the formulation is complex, the benefits are multiple in terms of the quality of the recovered trajectory and on the increased controllability between respective observations.

References [9], [10], [11] (in Excel table [61 – 63])

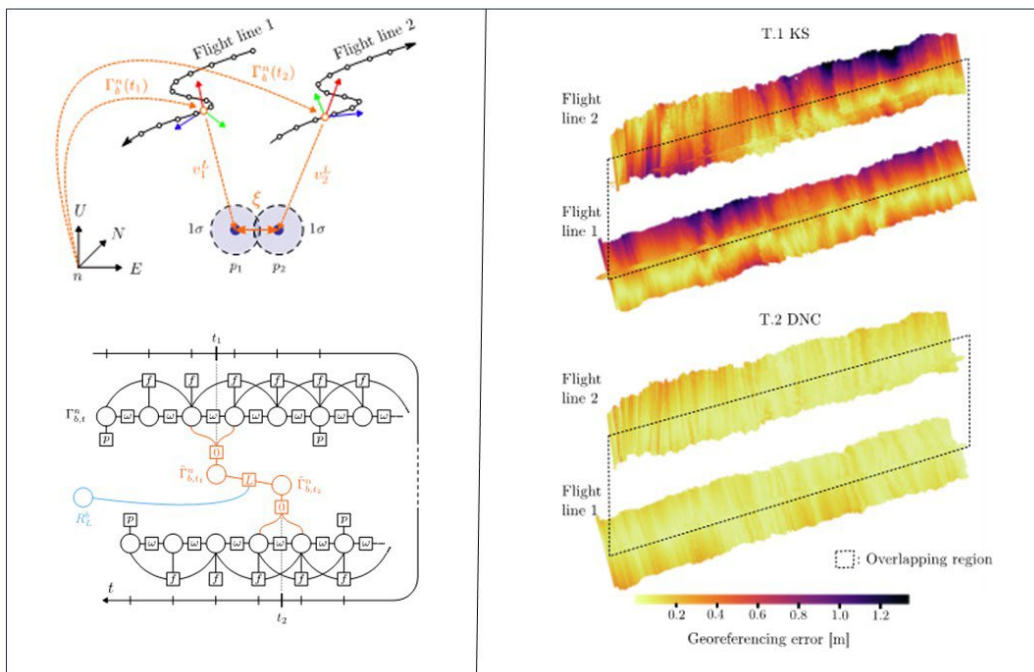


Figure 4.49: Left: (top - graphical representation of the geometrical constraint formulated for matched laser point between two point-clouds, (bottom) – a simplified Dynamic Network relating such correspondence (in orange) via optional lidar unknown parameter boresight (blue) to inertial raw observations (omega, f) and GNSS positions (p).

Right: magnitude of error in lidar-point cloud coordinates in two flight-lines for trajectory obtained via (top) – Kalman filtering and optimal smoothing, (bottom) – dynamic network using lidar point-to-point correspondences.

Fusion between navigation and optical sensors for precise mapping

E. Cledat¹, D.A. Cucci¹, K. Joseph-Paul¹, L.V. Jospin¹, J. Skaloud¹

¹ Ecole Polytechnique Fédérale de Lausanne, EPFL

The low weight Unmanned Aerial Vehicle (UAV) systems with imaging capability are now standardly deployed as carriers for surveying and mapping purposes. The optical sensors are small digital cameras or short-range lidar. This research focuses on the improvement of mapping efficiency achieved with this approach by maximising the geometrical accuracy while minimizing the need for ground control. This can be on one side improved by better mission planning that considers the physical obstructions of GNSS signal reception along drone trajectory due to its surroundings together with all other aspects of 3D reconstructions via imagery (e.g. planned camera positions, variations of the height above the terrain, texture of the scenery, location of some ground control etc.). Other improvements can be obtained by introduction of cameras with faster shutter, better optical properties of a lens, and good temporal stability of the sensor-lens-IMU assembly. Processing improvements can also be procured by a tighter fusion between active and passive optical sensing.

References [12], [13], [14] (in Excel table [64-66])

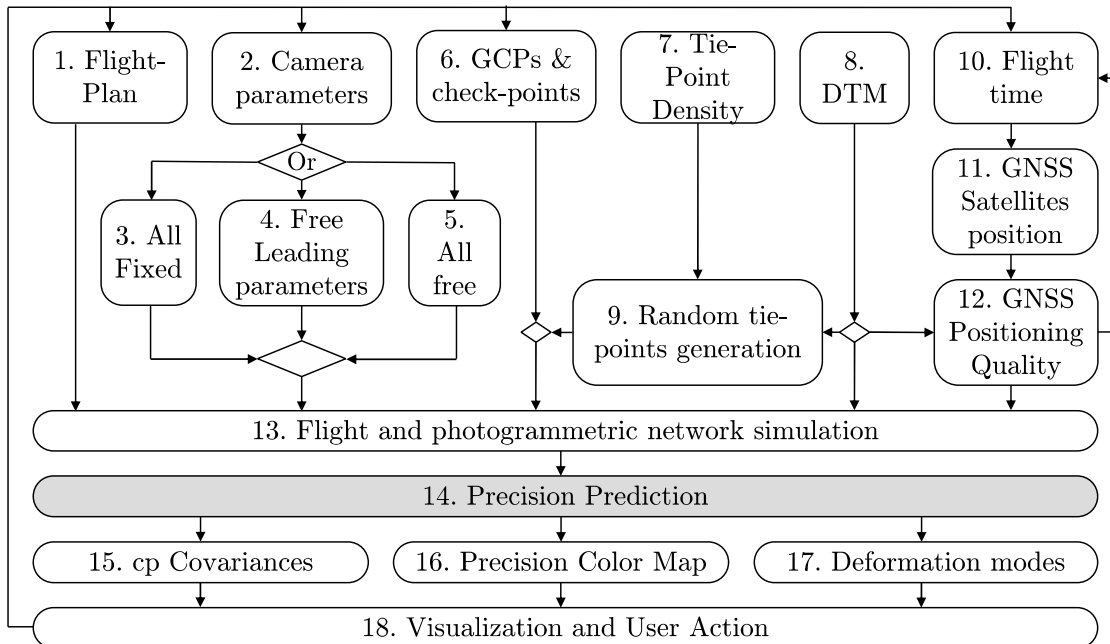


Figure 4.50: Workflow of accurate prediction of mapping precision.

REFERENCES

- [1] G. Laupre, M. Khaghani, and J. Skaloud, "Sensitivity to time delays in VDM-based navigation," *Drones*, vol. 3, p. 12, 2019, DOI:10.3390/drones3010011.
- [2] G. Laupre and J. Skaloud, "On the self-calibration of aerodynamic coefficients in vehicle dynamic model-based navigation," *Drones*, vol. 4, no. 1, p. 32, 2020.
- [3] P. Longobardi, G. Laupre, and J. Skaloud, "Aerodynamic characterization of a delta-wing UAV based on real flight data," in *2021 IEEE 8th Int. Workshop on Metrology for AeroSpace (MetroAeroSpace)*, 2021, pp. 69-74. [Online]. Available: DOI:10.1109/MetroAeroSpace51421.2021.9511742.
- [4] F. Nex et al., "UAV in the advent of the twenties: where we stand and what is next," *ISPRS J Photogramm. Remote Sens.*, vol. 184, pp. 215-242, 2022.
- [5] G. Laupre, P. Longobardi, J. Skaloud, and J.-C. Charlaix, "Model based navigation of delta-wing UAV - in-flight calibration and autonomous performance," *Eur. J. Navig.*, vol. 21, no. 1, pp. 22-30, 2021.
- [6] M. Khaghani, S. Guerrier, J. Skaloud, and Y. Zhang, "Optimal stochastic sensor error modeling based on actual impact on quality of GNSS-INS integrated navigation," in *ION GNSS+*, 2019, DOI:10.33012/2019.17057.
- [7] P. Clausen and J. Skaloud, "On the calibration aspects of MEMS-IMUs used in micro UAVs for sensor orientation," in *IEEE-ION Position Location and Navigation Symposium (PLANS)*, 2020, pp. 1457-1466. [Online]. DOI:10.1109/PLANS46316.2020.9110160.
- [8] S. Guerrier et al., "Wavelet-based moment-matching techniques for inertial sensor calibration," *IEEE Trans. Instrum. Meas.*, vol. 69, no 10, pp. 7542-7551, Apr. 2020., DOI:10.1109/TIM.2020.2984820.
- [9] D. Cucci and J. Skaloud, "On inertial measurements in dynamics networks," *ISPRS Ann Photogramm* DOI:10.5194/isprs-annals-IV-2W5-549-2019.
- [10] K. Mouzakidou, D.A. Cucci, and J. Skaloud, "On the benefit of concurrent adjustment of active and passive optical sensors with GNSS & raw inertial data," *ISPRS Ann. Photogramm. Remote Sens. Spat. Inf Sci*, vol. VI-2022, pp. 161-168, 2022.
- [11] A. Brun, A. Cucci, and J. Skaloud, "Lidar point-to-point correspondences for rigorous registration of kinematic scanning in dynamic networks," *ISPRS J. Photogramm. Remote Sens.*, vol. 189, pp. 185-200, 2022.
- [12] E. Cledat, L. V. Jospin, D. A. Cucci, and J. Skaloud, "Mapping quality prediction for RTK/PPK-equipped micro-drones operating in complex natural environment," *ISPRS J. Photogramm. Remote Sens.*, vol. 16, pp. 24-38, 2020.
- [13] E. Cledat and J. Skaloud, "Fusion of photo with airborne laser scanning," *ISPRS Ann Photogramm Remote Sens Spat. Inf Sci*, vol. V-1-2020, pp. 173-180, 2020.
- [14] J. Skaloud, D. A. Cucci, and K. Joseph-Paul, "Fixed-wing micro UAV open data with digicam and raw INS/GNSS," *ISPRS Ann Photogramm Remote Sens Spat. Inf Sci*, vol. V-1, pp. 105-111, 2021.
- [15] Nasser, Hamdi, Berz, Gerhard, Gómez, Mario, la Fuente, Alberto de, Fidalgo, Javier, Li, Wenjun, Pattinson, Michael, Truffer, Pascal, Troller, Marc, "GNSS Interference Detection and Geolocalization for Aviation Applications," *Proceedings of the 35th International Technical Meeting of the Satellite Division of The Institute of Navigation (ION GNSS+ 2022)*, Denver, Colorado, September 2022, pp. 192-216.

TABLE OF CONTENTS

Bibliography Commission 4

- Aichinger-Rosenberger, M., Brockmann, E., Moeller, G. (2021). Detection of Alpine Foehn in GNSS-ZWD time series: An innovative application of GNSS Meteorology. In EMS Annual Meeting.
- Aichinger-Rosenberger, M., Brockmann, E., Crocetti, L., Soja, B., and Moeller, G. (2022). Machine learning-based prediction of Alpine foehn events using GNSS troposphere products: first results for Altdorf, Switzerland, *Atmos. Meas. Tech.*, 15, 5821–5839. DOI:0.5194/amt-15-5821-2022.
- Aichinger-Rosenberger, M., Wolf, A., Senn, C., Hohensinn, R., Glaner, M.F., Moeller, G., Soja, B., Rothacher, M. (2023). Mpg-Net: A Low-Cost, Multi-Purpose Gns Co-Location Station Network for Environmental Monitoring. Preprint, DOI:10.2139/ssrn.4363729.
- Aichinger-Rosenberger, M., Brockmann, E., Crocetti, L., Soja, B., Moeller G. (2022). Machine learning-based prediction of Alpine foehn events using GNSS troposphere products: first results for Altdorf, Switzerland. In *Atmospheric Measurement Techniques*, Vol. 15(19), 5821-5839.
- Aschbacher, J., Milagro-Pérez, M. (2012). The European Earth monitoring GMES programme: Status and perspectives. *Remote Sensing of Environment*, 120:3-8, DOI:10.1016/j.rse.2011.08.028.
- Brun, A. Cucci, A, Skaloud, J. (2022). Lidar point-to-point correspondences for rigorous registration of kinematic scanning in dynamic networks. *ISPRS J. Photogramm. Remote Sens.*, vol. 189, pp. 185–200.
- Clausen, P., Skaloud, J. (2020). On the calibration aspects of MEMS-IMUs used in micro UAVs for sensor orientation. In *IEEE-ION Position Location and Navigation Symposium (PLANS)*, pp. 1457–1466. [Online]. DOI:10.1109/PLANS46316.2020.9110160
- Cledat, E., Jospin, L.V., Cucci, D.A., Skaloud, J. (2020). Mapping quality prediction for RTK/PPK-equipped micro-drones operating in complex natural environment. *ISPRS J. Photogramm. Remote Sens.*, vol. 16, pp. 24–38.
- Cledat, E., Skaloud, J. (2020). Fusion of photo with airborne laser scanning. *ISPRS Ann Photogramm Remote Sens Spat. Inf Sci*, vol. V-1–2020, pp. 173–180.
- Crocetti, L., Schartner, M., Zus, F., Zhang, W., Moeller, G., Navarro, V., See, L., Schindler, K., and Soja, B. (2023). Global, spatially explicit modelling of zenith wet delay with XGBoost. *Journal of Geodesy*. Submitted.
- Cucci, D., Skaloud, J. (2019). On inertial measurements in dynamics networks. *ISPRS Ann Photogramm Remote Sens Spat. Inf Sci*, vol. IV-2/W5, no. (Eurocow), pp. 549–557, DOI:10.5194/isprs-annals-IV-2-W5-549-2019.
- Dach, R., S. Lutz, P. Walser, P. Fridez (Eds); 2015: Bernese GNSS Software Version 5.2. User manual, Astronomical Institute, University of Bern, Bern Open Publishing. DOI: 10.7892/boris.72297; ISBN: 978-3-906813-05-9.
- Dach, R., Schaer, S., Arnold, D., Kalarus, M., Prange, L., Stebler, P., Villiger A., Jäggi, A. (2020a). CODE rapid product series for the IGS. Published by Astronomical Institute, University of Bern. URL: <http://www.aiub.unibe.ch/download/CODE>; DOI:10.7892/boris.75854.4.
- Dach, R., Schaer, S., Arnold, D., Kalarus, M., Prange, L., Stebler, P., Villiger A., Jäggi, A. (2020b). CODE final product series for the IGS. Published by Astronomical Institute, University of Bern. URL: <http://www.aiub.unibe.ch/download/CODE>; DOI:10.7892/boris.75876.4.

- Dach, R., Selmke, I., Villiger, A., Arnold, D., Prange, L., Schaer, S., Sidorov, D., Stebler, P., Jäggi, A., Hugentobler, U. (2021). Review of Recent GNSS Modelling Improvements Based on CODEs Repro3 Contribution. *Advances in Space Research*, 68(3):1263–1280, DOI:10.1016/j.asr.2021.04.046.
- Dach, R. and the BSW Development team (2022). Upcoming features of Bernese GNSS Software, Version 5.4 EUREF 2022 Symposium, online, 01–03 June, 2022, hosted by Zagreb, Croatia.
- Dach, R., Schaer, S., Arnold, D., Kalarus, M., Prange, L., Stebler, P., Sidorov, D., Villiger, A., Jäggi, A. (2023a). CODE Contributions to the IGS. This volume.
- Dach, R., Schaer, S., Arnold, D., Kalarus, M., Prange, L., Stebler, P., Sidorov, D., Villiger, A., Jäggi, A. (2023b). EUREF Activities at CODE. This volume.
- Fernández, J., Escobar, D., Águeda, F., Féménias, P. (2014). Sentinels POD Service Operations. *SpaceOps 2014 Conference*, SpaceOps Conferences, AIAA 2014-1929, DOI:10.2514/6.2014-1929.
- Fernández, M., Peter, H., Arnold, D., Duan, B., Simons, W., Wermuth, M., Hackel, S., Fernández, J., Jäggi, A., Hugentobler, U., Visser, P., Féménias, P. (2022). Copernicus Sentinel-1 POD reprocessing campaign. *Advances in Space Research*, 70(2), 249-267, DOI:10.1016/j.asr.2022.04.036.
- Friedli, E. (2020). Point Cloud Registration and Mitigation of Refraction Effects for Geomonitoring Using Long-Range Terrestrial Laser Scanning. Doctoral thesis, 26577, ETH Zürich, DOI:10.3929/ethz-b-000409052.
- Friedli, E., Presl, R., Wieser, A. (2019). Influence of atmospheric refraction on terrestrial laser scanning at long range. In: *Proc. JISDM 2019*, Athens, Greece, May 15-17, <http://jisdm2019.survey.ntua.gr/wp-content/uploads/2019/05/18.pdf>.
- Glaner, M.F. (2022). Towards instantaneous PPP convergence using multiple GNSS signals, Ph.D. thesis, Department of Geodesy and Geoinformation, TU Wien, DOI:10.34726/hss.2022.73610.
- Gojic, Z., Zhou, C., Wegner, J., Wieser, A. (2019). The Perfect Match: 3D Point Cloud Matching With Smoothed Densities. In *Proc: 2019 IEEE/CVF Conference on Computer Vision and Pattern Recognition (CVPR)*, Long Beach, CA, USA, 5540–5549, DOI:10.1109/CVPR.2019.00569
- Gojic, Z., Zhou, C., Wieser, A. (2020). F2S3: Robustified determination of 3D displacement vector fields using deep learning. *J Appl. Geodesy* 14(2): 177–189, DOI:10.1515/jag-2019-0044
- Gojic, Z. (2021). Benefiting from local rigidity in 3D point cloud processing. Doctoral thesis, 28017, ETH Zürich, DOI:10.3929/ethz-b-000523368
- Gojic, Z., Schmid, L., Wieser, A. (2021). Dense 3D displacement vector fields for point cloud-based landslide monitoring. *Landslides* 18: 3821–3832, DOI:10.1007/s10346-021-01761-y
- Guerrier, S. et al. (2020). Wavelet-based moment-matching techniques for inertial sensor calibration. *IEEE Trans. Instrum. Meas.*, vol. 69, no. 10, pp. 7542–7551, Apr. 2020, DOI:10.1109/TIM.2020.2984820.
- IERS Conventions (2010). Petit, G. and Luzum, B. (eds.). (IERS Technical Note ; 36) Frankfurt am Main: Verlag des Bundesamts für Kartographie und Geodäsie, 2010. 179 pp., ISBN 3-89888-989-6.
- Johnston, G., Riddell, A., Hausler, G. (2017). The International GNSS Service. In Teunissen, Peter J.G., & Montenbruck, O. (Eds.), *Springer Handbook of Global Navigation Satellite Systems* (1st ed., pp. 967-982). Cham, Switzerland: Springer International Publishing, DOI:10.1007/978-3-319-42928-1.

- Khaghani, M., Guerrier, S., Skaloud, J., Zhang, Y. (2019). Optimal stochastic sensor error modeling based on actual impact on quality of GNSS-INS integrated navigation. In ION GNSS+, 2019. DOI:10.33012/2019.17057.
- Kłopotek, G., Soja, B., Crocetti, L., Awadaljeed, M., Pan, Y., Rothacher, M., See, L., Weinacker, R., Sturn, T., McCallum, I., Navarro, V. (2022). Exploring Crowdsourced GNSS Observations for Data Fusion with the Use of Machine Learning. 8th International Colloquium on Scientific and Fundamental Aspects of GNSS. Sofia, Bulgaria, September 14–16, DOI:10.3929/ethz-b-000571141.
- Kobel, C., Arnold, D., Jäggi, A. (2019). Combination of precise orbit solutions for Sentinel-3A using Variance Component Estimation, *Adv. Geosci.*, 50, 27-37, DOI:10.5194/adgeo-50-27-2019.
- KUKA. 2018. KR AGILUS sixx specification. Augsburg, Germany: KUKA Deutschland.
- Landskron, D., Böhm, J. (2018). VMF3/GPT3: refined discrete and empirical troposphere mapping functions. *J Geod* 92, 349–360. DOI:10.1007/s00190-017-1066-2.
- Larson, K., Small, E., Gutmann, E., Bilich, A., Axelrad, P., Braun, J. (2008). Using GPS multipath to measure soil moisture fluctuations: Initial results, *GPS Solutions*. 12, 173–177. DOI:10.1007/s10291-007-0076-6.
- Laupre, G., Khaghani, M., Skaloud, J. (2019). Sensitivity to time delays in VDM-based navigation. *Drones*, vol. 3, p. 12, 2019, DOI:10.3390/drones3010011.
- Laupre, G., Skaloud, J. (2020). On the self-calibration of aerodynamic coefficients in vehicle dynamic model-based navigation. *Drones*, vol. 4, no. 1, p. 32, 2020.
- Laupre, G., Longobardi, P., Skaloud, J., Charlaix, J.-C. (2021). Model based navigation of delta-wing UAV - in-flight calibration and autonomous performance. *Eur. J. Navig.*, vol. 21, no. 1, pp. 22–30, 2021.
- Longobardi, P., Laupre, G., Skaloud, J. (2021). Aerodynamic characterization of a delta-wing UAV based on real flight data. in 2021 IEEE 8th Int. Workshop on Metrology for AeroSpace (MetroAeroSpace), 2021, pp. 69–74. [Online]. DOI:10.1109/MetroAeroSpace51421.2021.9511742
- Mao, X., Arnold, D., Girardin, V., Villiger, A., Jäggi, A. (2021). Dynamic GPS-based LEO orbit determination with 1 cm precision using the Bernese GNSS Software. *Advances in Space Research*, 67(2), 788-805, DOI: 10.1016/j.asr.2020.10.012.
- Meyer, U. (2020). CODE Associated Analysis Center Report. In: International Laser Ranging Service (ILRS) 2016-2019 Report, edited by C. Noll and M. Pearlman, NASA/TP-20205008530, NASA Goddard Space Flight Center, Greenbelt, MD, USA, 2020.
- Miotti L., Shehaj, E., Geiger, A., D'Aronco, S., Wegner, J.D., Moeller, G., Rothacher, M.. Tropospheric delays derived from ground meteorological parameters: comparison between machine learning and empirical model approaches, in IEEE proceedings of European Navigation Conference (ENC) 2020, online Conference, November 2020, 10.23919/ENC48637.2020.9317442.
- Moeller, G., Ao, C., Adavi, Z., Brenot, H., Sá, A., Hajj, G., Hanna, N., Kitpracha, C., Pottiaux, E., Rohm, W., Shehaj, E., Trzcina, E., Wang, K.-N., Wilgan, K., Zhang, K. (2020): Sensing small-scale structures in the troposphere with tomographic principles (IAG working group), EGU General Assembly 2020, Online, 4–8 May 2020, EGU2020-8469, DOI:10.5194/egusphere-egu2020-8469.
- Moeller G. (2023): Nanosatellites: The Next Big Chapter in Atmospheric Tomography. In: Inverse Problems - Recent Advances and Applications. IntechOpen; 2023. DOI:10.5772/intechopen.108522.

- Moeller, G., Piringer, F., Pérez Ortega, M., Presl, R., and Rothacher, M.: Absolute phase center calibration of low-cost GNSS patch antennas – Is it worth the effort?, EGU General Assembly 2021, online, 19–30 Apr 2021, EGU21-5700. DOI:10.5194/egusphere-egu21-5700, 2021.
- Montenbruck, O., Kunzi, F., Hauschild, A. (2022): Performance assessment of GNSS-based real-time navigation for the Sentinel-6 spacecraft. *GPS Solutions*, 26(1), 1–11.
- K. Mouzakidou, D. A. Cucci, and J. Skaloud, “On the benefit of concurrent adjustment of active and passive optical sensors with GNSS & raw inertial data,” *ISPRS Ann. Photogramm. Remote Sens. Spat. Inf Sci*, vol. VI-2022, pp. 161–168, 2022.
- Müller, L., Chen, K., Moeller, G., Rothacher, M., Soja, B., Lopez, L. (2023): Real-time navigation solutions of low-cost off-the-shelf GNSS receivers on board the Astrocast constellation satellites. Submitted to *Advances in Space Research*.
- Müller, L., Rothacher, M., and Chen, K. (2021): Systematic biases in the on-board navigation solution of a CubeSat GNSS payload board. EGU General Assembly 2021, online, April 19-30.
- Nasser, Hamdi, Berz, Gerhard, Gómez, Mario, la Fuente, Alberto de, Fidalgo, Javier, Li, Wenjun, Pattinson, Michael, Truffer, Pascal, Troller, Marc, "GNSS Interference Detection and Geolocalization for Aviation Applications," Proceedings of the 35th International Technical Meeting of the Satellite Division of The Institute of Navigation (ION GNSS+ 2022), Denver, Colorado, September 2022, pp. 192-216.
- Navarro, V., Grieco, R., Soja, B., Nugnes, M., Kłopotek, G., Tagliaferro, G., See, L., Falzarano, R., Weinacker, R., and Ventura-Traveset, J. (2021). Data Fusion and Machine Learning for Innovative GNSS Science Use Cases. In Proceedings of the 34th International Technical Meeting of the Satellite Division of The Institute of Navigation (ION GNSS+ 2021), pages 2656 – 2669. The Institute of Navigation, DOI:10.33012/2021.18115.
- F. Nex et al., “UAV in the advent of the twenties: where we stand and what is next,” *ISPRS J Photogramm. Remote Sens.*, vol. 184, pp. 215–242, 2022.
- Pacione, R., Douša J. (2020): SINEX_TRO - Solution (Software/Technique) INdependent Exchange, Format for TROpospheric and meteorological parameters, Version 2.00 (December 2020), Format description.
- Roesler, C., Larson, K. (2018): Software tools for GNSS interferometric reflectometry (GNSS-IR), *GPS Solutions* 22. DOI:10.1007/s10291-018-0744-8.
- Scaramuzza, S., R. Dach, G. Beutler, D. Arnold, A. Sušnik, A. Jäggi (2017): Dependency of geodynamic parameters on the GNSS constellation. *J Geod* 92(1):93-104. DOI:10.1007/s00190-017-1047-5
- Schaer, S., Villiger, A., Arnold, D., Dach, R., Prange, L., Jäggi, A. (2021): The CODE ambiguity-fixed clock and phase bias analysis products: generation, properties, and performance. *Journal of Geodesy*, Vol. 95, 1-25, DOI:10.1007/s00190-021-01521-9.
- Schreiter, L., Arnold, D., Sterken, V., Jäggi, A. (2021): “Mitigation of ionospheric signatures in Swarm GPS gravity field estimation using weighting strategies,” *Annales Geophysicae*, vol. 37, pp. 111–127, Feb. 2019. DOI:10.5194/angeo-37-111-2019.
- Schreiter, L., Montenbruck, O., Zangerl, F., Siemes, C., Arnold, D., Jäggi, A. (2021): “Bandwidth correction of Swarm GPS carrier phase observations for improved orbit and gravity field determination,” *GPS Solutions*, vol. 25, no. 2, p. 70, 2021, issn: 1521-1886. DOI:10.1007/s10291-021-01107-0.

- Schreiter, L. (2022): “Analysis and Quality Assessment of LEO GPS Data for Geophysical and Ionospheric Applications,” Swiss Geodetic Commission, ISBN: 978-3-908440-54-3, vol. 107, 2022.
- Shehaj, E., Frey, O., Moeller, G., Geiger, A., Rothacher, M. (2023): On the consistency of InSAR GNSS and NWP-derived tropospheric delays over complex terrain. Submitted to IEEE Transactions on Geoscience and Remote Sensing.
- Shehaj, E., Miotti, L., Geiger, A., D'Aronco, S., Wegner, J.D., Moeller, G., Soja, B., Rothacher, M. (2022): High-Resolution Tropospheric Refractivity Fields by Combining Machine Learning and Collocation Methods to Correct Earth Observation Data, *Acta Astronautica*. DOI:10.1016/j.actaastro.2022.10.007
- Shehaj, E., Geiger, A., Rothacher, M., Moeller, G.: Retrieval of Refractivity Fields from GNSS Tropospheric Delays: Theoretical and Data-based Evaluation of Collocation Methods and Comparison with GNSS Tomography. Submitted to *Journal of Geodesy*.
- Shehaj, E., Leroy, S., Cahoy, K., Geiger, A., Crocetti, L., Moeller, G., Soja, B., Rothacher, M.: GNSS Radio Occultations interpolated by Machine Learning and Bayesian Interpolation. Planned to be submitted in *Atmospheric Measurements Techniques*.
- Shehaj E., Wilgan K., Frey O., Geiger A (2020a): A collocation framework to retrieve tropospheric delays from a combination of GNSS and InSAR. *Navigation*, Issue 67, p. 823-842, DOI:10.1002/navi.398.
- Shehaj, E., Geiger, A., Moeller, G. (2020b): Total Refractivity Fields from GNSS Tropospheric Delays Reconstructed with Collocation Methods. *IGARSS 2020 - 2020 IEEE International Geoscience and Remote Sensing Symposium*, Waikoloa, HI, USA, 2020, pp. 457-460, DOI:10.1109/IGARSS39084.2020.9324073.
- Shehaj E. (2023): *Space Geodetic Techniques for Retrieval of High-Resolution Atmospheric Water Vapor Fields*. PhD thesis. ETH Zurich.
- Skaloud, J., Cucci, D.A., Joseph-Paul, K. (2021). Fixed-wing micro UAV open data with digicam and raw INS/GNSS, *ISPRS Ann Photogramm Remote Sens Spat. Inf Sci*, vol. V-1, pp. 105-111, 2021.
- Soja, B., Navarro, V., Kłopotek, G., Pan, Y., Crocetti, L., Awadaljeed, M., Rothacher, M., See, L., Sturn, T., Weinacker, R., and McCallum, I. (2022). Determination of atmospheric parameters from globally crowdsourced GNSS data. *American Geophysical Union Fall Meeting 2022*, DOI:10.3929/ethz-b-000590258.
- Sprenger, M., Schemm, S., Oechslin, R., and Jenkner, J. (2017): Nowcasting Foehn Wind Events Using the AdaBoost Machine Learning Algorithm, *Weather and Forecasting*, 32, 1079 – 1099. DOI:10.1175/WAF-D-16-0208.1
- SWPC (2023): Space Weather Prediction Center: Solar cycle progression. <https://www.swpc.noaa.gov>.
- Villiger, A., Dach, R., Arnold, D., Schaer, S., Selmke, I., Kalarus, M., Prange, L., Stebler, P., Jäggi, A. (2020): CODE repro3-IGb14 product series. Published by Astronomical Institute, University of Bern. URL: http://www.aiub.unibe.ch/download/REPRO_I20; DOI:10.7892/boris.135946.
- Willi D (2019): GNSS receiver synchronisation and antenna calibration. Doctoral Thesis, ETH Zurich, Zurich, Switzerland. DOI:10.3929/ethz-b-000308750